Particle-Laden Drop Impingement on a Solid Surface

A Dissertation
Presented to
The Academic Faculty

By

Hyunyoung Ok

In Partial Fulfillment
Of the Requirements for the Degree
Doctor of Philosophy in the
School of Polymer, Textile and Fiber Engineering

Georgia Institute of Technology
August 2005

Particle-Laden Drop Impingement on a Solid Surface

Approved by:

Dr. Wallace W. Carr, Advisor
School of Polymer, Textile and
Fiber Engineering
Georgia Institute of Technology

Dr. F. Joseph Schork
School of Chemical and
Biomolecular Engineering
Georgia Institute of Technology

Dr. Karl Jacob
School of Polymer, Textile and
Fiber Engineering
Georgia Institute of Technology

Dr. Jeffrey F. Morris
Chemical Engineering Department
City College of New York

Dr. Mary Lynn Realff
School of Polymer, Textile and
Fiber Engineering
Georgia Institute of Technology

Date Approved: July 11, 2005

ACKNOWLEDGEMENTS

First and foremost I would like to thank my advisor, Dr. Wallace Carr. Dr. Carr has provided me with a rich and rewarding graduate school experience on many levels, and I am truly thankful for his guidance, patience, and enthusiasm. I am very grateful to have had Dr. Carr as my dissertation advisor. I would also like to thank Dr. Jeffrey Morris for his input and discussion. I would also like to thank Dr. F. Joseph Schork for his involvement in my research and for giving me valuable advice. I would also like to thank Dr. Mary Lynn Realff and Dr. Karl Jacob for their critical reading of my work.

I would also like to thank Dan Brooks for always being willing to help me with all of my problems. Thanks to Hongming Dong for many discussions which have helped me in my research. Thanks to Arum Han in Electronic Engineering department for all the help with the experimental materials. I would also like to thank Dr. Paul Neitzel for his valuable input. Special thanks Dr. Ming Xu, in Sawgrass Technologies, Inc., for all information regarding inkjet printing.

I would like to recognize the National Textile Center (NTC) for funding this research.

I would also like to thank my parents, my brothers, and my mother-in-law, for their support over the years. Most of all, I would like to thank my husband, Heungsup Park, who gave never ending love and support. Without him, none of this would have been possible.

TABLE OF CONTENTS

LIST OF TABLES

LIST OF FIGURES

SUMMARY

An experimental study on impaction of a single drop on solid surfaces was conducted to show the effects of particles on the impact process. The effects of the following particle parameters were investigated: volume fraction of particles (0 to 0.3), particle size (0.47 to 250 μm), and ratio of particle size to drop size (0.00017 to 0.074).

The effect of particle volume fraction on the spreading process depends on impact speed and substrate. At low impact speed, particles have little effect on the spreading except for surfaces where the equilibrium contact angle is low. For this case, the maximum spreading ratio of particle-laden drop is lower than that of pure liquid drop. The liquid spreads to the equilibrium spreading ratio with almost no overshoot for the glass slide and silicon oxide wafer, and with a small overshoot for the Teflon® film (for the 690-μm drop, no overshoot occurs on Teflon® film). For high impact speed, the influence of particles on spreading can largely be described by the effective viscosity: as particle volume fraction is increased, viscosity increases, and Re is decreased; as a result, the particle-laden liquid does not spread as far as pure liquid.

The effect of particle size on the spreading process also depends on impact speed and substrate. Since spreading is dominated by liquid-surface interfacial energy at low impact speed, the drop does not have enough kinetic energy to overcome the energy

barrier associated with the large particles, consequently D_m^* is lower for the drop containing 250-μm particles. The effect of particle size is small for the impact speed of 2 m/s and for $\phi = 0.1$ and 0.2. For all surfaces and $\phi = 0.3$, D_m^* is largest for $d_p = 40$ μm, second largest for $d_p = 250$ μm, and smallest for $d_p = 6$ μm; however, the difference in D_m^* for the glass slide and silicon oxide wafer is small.

For particle-laden liquids, retraction depends on particle volume fraction, ϕ, and ratio of particle diameter to drop diameter, d_p/d. When pure liquid drops retract from D_m^*, the retraction appears to be symmetric around the point of impaction. In contrast, sometimes retraction of the particle-laden drop is asymmetric. The wetted area is not circular and particle distribution appears to be non-uniform. Drops containing 250-μm particles do not retract beyond the equilibrium position even for $\phi = 0.1$ while other drops retract beyond the equilibrium position.

Rebounding on the Teflon® surface depends on impact speed, particle volume fraction and particle size. The impact speed must reach a critical value for rebounding to occur. For 3.2-mm water drops, rebounding is observed at an impact speed as low as 0.42 m/s. The addition of particle affects rebounding. At low concentrations, the drop stretches further up before a drop is pinched off; however, if particle fraction is increased sufficiently, no rebounding occurs. Particles increase the viscosity of the liquid, and at high ϕ, the viscosity is sufficiently high to prevent pinch-off. At low ϕ, stretching for

the particle-laden fluid is greater that of pure liquid and pinch-off can occur at a weak point devoid of particles.

For larger pure liquid drops, Mao *et al.*'s rebounding model (1997) correctly predicts when rebounding occurs; however, it fails for the 690-μm pure liquid drop and for most of the particle-laden drops, especially for high ϕ. The failure of the model indicates that the effect of particles on rebounding are due to factors other than apparent viscosity.

Bouncing results suggest that the probability of bouncing decreases as viscosity increases, impact speed increases, and surface tension decreases. The non-wetting behavior and bouncing probably involves an air layer between the surface and the drop, and further work is needed.

When a low-velocity liquid drop impacts on a surface, ejection of a secondary drop from the top of the impacting drop is sometimes observed. Drop ejection is due to a spreading capillary wave, which is initiated at the impact point and progresses from the bottom of the drop to the top of the drop. The ejected drop eventually falls due to gravity, impacts on the mother drop which is spread over the surface, and then bounces several times on the mother drop and coalesces with it. During coalescence, the ejected drop sometimes ejects a daughter drop. When Renardy *et al.*'s (2003) criteria for the range of velocities for existence of a capillary wave is applied to for a 3.2-mm water drop, the

range is found to be between 0.2 to 1.5 m/s. However, drop ejection was observed at impact speed of 0.08 m/s.

Smaller drops spread faster and reach the equilibrium spreading ratio, D_e^*, sooner than the bigger drops for low and high impact speeds.

When apparent viscosity of the particle-laden liquid obtained from Krieger's equation (1972) was used in the pure liquid models for predicting D_m^*, good agreement between model predictions and experimental results was obtained. For impact speeds of 0.01 m/s and 0.3 m/s, Pasandideh-Fard *et al.*'s (1996) and Mao *et al.*'s (1997) model greatly over estimate D_m^*, especially for the low contact angle; however, Park *et al.*'s model (2003) is in close agreement with the experimental results. For an impact speed of 2 m/s, Mao *et al.*'s (1997) model overestimated some values while Pasandideh-Fard *et al.* (1996) and Park *et al.*'s (2003) models are good agreement with the measured maximum spreading ratio.

CHAPTER 1

INTRODUCTION

Studies of the effect of particles in the liquid on the impacting process are needed because solids, serving as colorant or binder, are required in "inks" needed for a number of nontraditional applications of inkjet technology such as textile printing. In addition to inks in textile printing, particles may also be ceramic or metallic particles in other applications. Although progress has been made in the design, formulation and utilization of such inks, impaction of particle-laden drops on surfaces has received little attention (Ok *et al.*, 2004; Carr *et al.,* 2004). For that reason, an impaction study using particle-laden-liquid drops impacting on solid surfaces was conducted.

The impaction of pure liquid drops is relatively well-understood, and processes using inks with soluble dyes have benefited from this understanding. The goal of the particle-laden drop impaction study is to develop understanding of how and why solid particles at a range of concentration affect the drop impaction process in order to support improved engineering of textile inkjet printing. Prior works (Park, 2003; Park *et al.,* 2003) have established a sufficient database for comparison of the behavior

of pure liquid impingement with that of drops with the particles at varying fractions and size so that the particulate effects can be identified. In the study presented here, the impact dynamics of particle-laden fluid are discussed, and the effects of the following particle parameters are studied: volume fraction of particles, particle size, and ratio of particle size to drop size. An existing model for maximum spreading ratio of pure liquid drop is used to predict the maximum spreading ratio for particle laden liquid.

When a low-velocity droplet impacts on a surface, sometimes the drop does not wet the surface and bouncing occurs. Bouncing reported in the literature is believed to be due to either the hydrophobicity of the surface (Onda *et al.*, 1996; Bico *et al.*, 1999; Quéré, 2002; Richard *et al.*, 2000, 2003; Okumura *et al.*, 2003) or surface roughness of the droplet (Aussillous *et al.*, 2001). However, in the present study, bouncing was observed on a hydrophilic surface at extremely low impact speed. Since this phenomenon has not been reported in the literature, this study includes bouncing, as well as spreading and rebounding.

In this dissertation, the background and literature review are presented in Chapter 2. In Chapter 3, the experimental details are discussed, and the results are presented in Chapter 4. Models for spreading and rebounding are discussed in Chapter 5. Conclusions and recommendations are in Chapter 6 and 7, respectively.

CHAPTER 2

BACKGROUND AND LITERATURE REVIEW

The impaction of pure liquid drop on solid surfaces has been studied for over 100 years (Worthington, 1876), and there is much in the literature about this subject. In contrast to the situation for pure fluids, impaction of particle-laden drop on surfaces have received little attention (Ok *et al*., 2004) despite their importance in a variety of applications such as inkjet printing. Ink properties (viscosity, surface tension, and density), substrate properties (surface energy and hydrophilicity/hydrophobicity), and drop parameters (drop size and impact velocity) affect the interaction of the impinging inkjet drop with the surfaces (Bergeron *et al.*, 2000; Funk, 1985; Oliver, 1988; Park, 2003; Park *et al*., 2003; Proebster *et al.*, 1989). These properties and parameters are used to form the significant dimensionless numbers, which are very useful in developing models for the droplet impact process on substrates. The most important dimensionless numbers are Reynolds number (Re), Weber number (We), and Capillary number (Ca). Also, contact angle (θ) is used for modeling the maximum spreading ratio. The Reynolds number is the ratio of inertial force to viscous force, and Weber number is the ratio of inertial force to surface energy of the impacting droplet. The

Capillary number, which is the ratio of viscously dissipated energy to surface energy, equals Weber number over Reynolds number. The definitions of Re, We, and Ca are shown in equations (2.1) through (2.3).

$$\mathrm{Re} = \frac{\rho v d}{\eta} \tag{2.1}$$

$$\mathrm{We} = \frac{\rho v^2 d}{\gamma} \tag{2.2}$$

$$Ca = \frac{We}{Re} = \frac{v\eta}{\gamma} \tag{2.3}$$

where ρ, η, and γ are the density, viscosity and surface tension of liquid, respectively, and d and v are drop diameter and impact speed, respectively. Table 2-1 shows the ranges of the physical properties of inks and operating parameters that can be used with the different inkjet engines, as well as the dimensionless numbers (Re, We, and Ca) associated with them (Tincher *et al.*, 1998a, 1998b; Tincher, 1999; Park, 2003). The continuous inkjet engines produce bigger drop sizes and higher impact velocities, and require higher ink surface tension and conductivity. Re and We for continuous inkjet engines are higher than for the drop-on demand engines.

Table 2-1. Properties of inkjet ink for textile printing (Tincher *et al.*, 1998a, 1998b; Tincher, 1999; Park, 2003).

Properties	Inkjet type			Present study
	Continuous Inkjet (CIJ)	Drop-on Demand (DOD)		
		Piezo	Thermal Inkjet	
Viscosity (cps)	1 – 10	5 – 30	1 – 3	1-6.2
Maximum Drop Size (μm)	~ 100	~ 30	~ 35	690 - 4000
Surface Tension (mN/m)	> 40	> 32	> 35	33 – 72
Velocity (m/s)	8 – 20	2.5 – 20	5 – 10	0.01 – 2.55
Conductivity (microsiemens)	> 1000	No Requirement	No Requirement	N/A
Re	80 – 2000	2.5 – 120	58 – 350	6.4 – 7900
We	87.6 – 1000	2.7 – 373	12 – 100	0.0084 – 390

In 1876, Worthington observed milk and mercury drops impacting on glass plates; however, most significant study of droplet impaction has been done in the last twenty years due to development of high-speed photographic techniques. The two major types of investigation of impact dynamics are classified as experimental and numerical.

Experimental studies have been done mostly using imaging capture systems. Two main categories of numerical studies are computer simulation and theoretical calculation. Computer simulation models fluid behavior as a function of time using computational program code. On the other hand, theoretical calculation is done to model the maximum spreading ratio, D_m^* (D_m/d, i.e. ratio of the maximum drop/surface contact diameter to drop diameter before impact). Some literature about experimental studies and numerical models for pure liquid impingement are reviewed in section 2.2 and 2.3.

2.1. Dynamics of Liquid Drop Impingement

When a drop impinges on a surface, several things can happen (Park *et al.*, 2003; Ok *et al.*, 2004). The impact speed of the drop greatly affects the impacting process. At high impact speeds, the drop may break up or flow out radially in what is

referred to as crown shape, where the axisymmetric flow is not stable and thus the flow is not uniform in all directions (Engel *et al.*, 1955; Ford *et al.*, 1967). If the spreading drop does not break up, the drop/substrate interaction can be separated into three stages: spreading, retraction, and equilibrium.

These processes are illustrated in Figure 2-1, which shows the spreading ratio, $D^* = D/d$, as a function of time. The shape of the curve depends on contact angle, Re, and We. In addition to these parameters, roughness may be important (Range *et al.*, 1998). Before the drop impacts on the surface, the drop has kinetic, surface, and potential energies. When the drop impacts on the surface, it spreads over the surface until it reaches a maximum spreading diameter, D_m, where the surface energy of the drop is at a maximum while its kinetic energy is zero. At the maximum spreading state, the liquid flow changes its direction and recoils inward due to surface energy. The amount of retraction depends on several factors including the initial kinetic energy of the impacting drop, the surface energy of the liquid, and the interaction energy between the liquid and the surface. In some cases, the liquid will retract to the equilibrium position and stop. In other cases, the liquid will retract beyond the equilibrium position and rise in the region of the initial impact. Under appropriate conditions, rebounding will occur where the liquid separates from the surface, rises a short distance and returns to the surface (Ok *et al.*, 2004).

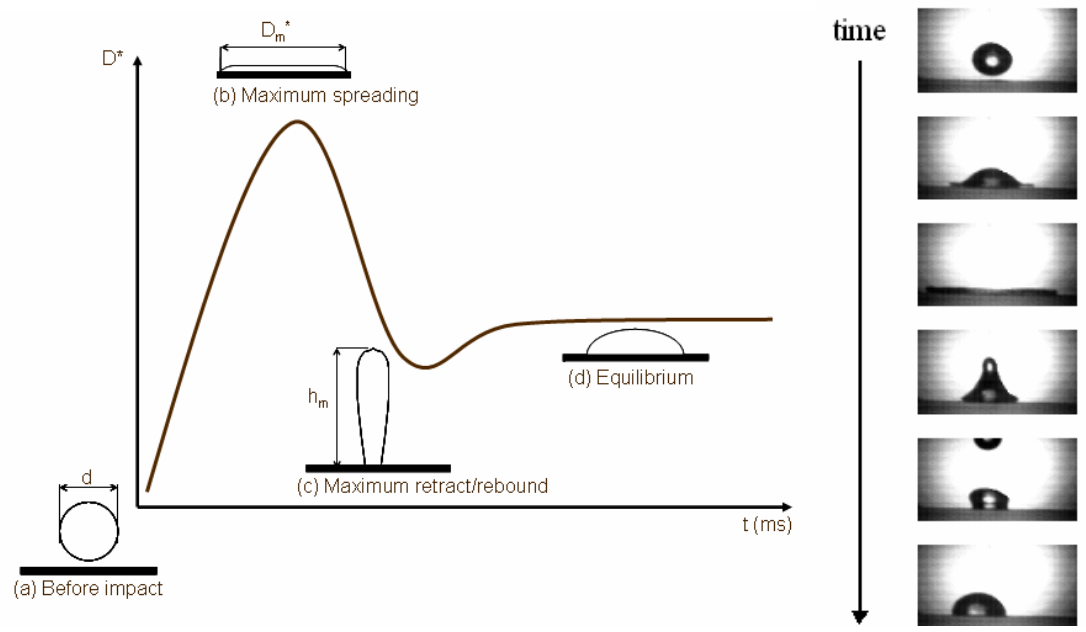

Figure 2-1. Impact and spreading process: (a) before impact, (b) maximum spreading, (c) maximum retract/rebound, and (d) equilibrium.

2.2 Experimental Studies of Pure Liquid Drop Impingement

Most of previous studies (Table 2-2) have been conducted using single-phase liquids on smooth surfaces. In spite of its importance, particle-laden droplet impingement has not been reported; however, some studies considered the effects of additives in pure liquids such as alcohol, surfactant, and polymer. In addition, there are some interesting droplet impact studies showing the effects of changing temperature and impact speed, etc.

Table 2-2. Significant parameters in important drop impact studies.

Authors (Year)	Liquids	Surfaces	v (m/s)	d (mm)	η (cP)	γ (mN/m)	Contact Angle (degree)			Re	We	D_m^*
							θ_e [a]	θ_a [a]	θ_r [a]			
Worthington (1876)	Milk, Mercury	Smoked and unsmoked glass	1, 1.4, 1.7, 2.0, 2.2	6.0 and 4.1	b	b	b	b	b	b	b	b
Engel (1955)	Water, surfactant solution	glass and filter paper	3 and 11	b	b	b	b	b	b	b	b	b
Ford *et. al.* (1967)	Water, surfactant solution	beeswax, cellulose acetate, glass	2.6-4.3	0.62, 0.78, 0.89, 0.98, and 1.1	1	72.8, other	b	27, 62, and 111	7, 31, and 54	1600-4496	57-256	2.65 to 4.40
Tsurutani *et al.* (1990)	fluorescent dye solution	glass	~3.1	5.2	1	60	b	27	b	16300	1020	5.5
Chandra *et.al.* (1991)	n-heptane	stainless steel surface, ceramic	0.93	1.50	0.42	20.8	b	32 - 180	b	2300	43	4.0
Asai *et al.* (1993)	3 water-based ink jet ink	copy and bond paper and transparent film	2.5-20	(44 to 81) × 10^{-3}	2.0 – 7.5	50-54	b	b	b	56 -59	5.3 – 5.5	~1.42
Fukai *et al.* (1995)	Water	3 Pyrex glass plates and a plate coated with a commercial wax	1.5-3.8	3.6	1	72.8	34-76	49 - 92	22-60	~3000 and ~8800	~60 and ~360	~2 to ~6
Scheller *et al.* (1995)	Glycerin-water-ethanol mixture	polystyrene and glass	4.9	0.8 to 4	1-300	72 – 65	b	b	b	20-20,000	0.00204-0.585 (Oh)	1.5 to 5.5
Pasandideh-Fard *et al.* (1996)	Water, 100 and 1000 ppm SDS solution	stainless steel	1	~2.0	1	73, 70, and 50	b	110	b	2112	27	2.15 to 2.62
Mao *et al.* (1997)	Water, 20% and 50% aqueous sucrose solution	wax, stainless steel, and glass	0.55, 1.86, 2.77, 4.58	2.7, 2.6, 2.5	1.0, 2.0, and 16.4	72.8	37, 67, and 97	b	b	1485-10,044	11.2-513	1.65 to 4.94

a. θ_e is equilibrium contact angle
θ_a is advancing contact angle
θ_r is receding contact angle
b. no information in the paper.
c aqueous solution of nonionic surfactant nonylphenol polyoxyethylene polyoxipropylene (NPOEOP) and the anionic surfactant sodium dioctyl sulfosuccinate (DOS).
d. surfactants are sodium dodecyl sulphate (SDS), octylphenoxy polyethoxyethanol (Triton X-100), and 2-butanol.
e. powder is lycopodium grains having typical size of 20 μm.

Table 2-2. (continued).

Authors (Year)	Liquids	Surfaces	v (m/s)	d (mm)	η (cP)	γ (mN/m)	Contact Angle (degree)			Re	We	D_m*
							θ_e[a]	θ_a[a]	θ_r[a]			
Thoroddsen *et al.* (1998)	Fluorescent water solution (6mg/l)	glass	f	5.5	1	60	b	27 and 110	b	~ 15,000	~ 1000	4.5 to 5.2
Mourougou-Candoni *et al.* (1999)	Water and surfactant solutions (NPOEOP and DOS[c])	glass plated coated by complexed stearic acid	4.06-4.48 and 3.20-3.51	0.70 to 0.89 and 2.28 to 2.75	1	72.58, 36.9, and 27	b	110-85	104-11	3367-3648 and 7524-9652	200-600 and 460-920	3.51 to 4.66
Bergeron *et al.* (2000)	Water and dilute poly-ethylene oxide solution	glass coated with a stearic acid complex agent	~3	~2	1	73	b	b	120	6000	250	~4.2
Crooks *et al*. (2001)	Water, glycerol and PEO solution, PEO solution, glycerol and surfactant solution[d]	glass, Parafilm M, Perspex, dichloro-silane, and PS	1-3	2.3	1-64	35 – 73	6-106	b	b	440-1320	30-300	2 to 4
Kim *et al.* (2001)	Deionized water, Ink, Silicone oil	Polycarbo-nate, Silicon oxide	0.77-3.47	2.8-3.7	0.867, 2.6, 36.3	71.7, 55, 37.3	6.2-87.4	b	b	120-14000	30-582	2.3-3.2
Aussillous *et al.* (2001)	Water and glycerine/ water coated with powder[e]	Glass, Teflon®	b	2	1-1150	b	180	b	b	b	b	N/A
Šikalo *et al.* (2002)	water, isopropanol , and glycerin	glass, wax, and PVC	1.17-4.55	2.7 - 3.3	1, 2.4, and 116	73, 63, and 21	b	0-105	0-95	500-15000	50-1000	2 to 6
Richard *et al.* (2002)	Water	Super hydro-phobic surface	0.2-2.3	0.2 -8	1	73	180	b	b	b	0.3-37	N/A

a. θ_e is equilibrium contact angle
θ_a is advancing contact angle
θ_r is receding contact angle
b. no information in the paper.
c aqueous solution of nonionic surfactant nonylphenol polyoxyethylene polyoxipropylene (NPOEOP) and the anionic surfactant sodium dioctyl sulfosuccinate (DOS).
d. surfactants are sodium dodecyl sulphate (SDS), octylphenoxy polyethoxyethanol (Triton X-100), and 2-butanol.
e. powder is lycopodium grains having typical size of 20 μm
f. Impact speeds were not given. Height of needle above surfaces were 0.20 and 0.29 m.

Table 2-2. (continued).

Authors (Year)	Liquids	Surfaces	v (m/s)	d (mm)	η (mPa·s)	γ (mN/m)	Contact Angle (degree)			Re	We	D_m*
							θ_e[a]	θ_a[a]	θ_r[a]			
Rioboo *et al*. (2002)	Acetone, isopropanol, ethanol, water, silicone oils, glycerine/water	Glasses, PVC, wax, polymer coatings, AKD	0.78-4.1	1.2-4.9	0.3-934	b	b	0-162	0-154	9-8842	33-396	2.3-5.2
Park *et al.* (2003)	Water, n-ocxane, n-tetradecane, and n-hexadecane	glass, silicon wafers, Teflon®	0.082-4	2.3	1	73	30-120	b	b	180-5513	0.2-176	2-4
Kim *et al.* (2003)	Distilled water	Poly-carbonate surface	8-16.2	0.213-0.26	1	73	b	b	b	1700-3900	190-860	3.2-4.4

a. θ_e is equilibrium contact angle
θ_a is advancing contact angle
θ_r is receding contact angle
b. no information in the paper.
c aqueous solution of nonionic surfactant nonylphenol polyoxyethylene polyoxipropylene (NPOEOP) and the anionic surfactant sodium dioctyl sulfosuccinate (DOS).
d. surfactants are sodium dodecyl sulphate (SDS), octylphenoxy polyethoxyethanol (Triton X-100), and 2-butanol.
e. powder is lycopodium grains having typical size of 20 μm.

2.2.1. Effect of polymer additives

Bergeron *et al.* (2000) found that rebound of water droplet occurred when the retraction speed is high. However, the rebound is suppressed when a small amount of polyethylene oxide (PEO) is added to water due to its high extensional viscosity of the fluid. Extensional viscosity is a material property of a fluid which characterizes the resistance of a material to stretching; therefore, a fluid having higher extensional viscosity tends to have lower rebound. Crook *et al.*'s study (2001) confirmed the

effect of polymer additives by using a Boger fluid, a liquid whose extensional viscosity changes while shear viscosity remains constant. Several PEO's with different molecular weights were added to water to obtain solutions having the same shear viscosity, but different extensional viscosities. They showed the height of the rebounding is reduced as extensional viscosity is increased.

2.2.2. Effects of surfactant additives

Effects of surface tension of liquid were mainly studied using surfactant in liquids. Zhang and Basaran (1995) found that adding surfactant increases spreading of the drop; however, the non-uniform distribution of surfactant along the fluid interface gives rise to Marangoni stresses (i.e., surface-tension gradient forces) that reduce drop spreading. They also stated that since the contact line between the liquid and the substrate is not constant during spreading and retracting, the influence of dynamic surface tension on behavior of drops of surfactant solutions is important. Mourougou-Candoni *et al.* (1999) claimed that the surface tension of the drop and the adsorption kinetics of the surfactant are the most important factors that control the impaction process.

2.2.3 Effect of temperature

Chandra and Avedisian (1991) studied the effect of surface temperature on the drop impingement process and developed a model for maximum spreading. When water drops impact on a stainless steel surface, they found that the population of bubbles within the droplet increased as surface temperature was increased because of progressive activation of nucleation sites on the stainless steel surface. They also found that overall droplet shape, particularly in the early stages of impact, was unaffected in spite of the presence of bubbles; however, the resting state was significantly different. For higher temperature, the resting diameter was less than that for lower temperature because of increased surface energy of the liquid-solid interface.

2.2.4. Bouncing droplet

Droplet bouncing has been observed for two drops impacting each other and a single drop impacting a surface. Lord Rayleigh (1945) noted that small rain droplets bounced upon collision with a larger pool of water and attributed the failure to achieve coalescence was caused by a layer of air trapped between the two colliding surfaces which prevented true contact.

Orme (1997) discusses the events that occur when two or more droplets collide. Droplet bounce occurs if the surfaces of the droplets do not make contact due to the presence of a thin intervening gas film. The colliding droplets will coalesce when the air film thickness reaches a critical value. This critical value is typically of the order of 100 Å. When two droplets interact during flight, several events may occur, including bouncing, stable coalescence, temporary coalescence followed by disruption or temporary coalescence followed by fragmentation. The outcome depends on two parameters (Weber number and the distance (b) from the center of one drop to the relative velocity placed on the center of the other drop), and the fluid properties (viscosity and surface tension of the liquid and viscosity and density of air). Orme points out that the behavior of fuel droplet collisions has been found to be notably different from the behavior of water droplet collisions. The behavior of droplet collisions is found to be dependent on viscosity of the fluid as well as the surface tension and gas properties. Since the two parameter We and b do not include viscosity, critical values of these parameters defining regions of behavior will vary with droplet fluid as well as background gas.

Dell'Aversana *et al.* (1996, 1998, 2002) showed that noncoalescence occurred due to thermocapillary convection. When drops approach one another, a locally hotter region is formed in the center of the cold drop and a locally cooler region is

formed in the center of the hot drop. These temperature variations give rise to thermocapillary motion within the drops. The resultant surface motion of the drops gives rise to bulk flow within the ambient gas surrounding the drops, causing gas to be swept into the space between them. This motion produces enough pressure to prevent the surfaces from coming into contact.

The bouncing of a single drop impacting a surface may occur due to the hydrophobicity of the substrate (Richard *et al*., 2000, 2002; Okumura *et al.*, 2003) and the surface roughness of the droplet (Aussillous *et al.*, 2001).

In a study of the impaction of a water droplet on a super-hydrophobic surface, Richard *et al.* (2000, 2002) showed that the water drop could fully bounce on the surface without wetting. The contact remained close to 180° during the whole shock (period when the drop is in contact with the surface). Thus, the drop was not wetting the surface during shock; however, the static contact was approximately 170°. The drop deforms during impact, and kinetic energy is converted into surface energy. Then surface energy causes the drop to move away from the surface as surface energy is converted into kinetic energy. As the drop rises, kinetic energy is converted into the potential energy until kinetic energy reaches zero, and the drop reverses its directions. The degree of deformation of impacting droplet depends on We; however, contact time is independent of impact velocity over the range of velocities studied.

Aussillous and Quéré (2001) encapsulated an aqueous liquid droplet with a very hydrophobic powder (20-micron size lycopodium grains covered with fluorinated silanes) that gave hydrophobicity to the droplet surface. The contact angle between the droplet and a glass surface was 180^{o}. Drop impaction on glass gave results similar to those reported by Richard *et al.* (2000, 2002).

2.2.5. Ejection of secondary droplet

When a low-velocity liquid drop impacts on a surface, the ejection of a secondary drop from the top of the impacting drop is sometimes observed. Thoroddsen *et al.* (2000) reports the ejection of secondary drops when a drop is deposited gently onto the surface of the same liquid. They describe the phenomenon as follows: "The drop hesitates briefly before coalescing into the bulk fluid, due to the draining of a thin layer of air sitting between the two liquid masses. As contact is established between the drop and the liquid layer, the unbalanced surface tension forces initiates a capillary wave that greatly deforms the drop that coalesces only partially, pinching off a new drop at its top. The daughter drop bounces and comes to rest at the surface, repeating this partial coalescence. We have observed up to six steps in this cascade, starting with drop diameters around 3 mm and decreasing in diameter

by approximately one-half during each step."

The ejection of a drop during the impaction process occurs due to a capillary wave in the vertical direction. Renardy *et al.* (2003) give the following two criteria for a capillary wave to exist for drop impacting on a solid surface: $We > 2$ and $We \cdot Ca < 2$. Although they do not discuss drop ejection, they state that "..... the oscillation of the top can lead to the formation of a small cavity of air. The collapse of this cavity eventually produces the eruption of a very thin jet".

Roux *et al.* (2004) observed the ejection of a secondary drop when a 2.4-mm water drop impacted a glass surface at an impact speed of 0.22 m/s. They applied Renardy *et al.*'s criteria for existence of a capillary wave and found that it was satisfied. They state that the secondary drop bounces, but did not mention the generation of a series of successively smaller drops as reported by Thoroddsen *et al.* (2000).

2.3. Modeling of Pure Liquid Drop Impingement

Two main approaches to study drop impingement on a smooth surface are computer simulation and theoretical calculation using energy balance. A model for predicting whether or not rebounding occurs has also been developed by Mao *et al.* (1997).

2.3.1 Computational modeling

The earlier computational simulations used the Marker-and-Cell (MAC) finite difference method. Since the MAC method neglects effects of surface tension and viscosity of liquid, it is not very useful. A modified method developed from MAC referred to as the Volume-of-Fluid (VOF) method has also been used. It includes effects of surface tension and viscosity of liquid. To determine the shape of the free surface of the impacting droplet, contact angle is needed. Both equilibrium and dynamic contact angles have been used in computations (Fukai *et al.*, 1995; Pasandideh-Fard *et al.*, 1996). The results using equilibrium contact angle are not accurate. Dynamic contact angle gives much better predictions; however, it has to be measured from the photographs of the drop during spreading. Thus, experiments must be conducted before the model can be used, making the model much less useful. If experiments are run, then important information such as maximum spreading ratio can be determined directly from the photographs.

2.3.2 Theoretical modeling

Theoretical modeling uses an energy balance before and after drop impact to

predict D_m^* as a function of the Re, We, and contact angle (θ). Kinetic energy, viscous dissipation, and surface energy are included in the energy balance. This method gives no information about pressure, velocity, and temperature distributions.

An energy balance to obtain D_m^* was first used by Ford and Furmidge (1967). The balance between the energy of the impacting drop and the energy at maximum spread is expressed as

$$E_{1k} + E_{1p} + E_{1s} = E_{2p} + E_{2s} + E_{2d} \tag{2.4}$$

where E_{1k} is the kinetic energy at the point of impact, E_{1p} is the potential energy at the point of impact, E_{1s} is the surface energy at the point of impact, E_{2p} is the potential energy at the maximum spread, E_{2s} is the surface energy at the maximum spread, and E_{2d} is the energy dissipated during the deformation of the drop. They were unable to calculate the spreading ratio due to difficulty of estimating dissipation energy.

Chandra and Avedisian (1991) neglected the potential energy term from the energy balance, set kinetic energy equal to zero at maximum spread, and set the dissipation energy equal to viscous dissipation. Viscous dissipation was estimated using the following equation:

$$\int_0^{t_c}\int_{\Omega}\phi d\Omega dt \approx \phi\Omega t_c \approx \left(\mu\left(\frac{u}{h}\right)^2\right)\left(\frac{1}{4}\pi D_m^2 h\right)\left(\frac{d}{u}\right) = \frac{\pi}{4}\frac{\mu\, u d D_m^2}{h} \tag{2.5}$$

where ϕ is the dissipation function, Ω is the volume of the liquid drop, t_c is the time taken for the drop to spread from impact to maximum spreading, and u is the impact speed. Since then, the viscous dissipation was included in models to obtain D_m^*. Table 2-3 summarized some important models from the literature. Park *et al.* (2003) recently developed a model, which gives improved predictions for low drop impact velocities, as discussed below. The key feature of the model was that the shape of the drop was assumed to be a spherical cap at the maximum spread as shown in Figure 2-2 while other models assumed the shape of the drop to be cylindrical at the maximum spread. There are two equations for the maximum spreading ratio. Equation (2.6) is for Re < $81(D_m^*)^4$, and equation (2.7) is for Re > $81(D_m^*)^4$.

$$0.53\frac{We}{\mathrm{Re}}D_m^{*4} + \left(\frac{1}{2}\left(\frac{1-\cos\alpha}{\sin^2\alpha}\right) - \frac{1}{4}\cos\theta\right)D_m^{*2} - 1 - \frac{We}{12} + \frac{\Delta E_{SP}}{\pi d^2 \gamma_{LV}} = 0 \tag{2.6}$$

$$\left(0.33\frac{We}{\sqrt{\mathrm{Re}}} - \frac{1}{4}\cos\theta + \frac{1}{2}\left(\frac{1-\cos\alpha}{\sin^2\alpha}\right)\right)D_m^{*2} - 1 - \frac{We}{12} + \frac{\Delta E_{SP}}{\pi d^2 \gamma_{LV}} = 0 \tag{2.7}$$

where ΔE_{SP} is the decrease in surface and interfacial energies for spontaneous spreading from state 1 to state 2 (Figure 2-2), γ_{LV} is the surface energy of liquid-vapor interface, and α is the contact angle at the maximum spreading calculated using the assumptions that the shape of the fluid in state 2 is a cap of a sphere and that the fluid volume is constant. The relationship for calculating of ΔE_{SP} is shown in equation (2.8).

$$\Delta E_{SP} = \pi d^2 \gamma_{LV} \left(\frac{\cos\theta}{4} g(\alpha) + 1 - \frac{1}{2}\left(\frac{1-\cos\theta}{\sin^2\theta} \right) g(\theta) \right) \qquad (2.8)$$

where the function $g(\theta)$ is the square of spreading ratio at equilibrium contact angle. Ford and Furmidge (1967) expressed $g(\alpha)$ as

$$g(\alpha) = D^{*2}_{m} = \left[\frac{4\sin^3\alpha}{2 - 3\cos\alpha + \cos^3\alpha} \right]^{\frac{2}{3}} \qquad (2.9)$$

Equation (2.9) can be solved simultaneously with equation (2.6) or (2.7) to obtain D_m^*.

Table 2-3. Summary of previous models.

	Models
Chandra *et al.* (1991)	$\left(\frac{3}{2}\frac{\mathrm{We}}{\mathrm{Re}}\right)D^{*}_{m}{}^{4}+(1-\cos\theta_e)D^{*}_{m}{}^{2}-\left(\frac{1}{3}\mathrm{We}+4\right)=0$
Asai *et al.* (1993)	$D^{*}_{m}=1+0.48We^{0.5}\,exp\left[-1.48We^{0.22}\,Re^{-0.21}\right]$
Scheller *et al.* (1995)	$D^{*}_{m}=0.61(\mathrm{Re}^2\mathrm{Oh})^{0.166}$
Fukai *et al.* (1995)	$\frac{1}{2}\frac{We}{\mathrm{Re}^{0.772}}D^{*}_{m}{}^{4}+2.29(1-\cos\psi)D^{*}_{m}{}^{2}-\left(\frac{We}{3}+4\right)=0$
Pasandideh-Fard *et al.* (1996a, 1996b)	$D^{*}=\sqrt{\frac{We+12}{3(1-\cos\theta_a)+4(We/\sqrt{\mathrm{Re}})}}$
Mao *et al.* (1997)	$\left[\frac{1}{4}(1-\cos\theta_e)+0.2\left(\frac{We^{0.83}}{\mathrm{Re}^{0.33}}\right)\right]D^{*3}-\left(\frac{We}{12}+1\right)D^{*}+\frac{2}{3}=0$

Notation:

D^{*}_{m} : maximum spreading ratio

θ_e : equilibrium contact angle

Oh : Ohnesorge number, $Oh=\frac{\mu}{\sqrt{\rho d\sigma}}=\frac{\sqrt{We}}{\mathrm{Re}}$

ψ : dynamic contact angle

θ_a :advancing contact angle between liquid and solid

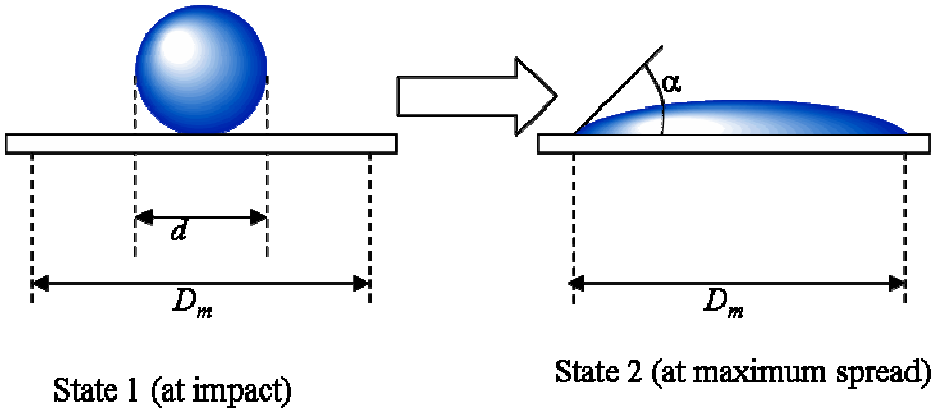

Figure 2-2. Schematics of: state 1 (at impact) and state 2 (at maximum spread).

2.3.3 Rebounding modeling

Mao *et al.* (1997) developed a rebounding model using energy difference between the maximum spreading stage and a fictitious stage after retraction. Assumptions for this model are: 1) only potential energy and surface energy are considered at the maximum extent to which a drop recoils or bounces, 2) the drop is just above the solid surface and is considered to be momentarily at rest in the fictitious stage, and 3) shape at the maximum spread is a thin cylinder. According to their model, whether a drop rebounds or not depends on the maximum spreading ratio and

the equilibrium contact angle. The resulting equation for predicting whether or not rebounding occurs is

$$E^*_{ERE} = \frac{1}{4}\left(\frac{D_m}{d}\right)^2 (1-\cos\theta) - 0.12\left(\frac{D_m}{d}\right)^{2.3} (1-\cos\theta)^{0.63} + \frac{2}{3}\left(\frac{D_m}{d}\right)^{-1} - 1 \quad (2.10)$$

where, E^*_{ERE} is the excess rebound energy normalized with respect to the energy possessed in fictitious stage. A drop will be rebound when E^*_{ERE} is greater than zero. In their study, rebounding occurred on the paraffin wax surface ($\theta = 97^o$ with distilled water) with D_m^* of 3.01, 3.60, and 4.32. In Figure 2-3, E^*_{ERE} is illustrated according to Mao *et al.*'s equation as a function of the maximum spreading ratio for $\theta = 97^o$. For D_m^* of 3.01, 3.60, and 4.32, ΔE^*_{ERE} is greater than zero, rebound is predicted. This model's ability to predict rebounding of a particle-laden drop is discussed in Chapter 5.

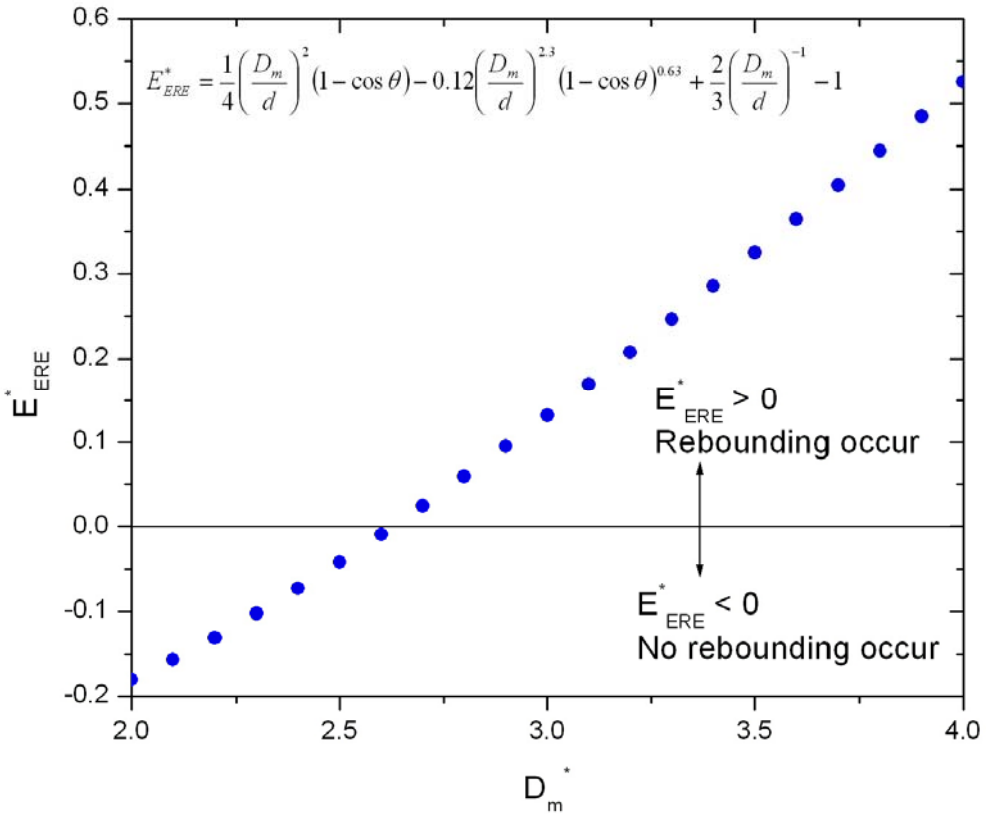

Figure 2-3. Excess rebound energy (Mao *et al*., 1997) as a function of the maximum spreading ratio for a contact angle of 97^o.

CHAPTER 3

EXPERIMENTAL

The impaction of a particle-laden drop on different surfaces was studied. The particle-laden drops were formed from particulate suspensions composed of spherical, neutrally buoyant, non-colloidal particles in a viscous liquid. The impaction process was recorded using a high-speed CCD camera, and the captured images were analyzed. The following particle-related parameters were considered: 1) volume fraction of particles, ϕ, 2) particle size, d_p, and 3) the ratio of particle size (d_p) to drop size (d), d_p/d. The results were analyzed during spreading and retracting/rebounding. The special case of bouncing of a low-velocity drop impacting on silicon oxide wafer (a hydrophilic surface) was investigated. Table 3-1 shows drop and particle size found in a typical inkjet printing system and present study.

3.1. Apparatus

The experimental setup for producing a single drop and recording the impact process is shown in Figure 3-1. A syringe pump (KD Scientific Model 230) forces

Table 3-1. Comparison of drop size and particle size in a typical inkjet with present study.

System	Drop size, d (μm)	Particle size, d_p (μm)	d_p/d^*
Typical inkjet**	30	0.25 (0.1 – 0.7)	0.0083 (0.0033 – 0.0233)
Present study	690	20 40	0.029 0.058
	2700	0.47	0.00017
	2900	20 40	**0.0069** **0.014**
	3900 4000 3400	6 40 250	0.0015 **0.010** 0.074

** Private communication with Xu, M (2003).

*Bolded numbers indicate d_p/d falls in the typical inkjet range.

the suspension out of a flat-tipped needle in Figure 3-1 (a). The drop falls by gravity, and the impact speed is controlled by adjusting the height of the needle. A high speed camera records the impact process. The captured images are transferred to computer and stored for further analysis. For drops containing 20- and 40-μm particles, a 22-gauge needle was used; however, for larger particles, a stainless tube with an inside diameter of approximately 3 mm was used to form the drops because the 250-μm particles clogged the 22-gauge needle. The resultant drop size ranged from 3.4 to 4.0 mm, depending on particle size. With this setup, producing drops with diameter less than 2 mm is difficult because drop size is proportional to 1/3 power of needle diameter. To reduce the drop size by factor of 2, the needle size needs to be reduced by factor of 8. Particle-laden liquid cannot be used with small needles due to clogging.

Small drops were produced using a special device designed and fabricated at Georgia Tech. It is shown schematically in Figure 3-1 (b). The device uses a piezo engine (PAR Technologies, LLC) to force liquid from a pinhole, a disk with a hole in its center. The pinhole size is varied to produce a range of drop size. This apparatus uses a piezo pump to push out the liquid through the pinhole. Various sizes of pinhole are available commercially. Amplitude and frequency of the voltage applied to the piezo engine was adjusted to produce a single drop. With this system, the drop

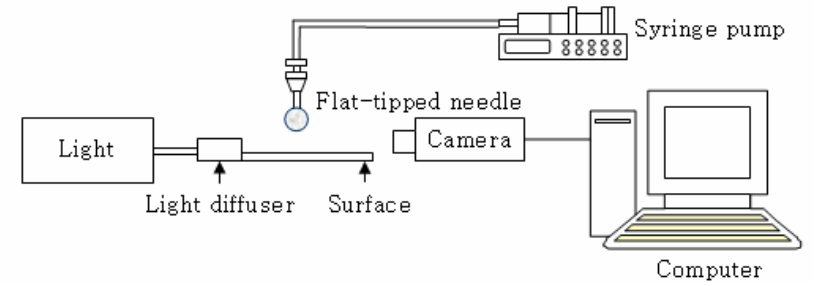

(a) Setup for large drops

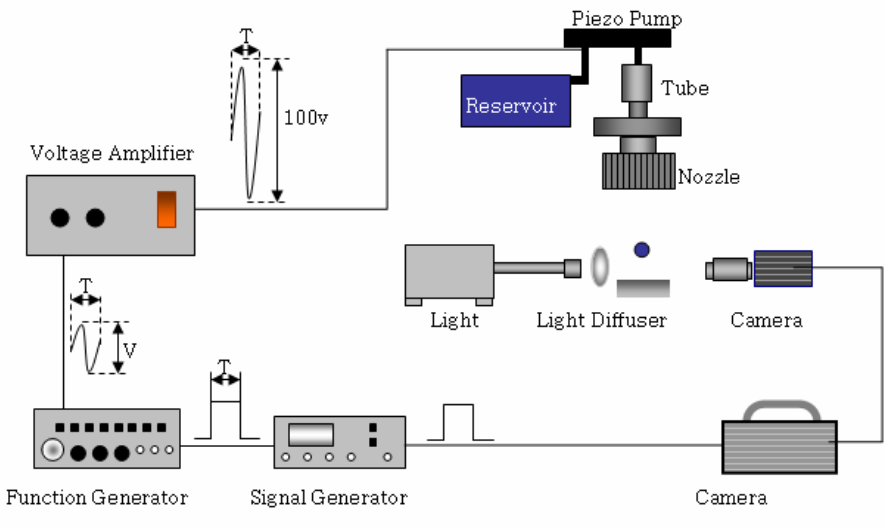

(b) Setup for small drops

Figure 3-1. Schematic of experimental apparatus: (a) setup for large drops and (b) setup for small drops.

ejection speed is low; therefore, impact speed was controlled by varying the distance between pinhole and surface. An example of the variation of drop ejection speed and drop size versus frequency as a function of voltage is shown in Figure 3-2.

A Kodak MotionCorder Analyzer (Eastman Kodak Company, Model 10K, San Diego, CA) was used to record continuous images of the impaction of a single droplet. A Nikon MKII Fiber Optic Illuminator was used to provide back lighting. A series of pictures was recorded from one drop impingement event using a camera speed of 5000 frames per second. A 50-μs exposure time was used to obtain sufficient sharpness of

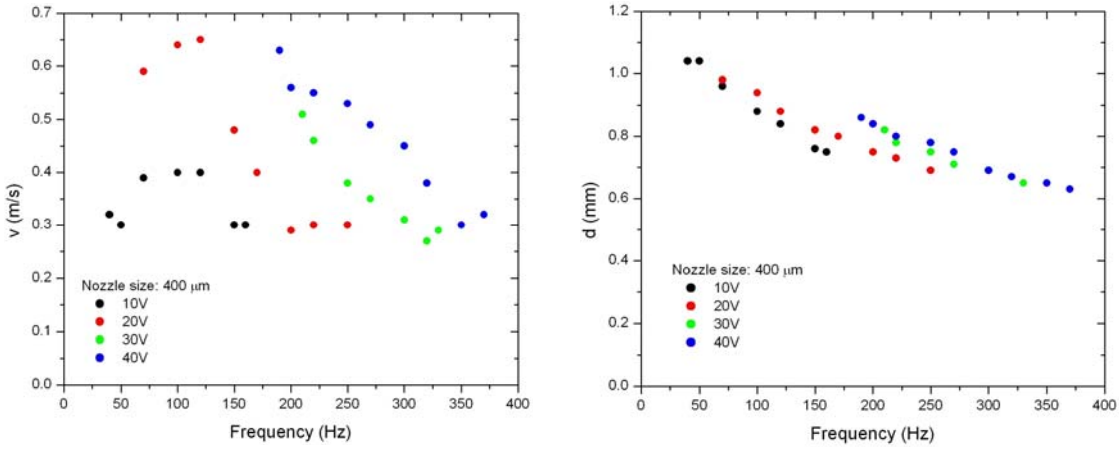

(a) Ejection speed versus frequency as a function of voltage.

(b) Drop diameter versus frequency as a function of voltage.

Figure 3-2. Operation range of the piezoelectric device with nozzle size of 400μm: (a) ejection speed versus frequency as a function of voltage and (b) drop diameter versus frequency as a function of voltage.

images. For this setting, the camera has 128 × 80 pixels spatial resolution and 8 bit gray scale in black and white. Drop impaction speed was calculated from droplet displacement measured using two different frames and a calibrated scale, and time between frames.

3.2. Materials

The impaction of particle-laden drop on different surfaces was studied. The particle-laden drops were formed from particulate suspensions composed of spherical, neutrally buoyant, non-colloidal particles in a viscous liquid. Polystyrene particles having density of 1.06 g/cm^3 were used to produce the particle-laden liquids. Particle size was varied from 0.47 to 250 μm.

The 0.47-μm polystyrene particles dispersed in water-based solution were produced in the laboratory by emulsion polymerization. The steps for producing the particles via emulsion polymerization are shown in Table 3-2. The particle size produced from step 1 was 0.12 μm. The bigger particles were produced via swelling process (Ugelstad *et al.*, 1979). The swelling process is shown in step 2 to 4 in Table 3-2. After the first and second cycles of swelling, the particle sizes were 0.22 and 0.47 μm, respectively; however, the particles did not get bigger in the third cycle. The

Table 3-2. Steps for producing polystyrene particles.

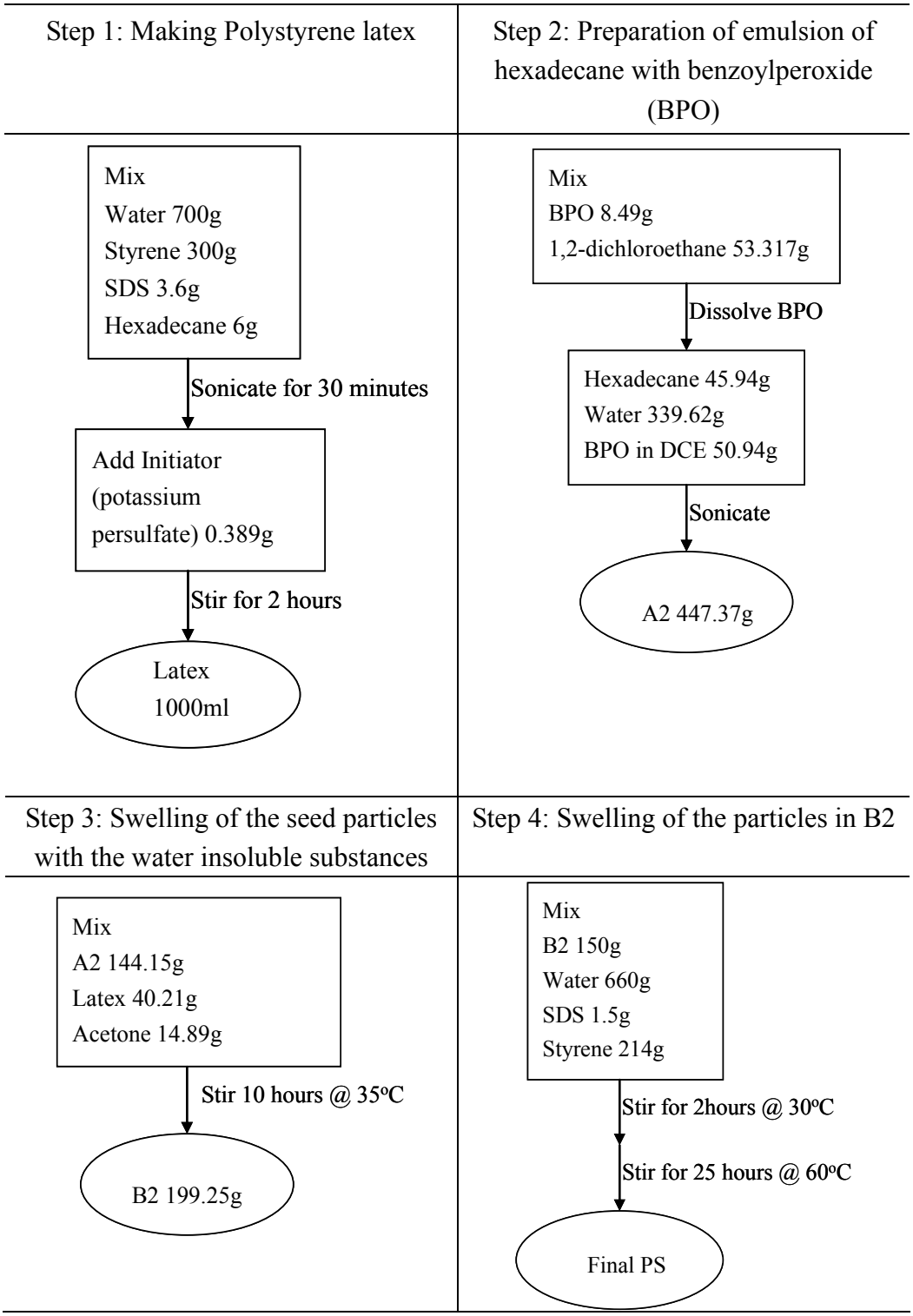

particle volume fraction of the final product was 0.15. Particles were filtered from the final product to obtain a particle-free base solution that was used for comparison tests.

Other particles were from Sekisui Chemical Co., Ltd (6-μm particles), Bangs Laboratories, Inc. (20 and 250-μm particles), and Kodak (40-μm particles). Three solutions were used for the particle-laden liquid tests. The first solution (Mixture 1) contained 77% water and 23% glycerin, which matched the density (1.06 g/cm^3) of the particles. The tests were conducted using 20- and 40-μm particles that dispersed well in Mixture 1. Since the 6- and 250- μm particles were uncoated, 100 ppm of polyoxyethylene 3 decyl ether (Aldrich inc.) was added to Mixture 1 to obtain second solution (M1S100). Tests with 6-, 40-, and 250-μm dispersed in M1S100 were conducted. The third solution (S1) was the liquid in which the 0.47-μm particles were dispersed in following the last step in the polyethylene process (Table 3-2).

Surface tension was measured using a Bubble Pressure Tensiometer (BP2 Krűss GmbH) over a range of frequencies. The surface tension of Mixture 1 was almost constant (about 72 dyne/cm); however, the surface tension of M1S100 and S1 varied with frequency as shown in Figure 3-3. Weber numbers are calculated based on static surface tension, which is the value at the lowest frequency in dynamic surface tension curve. The surface tension of Mixture 1 with surfactant is 43 dyne/cm, and

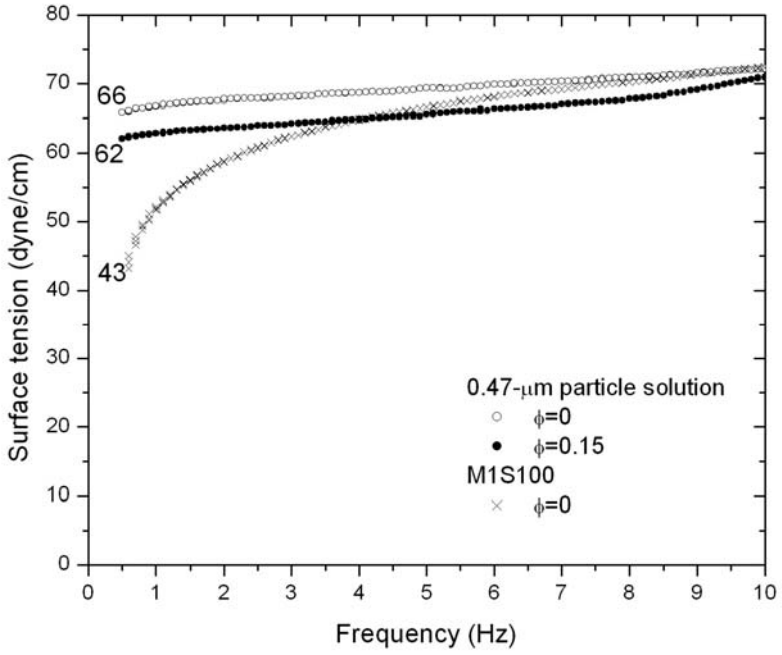

Figure 3-3. Dynamic surface tension of liquids containing surfactant.

that of ϕ = 0 and 0.15 of solution of 0.47-μm polystyrene particles are 62 and 66 dyne/cm, respectively. Apparent viscosities of the fluids were measured using a Brookfield Viscometer (model DV-1). Surface roughness of silicon oxide wafer, silicon wafer, and Teflon® film was measured using Atomic Force Microscopy (AFM, Digital Instruments NanoScope).

Six different surfaces were used: glass slide, silicon oxide wafer, silicon wafer, polycarbonate surface, fluorocarbon plasma treated silicon wafer, and a Teflon® coated aluminum film (Bytac® Teflon® Surface Protectors). Contact angles of liquids on the

surfaces were measured using a VCA2500KE Contact Angle Surface Analysis System (AST Products Inc.). Equilibrium contact angles of distilled water on six surfaces are shown in Table 3-3. Table 3-4 and 3-5 show the equilibrium contact angles of M1S100 and S1.

3.3. Tests Conducted

Experiments were conducted to show the effect of particle volume fraction on spreading ratio (D^*), which is an important parameter that affects printing quality. Spreading ratio is the ratio of spreading diameter (D) to the initial drop diameter (d). Tests were conducted where the impact speed and surface were held constant, and the particle volume fraction was varied; therefore, the Weber number (We) remained nearly constant and the Reynolds number (Re) changed with particle volume fraction since Re is based on the apparent viscosity of the suspension.

Test were also conducted to determine if the effects of particles were due solely to the increase in viscosity associated with the addition of particles. Thus, it is meaningful to compare the impact process of particle-laden fluid with that of pure fluid having the same Re and We. In addition to the measured viscosity, viscosity of particle-laden fluid was estimated using Krieger's equation (Krieger, 1972):

Table 3-3. Equilibrium contact angles of distilled water on surfaces*.

Surface	Contact angle (°)
Glass slide	17
Silicon oxide wafer	38
Silicon wafer	47
Polycarbonate surface	89
Teflon® film	112
Fluorocarbon plasma treated silicon wafer	113

* Contact angle of Mixture 1 on each surface is similar with that of distilled water.

Table 3-4. Equilibrium contact angle of M1S100.

Surface	Contact angle (°)
Glass slide	5
Silicon oxide wafer	20
Teflon® film	90

Table 3-5. Equilibrium contact angle of S1.

Surface	Contact angle (°)
Glass slide	10
Silicon oxide wafer	25
Teflon® film	95

$$\eta = \eta_0 \left(1 - \frac{\phi}{\phi_m} \right)^{-2.5\phi_m} \tag{3.1}$$

where, η_0 is viscosity of pure fluid, and ϕ_m is the maximum particle volume fraction. The comparison of measured viscosity and Krieger's viscosity is shown in the Table 3-6. Measured viscosities are higher than viscosity from Krieger equation, especially for high ϕ. The measured viscosities of the particle-laden fluid having particle volume fractions of 0.10 and 0.20 were matched with a pure fluid produced by mixing water and glycerin (Mixtures 2 and 3 in Table 3-7), and Krieger's viscosities having $\phi = 0.1$, 0.2, and 0.3 were also matched with mixture of water and glycerin (Mixture 4, 5, and 6 in Table 3-7). Since the actual maximum spreading ratio of particle-laden drop is closer to that of Mixture 4, 5, and 6 (Figure 3-4) than Mixture 2 and 3 (Figure 3-5), Re and We are calculated based on Krieger's viscosity in this study. Comparisons on other surfaces are illustrated in Appendix A.

Experiments were conducted to show the effects of particles during various stages of the impacting process: spreading and retracting/rebounding. In addition, the phenomenon of bouncing of a low-speed hydrophilic drop impacting a hydrophilic surface (silicon oxide wafer) was studied. The conducted tests for spreading, rebounding, and bouncing are summarized in Table 3-8, 3-9, and 3-10, respectively.

Table 3-6. Viscosities of particle-laden fluid.

Particle volume fraction, ϕ	Measured viscosity, η	Kreiger's viscosity, η_k
0	2.3	2.3
0.1	3.4	3.0
0.2	7.1	4.2
0.3	20	6.2

Table 3-7. Test conditions and fluid properties.

v (m/s)	Liquid	Volume fraction, ϕ	Viscosity, η (cP)	Re	We	Ca
0.01	Mixture 1[a]	0	2.3	19	0.0084	0.00045
		0.1	3.0	14		0.00058
		0.2	4.2	10		0.0082
	Mixture 2[b]	0	3.4	13	0.0087	0.00066
	Mixture 3[c]	0	7.1	6.5	0.0089	0.0014
	Mixture 4[d]	0	3.0	15	0.0085	0.00058
	Mixture 5[e]	0	4.2	11	0.0087	0.00082
	Mixture 6[f]	0	6.2	7.4	0.0089	0.0012
2	Mixture 1[a]	0	2.3	2700	170	0.064
		0.1	3.0	2000		0.083
		0.2	4.2	1500		0.120
	Mixture 2[b]	0	3.4	1900	180	0.094
	Mixture 3[c]	0	7.1	920	180	0.200
	Mixture 4[d]	0	3.0	2100	170	0.083
	Mixture 5[e]	0	4.2	1500	180	0.12
	Mixture 6[f]	0	6.2	920	180	0.17

[a] Mixture 1: mixture of water/glycerin (77/23).
[b] Mixture 2: mixture of water/glycerin (62/38).
[c] Mixture 3: mixture of water/glycerin (51/49).
[d] Mixture 4: mixture of water/glycerin (70/30).
[e] Mixture 5: mixture of water/glycerin (60/40).
[f] Mixture 6: mixture of water/glycerin (52/48).

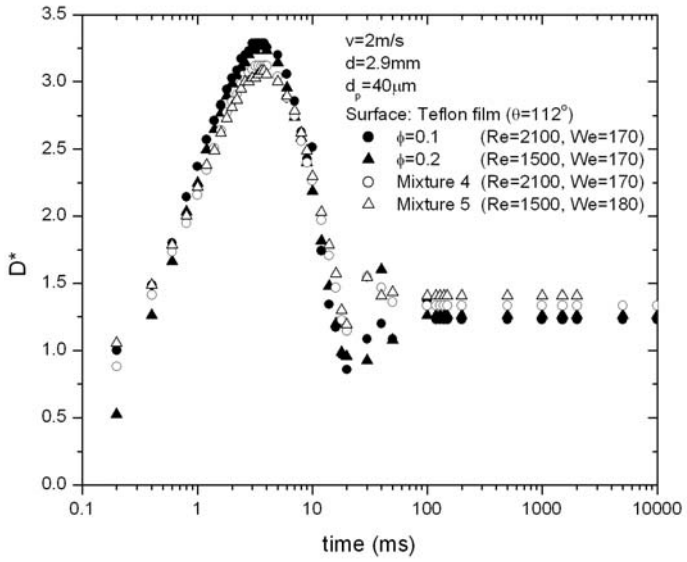

Figure 3-4. Comparison of impact process of particle-laden drop with Mixture 4, 5, and 6. Re of particle-laden drop was calculated based on Krieger's viscosity (Krieger, 1972). Drop impacts on Teflon® film surface at impact speed of 2 m/s.

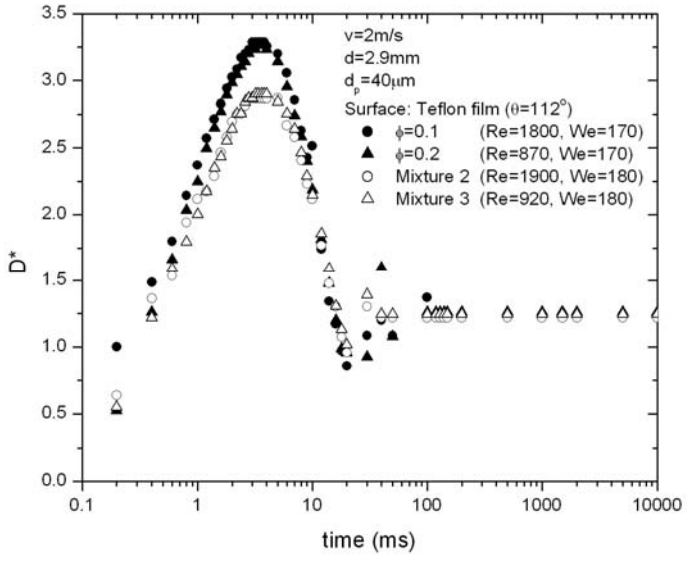

Figure 3-5. Comparison of impact process of particle-laden drop with Mixture 2 and 3. Re of particle-laden drop was calculated based on measured viscosity. Drop impacts on Teflon® film surface at impact speed of 2 m/s.

Table 3-8. Summary of experiments for spreading.

Liquid	d (mm)	d_p (μm)	d_p/d	v (m/s)	ϕ	η (cP)	γ (mN/m)	Re	We	Ca
Mixture 1	0.69	20	0.029	0.3	0	2.3	72	95	0.91	0.0096
					0.1	3.0		73		0.013
					0.2	4.2		52		0.018
				2	0	2.3		640	41	0.064
					0.1	3.0		490		0.083
					0.2	4.2		350		0.12
		40	0.058	0.3	0	2.3		95	0.91	0.0096
					0.1	3.0		73		0.013
					0.2	4.2		52		0.018
				2	0	2.3		640	41	0.064
					0.1	3.0		490		0.083
					0.2	4.2		350		0.12
S1	2.7	0.47	0.00017	0.01	0	1.0	66	38	0.0080	0.00021
					0.15	1.5	62	25	0.0085	0.00034
				2	0	1.0	66	5400	160	0.030
					0.15	1.5	62	3600	170	0.047
Mixture 1	2.9	20	0.0069	0.01	0	2.3	72	19	0.008 4	0.00045
					0.1	3.0		14		0.00058
					0.2	4.2		10		0.00082
				1	0	2.3		1300	43	0.032
					0.1	3.0		1000		0.042
					0.2	4.2		730		0.058
				2	0	2.3		2700	170	0.064
					0.1	3.0		2000		0.083
					0.2	4.2		1500		0.12
		40	0.014	0.01	0	2.3		19	0.0084	0.00045
					0.1	3.0		14		0.00058
					0.2	4.2		10		0.00082
					0.3	6.2		6.9		0.0012
				0.2	0	2.3		2700	170	0.064
					0.1	3.0		2000		0.083
					0.2	4.2		1500		0.12
					0.3	6.2		990		0.17

Table 3-8. (continued).

Liquid	d (mm)	d_p (μm)	d_p/d	v (m/s)	ϕ	η (cP)	γ (mN/m)	Re	We	Ca
Mixture 1	2.9	N/A	N/A	0.01	0	2.3	72	19	0.0084	0.00045
						3.0		15	0.0085	0.0058
						3.4		13	0.0087	0.00066
						4.2		11	0.0087	0.00082
						6.2		7.4	0.0089	0.0012
						7.1		6.4	0.0089	0.0014
				2	0	2.3		2700	170	0.064
						3.0		2000	170	0.083
						3.4		1900	180	0.094
						4.2		1500	180	0.12
						6.2		1100	180	0.17
						7.1		920	180	0.20
M1S100	3.9	6	0.0015	0.01	0	2.3	43	25	0.019	0.00075
					0.1	3.0		19		0.00098
					0.2	4.2		14		0.0014
					0.3	6.2		9.3		0.0020
				2	0	2.3		3600	380	0.11
					0.1	3.0		2800		0.14
					0.2	4.2		2000		0.20
					0.3	6.2		1300		0.29
	4.0	40	0.01	0.01	0	2.3		25	0.019	0.00075
					0.1	3.0		20		0.00098
					0.2	4.2		14		0.0014
					0.3	6.2		9.6		0.0020
				2	0	2.3		3600	380	0.11
					0.1	3.0		2800	390	0.14
					0.2	4.2		2000	390	0.20
					0.3	6.2		1400	390	0.29
	3.4	250	0.074	0.01	0	2.3		25	0.019	0.00075
					0.1	3.0		17	0.016	0.00098
					0.2	4.2		12	0.016	0.0014
					0.3	6.2		8.1	0.016	0.0020
				2	0	2.3		3600	380	0.11
					0.1	3.0		2400	340	0.14
					0.2	4.2		1700	340	0.20
					0.3	6.2		1200	340	0.29

Table 3-9. Summary of experiments for rebounding on hydrophobic surfaces.

Liquid	d (mm)	d_p (μm)	d_p/d	v (m/s)	ϕ	η (cP)	γ (mN/m)	Re	We	Ca
Mixture 1	0.69	20	0.029	2	0	2.3	72	640	41	0.064
					0.1	3.0		490		0.083
					0.2	4.2		350		0.12
		40	0.058	2	0	2.3		640	41	0.064
					0.1	3.0		490		0.083
					0.2	4.2		350		0.12
S1	2.7	0.47	0.00017	2	0	1.0	66	5400	160	0..030
					0.15	1.5	62	3600	170	0.047
Mixture 1	2.9	20	0.0069	2	0	2.3	72	2700	170	0.064
					0.05	2.6		2400		0.072
					0.1	3.0		2000		0.083
					0.15	3.5		1800		0.097
					0.2	4.2		1500		0.12
				2.55	0	2.3		3400	280	0.081
					0.05	2.6		3000		0.092
					0.10	3.0		2600		0.11
					0.15	3.5		2200		0.12
					0.20	4.2		1900		0.15
					0.25	5.0		1600		0.18
					0.30	6.2		1300		0.22
		40	0.014	2	0	2.3		2700	170	0.064
					0.1	3.0		2000		0.083
					0.2	4.2		1500		0.12
					0.3	6.2		990		0.17
				2.55	0	2.3		3400	280	0.081
					0.05	2.6		3000		0.092
					0.10	3.0		2600		0.11
					0.15	3.5		2200		0.12
					0.20	4.2		1900		0.15
					0.25	5.0		1600		0.18
					0.30	6.2		1300		0.22

Table 3-9. (continued).

Liquid	d (mm)	d_p (μm)	d_p/d	v (m/s)	ϕ	η (cP)	γ (mN/m)	Re	We	Ca
Mixture 1	1.98	N/A	N/A	2.55	0	2.3	72	2300	190	0.081
	2.1	N/A	N/A	2.55	0	2.3	72	2500	200	0.081
	2.3	N/A	N/A	2.55	0	2.3	72	2700	220	0.081
Mixture 1	2.9	N/A	N/A	2.55	0	2.3	72	3400	280	0.081
Mixture 4						3.0		2700	280	0.11
Mixture 2						3.4		2400	290	0.12
Mixture 5						4.2		1900	290	0.15
Mixture 6						6.2		1300	290	0.22
Mixture 3						7.1		1200	300	0.25
Distilled water	3.2	N/A	N/A	2.48	0	1	72	7900	270	0.034
				2.35				7500	250	0.033
				2.28				7300	230	0.032
				2.15				6900	210	0.030
				1.80				5800	140	0.025
				1.57				5000	110	0.022
				1.34				4300	80	0.019
				1.07				3400	51	0.015
				0.88				2800	34	0.012
				0.75				2400	25	0.010
				0.42				1300	7.8	0.0058
				0.28				900	3.5	0.0039
M1S100	3.9	6	0.0015	2	0	2.3	43	3600	380	0.11
					0.1	3.0		2800		0.14
					0.2	4.2		2000		0.20
					0.3	6.2		1300		0.29
	4.0	40	0.01	2	0	2.3		3600	380	0.11
					0.1	3.0		2800	390	0.14
					0.2	4.2		2000	390	0.20
					0.3	6.2		1400	390	0.29
	3.4	250	0.074	2	0	2.3		3600	380	0.11
					0.1	3.0		2400	340	0.14
					0.2	4.2		1700	340	0.20
					0.3	6.2		1200	340	0.29

Table 3-10. Summary of experiments for bouncing on silicon oxide wafer.

Liquid	d (mm)	d_p (μm)	d_p/d	v (m/s)	ϕ	η (cP)	γ (mN/m)	Re	We	Ca
Mixture 1	2.9	20	0.0069	0.01	0 0.1 0.2	2.3 3.0 4.2	72	19 14 10	0.0084	0.00045 0.00058 0.00082
Water /surfactant	2.16	N/A	N/A	0.16	0	1	33	350	1.7	0.0048
Glycerin	2.58	N/A	N/A	0.16	0	1490[a]	48.09[b]	0.35	1.7	4.9
Water Mixture 1 Mixture 3	2.9	N/A	N/A	0.08	0	1 2.3 7.1	72	230 110 37	0.26 0.27 0.29	0.0011 0.0025 0.0078
Water	3.2	N/A	N/A	0.01 0.08 0.16 0.18 0.27	0	1	72	32 260 510 580 860	0.0044 0.28 1.1 1.4 3.2	0.00014 0.0011 0.0022 0.0025 0.0038

[a] Viscosity of glycerin taken from a reference (David R. Lide, CMC Handbook of Chemistry and Physics, 71st Edition, CRC Press, Boca Ranton, 1990, p. 6-144).

[b] Surface tension of glycerin taken from a reference (Arthur W. Adamson and Alice P. Gast, Physical Chemistry of Surfaces, 6th Edition, John Wiley & Sons, Inc., New York, 1997, p. 36).

CHAPTER 4

RESULTS AND DISCUSSION

The impaction process was studied over a range of drop sizes for particle-laden drop on smooth substrates; however, for drops smaller than 1 mm, impact speed limitation and clogging problems associated with the drop ejection system used to produce the smaller drops were encountered. Data are available for the smaller pure liquid drops down to 340 μm in diameter and for particle-laden drops with diameters of 560 and 690 μm at particle volumetric concentrations of 0.05 and 0.2, respectively.

The effects of particle volume fraction and particle size on the impact process will be presented first, and then the effects of particles on retraction/rebounding will follow. In addition to the particle effect on impaction process, the effect of drop size will be discussed.

For each test condition, at least three tests were run. Representative plots of D^* versus time are shown in this chapter. Reproducibility of results was generally very good; however, in some cases for low impact speed, the impacting drop did not immediately wet the surface. This occurred infrequently on most of the surfaces except silicon oxide wafer, where bouncing of the drop occurred. Bouncing will be

discussed in a section in this chapter. When bouncing occurs, time in the D^* versus time plots begins when the drop hits the surface and begins to spread.

4.1 Effects of Particle Volume Fraction

4.1.1. Low impact speed

The effect of particle volume fraction on the spreading process depends on impact speed and substrate as illustrated in Figure 4-1. At low impact speed for most cases, particles have little effect on the spreading except for surfaces where the equilibrium contact angle is low. The liquid spreads to the equilibrium spreading ratio with almost no overshoot (spreading beyond the equilibrium value) for the glass slide and silicon oxide wafer, and with a small overshoot for the Teflon® film. This occurred for drop sizes of 2.7, 2.9, 3.4, and 3.9 mm; however, for the 690-μm drop, no overshoot occurred as was observed for the larger drops while overshoot was expected based on Re and We.

In Figure 4-1, spreading ratio, D^*, is plotted as a function of time for drops impacting at speed of about 0.01 m/s on three types of surfaces: glass slide, silicon

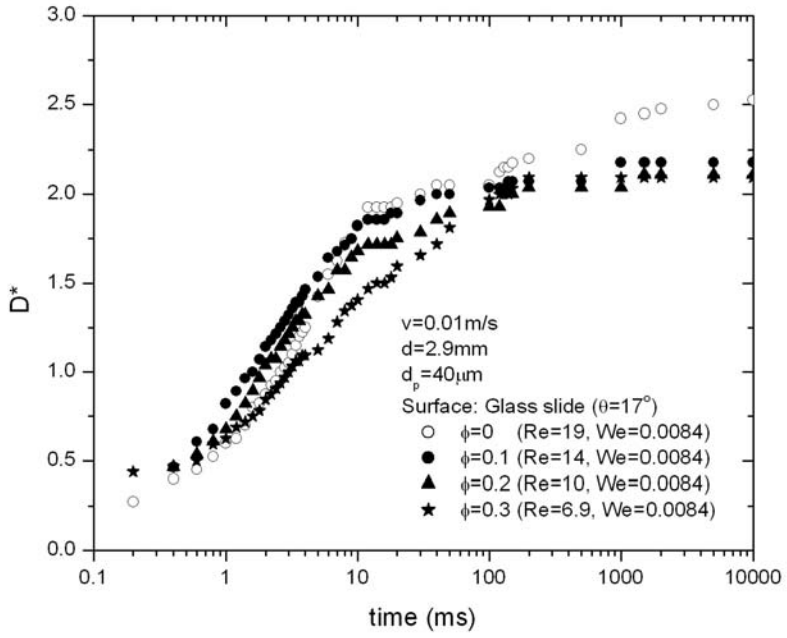

(a) Glass slide

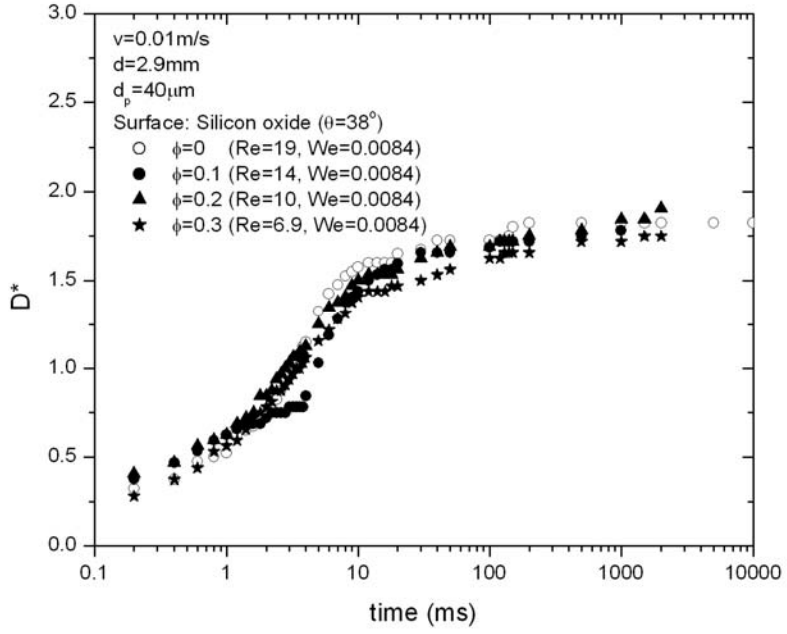

(b) Silicon oxide wafer

Figure 4-1. Impact process of particle-laden fluid. The 40-μm particles are dispersed in Mixture 1, the drop size is 2.9mm, and the impact speed is about 0.01m/s: (a) glass slide, (b) silicon oxide wafer, and (c) Teflon® film.

Figure 4-1. (continued)

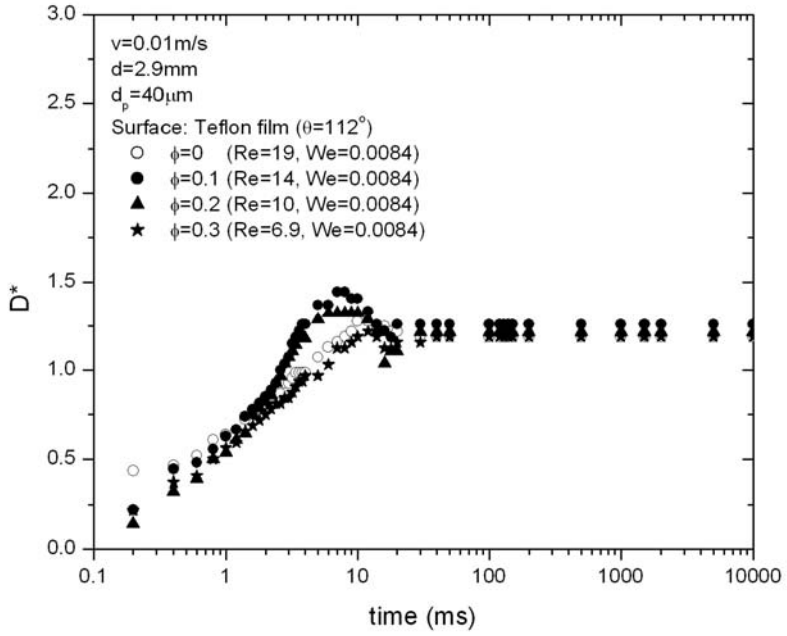

(c) Teflon® film

oxide wafer, and Teflon® film. These results are for 2.9-mm drops containing 40-μm particles, and similar results are obtained for large drops containing 0.47-, 6-, 20-, and 250-μm particles (see Appendix B). The behavior on the glass slide is different from the other two surfaces as can be seen in Figure 4-1 (a). For the glass slide, D^* is similar for the pure liquid and the particle-laden liquid for times up to about 100 ms. It should be noted that as ϕ increases, the drops spreads slower and takes longer to reach D_e^*. This is probably due to increasing viscosity with increasing ϕ. From about 100 to 1000 ms, the pure liquid spontaneously spreads to a value of D_m^* of about 2.5 which is close to the theoretical equilibrium value of 2.6 (Appendix C), based on the measured equilibrium values of θ. However, over time from about 100 to 1000 ms, the particle-laden drops do not spontaneously spread, and D_m^* remains at about 2.2. This is not expected based on the equilibrium contact measurements since measured θ values for the particle-laden liquids are almost identical with those for the pure liquid. The reason for this has not been determined; however, it is conjectured that particles may prevent from further spreading due to pinning on the solid surface.

4.1.2. High impact speed

At a higher impact speed (2 m/s), D_m^* is much larger than for the low impact

speed. Inertial forces dominate at impact, and initial spreading is similar on glass slide, silicon oxide, and Teflon® film, as shown in Figure 4-2. These results are for 40-μm particles, but similar results are obtained for drops having particle sizes of 0.47, 6, 20, and 250 μm. For pure liquid, D_m^* is similar for the three surfaces, but is slightly lower for the Teflon® film ($\theta = 112^o$). Retraction from D_m^* depends greatly on liquid-surface interaction, indicated by the equilibrium contact angles given in Table 3-3.

For the glass slide which has a favorable interaction with the aqueous liquid, and hence a small contact angle, retraction occurs neither for pure nor particle-laden liquid. The theoretical equilibrium value of D^*, based on the measured value of equilibrium contact angle of 17^o is about 2.6 (Appendix C). However, once inertia spreads the liquid over the low contact angle surface, the liquid does not retract due to the strong liquid/surface interaction. For this case, the influence of particles can largely be described by the effective viscosity: as particle volume fraction is increased, viscosity increases, and Re is decreased; as a result, the particle-laden liquid does not spread as far as pure liquid.

As contact angle is increased, both the rate of retraction and the magnitude of retraction increase. The interaction between the surface and the liquid is less favorable and less energy is required to pull the liquid away from the surface.

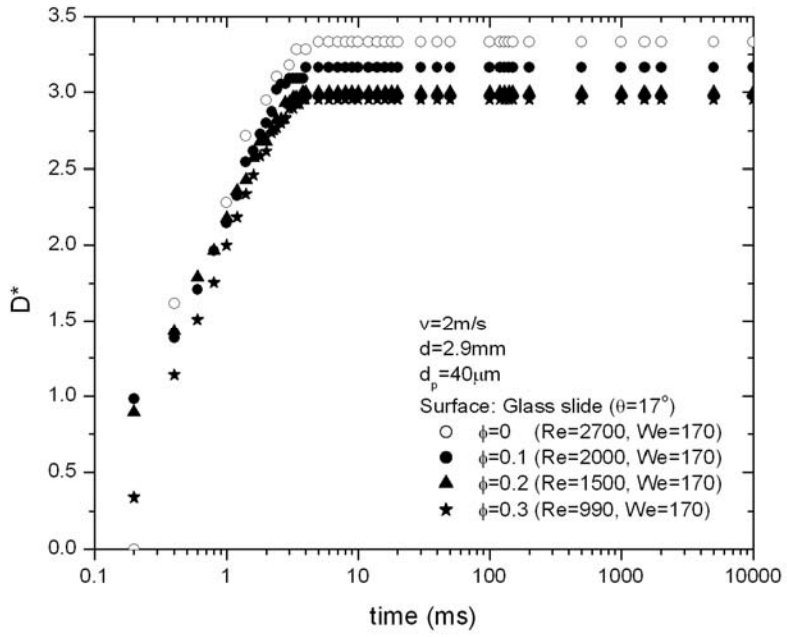

(a) Glass slide

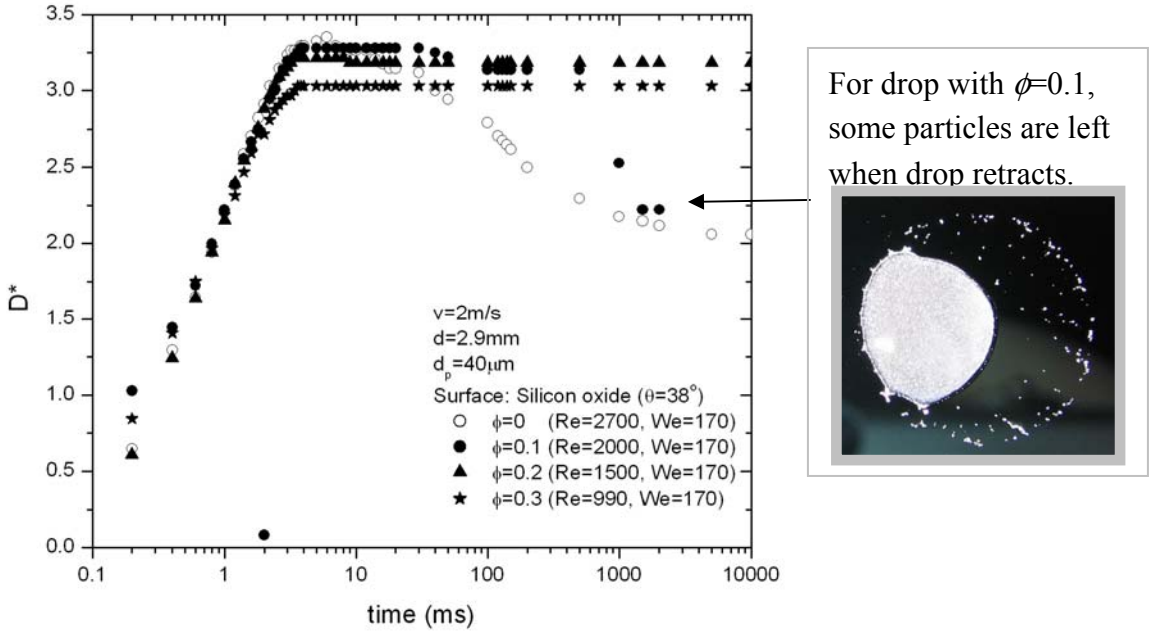

(b) Silicon oxide wafer

Figure 4-2. Impact process of particle-laden fluid. The 40-μm particles are dispersed in Mixture 1, the drop size is 2.9mm, and the impact speed is about 2m/s: (a) glass slide, (b) silicon oxide wafer, and (c) Teflon® film.

Figure 4-2. (continued)

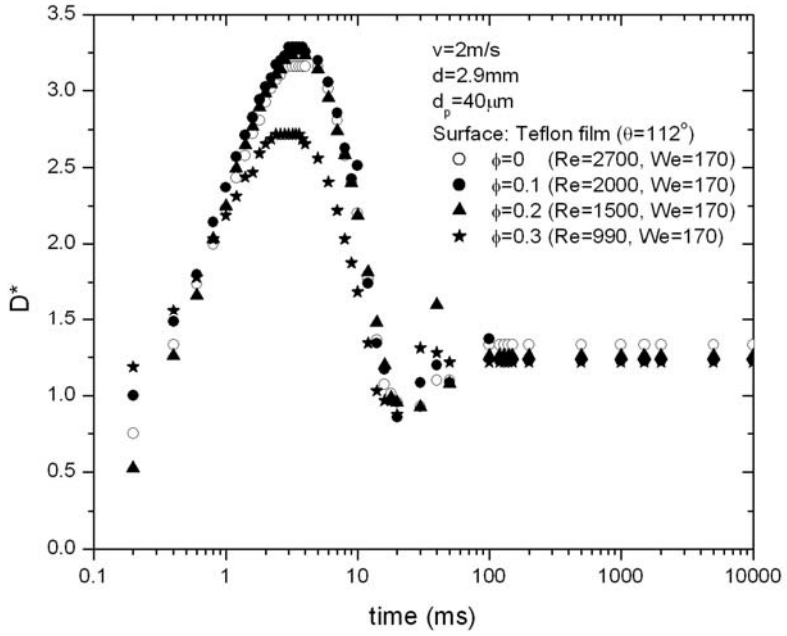

(c) Teflon® film

For the silicon oxide wafer, the pure liquid retracts from D_m^*; however, the equilibrium value of D^* (approximately 2.1) is slightly above the predicted value of 1.95 based on the measured value of equilibrium contact angle of 38°. D_m^* for $\phi = 0.2$ and 0.3 are about 5% and 10% lower than that for pure liquid, respectively. No retraction is observed for the particle-laden drops with $\phi = 0.2$ and 0.3 due to particle pinning on the surface, which prevents liquid retraction. For drop with ϕ = 0.1, retraction is observed; however, the retraction occurs slower than that of pure liquid. The drop with ϕ = 0.1 left particles behind, and the particle traces can be seen in Figure 4-2 (b). This behavior is found for drops having 20- and 40-μm particles with $\phi = 0.1$ and 0.2 impacting on either silicon oxide wafer or silicon wafer at an impact speed of 2 m/s. It is also observed for a drop having 6-μm particles with ϕ = 0.3 impacting on Teflon® film at an impact speed of 2 m/s, but not $\phi = 0.1$ or 0.2. This will be discussed later.

As shown in Figure 4-2 (c), for Teflon® film, 40-μm particles have little effect on spreading ratio for $\phi \leq 0.2$ for an impact speed of 2.0 m/s. Very similar results are found for 20-μm particles when D^* is plotted versus time (see Appendix B). For both particle sizes and an impact speed of 2 m/s, the rebound behavior depends on particle volume fraction. Rebounding was largest for $\phi = 0.15$, but did not occur for $\phi \geq 0.2$ for 20-μm particles. For the 40-μm particles, rebounding did not occur for $\phi \geq 0.15$,

and the degree of rebounding is smaller than 20-μm particles. Rebounding behavior will be discussed in section 4.4.

At an impact speed of 2.55 m/s, the particulate effect on D_m^* is small at $\phi = 0.1$ and 0.2, but increases rapidly when ϕ is increased to 0.25 and then to 0.30, as can be seen in Figure 4-3. This is a consequence of the viscosity increasing nonlinearly with particle volume fraction. Also note that even though the maximum spreading ratios of each particle volume fraction are different, D^* at maximum retraction is almost the same for all ϕ (Figure 4-3 (b) and (c)).

4.2. Effects of Particle Size

The effect of particle size on the impaction process is investigated using 6-, 20-, 40-, and 250-μm particles. Since the surface coatings on the particles are different, two different liquids (M1S100 and Mixture 1) are used. The 6-, 40-, and 250-μm particles are dispersed in M1S100 liquid, and the syringe and needle system is used to form drops. Drop size for drops containing no particles, 6-, 40-, and 250-μm particles are 3.9, 3.9, 4.0, and 3.4 mm, respectively. The effect of particle size for smaller drops is not investigated for M1S100 containing 6-, 40-, and 250-μm particles because the 250-μm particles clogged the pinhole even at low ϕ. Mixture 1 containing

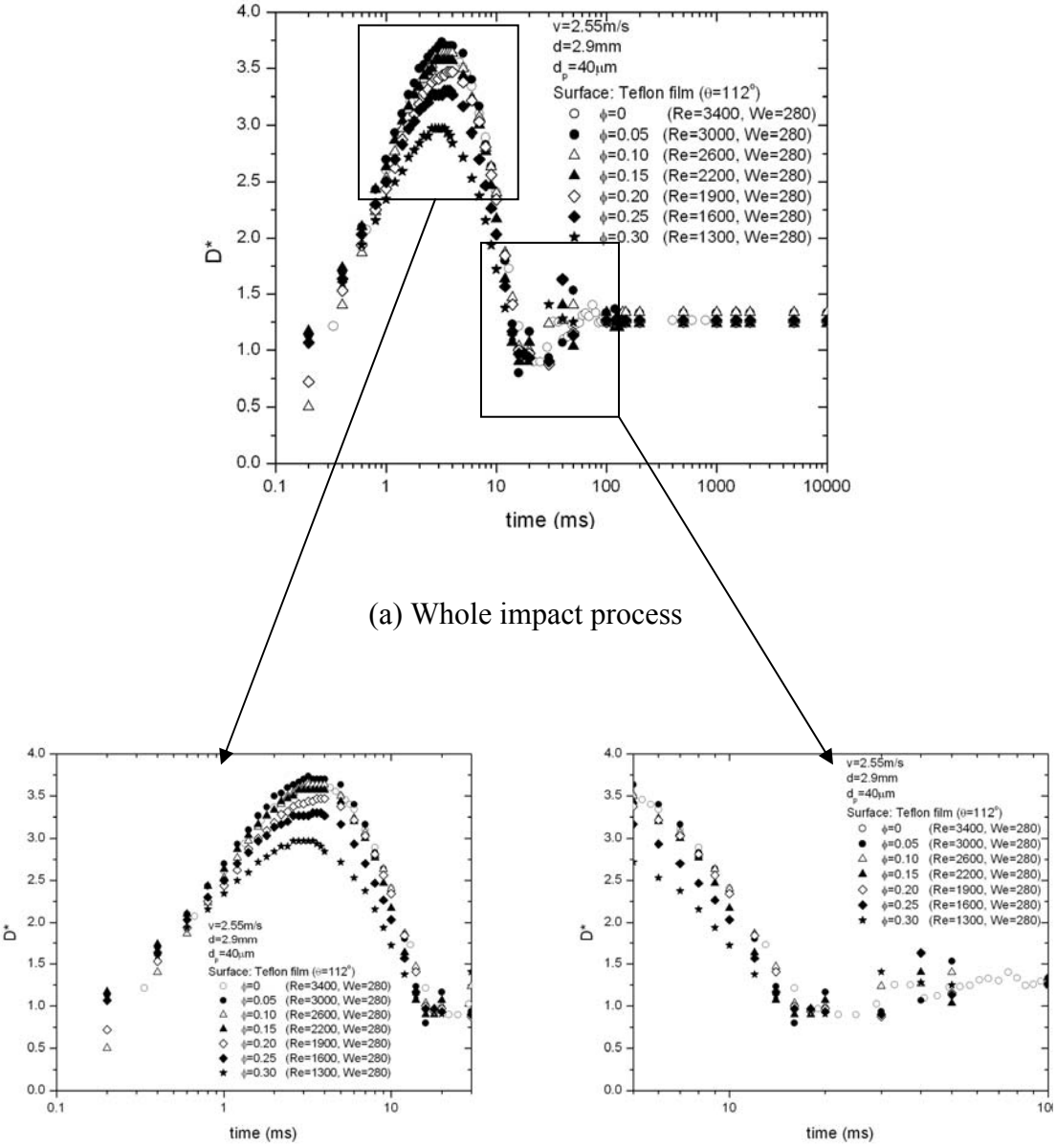

(a) Whole impact process

(b) At D_m^*

(c) At the maximum retraction

Figure 4-3. Impact process of particle-laden fluid. The 40-μm particles were dispersed in Mixture 1, the drop size is 2.9mm, and the impact speed is about 2.55m/s on Teflon® film: (a) whole impact process, (b) at D_m^*, and (c) at the maximum retraction.

either 20- or 40-μm particles was used to study the effect of particle size for two size drops (690 μm and 2.9 mm).

4.2.1 Particles dispersed in M1S100 liquid

Low impact speed

For an impact speed of 0.01 m/s, particle size has little effect on the impact process for ϕ = 0.1 and 0.2 (see Appendix D). The effect of particle size on D^* for a 3.9-mm drop with ϕ = 0.3 impacting at a speed of 0.01 m/s can be seen in Figure 4-4.

On the glass slide, D_m^* of a 250-μm particle-laden drop is lower than that of 6- and 40-μm particles. This is probably due to the 250-μm particles being large relative to the thickness of the spreading drop. Calculation is made to estimate the height (h), referred to below as drop thickness, of the liquid-air interface above the substrate. This allowed calculations of the ratio, h/d_p (see Figure 4-5 and Table 4-1). In estimating h, it was assumed that the shape of the drop at D_m^* can be approximated as a cap of a sphere, which is a good assumption for low impact speeds. The experimentally determined value of D_m^* for a pure liquid drop impacting a given substrate was used to obtain the results shown in Table 4-1. The ratio, h_m/d_p, is the drop thickness at the center of the drop divided by the particle diameter. The ratios

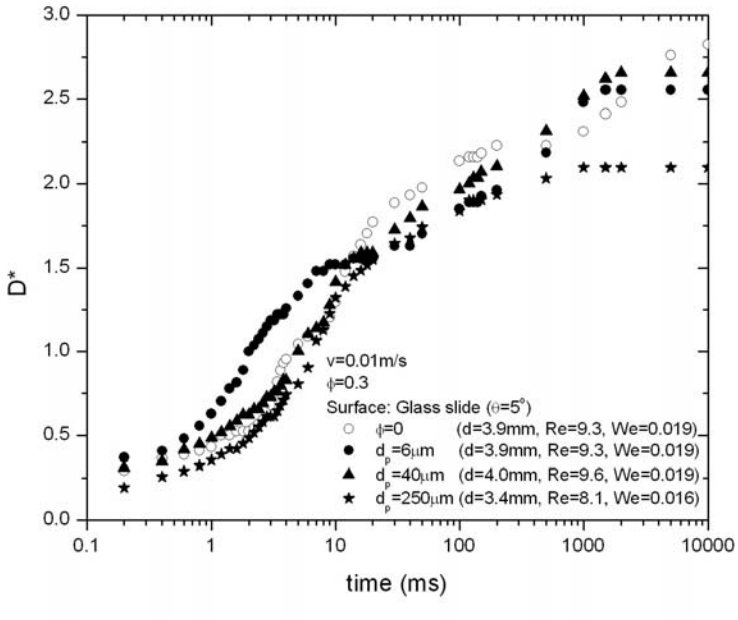

(a) Glass slide

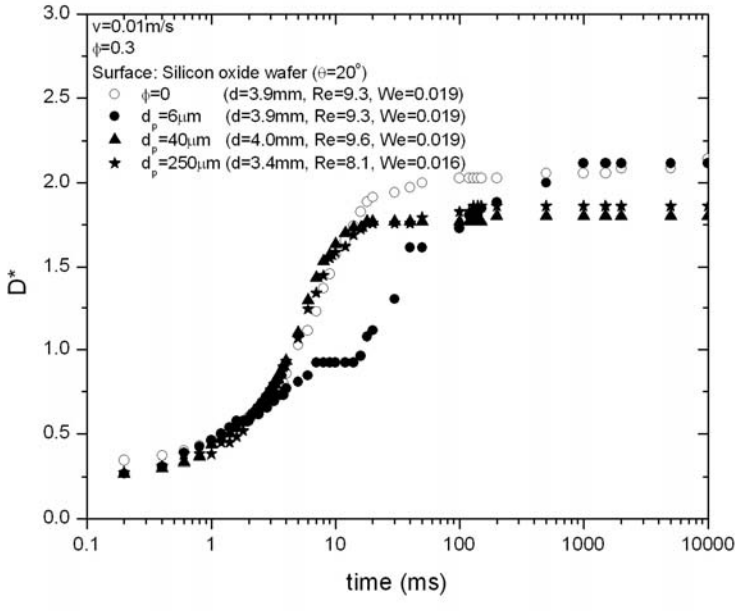

(b) Silicon oxide wafer

Figure 4-4. Effect of particle size on impact. ϕ = 0.3 and the impact speed is about 0.01m/s: (a) glass slide, (b) silicon oxide wafer, and (c) Teflon® film.

Figure 4-4. (continued).

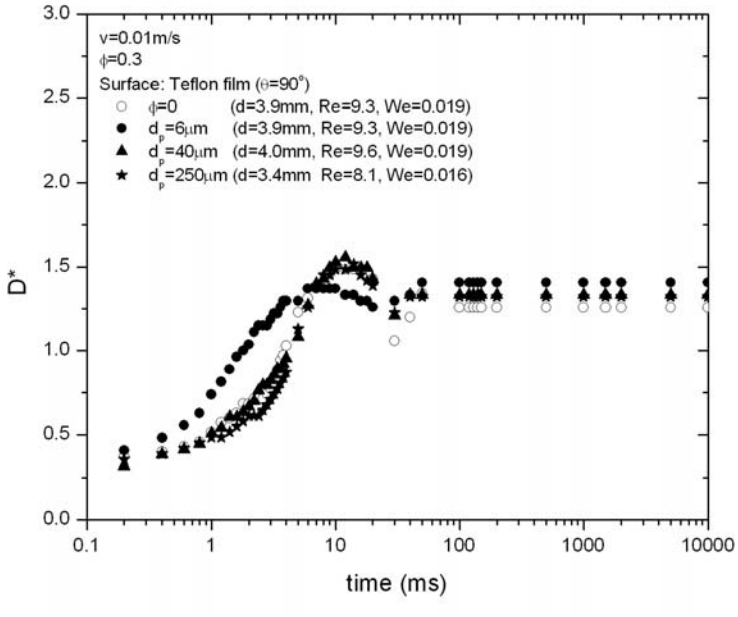

(c) Teflon® film

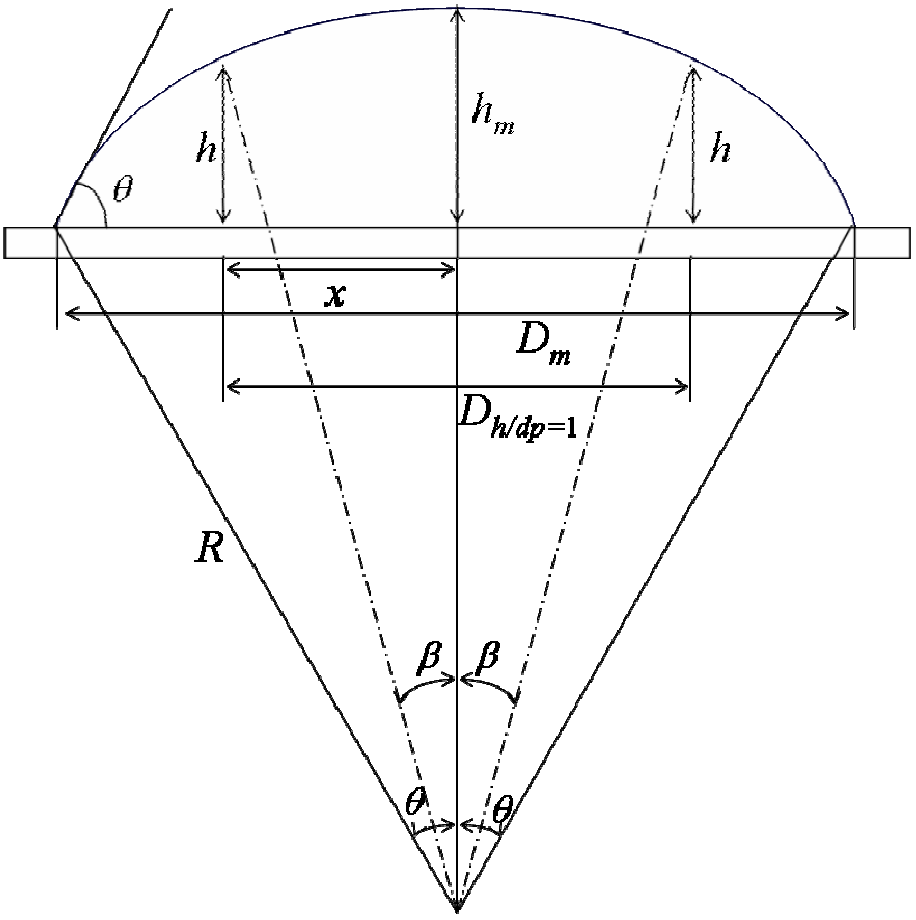

Figure 4-5. Schematics of a drop at D_m^* with contact angle θ. θ was calculated using experimentally measured D_m^* in the equation for a cap of sphere developed by Ford *et al.* (1967).

Table 4-1. Comparison of D^* at $h = d_p$ for each surface and particle size for $\phi = 0.3$.

Surface	Measured D_m^* for pure liquid	θ(°) based on the measured D_m^* for pure liquid	d_p (μm)	$\frac{h_m}{d_p}$	$D^*_{h=d_p}$	Measured D_m^* for $\phi = 0.3$
Glass slide	2.8	14	6	112	2.79	2.56
			40	17	2.72	2.66
			250	2.3	2.12	2.10
Silicon oxide wafer	2.14	30	6	185	2.13	2.12
			40	29	2.10	1.80
			250	3.9	1.86	1.86
Teflon® film	1.48	70	6	334	1.48	1.37
			40	52	1.47	1.56
			250	7.0	1.42	1.52

for a drop on glass are 112, 17, and 2.3 for the 6-, 40-, and 250-μm particles, respectively. Even at the center of the drop the size of the 250-μm particles is large relative to the drop thickness.

Since h decreases with increasing distance (x) from the center until it is zero at the contact line, the ratio, h/d_p, will also decrease with x until it equals to one. For the value of x where $h/d_p = 1$, the drop thickness and particle diameter are equal. Interaction of the particle with the substrate surface and the liquid-air interface would tend to inhibit spreading beyond this point. The dimensionless parameter, $D_{h/dp=1}^* = 2x/d$, is given in Table 4-1. It represents the spreading ratio in pure liquids where the

drop thickness is equal to particle diameter. The values of $D_{h/dp=1}^{*}$ on glass slide are 2.79, 2.72, and 2.12, for the 6-, 40-, and 250-μm particles, respectively. It is interesting that D_m^{*} for the particle-laden drops containing the 40- and 250-μm particles were 2.66 and 2.10, respectively, which are close to the values of $D_{h/dp=1}^{*}$. This suggests that for low impact speed, when the size of the particles approaches the drop thickness, spreading is inhibited. However, for the 6-μm particles, the value of $D_{h/dp=1}^{*}$ is 2.79 while D_m^{*} is only 2.56. The 6-μm particles inhibit spreading even though the particles are relatively small. Similar observations are made for the high impact speed tests in the next section.

For time from 0 to approximately 2 ms, spreading on the silicon oxide wafer was similar for all three drops. For t from 2 to 20 ms, spreading for the drop containing 6-μm particles is much slower than for the other two particle sizes. The drop apparently has contacted the surface, but has not wet it. It is not known why the drop containing 6-μm particles are slow at wetting the silicon oxide wafer, but was repeatedly observed for this case. This will be discussed further in the section on bouncing. For t from 20 ms to about 100 ms, the drop containing 6-μm particles spreads much faster than other two particle sizes, and at t above 100 ms, D_m^{*} is approximately the same for all three sizes. The drop containing 6-μm particles continue spreading until t of about 1,000 ms, but spreading stops at t of about 100 ms

for the other two particles sizes. D_m^* of the drops containing 6-μm particles was larger than that of the other drops.

In contrast to behavior on the hydrophilic surface, the drop containing 6-μm particles impacts Teflon® film, it spread faster than the drops containing the bigger particles. Although the drop containing 6-μm particles spread faster, the D_m^* was lower than for the drops containing larger particles.

High impact speed

The effect of particle size is small for the impact speed of 2 m/s and for $\phi = 0.1$ and 0.2 (see Appendix D) except for the retraction behavior on silicon wafer. Retraction on silicon wafer for $\phi = 0.1$ and 0.2 will be discussed in the section 4.4. Figure 4-6 shows the effect of particle size on D^* for $\phi = 0.3$ and an impact speed of 2 m/s. Particle-laden drops with $\phi = 0.3$ do not retract on the glass slide or silicon oxide wafer while retraction occurs on the Teflon® film.

On the Teflon® film, the drop containing $d_p = 40$ μm retracts beyond its equilibrium spreading ratio; however, drops with other particle sizes retract directly to the equilibrium state. While retracting, the drop having 6-μm particles leaves particles behind as shown in Figure 4-6 (c). The trace of particles on Teflon® film was not seen at lower concentration or for other particle sizes, which indicates that the particles are

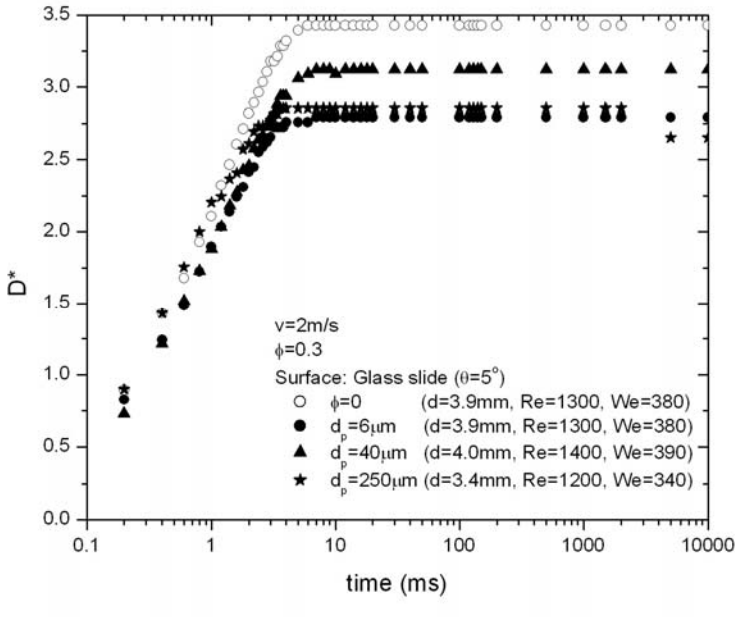

(a) Glass slide

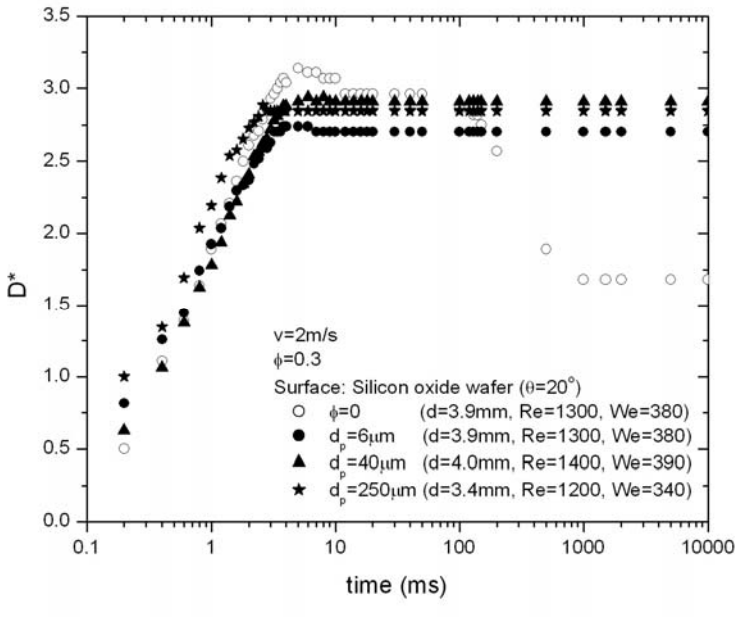

(b) Silicon oxide wafer

Figure 4-6. Effect of particle size on impact process for $\phi = 0.3$ and $v = 2$ m/s: (a) glass slide, (b) silicon oxide wafer, and (c) Teflon® film.

Figure 4-6. (continued).

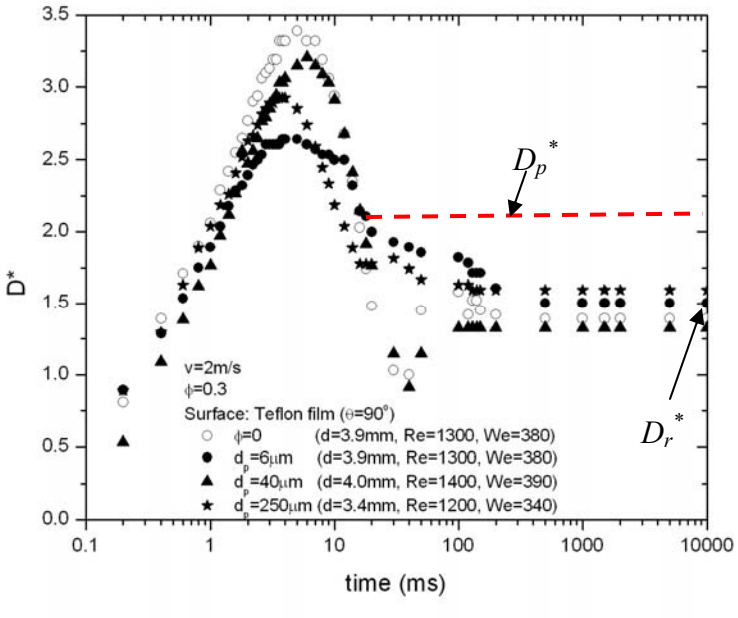

For drop having d_p=6 μm with ϕ=0.3, some particles are left when drop retracts.

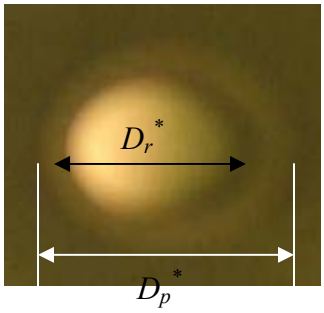

(c) Teflon® film

in contact with the surface at high ϕ. The test was repeated 10 times to confirm the results.

For all surfaces, D_m^* is largest for d_p = 40 μm, second largest for d_p = 250 μm, and smallest for d_p = 6 μm; however, the difference in D_m^* for the glass slide and silicon oxide wafer is small. For impaction on the Teflon® film, D_m^* of drops containing 6-μm, 40-μm, and 250-μm are about 2.64, 3.20, and 2.93, respectively.

4.2.2 Particles dispersed in Mixture 1

The effect of particle size on the impaction process was investigated using 20- and 40-μm particles dispersed in Mixture 1. There are two drop sizes: 690-μm drop produced using piezo engine system and 2.9-mm drop produced using syringe and needle system.

690-μm drop

For the 690-μm drops, two impact speeds (0.3m/s and 2 m/s) and three surfaces (glass slide, silicon oxide wafer, and fluorocarbon plasma treated silicon wafer) were used. The results for v = 0.3 m/s are shown in Figure 4-7. The drops spread to the equilibrium spreading ratio with almost no overshoot for all surfaces. For glass slide

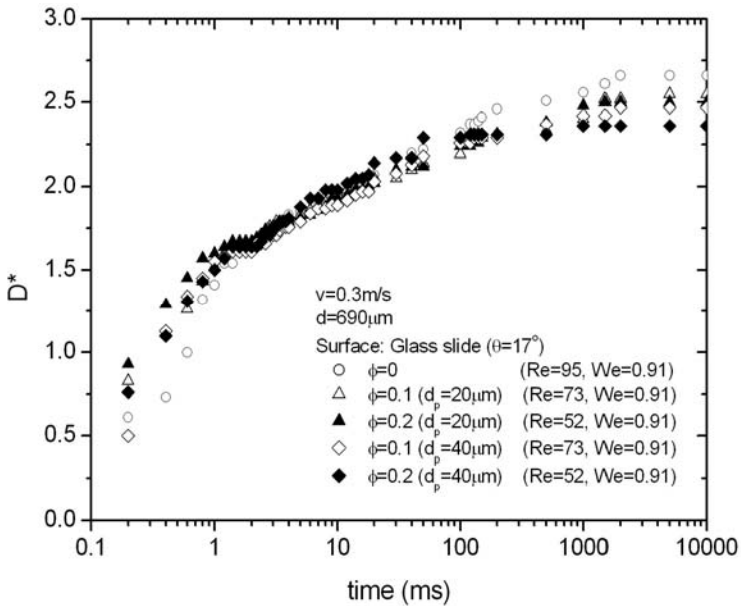

(a) Glass slide

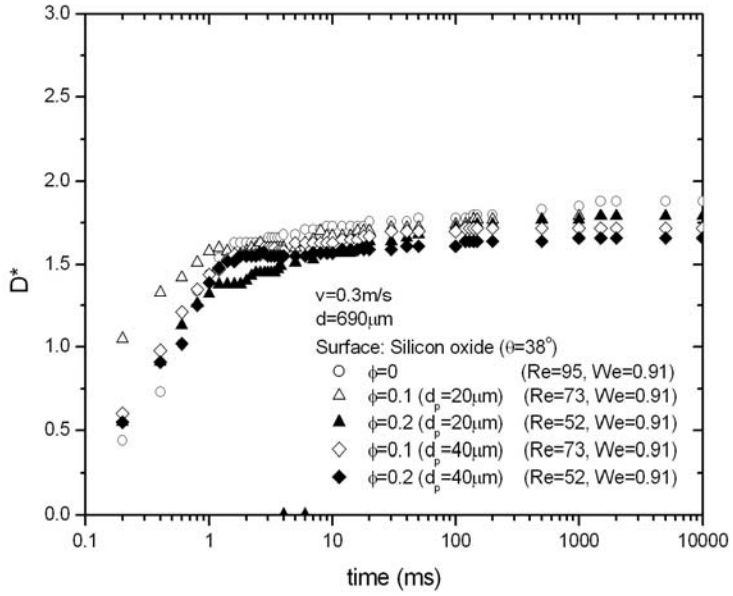

(b) Silicon oxide wafer

Figure 4-7. Impact process of particle-laden fluid. The particles were dispersed in Mixture 1, the drop size is 690 μm, and the impact speed is about 0.3 m/s: (a) glass slide, (b) silicon oxide wafer, and (c) fluorocarbon plasma treated silicon wafer.

Figure 4-7. (continued).

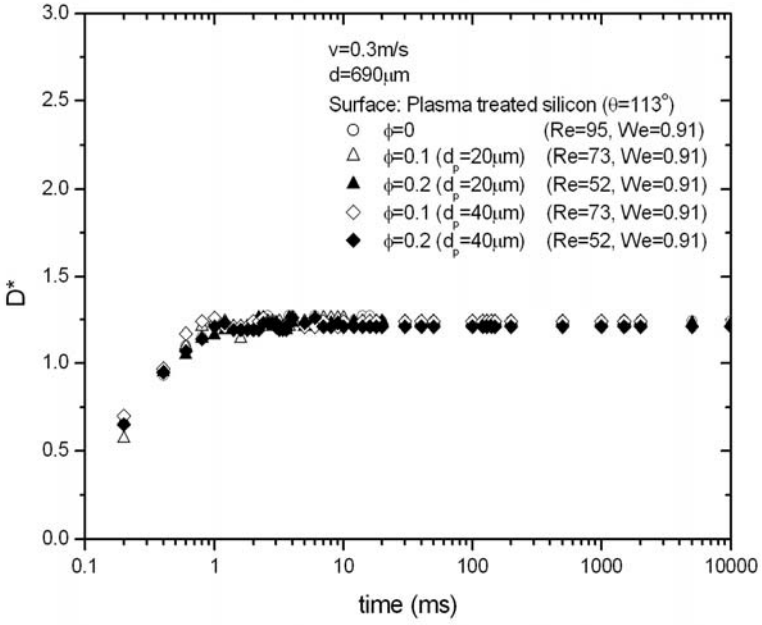

(c) Fluorocarbon plasma treated silicon wafer

and silicon oxide wafer surfaces, D_m^* of drops containing 40-μm particles is little lower than that of drops having 20-μm particles; however, the difference is small.

The maximum spread ratio, D_m^*, is greatest for the glass slide surface because the liquid-surface interactions are strongest. The pure liquid spread a little further than the particle-laden liquid; however, varying particle fraction from 0 to 0.2 has little effect on the impact process.

When 690-μm drops containing 20- and 40-μm particles impact on surfaces at an impact speed of 2 m/s, there is little effect associated with particle size, as illustrated in Figure 4-8.

2.9-mm drop

For the 2.9-mm drops, two impact speeds (0.01 m/s and 2 m/s) and four types of surfaces (glass slide, silicon oxide wafer, silicon wafer and Teflon® film wafer) were used. There is little effect associated with particle size (see Appendix B).

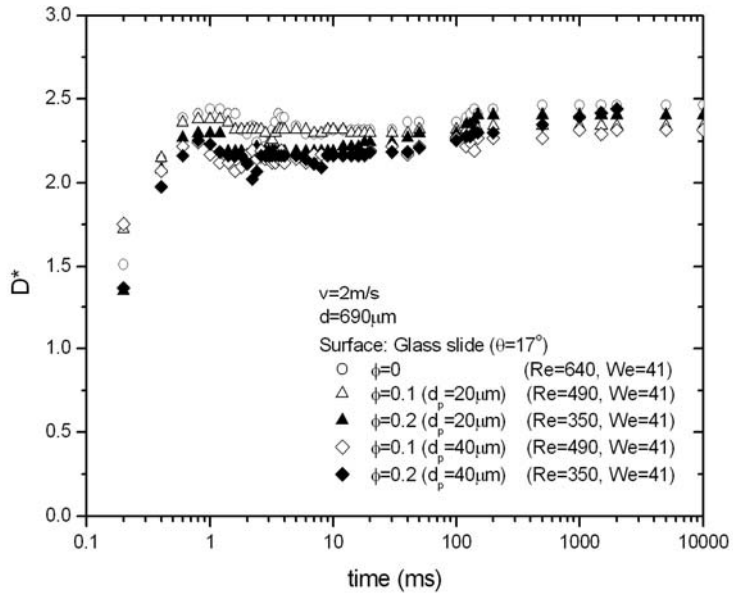

(a) Glass slide

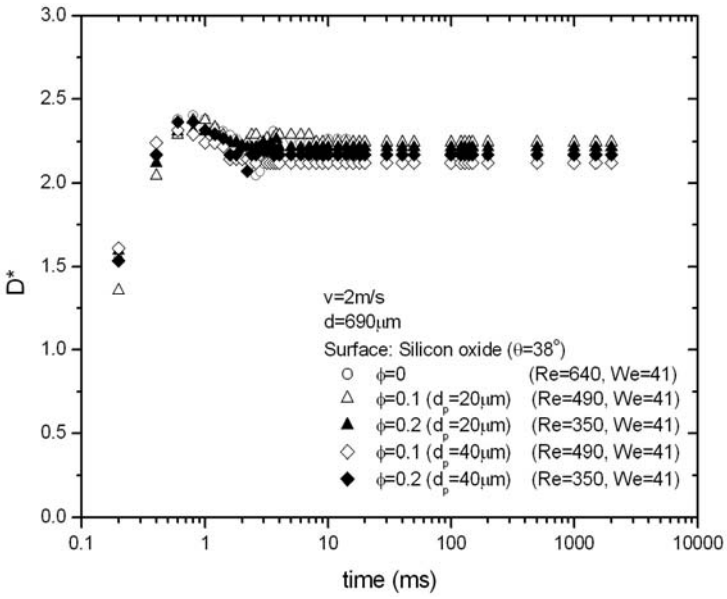

(b) Silicon oxide wafer

Figure 4-8. Impact process of particle-laden fluid. The particles were dispersed in Mixture 1, the drop size is 690 μm, and the impact speed is about 2 m/s: (a) glass slide, (b) silicon oxide wafer, and (c) fluorocarbon plasma treated silicon wafer.

Figure 4-8. (continued)

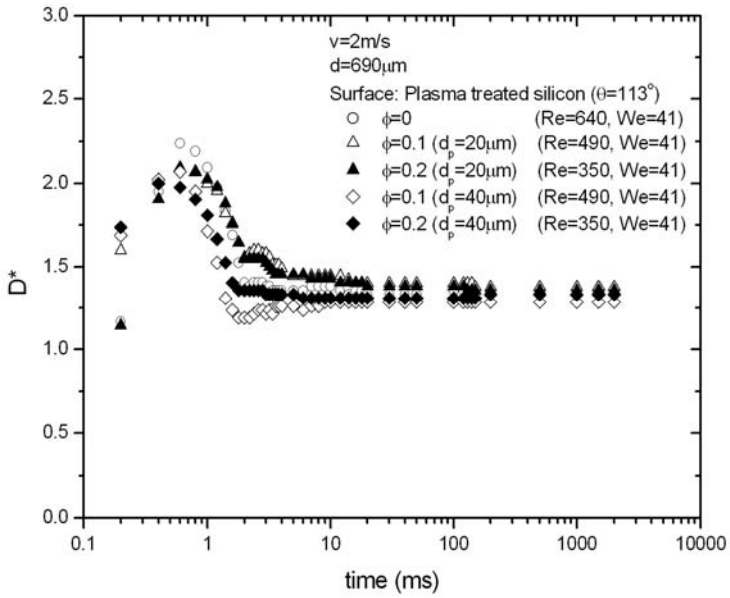

(b) Fluorocarbon plasma treated silicon wafer

4.3 Retraction and Rebounding

When a drop impacts on a surface where the equilibrium contact angle is greater than zero, it spreads over the surface until it reaches a maximum spreading diameter, D_m^*, where the surface energy of the drop is at a maximum while its kinetic energy is nearly zero. In some cases, at the maximum spreading state, the liquid flow changes its direction and recoils inward due to surface energy.

For pure liquids, the amount of retraction has been shown to depend on the following dimensionless numbers: Re, We and cos θ. These parameters include the effects of initial kinetic energy of the impacting drop, the surface energy of the liquid, viscous dissipation in the spreading liquid, and the interaction between the liquid and the surface. When liquid/surface interaction is strong and/or the impact speed is low, the liquid will retract to the equilibrium position and stop. If liquid/surface interaction is weak and a drop has high kinetic energy, the liquid will retract beyond the equilibrium position and rise in the region of the initial impact. Under appropriate conditions, rebounding will occur where the liquid separates from the surface, rises a short distance and returns to the surface (Mao *et al.*, 1996).

A study was conducted to determine how particles affect retraction and rebounding. For particle-laden liquids, the amount of retraction may be affected by

particle parameters such as the particle volume fraction, ϕ, and ratio of particle diameter to drop diameter, d_p/d.

4.3.1 Low impact speed

As discussed in earlier sections, particles did not have much effect on the spreading of an impacting drop. In most cases, the drops spread to the equilibrium spreading ratio without retraction.

4.3.2 Retraction at a high impact speed

Retraction on glass slide

At high impact speed, no retraction was observed on the glass slide for both pure and particle-laden liquids. Since the equilibrium contact angles of the pure liquids with glass slide are low, the interaction of the liquids with the glass slide is high and prevents retraction.

Retraction on silicon oxide wafer

The behavior of the particle-laden liquids on the silicon oxide wafer is quite

different from that of the pure liquids. The particle-laden liquid spreads to D_m^* similar to the pure liquid, but retracts very little for the higher values of ϕ. This is illustrated in Figure 4-9, where D^* is plotted versus time for MS100 containing 6-, 40- and 250-μm particles. The pure liquid drop retracts to an equilibrium spreading ratios, D_e^*, of about 1.75 from D_m^* of about 3.25. The retraction for drops with ϕ = 0.1 was different for the three particle sizes. For the drops containing the 6- and 250-μm particles retraction was small, but the drop containing the 40-μm particles retracts from D_m^* of about 3.25 to about 2.0. It should be noted that the tests using 20- and 40-μm particles in Mixture 1, similar results to that for the 40-μm particles in MS100 were observed. At ϕ = 0.2 and 0.3, little retraction occurred for all three particle sizes. Similar results were obtained in the tests using 20- and 40-μm particles in Mixture 1.

Retraction from the contact line is probably related to both the number of particles in the drop, n, and the ratio of drop thickness to particle size at maximum spreading, h_m/d_p. The effects of changing d_p/d and ϕ on n are shown in Table 4-2. The table also shows h_m/d_p, based on the assumption that the drop shape can be approximated by a circular cylinder of diameter D_m and height h_m (D_m for a pure liquid is used in the calculation) at the maximum spreading. These calculations are useful in attempting to explain the effect of particles on the impact process. When a drop impacts on the silicon oxide wafer, the drop does retracts for the pure liquid and ϕ =

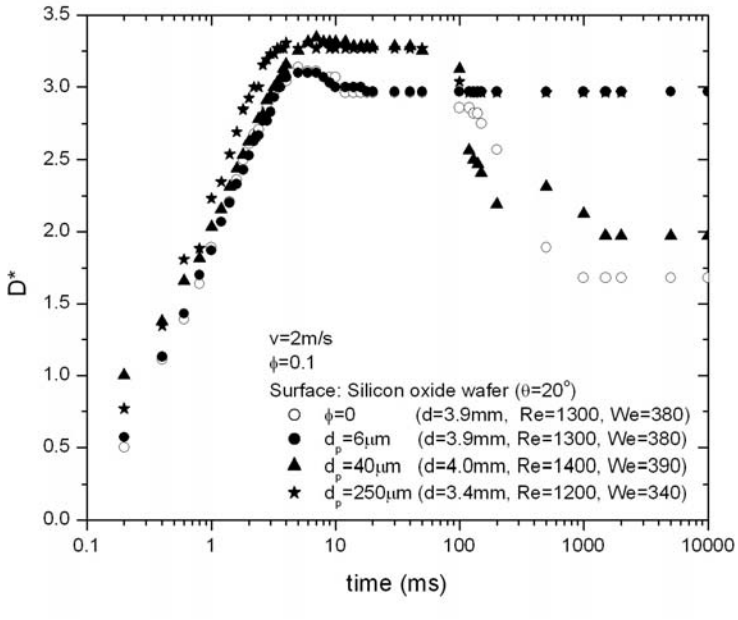

(a) $\phi = 0.1$

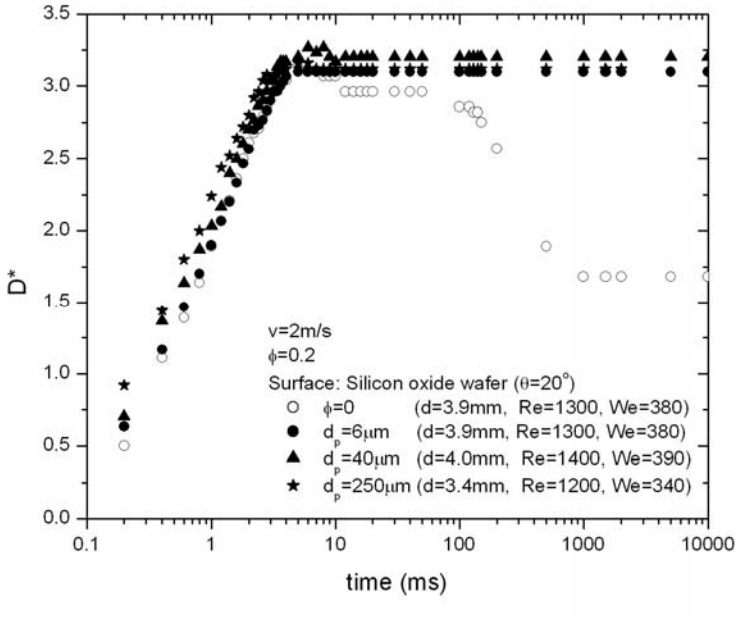

(b) $\phi = 0.2$

Figure 4-9. Effect of particle size on retraction on the silicon oxide wafer. The 6-, 40-, and 250- μm particles are dispersed in M1S100 liquid: (a) $\phi = 0.1$, (b) $\phi = 0.2$, and (c) $\phi = 0.3$.

Figure 4-9. (continued).

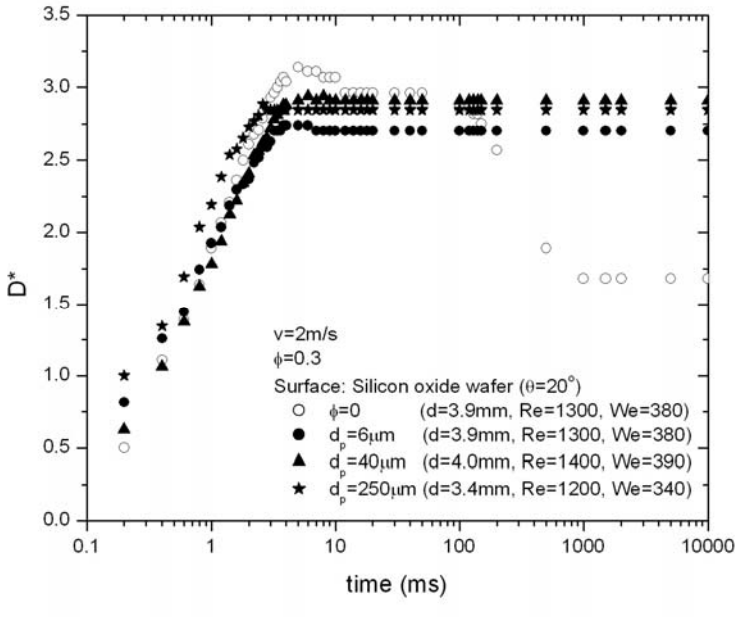

(c) $\phi = 0.3$

Table 4-2. The number of particles per drop and h_m/d_p as a function of d_p/d.

d_p (μm)	d (mm)	d_p/d	ϕ	n, Total number of particles per drop	h_m/d_p
6	3.9	0.0015	0.1 0.2 0.3	27,462,500 54,925,000 82,387,500	37
40	4.0	0.01	0.1 0.2 0.3	100,000 200,000 300,000	7
250	3.4	0.074	0.1 0.2 0.3	252 503 755	0.8

0.1 of 40-μm particles, but does not retract for the other cases. For the 6-μm particles, there is a large number of particles, even for $\phi = 0.1$, close to the contact line at D_m^*. It can be conjectured that the large number of 6-μm particles pins the contact line and prevents retraction. For the drop containing 250-μm particles, h_m/d_p is about 0.8 which indicates that the particle size is bigger than the thickness of the drop and the particles are in contact with the surface. The interaction of these large particles with the surface presents an energy barrier being large for the liquid surface tension to overcome.

For the drop containing 40-um particles, the drop with $\phi = 0.1$ retracts, but not drops with $\phi = 0.2$ and 0.3. It is not clear why the drop containing 40-μm particles

retracts for $\phi = 0.1$; however, since no retraction occurs for $\phi = 0.2$ and 0.3, it may be related to the number of particles (N) at the contact line. For $\phi = 0.2$ and 0.3, N may be sufficient to pin the contact line; in contrast, for $\phi = 0.1$, N may be insufficient to stop retraction of the contact line.

When pure liquid drops retract from D_m^*, the retraction appears to be symmetric around the point of impaction. In contrast, sometimes retraction of the particle-laden drop is asymmetric, drop shape on the surface is not cylindrical and particle distribution appears to be non-uniform, as illustrated in Figure 4-10. In the case of particle size of 6-μm, the retraction is small for values of ϕ of 0.1, 0.2 and 0.3, and appears to be symmetric. With the 40-μm particles, the retraction for values of ϕ of 0.1 and 0.2 is asymmetric. When $\phi = 0.1$, the contact line on one edge (nine-o'clock position) of the drop appears to be pinned, but the contact line along the rest of the rim of the drop is not and retracts toward the nine-o'clock position. When the liquid retracts, particles are left on the surface, particularly around the rim of the drop at the maximum spreading position. When $\phi = 0.2$ for particle-laden liquid containing the 40-μm particles, the contact line appears to be pinned on two edges (three-o'clock and nine-o'clock positions), but the contact line along the rest of the rim of the drop is not and retracts toward the center.

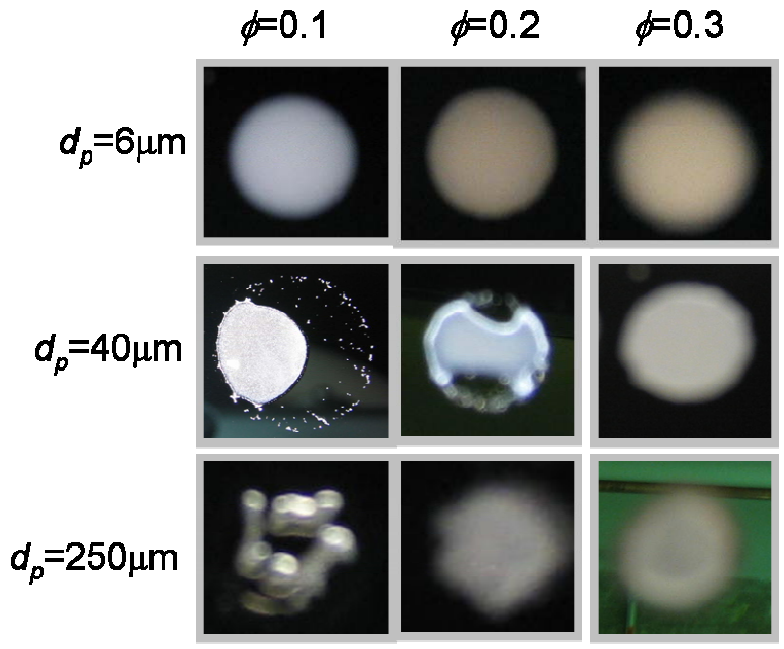

(a) Top view

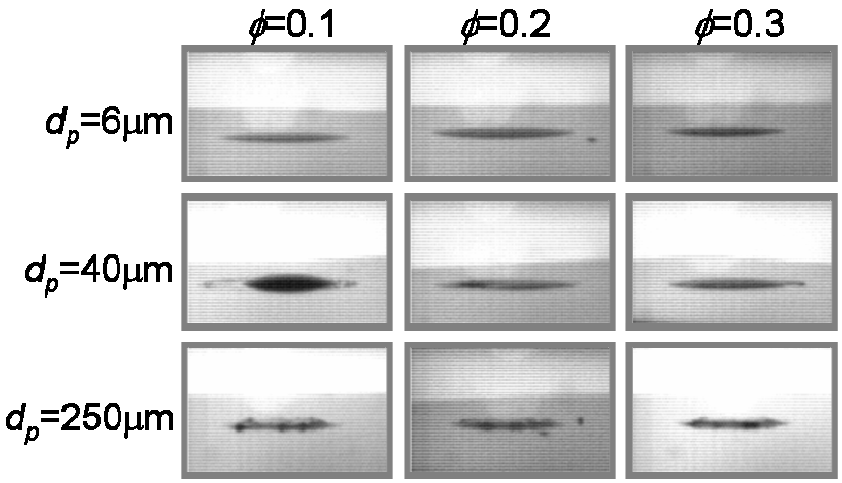

(b) Side view

Figure 4-10. Top and side views of drops resting on silicon oxide wafer. The 6-, 40-, and 250-μm particles are dispersed in M1S100: (a) Top view and (b) side view.

For the particle-laden liquid containing the 250-μm particles for all three values of ϕ, drop shape on the surface is not cylindrical and particle distribution appears to be non-uniform. Particle distribution appears to be highly non-uniform when $\phi = 0.1$.

Retraction on Teflon® film

Since the liquids used in the tests are hydrophilic, all drops with and without particles impacting Teflon® film retract after spreading to D_m^*. The retraction process depends on ϕ and particle size, as illustrated in Figures 4-11 and 4-12. Comparison of (a) – (c) in Figure 4-12 reveals that 40-μm particles have a much smaller effect on the retraction process than either the 6- or 250-um particles. For ϕ = 0.1 and 0.2, drops with 6-μm particles retract beyond the equilibrium position (D_e^*); however, for $\phi = 0.3$, the drop retracts directly to D_e^* leaving particles on the surface, as shown in Figure 4-12 (a). The 40-μm particles affect the spreading process much less, and drops containing these particles retract beyond D_e^* for all three values of ϕ. The 250-μm particles significantly affect the retraction process, and drops containing these particles do not retract beyond D_e^* even for $\phi = 0.1$.

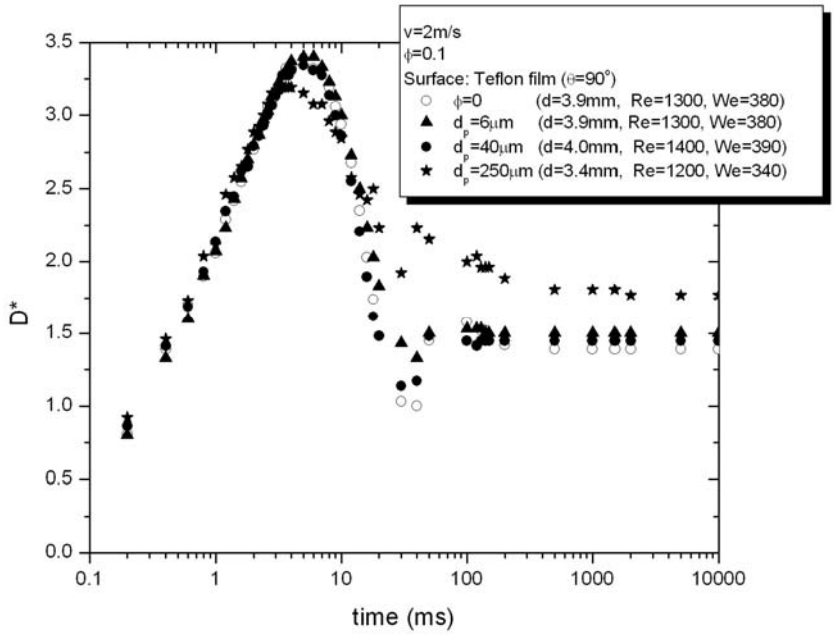

(a) $\phi = 0.1$

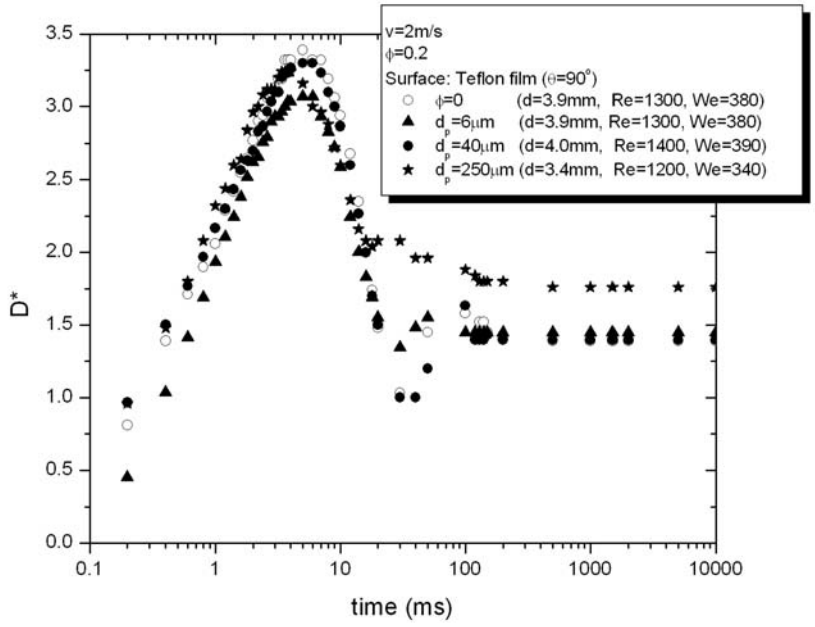

(b) $\phi = 0.2$

Figure 4-11. Effect of particle size on retraction on the Teflon® film. The 6-, 40-, and 250-μm particles are dispersed in M1S100: (a) $\phi = 0.1$, (b) $\phi = 0.2$, and $\phi = 0.3$.

Figure 4-11. (continued)

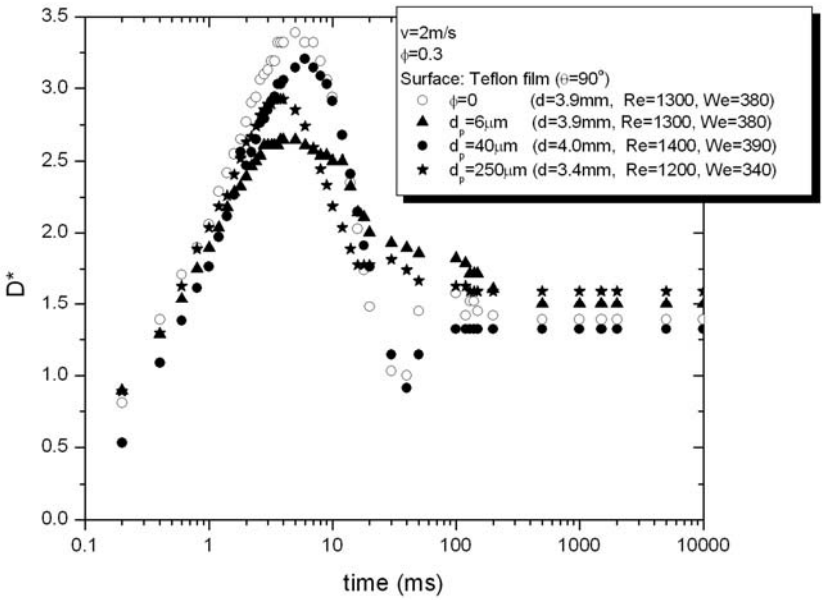

(c) $\phi = 0.3$

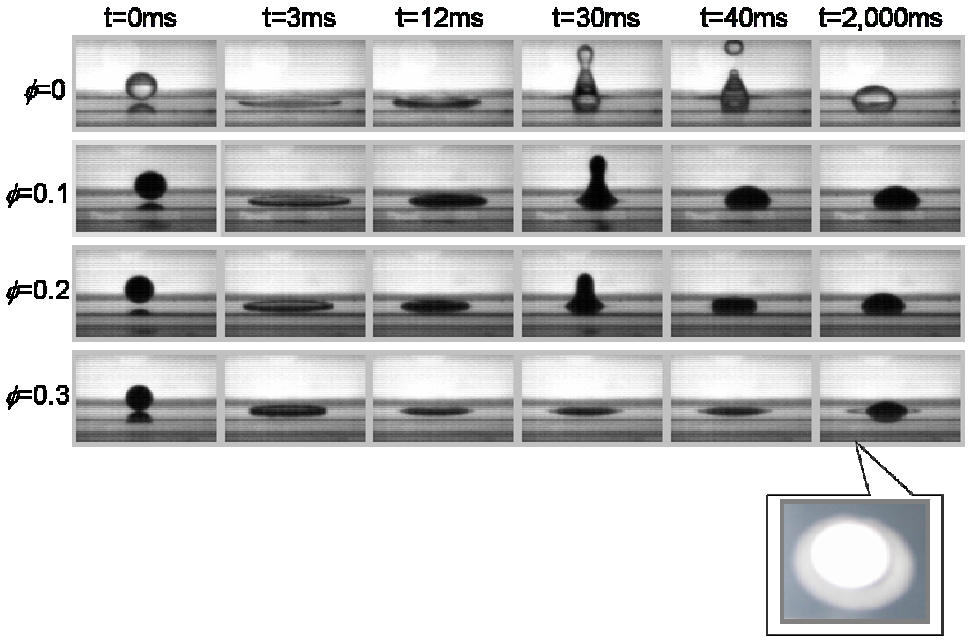

(a) 6-μm particles (d = 3.9 mm)

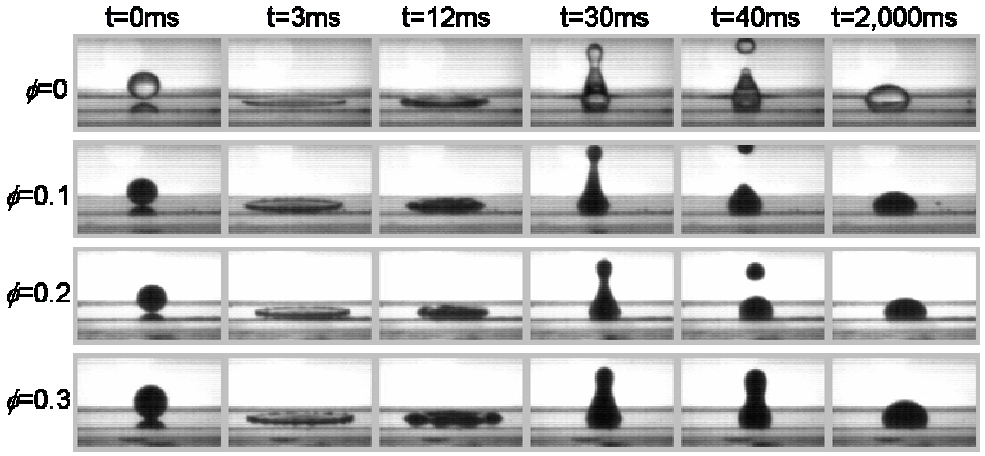

(b) 40-μm particles (d = 4.0 mm)

Figure 4-12. Photograph of particle-laden drops (M1S100) impacting Teflon® film at impact speed of 2 m/s: (a) 6-μm particles, (b) 40-μm particles, and (c) 250-μm particles

Figure 4-12. (continued).

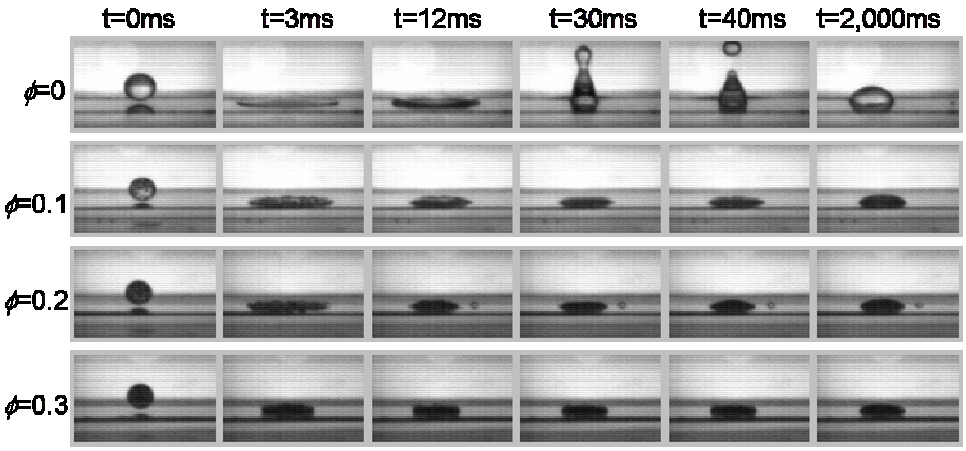

(c) 250-μm particles (d = 3.4 mm)

The reason that the 40-μm particles affect retraction much less than the 6- and 250-μm particles is not known, but believed to be associated with the surface tension being higher for the liquid containing the 40-μm particles than for the other particle-laden liquids (see Table 4-3). The higher surface tension of the liquid containing the 40-μm particles is believed to be due to the coating on the particles. As discussed in Chapter 3, the manufacturers of the 20- and 40-μm particles deposited coatings on the particles which allowed them to be dispersed easily into Mixture 1. Retraction for drops containing 20-μm and 40-μm particles in Mixture 1 is similar for ϕ = 0.1, 0.2, and 0.3. On the other hand, 6- and 250-μm particles were not coated by the manufacturers and would not disperse in Mixture 1; thus, surfactant was added to Mixture 1 to produce M1S100 so that suspensions of these particles could be made. M1S100 was also used with the 40-μm particles.

4.3.3 Rebounding at high impact speed

As pointed out in the previous section, for impaction on Teflon® film, all drops used in this study retract after spreading to D_m^*. This occurs because the liquid/surface interaction is weak. Depending on several factors, the retracting drop sometimes rebounds. Rebounding occurs when the drop reaches maximum retraction,

Table 4-3. Surface tension of M1S100 with and without particles.

d_p (μm)	ϕ	γ (dyne/cm)
M1S100 without particles	0	43
6	0.1	45
	0.2	52
	0.3	66
40	0.1	58
	0.2	68
	0.3	70
250	0.1	45
	0.2	46
	0.3	47

stretches up, necks and generates a secondary drop that moves vertically upward. In some cases, the upward stretching drop necks more than once, producing a series of secondary drops. The D^* versus t does not reveal that rebounding is occurring. For example, Figure 4-13 shows that the drops containing 20-μm particles impacting at a speed of 2 m/s on Teflon® film retract beyond the equilibrium position and then spread to the equilibrium position; however, this figure does not revealed that the drop rebounds from the surface. To better show the variation of D^* versus time, the data are plotted using a linear time scale in Figure 4-14. There appear to be regions (flat) where D^* stays relatively a constant for certain time, and then regions (curved) where

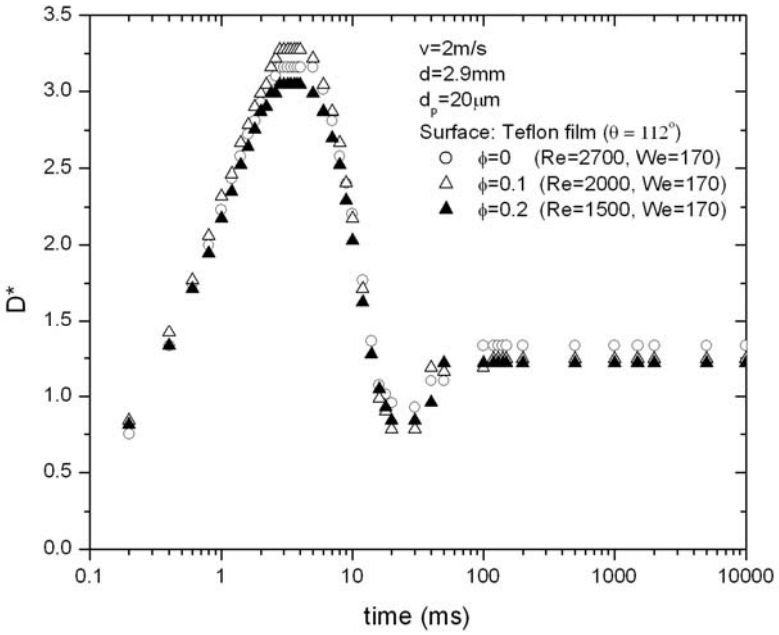

Figure 4-13. Impact process of 2.9-mm drop having 20-μm particles impacting on Teflon® film at v = 2 m/s.

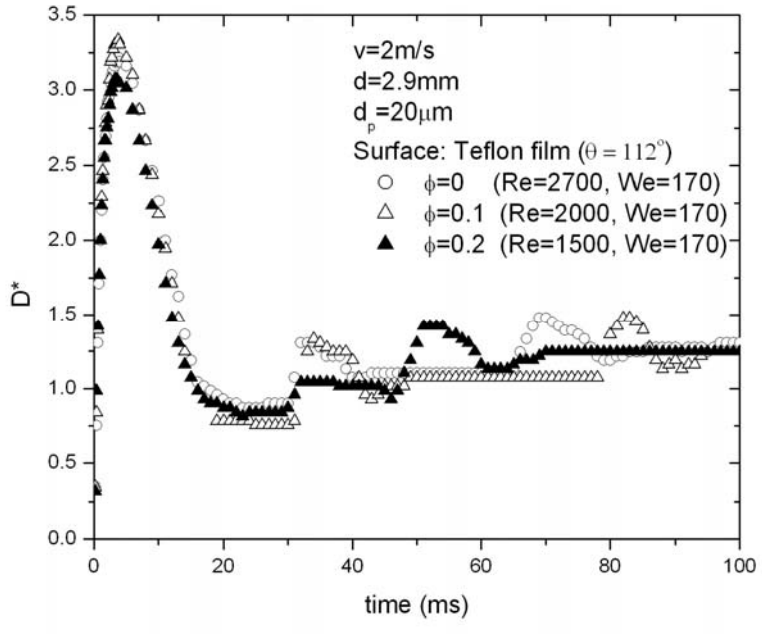

Figure 4-14. Impact process of 2.9-mm drop having 20-μm particles impacting on Teflon® film at v = 2 m/s in linear scale.

D^* changes. The locations of the flat and curved regions depend on particle volume fraction. To explain this behavior, the photographs of the retracting process for $\phi = 0$ and plots of D^* versus time are shown in Figure 4-15. The image shown on the left side of the bottom is at $t = 20$ ms when the spreading ratio is at its minimum at the end of retraction. Between $t = 20$ ms and 30 ms, the spreading ratio stays constant. In this region, the drop stretches up and necks. Necking continues until a secondary drop is generated at t ~ 25 ms. From $t = 25$ ms, the secondary drop is airborne. While this occurs, the drop on the surface spreads, retracts, and reaches an equilibrium state (flat region) until the secondary drop falls down by gravity and impacts on and combines with the drop on the surface. The recombined drop spreads and retracts to its equilibrium position.

Since the rebounding behavior were different for $\phi = 0$, 0.1 and 0.2, further experiments were conducted using $\phi = 0.05$, 0.15, and 0.3. Some results are shown in Figure 4-16. The secondary drop stays airborne longest for ϕ of 0.15, but a secondary drop is not generated for either $\phi = 0.2$ or 0.3. In the region where the drop stretches up and necks, the shape depends on particle volume fraction. Furbank and Morris (2004) have studied the effect of particles on drop formation in the dripping mode. They observed that the pinch-off structures for the particle-laden systems are qualitatively different from the pure liquid case. During necking, particles in the

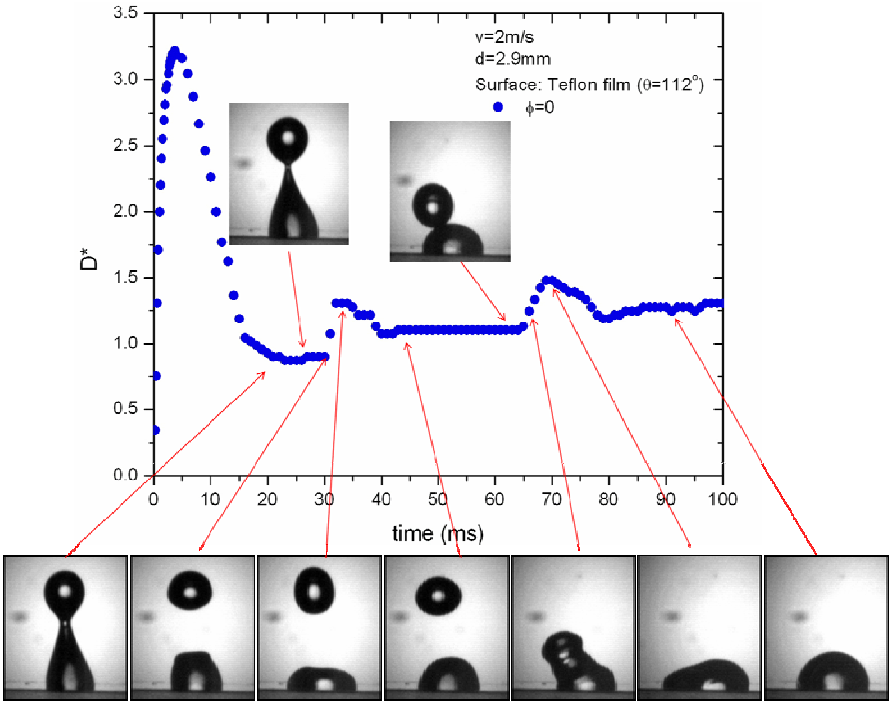

Figure 4-15. Images of rebounding behavior of a drop at an impact speed of 2m/s on Teflon® film.

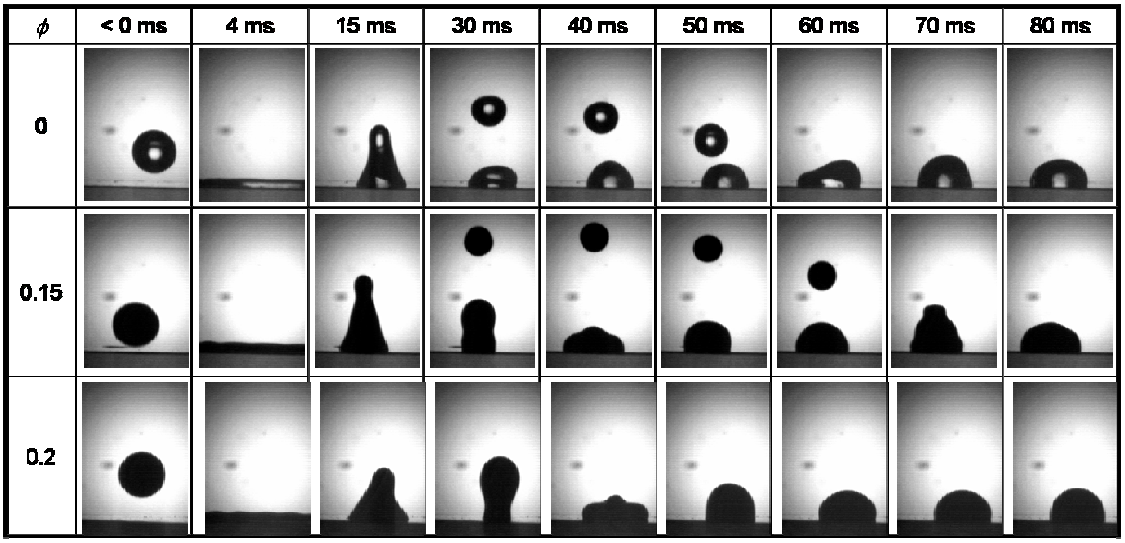

Figure 4-16. Images of drops having 20-μm particles with ϕ = 0, 0.15, and 0.2 impacting on Teflon® film at v = 2 m/s.

thread resist its further thinning, and depending on the number of particles present, this resistance can have either a destabilizing or a stabilizing effect on the thread relative to the case of the pure liquid. The presence of a small number of particles in the thread introduces regions within the thread which cannot thin beyond the size of an individual particle and leads to earlier rupture. A large number of particles in the thread tends to have a stabilizing effect both before and after pinch-off. In this case there are sufficient particles present in the thread that their individual motions are restricted and the necking of the thread is slowed. Based on their observations, we conjecture that at ϕ of 0.2 and 0.3, the particle volume fraction was sufficiently high to prevent pinch-off. At ϕ of 0.15, apparently the particle concentration is low enough that sufficient stretching and pinch-off can occur at a weak point devoid of particles. This is consistent with observation by Furbank and Morris (2004), where it was observed that for $\phi \approx 0.15$, drop formation changes drastically from behavior similar to that of pure fluid.

At a higher impact speed (2.55 m/s) for drops having 20-μm particles, rebound occurred at $\phi \leq 0.25$. For some volume fractions (ϕ = 0.1 and 0.2), two secondary drops are produced one by one, and the degree of rebound is maximum at ϕ = 0.10 as shown in Figure 4-17. The first image in each volume fraction shows necking at the maximum extent, and the last image shows returning of the secondary drop. When

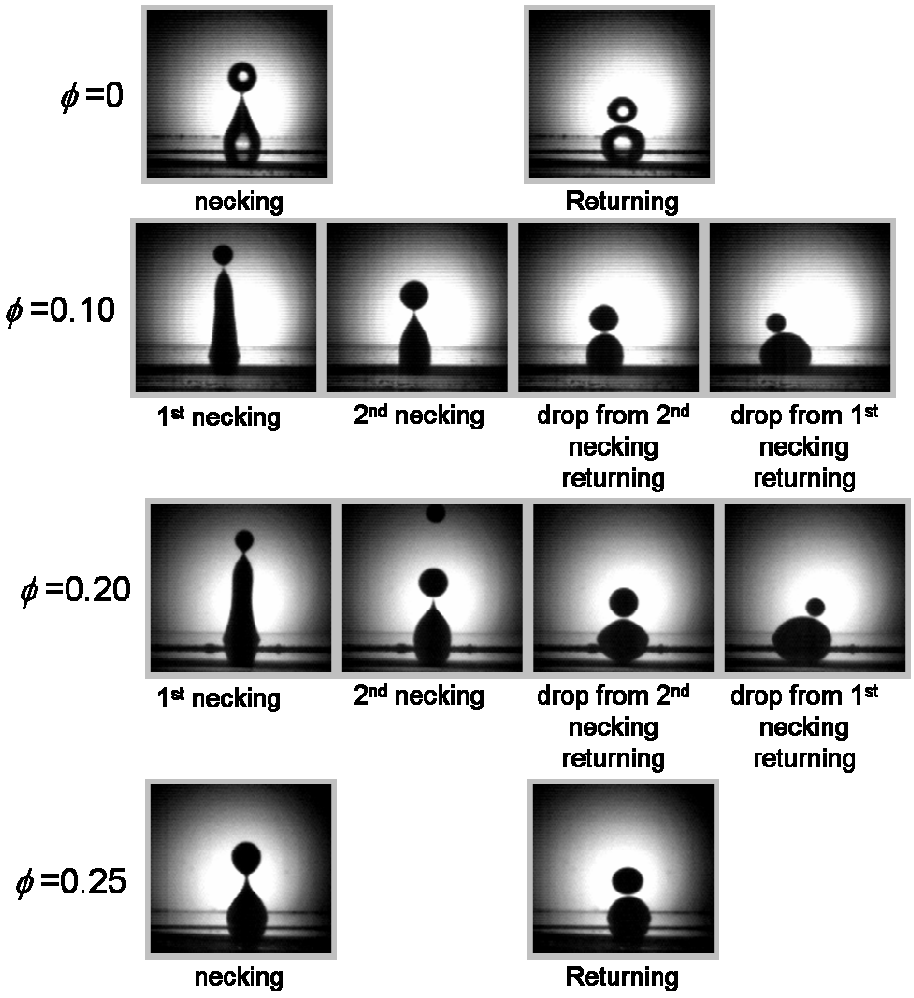

Figure 4-17. Images of necking and returning of secondary drops after drops containing 20-μm particles impact on Teflon® film at v = 2.55 m/s.

drop extension is high, the secondary drop size tends to be smaller and to stay airborne longer (Figure 4-18).

Following the test using 20-µm particles in Mixture 1, further testing of the effects of particles on rebounding on Teflon® film were conducted using different drop and particle sizes. These involved 40-µm particles in Mixture 1 with a drop size of 2.9 mm, 20- and 40-µm particles in Mixture 1 with drop size of about 690 µm, and 6-, 40- and 250-µm particles in MS100 with drop sizes of about 3.9, 4.0, and 3.4, µm, respectively. The results are summarized in Table 4-4.

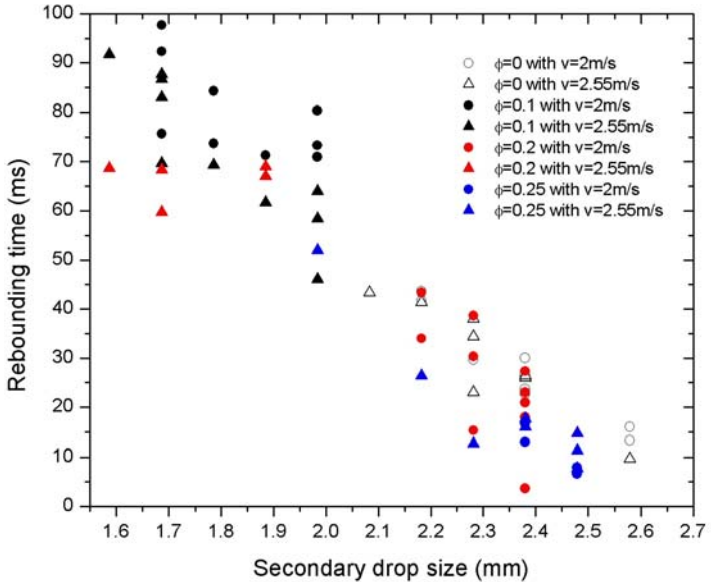

Figure 4-18. Airborne time as a function of secondary drop size.

Table 4-4. Summary of rebounding of particle-laden liquid on Teflon® film.

Liquid	d (mm)	d_p (μm)	v (m/s)	ϕ	θ	Re	We	Ca	D_m^*	Does rebounding occur?
Mixture 1	0.69	20	2	0	112	640	41	0.064	2.40	No
				0.1		490		0.083	2.38	No
				0.2		350		0.12	2.31	No
		40	2	0		640	41	0.064	2.40	No
				0.1		490		0.083	2.21	No
				0.2		350		0.12	2.16	No
S1	2.7	0.47	2	0	95	5400	160	0..030	3.65	Yes
				0.15		3000	170	0.058	3.75	Yes
Mixture 1	2.9	20	2	0	112	2700	170	0.064	3.35	Yes
				0.05		2400		0.072	3.35	Yes
				0.1		2000		0.083	3.22	Yes
				0.15		1800		0.097	3.24	Yes
				0.2		1500		0.12	3.09	No
			2.55	0		3400	280	0.081	3.62	Yes
				0.10		2600		0.11	3.59	Yes
				0.20		1900		0.15	3.52	Yes
				0.25		1600		0.18	3.38	Yes
				0.30		1300		0.22	3.01	No
		40	2	0		2700	170	0.064	3.11	Yes
				0.1		2000		0.083	3.34	Yes
				0.2		1500		0.12	3.27	No
				0.3		990		0.17	2.94	No
			2.55	0		3400	280	0.081	3.62	Yes
				0.05		3000		0.092	3.73	Yes
				0.10		2600		0.11	3.63	Yes
				0.15		2200		0.12	3.57	Yes
				0.20		1900		0.15	3.47	Yes
				0.25		1600		0.18	3.30	No
				0.30		1300		0.22	3.00	No
M1S100	3.9	6	2	0	90	3600	380	0.11	3.11	Yes
				0.1		2800		0.14	3.10	No
				0.2		2000		0.20	3.10	No
				0.3		1300		0.29	2.74	No
	4.0	40	2	0		3600	380	0.11	3.11	Yes
				0.1		2800	390	0.14	3.34	Yes
				0.2		2000	390	0.20	3.27	Yes
				0.3		1400	390	0.29	2.94	No
	3.4	250	2	0		3600	380	0.11	3.11	Yes
				0.1		2400	340	0.14	3.31	No
				0.2		1700	340	0.20	3.16	No
				0.3		1200	340	0.29	2.85	No

Effect of drop size on rebounding

The effect of drop size on rebounding was studied using Mixture 1 and a drop impact speed of 2.55 m/s. Drop diameter was varied from 1.98 to 2.9 mm by changing needle size.

As shown in Table 4-5, rebounding occurs for 2.3 and 2.9 mm drops, but not for 1.98 and 2.1 mm drops. This can be explained by the effect of drop size on Re and We. When all parameters are held constant except drop size, both Re and We increase (the ratios of inertial forces to viscous forces and inertial energy to surface energy increase). As a result, the maximum spreading ratio increases. Since the larger drops are stretched further beyond D_e^*, they have more liquid-air interfacial energy to cause them to retract, and the tendency to rebound is greater.

Table 4-5. Effect of drop size on rebounding of pure liquid. Drop of Mixture 1 impacting at 2.55 m/s on Teflon® film ($\theta = 112^o$).

d (mm)	v (m/s)	η (cP)	γ (mN/m)	Re	We	Ca	D_m^*	Does rebounding occur?
1.98	2.55	2.3	72	2300	190	0.081	3.12	No
2.1				2500	200	0.081	3.10	No
2.3				2700	220	0.081	3.36	Yes
2.9				3400	280	0.081	3.62	Yes

Effect of viscosity on rebounding

Tests were conducted to determine if the effect of particles on rebounding can be accounted for solely due to viscosity. A series of mixtures of water and glycerin were made to match the apparent viscosity of particle-laden liquid using 20- and 40-μm particles in Mixture 1. For the tests, the impact speed was 2.55 m/s, and liquid viscosity was varied from 2.3 to 6.2 cP. As shown in Table 4-6, rebounding for pure liquid drops occurred only at viscosity of 2.3 cP; however, rebounding of the particle-laden drops occurred at apparent viscosities of 3.0 and 4.2 cP. If the viscosity of pure liquid drop and particle-laden drop is same, the D_m^* is very close; therefore, it appears that fluid viscosity is more important than apparent viscosity for rebounding.

Table 4-6. Effect of liquid viscosity and particle volume fraction on rebounding on Teflon® film[a] ($\theta = 112^o$).

Liquid	d (mm)	d_p (μm)	ϕ	v (m/s)	η (cP)	Re	We	Ca	Does rebounding occur?
Mixture 1	2.9	N/A	0	2.55	2.3	3400	280	0.081	Yes
Mixture 4					3.0	2700	280	0.11	No
Mixture 5					4.2	1900	290	0.15	No
Mixture 6					6.2	1300	290	0.22	No
Mixture 1	2.9	20	0	2.55	2.3	3400	280	0.081	Yes
			0.1		3.0	2600	280	0.11	Yes
			0.2		4.2	1600	280	0.18	Yes
			0.3		6.2	1300	280	0.22	No

Effect of impact speed on rebounding

The effect of impact speed on rebounding was conducted by holding all parameters constant and varying impact speed. Distilled water was used for the tests because rebounding occurs over a wider range of impact speed than the water and glycerin solutions. Impact speed was varied from 0.28 to 2.48 m/s. As shown in Table 4-7, rebounding occurred except at v = 0.28 m/s. As impact speed is increased, more kinetic energy is in the system; therefore, the tendency to rebound increases.

Figure 4-19 shows water images of water drops at v = 0.28, 0.42, 1.80, and 2.48 m/s. For v = 0.42 m/s, the whole drop rebounded without any secondary drops. As impact speed is increased, the drop divides and a secondary drop is emitted vertically, but the mother drop remains attached to the surface. Further increase in impact speed results in additional secondary drops being emitted vertically, but the mother drop still remains attached to the surface.

Table 4-7. Effect of impact speed on rebounding of water drops on Teflon® film (θ = 112°).

d (mm)	v (m/s)	η (cP)	γ (mN/m)	Re	We	Ca	Does rebounding occur?
3.2	2.48	1	72	7900	270	0.034	Yes
	2.35			7500	250	0.033	Yes
	2.28			7300	230	0.032	Yes
	2.15			6900	210	0.030	Yes
	1.80			5800	140	0.025	Yes
	1.57			5000	110	0.022	Yes
	1.34			4300	80	0.019	Yes
	1.07			3400	51	0.015	Yes
	0.88			2800	34	0.012	Yes
	0.75			2400	25	0.010	Yes
	0.42			1300	7.8	0.0058	Yes
	0.28			900	3.5	0.0039	No

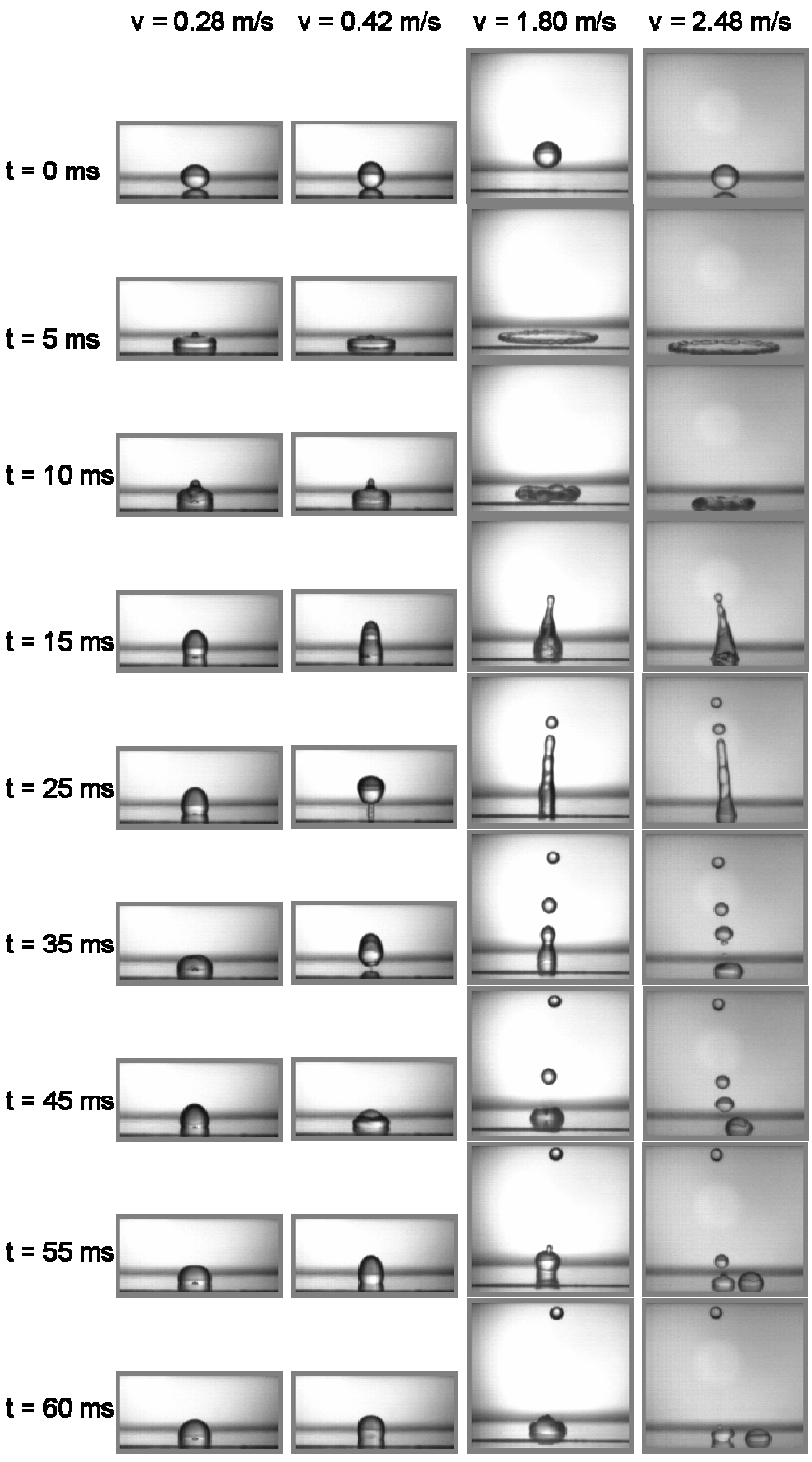

Figure 4-19. Rebounding of water drops at *v* of 0.28, 0.42, 1.80, and 2.48 m/s.

4.4 Bouncing of Drops at Low Impact Speed

When a low-velocity hydrophilic droplet impacts on a hydrophilic surface, sometimes the droplet will bounce off the surface without wetting it, as illustrated in Figure 4-20. This is not expected for a hydrophilic drop impacting on a smooth hydrophilic surface. Among the surfaces used in the present study, bouncing is observed mostly on silicon oxide wafer, and it is seldom found on glass slide. It should be noted that bouncing on the hydrophobic surfaces was not observed.

In the bouncing study, the following four parameters were considered: 1) surface tension, 2) viscosity, 3) impact speed, and 4) particle volume fraction. Since drop bouncing was mostly observed on silicon oxide wafers, the tests were conducted on this surface. In this study, most of the tests were conducted using distilled water without particles. To investigate the effect of particles, Mixture 1 and 20-μm particles at ϕ of 0, 0.1 and 0.2 were used. Impact speed of drops of glycerin mixture was 0.08 m/s, and those of glycerin and water/surfactant solution were 0.16 m/s. For each drop type, impaction test was repeated at least ten times. The important parameters (including We, Re, and Ca) for bouncing experiments on silicon oxide wafers are given in Table 4-8.

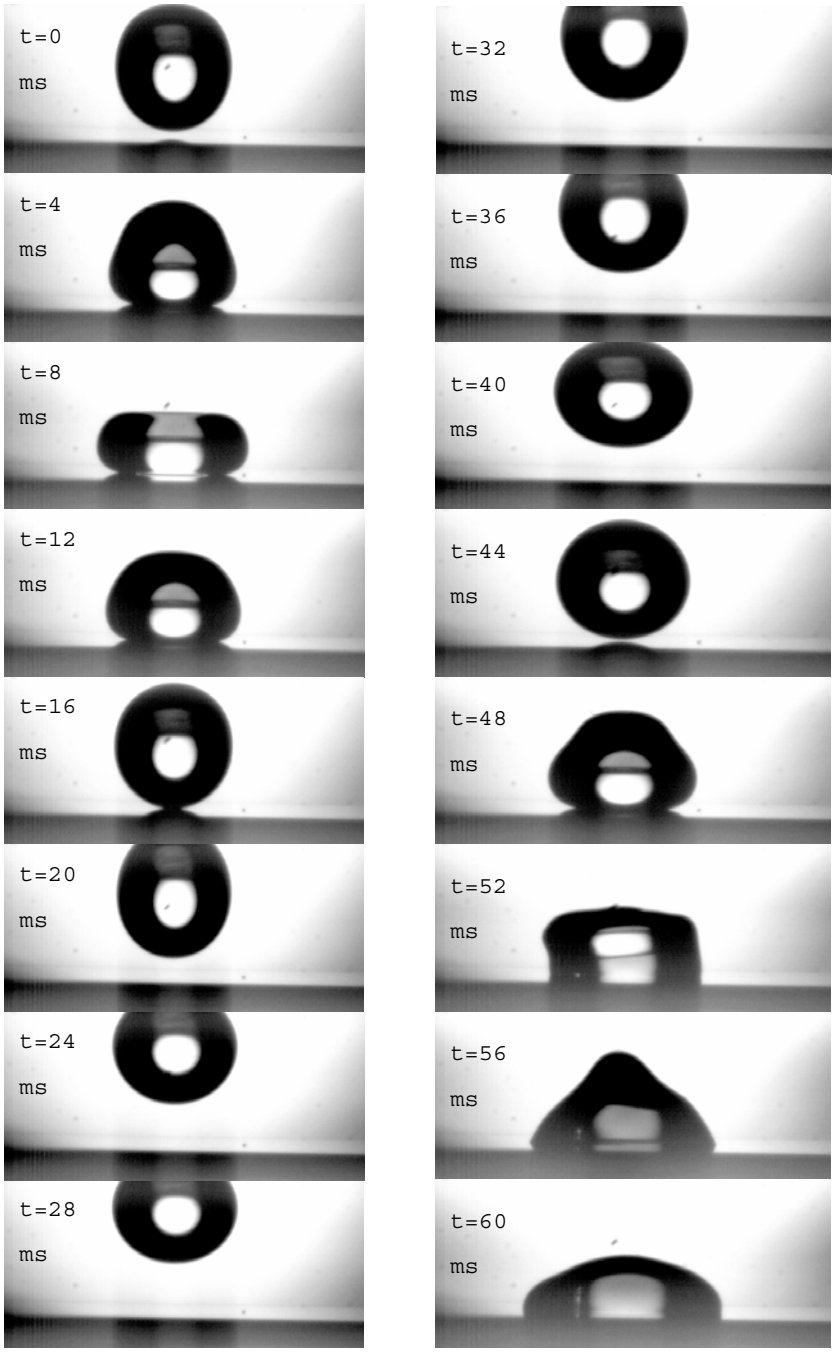

Figure 4-20. Water drop bouncing on silicon oxide wafer.

Table 4-8. Parameters for bouncing experiments on silicon oxide wafers.

Liquids	d (mm)	d_p (μm)	v (m/s)	ϕ	η (cP)	γ (mN/m)	Re	We	Ca
Water	2.9	N/A	0.08	0	1	72	230	0.26	0.0011
Mixture 1	2.9	20	0.08	0	2.3	72	110	0.27	0.0026
				0.1	3.0		82		0.0033
				0.2	4.2		59		0.0047
Mixture 3	2.9	N/A	0.08	0	7.1	72	37	0.29	0.0079
Water/ surfactant	2.16	N/A	0.16	0	1	33	350	1.7	0.0048
Glycerin	2.58	N/A	0.16	0	1490[a]	48.09[b]	0.31	1.5	5.0
Water	3.2	N/A	0.01	0	1	72	32	0.0044	0.00014
			0.08				260	0.28	0.0011
			0.16				510	1.1	0.0022
			0.18				580	1.4	0.0025
			0.27				860	3.2	0.0038

[a]From a reference (David R. Lide, CMC Handbook of Chemistry and Physics, 71st Edition, CRC Press, Boca Raton, 1990, p. 6-144).
[b]From a reference (Arthur W. Adamson and Alice P. Gast, Physical Chemistry of Surfaces, 6th Edition, John Wiley & Sons, Inc., New York, 1997, p. 36).

In Figure 4-21 (a), the probability of bouncing for pure liquids is plotted versus Re. The trend is for the probability of bouncing to decrease as Re increases. The point for glycerin clearly does not fit in with other data points. The apparent reason for this is that the viscosity is much higher than for the other fluids. Note that the chance of bouncing decreases as more glycerin is added to water. This can be seen in Table 4.9 by comparing the results for water, Mixture 1 and Mixture 3, which are for a drop size of 2.9 mm and an impact speed of 0.08 m/s. Note that viscosities of these three liquids are 1.0, 2.3 and 7.1 cP, respectively. Glycerin has a high viscosity (1490 cP), and the glycerin drop did not bounce at an impact speed of 0.16 m/s, but the water drop did bounce for the same impact speed. These observations suggest that the probability of bouncing decreases as viscosity increases and that some other dimensionless number other than Re may be better for characterizing bouncing.

In Figure 4-21 (b), the probability of bouncing for pure liquids is plotted versus We. The trend is for the probability of bouncing to decrease as We increases. The point for water/surfactant does not fit in with other data points. The apparent reason for this is that the surface tension of this liquid is much lower than for the other liquids.

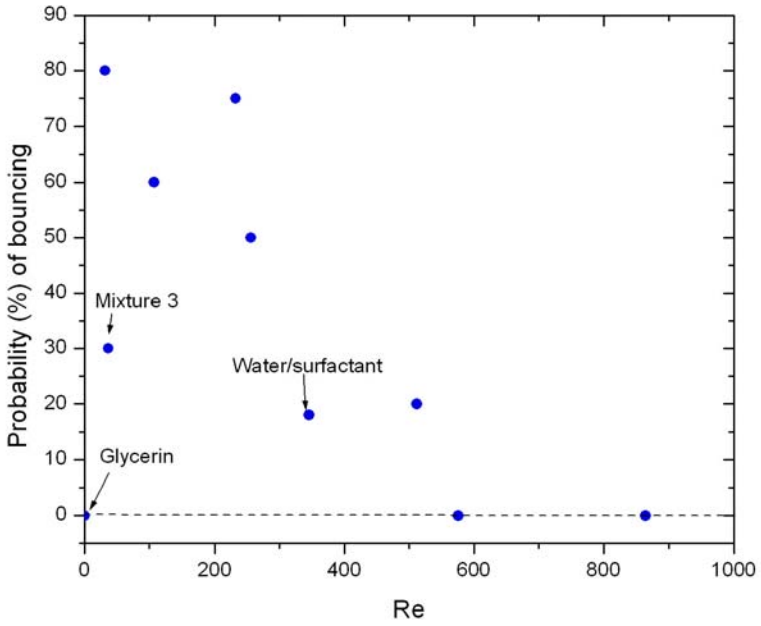

(a) Probability (%) of bouncing versus Re

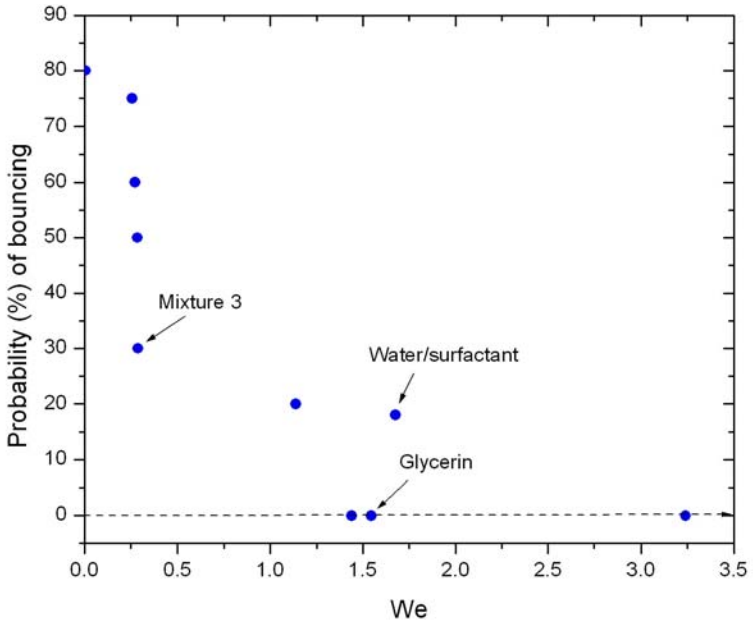

(b) Probability (%) of bouncing versus We

Figure 4-21. Probability (%) of bouncing of pure liquid as a function of Re, We, or Ca: (a) Probability (%) of bouncing versus Re, (b) Probability (%) of bouncing versus We, and (c) Probability (%) of bouncing versus Ca.

Figure 4-21. (continued).

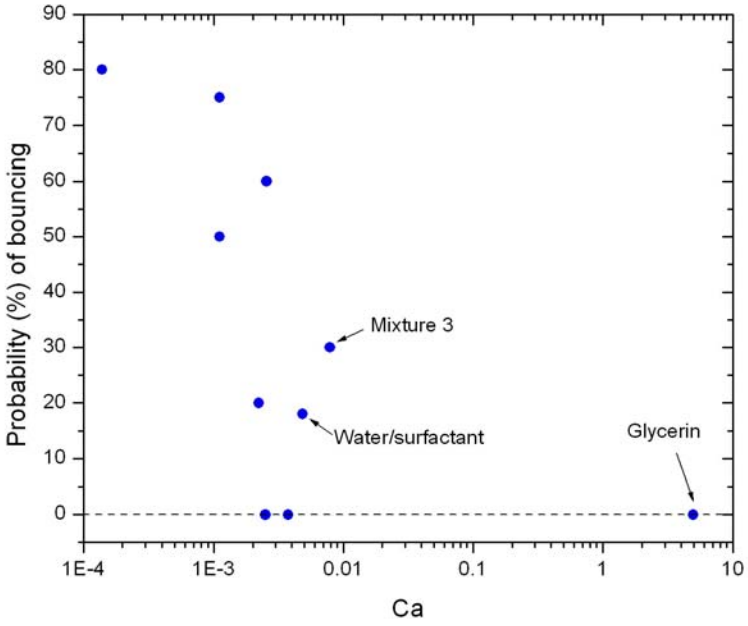

(c) Probability (%) of bouncing versus Ca.

Table 4-9. Results of bouncing tests on silicon oxide wafers for pure liquids.

Liquids (drop size)	*v* (m/s)	Re	We	Ca	Total no. of tests	No. of tests where bouncing occurred	% of tests where bouncing occurred
Water (2.9 mm)	0.08	230	0.26	0.0011	12	9	75
Mixture 1 (2.9 mm)	0.08	110	0.27	0.0026	10	6	60
Mixture 3 (2.9 mm)	0.08	37	0.29	0.0079	10	3	30
Glycerin (2.58 mm)	0.16	0.31	1.5	5.0	10	0	0
Water* (3.2mm)	0.01	32	0.0044	0.00014	10	8	80
	0.08	260	0.28	0.0011	10	5	50
	0.16	510	1.1	0.0022	10	2	20
	0.18	580	1.4	0.0025	10	0	0
	0.27	860	3.2	0.0038	10	0	0
Water/ surfactant (2.16 mm)	0.16	350	1.7	0.0048	11	2	18

* 3.2-mm water drops emit secondary drop after it wets the surface.

In Figure 4-21 (c), the probability of bouncing for pure liquids is plotted versus Ca. The trend is for the probability of bouncing to decrease as Ca increases. The points for water/surfactant and Mixture 3 do not fit in with other data points.

The effect of particles on bouncing was investigated using 20-μm particles added to Mixture 1 at ϕ of 0.1 and 0.2. As shown in Table 4-10, the addition of particles increases viscosity, and consequently Re and Ca, and decreases the probability of bouncing. This is consistent with earlier observations for pure liquids where the probability of bouncing decreased with increasing viscosity. In Figure E-1 through 3 in Appendix E, the probability of bouncing for both pure and particle-laden liquids is plotted versus Re, We and Ca.

Table 4-10. Results of bouncing tests on silicon oxide wafers for particle-laden liquids*.

Liquids (drop size)	v (m/s)	ϕ*	Re	We	Ca	Total no. of tests	No. of tests where bouncing occurred	% of tests where bouncing occurred
Mixture 1 (2.9mm)	0.08	0	110	0.27	0.0026	10	6	60
		0.1	82		0.0033	12	5	42
		0.2	59		0.0047	12	0	0

*Mixture 1 with 20-μm particles.

4.4.1 Initial non-wetting of drop

Even if a low-velocity drop does not bounce from the surface, non-wetting behavior of the drop is sometimes observed for hydrophilic drops on both hydrophilic and hydrophobic surfaces, but most frequently on the silicon oxide wafer. The drop contacts the surface, but appears not to wet it for sometime after the contact is made. When this happens, the D^* versus time curve is not straight from the origin to the maximum spreading ratio as usually occurs. An example is shown in Figure 4-22, where D^* is plotted versus time for a 3.9-mm drop containing 6-μm particles impacting at a speed of 0.01 m/s on a silicon oxide surface. The images in the first three regions of this figure show a drop that is in contact with the surface, but is not wetting the surface. In Region I, the drop impacts on surface, and the contact area increases. The contact area stays almost constant while the drop shape deforms slowly in Region II. The deformation of the drop is large in Region III; however, the drop still does not wet the surface in this region. The last image in Region III clearly shows the outer regions of the drop is not wetting the surface, and the curvature of the drop at the contact line resembles that of a bouncing drop at t = 8 ms shown in Figure 4-20. At the beginning of Region IV, the drop finally wets the surface. Notice that the drop wets the surface asymmetrically, beginning first on the right side and later on the left

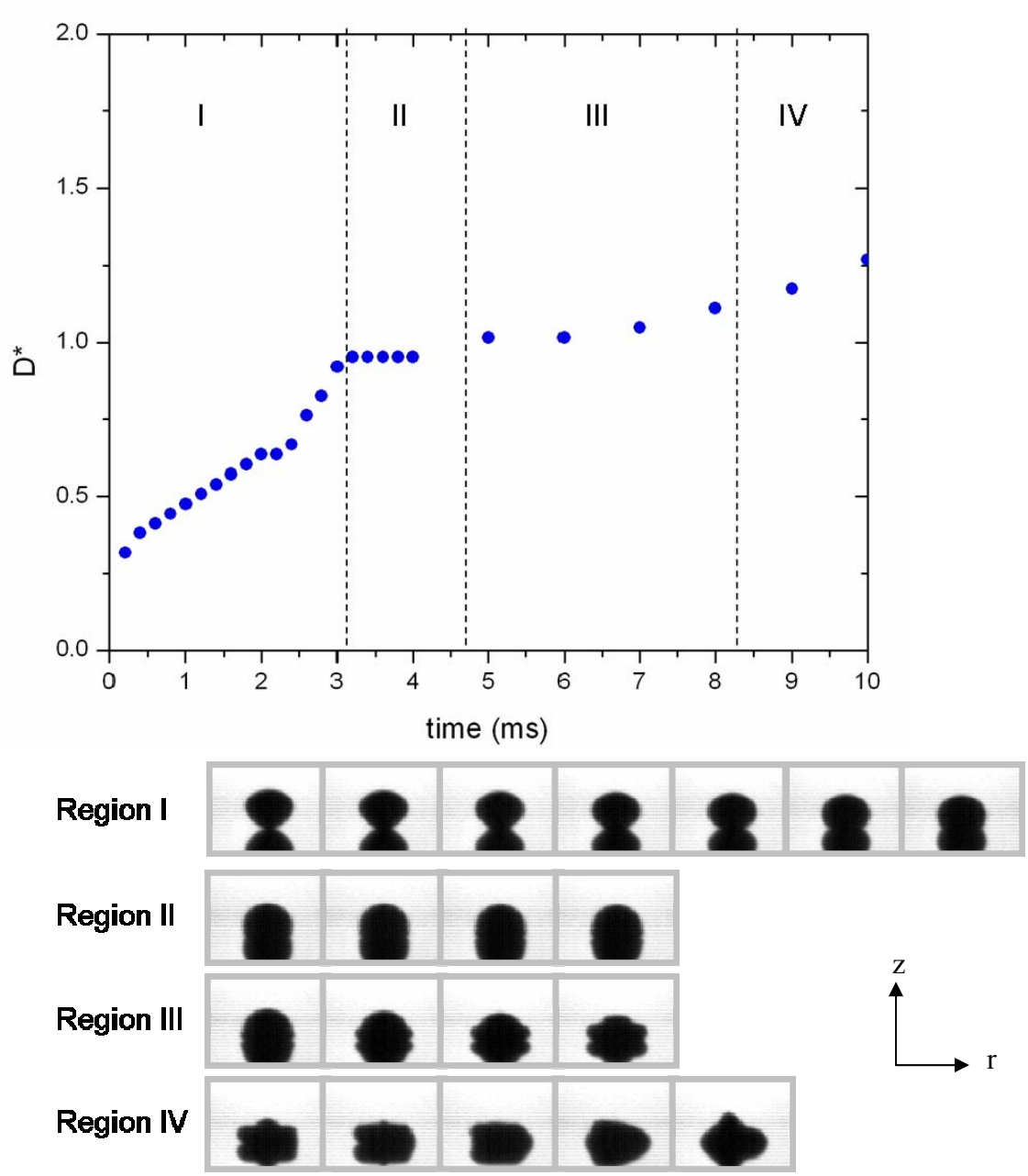

Figure 4-22. Changing of drop shape after impact on silicon oxide surface (d = 3.9mm, d_p = 6μm, ϕ = 0.1, and v = 0.01m/s).

side. Similar behavior was observed in many different cases, and some of them are shown in Appendix F. The non-wetting behavior for these cases and bouncing should be related, and a possible explanation for the non-wetting and bouncing behavior is that it is caused by air between the surface and the drop as discussed in Chapter 2.

4.4.2 Ejection of secondary drop

When a low-velocity liquid drop impacts on surface, ejection of a secondary drop from the top of the impacting drop is sometimes observed. Ejection of a drop is observed for cases when the impacting drop bounces and in other cases where the impacting drop does not bounce. Similar to Thoroddsen *et al.*'s (2000) observations for a liquid drop impacting a liquid surface, a series of up to three, progressively smaller drops, is observed.

Figure 4-23 illustrates drop ejection when a 3.2-mm water drop impacts on a silicon oxide wafer with impact speed of 0.08 m/s. The steps in generating the secondary drops are similar to those described by Thoroddsen *et al*. (2000). After the drop starts to wet the surface, the surface curvature near the contact line changes directions. This is due to spreading capillary waves, which are initiated at the impact point. Capillary waves progress from the bottom of the drop to the top of the drop.

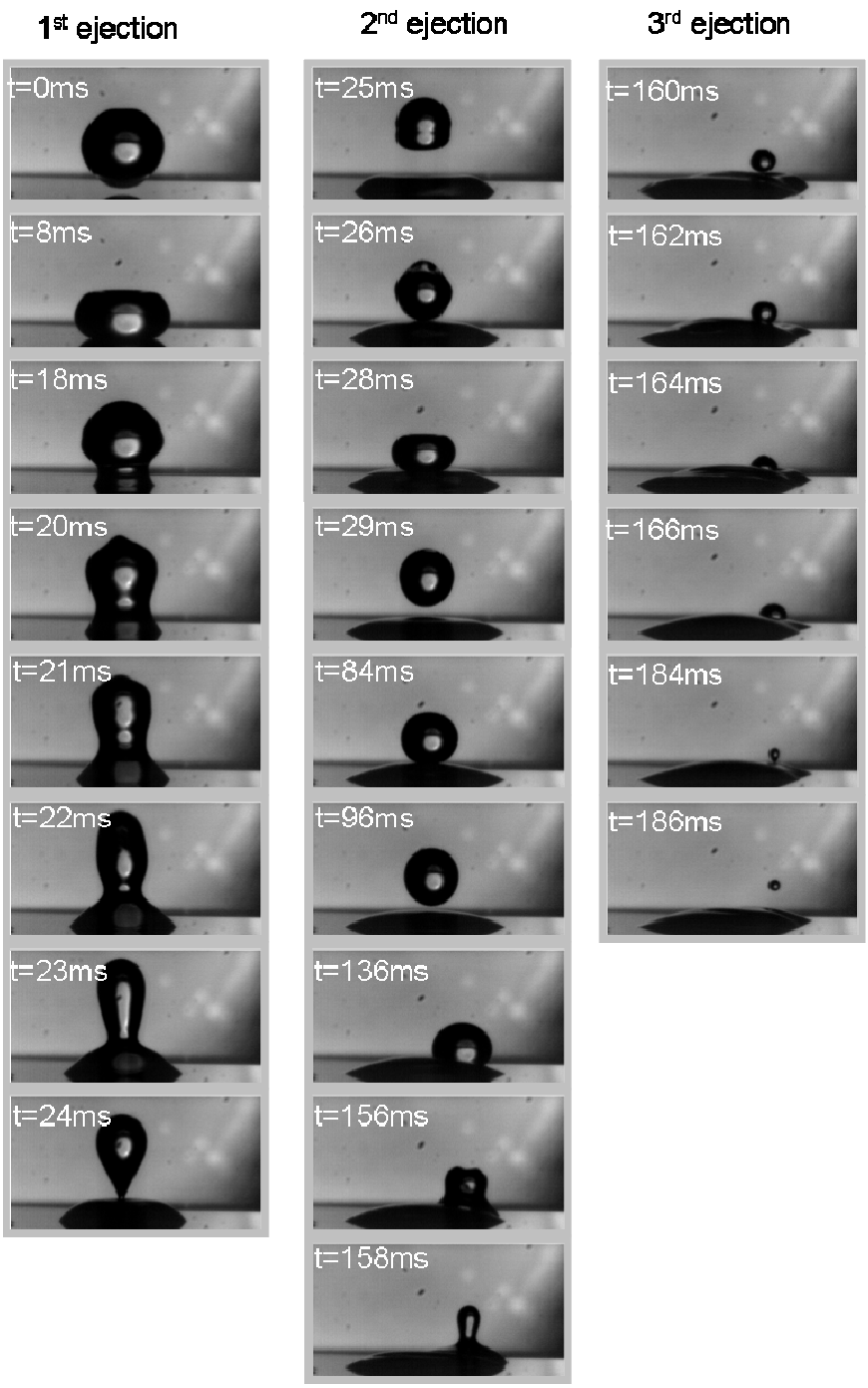

Figure 4-23. Ejection of secondary drops observed when a 3.2-mm water drop impacts at a speed of 0.08 m/s on a silicon oxide wafer.

Between 8 and 18 ms, wetting appears to have occurred, the contact line has moved outward, and the wave has moved upward, which gives the drop a mushroom-like shape. Between 18 and 24 ms, the contact line continues to move outward, the inflection point where the direction of curvature changes moves inward, and the wave continues to move upward. As a result, the drop divides into two parts for t between of 24 and 25 ms, producing an ejected drop that moves vertically upward. The ejected drop eventually falls due to gravity, impacts on the mother drop which is spread over the surface, and then bounces several times on the mother drop and coalesces with it. During coalescence, the ejected drop ejects a daughter drop.

Renardy *et al*.'s (2003) criteria for existence of a capillary wave is

$$\left(\frac{\sigma}{\rho r}\right)^{\frac{1}{2}} < v < \left(\frac{\sigma^2}{\eta\rho r}\right)^{\frac{1}{3}} \tag{4.2}$$

For a 3.2-mm water drop, the range is between 0.2 to 1.5 m/s. However, drop ejection is observed at impact speed lower than 0.2 m/s.

4.5 Effect of Drop Size on Impact Process for Pure Liquid

4.5.1. Low impact speed

Figure 4-24 (a) shows D^* versus time for different drop sizes (340, 690 and 2900 μm) for pure liquid drops (Mixture 1) impacting fluorocarbon plasma treated silicon wafer and Teflon® film at low impact speed. Values of Re and We are small, but different for each size drop. The smaller drops spread faster and reach the equilibrium spreading ratio, D_e^*, sooner than the bigger drops. This may be due to the extremely low We and small Re for the larger drop. Similar results (see Appendix F) are obtained for the hydrophilic surfaces (glass slide and silicon oxide wafer). In Figure 4-24 (b), D^* is plotted as a function of dimensionless time, t^*.

$$t^* = \frac{tv}{d} \tag{4.3}$$

In Figure 4-24 (b), t_m^* for d = 340, 690, and 2,900 μm are 1.41, 0.52, and 0.05, respectively. Pasandideh-Fard *et al.* (1996) suggested that the dimensionless time for the drop to reach its maximum spreading ratio is constant (t_m^* ~2.67). Pasandideh-Fard *et al*., (1999) found that t_m^* increased with impact speed, and ranged from 2 to 4 in their experiments; however, they used t_m^* = 2.67 for simplicity of numerical analysis.

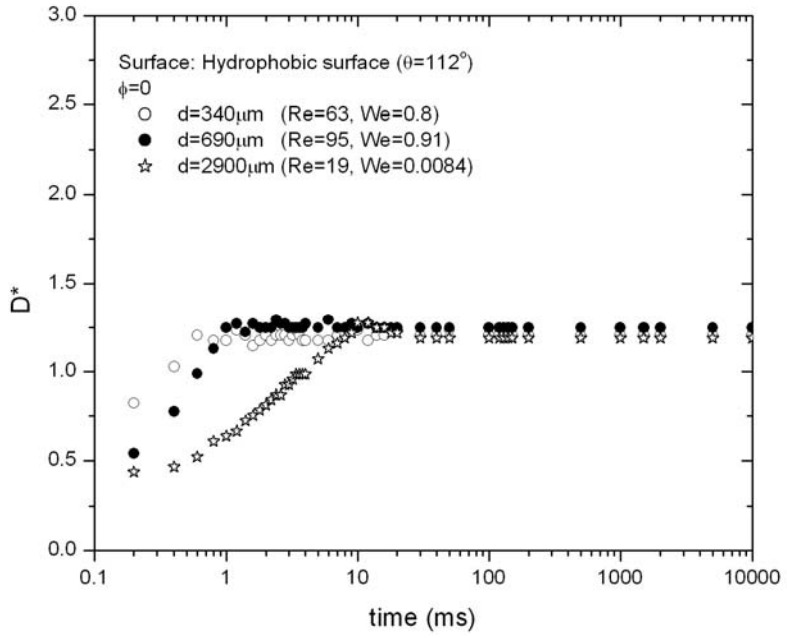

(a) D* versus time

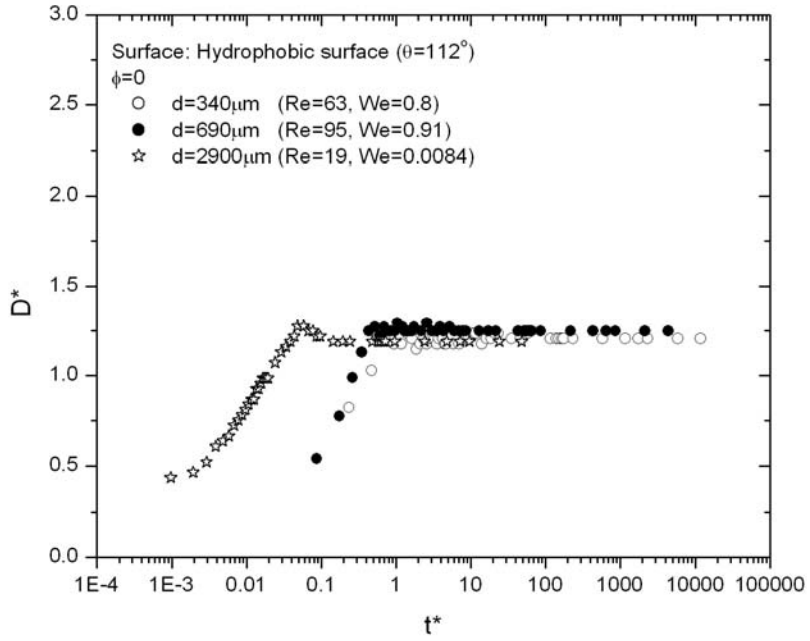

(b) *D** versus dimensionless time

Figure 4-24. Effect of drop size on impact process on hydrophobic surfaces (fluorocarbon plasma treated silicon wafer for 340- and 690-μm drops and Teflon® film for 2.9-mm drop) for Mixture 1. Impact speed is 0.4 m/s for 340-μm drop, 0.3 m/s for 690-μm drop, and 0.01 m/s for 2.9-mm drop: (a) *D** versus time and (b) *D** versus dimensionless time.

Moita *et al.* (2002) reported values of t_m^* ranged from 1.3 to 4.25 when a diesel oil drop impacted on a smooth Perspex surface for the following conditions and parameters: We of 4 – 487, Re of 198 – 2558, drop size of 2.5mm, and impact speed of 0.22 – 2.47 m/s. Although other studies (Bechtel *et al*, 1981; Haferl *et al*, 2002; Dietzel *et al*., 2003) used t^* for tracking time during the impact process, no values of t_m^* were given.

4.5.2 High impact speed

Figure 4-25 (a) shows D^* versus time for different drop sizes (340 and 2900 μm) for pure liquid drops impacting a hydrophobic surface (fluorocarbon plasma treated silicon wafer for 340-μm drop and Teflon® film for 2.9-mm drop) at 2 m/s. The small drop spreads faster and reaches the equilibrium spreading ratio, D_e^*, sooner than the bigger drop. Similar results (see Appendix G6 and 7)) are obtained for the hydrophilic surfaces (glass slide and silicon oxide wafer). When D^* is plotted against t^*, t_m^* of 690- and 2900-μm drops are similar and is in the range of 1.74 – 3.45.

For the small drops impacting the hydrophobic surfaces, oscillations around the equilibrium value of D_e^* is observed, as shown in Figure 4-26. The drop reaches its maximum spreading ratio very quickly (about 0.4 ms after impact); it still has enough

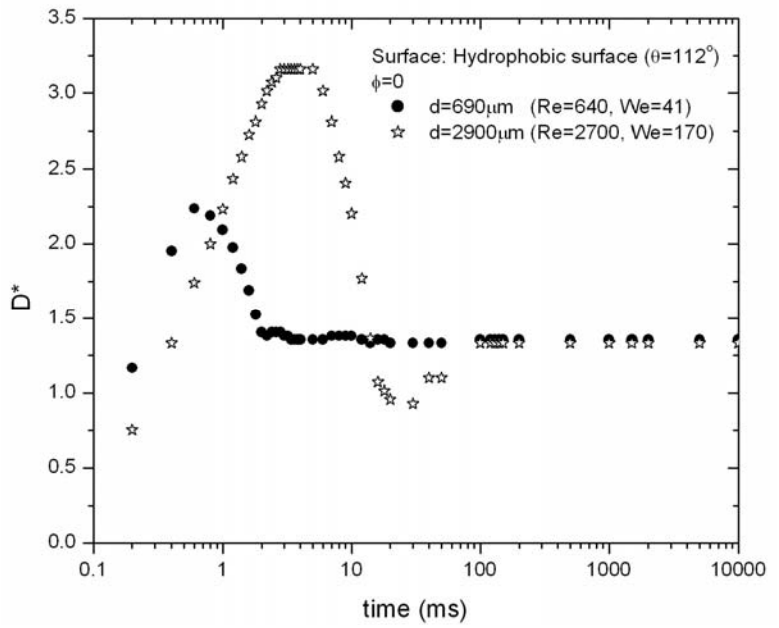

(a) D^* versus time.

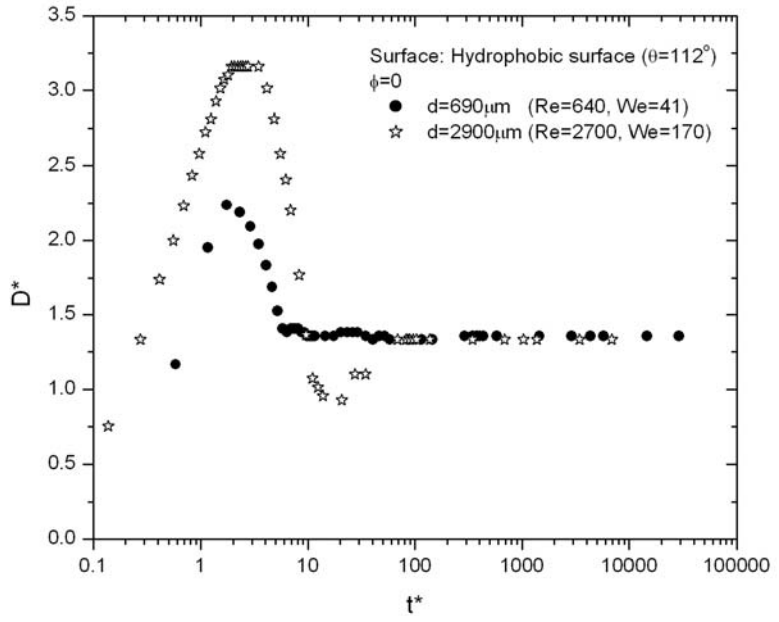

(b) D^* versus dimensionless time

Figure 4-25. Effect of drop size on impact process on hydrophobic surfaces for pure liquid. Impact speed is 2 m/s: (a) D^* versus time and (b) D^* versus dimensionless time.

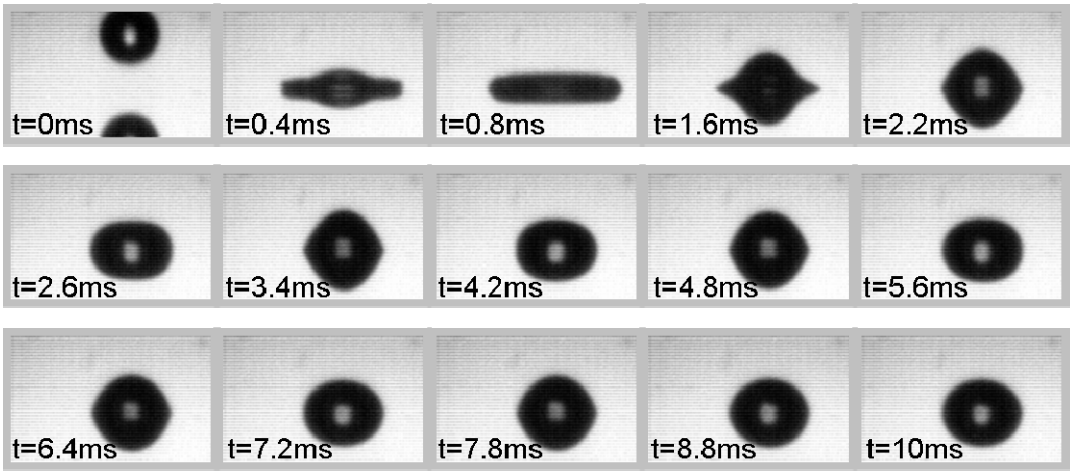

Figure 4-26. Oscillation of 690-μm pure liquid drop impacting a speed of 2 m/s on a fluorocarbon plasma treated silicon wafer.

kinetic energy to spread further. After it reaches its equilibrium spreading ratio ($t \sim 2$ ms), the drop expands and contracts until 20 ms and stops.

CHAPTER 5

THEORETICAL MODELS

5.1 Theoretical Model for D_m^*

A model for predicting D_m^* for particle-laden drops impacting solid surfaces was sought. The approach was to modify existing models for predicting D_m^* for pure liquid drops by including particle related parameter such as d_p/d and ϕ.

When apparent viscosity of the particle-laden liquid obtained from Krieger's equation (1972) was used in the pure liquid models, good agreement between model predictions and experimental results was obtained. Thus, particle volume fraction is used in the model, but d_p/d is not. Predictions based on three models (Pasandideh-Fard *et al.* (1996), Mao *et al.* (1997), and Park *et al.* (2003)) are discussed in this chapter. These models are shown in Table 5-1.

Figure 5-1 shows the comparison of the measured maximum spreading ratio and modeled predictions for the particle-laden drop on glass slide, silicon oxide wafer, and Teflon® film for low impact speed experiments. For impact speeds of 0.01 m/s

Table 5-1. Models used to predict D_m^* for particle-laden drops impacting solid surfaces.

Models	
Pasandideh-Fard *et al.* (1996a, 1996b)	$D^* = \sqrt{\dfrac{We + 12}{3(1-\cos\theta_a) + 4(We/\sqrt{\mathrm{Re}})}}$
Mao *et al.* (1997)	$\left[\dfrac{1}{4}(1-\cos\theta) + 0.2\left(\dfrac{We^{0.83}}{\mathrm{Re}^{0.33}}\right)\right] D_m^{*3} - \left(\dfrac{We}{12}+1\right) D_m^* + \dfrac{2}{3} = 0$
Park *et al.* (2003)	$\left(0.33\dfrac{We}{\sqrt{\mathrm{Re}}} - \dfrac{1}{4}\cos\theta + \dfrac{1}{2}\left(\dfrac{1-\cos\alpha}{\sin^2\alpha}\right)\right) D^{*2}_m - 1 - \dfrac{We}{12} + \dfrac{\Delta E_{SP}}{\pi d^2 \gamma_{LV}} = 0$

Notation:

D^*_m : maximum spreading ratio

θ : equilibrium contact angle

θ_a :advancing contact angle

$$We = \frac{\rho v^2 d}{\sigma}$$

$$\mathrm{Re} = \frac{\rho v d}{\eta_0 \left(1 - \dfrac{\phi}{\phi_m}\right)^{-2.5\phi_m}}$$

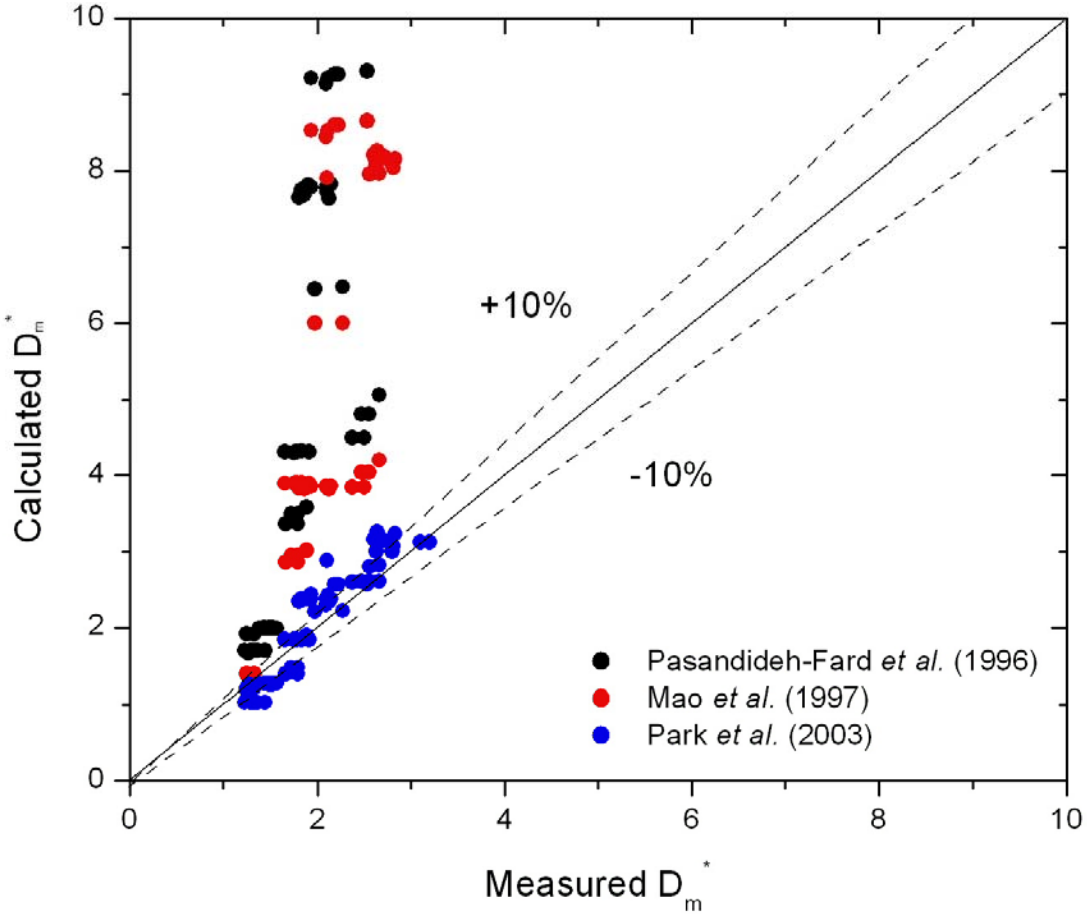

Figure 5-1. Comparison of measured D_m^* with predicted values for low impact speeds.

and 0.3 m/s, Pasandideh-Fard *et al.*'s and Mao *et al.*'s model greatly over estimate D_m^*, especially for the low contact angle; however, Park *et al.*'s model is in close agreement with the experimental results. For low impact speeds, Park *et al.*'s model gives better results because it is assumed that the drop shape is a cap of sphere at the maximum spreading state while other models (Pasandideh-Fard *et al.* (1996) and Mao *et al.* (1997)) assume that it is cylindrical.

For v = 2 m/s, Mao *et al.*'s model over estimates some values while Pasandideh-Fard *et al.* and Park *et al.*'s models are good agreement with the measured maximum spreading ratio as shown in Figure 5-2. For large drop sizes (3.4 to 4.0 mm), Pasandideh-Fard *et al.* and Park *et al.*'s model predictions are close to the experimental values, but Mao *et al.*'s model over estimates D_m^* for most of the cases.

Model predictions for all tests are compared with measured D_m^* in Appendix H.

5.2 Prediction of rebounding using Mao *et al.*'s (1997) Model.

The only available model for predicting whether or not rebounding will occur was developed by Mao *et al.* (1997), which was discussed in Chapter 2. Their model

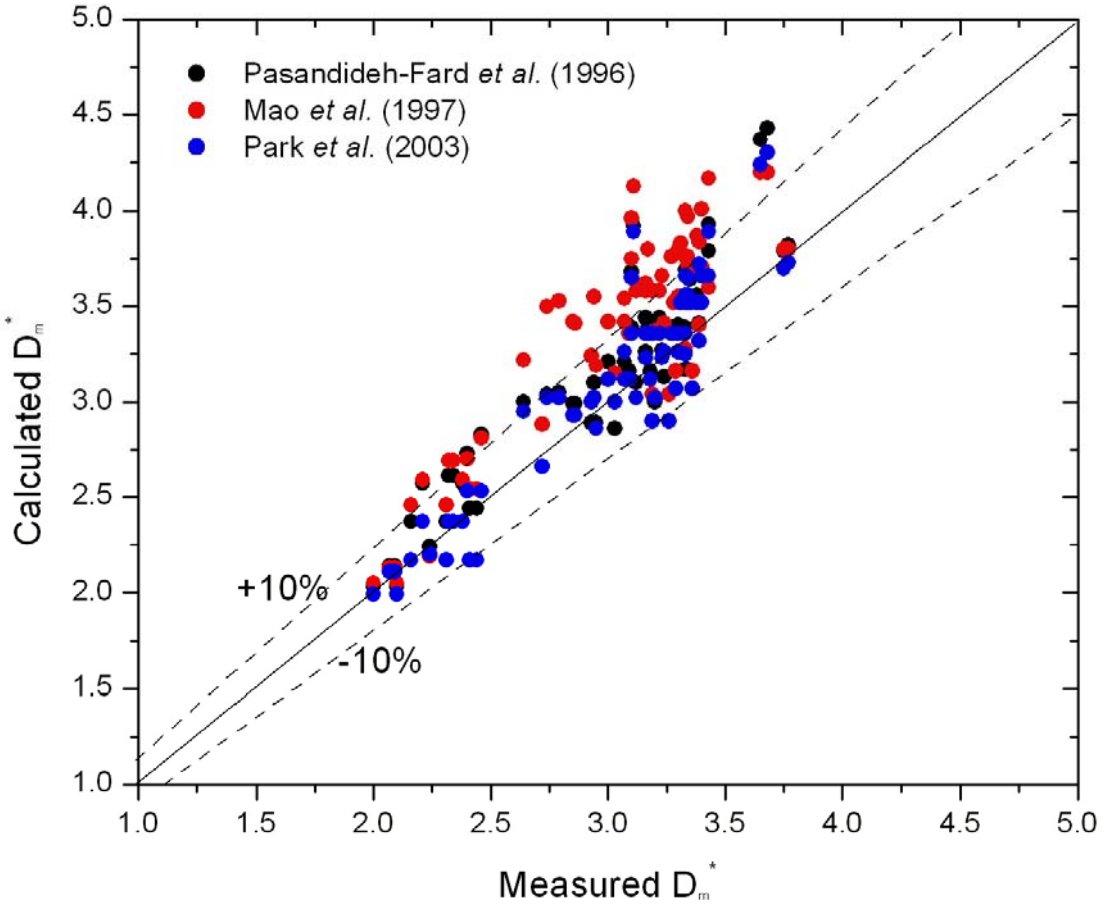

Figure 5-2. Comparison of measured D_m^* with predicted values for an impact speed of 2 m/s.

(1997) was developed using data for water drops ranging in size from 2.5 to 2.7 mm, impact speed ranging from 0.55 – 4.58 m/s, Re ranging from 1,485 to 10,044, and We ranging from 11.2 to 513. 5.2 Prediction of rebounding using Mao *et al.*'s Model (1997).

The only available model for predicting whether or not rebounding will occur was developed by Mao et al. (1997), which was discussed in Chapter 2. Their model was developed using data for water drops ranging in size from 2.5 to 2.7 mm, impact speed ranging from 0.55 – 4.58 m/s, Re ranging from 1,485 to 10,044, and We ranging from 11.2 to 513.

When excessive energy, ΔE^*_{ERE}, in Mao *et al.*'s model, is greater than zero, rebounding is predicted. In Figure 5-3, ΔE^*_{ERE} is plotted against D_m^* for several contact angles. The plot shows that for θ = 90, 95, and 112^o, rebounding is predicts when D_m^* is greater than 2.03, 2.74, and 3.11, respectively.

In Table 5-2, Mao *et al.*'s model predictions are compared with experimental results for pure liquids. For the larger drops, Mao *et al.*'s model correctly predicted that rebounding occurs for all of the drop sizes except for the 690-μm drop. It predicts that the 690-μm drops will rebound; however, rebounding is not observed in the experiments. It should be noted that the drop size and Re for the 690-μm drop experiments fall outside of the range of values used to develop Mao *et al.*'s model.

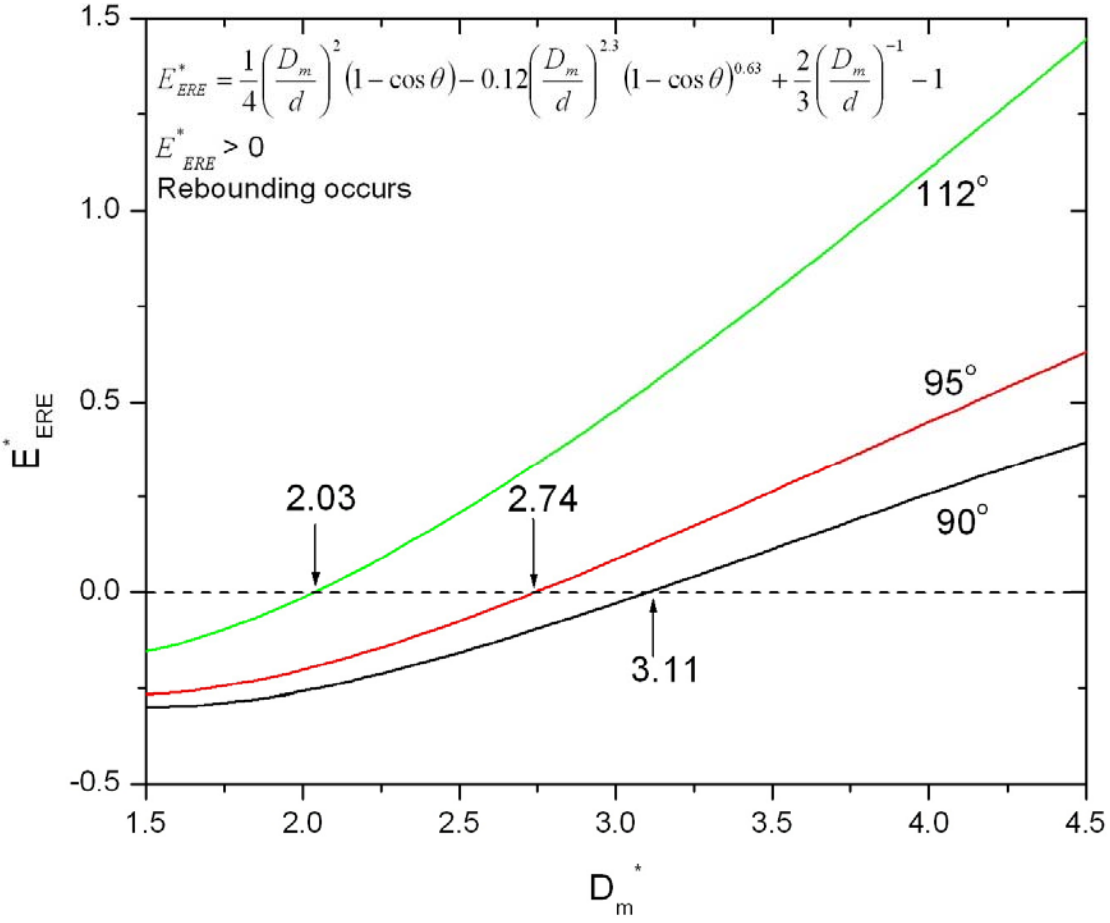

Figure 5-3. Excessive energy, E^*_{ERE}, versus the maximum spreading ratio for contact angles of 90, 95, and 112 ^{o}.

Table 5-2. Summary of rebounding results for pure liquid drops impacting on Teflon® film.

Liquid	d (mm)	v (m/s)	θ	Re	We	Ca	D_m^*	Does rebounding occur?	
								Experimental Result	Mao *et al.*'s prediction
Mixture 1	0.69	2	112	640	41	0.064	2.19	No	Yes
S1	2.7	2	95	5400	160	0.030	3.60	Yes	**Yes**
Mixture 1	2.9	2	112	2700	170	0.064	3.20	Yes	**Yes**
		2.55		3400	280	0.081	3.65	Yes	**Yes**
M1S100	3.9	2	90	3600	380	0.11	3.84	Yes	**Yes**
Water	3.2	2.48	112	7900	270	0.034	4.08	Yes	**Yes**
		2.35		7500	250	0.033	3.97	Yes	**Yes**
		2.28		7300	230	0.032	3.90	Yes	**Yes**
		2.15		6900	210	0.030	3.81	Yes	**Yes**
		1.80		5800	140	0.025	3.47	Yes	**Yes**
		1.57		5000	110	0.022	3.26	Yes	**Yes**
		1.34		4300	80	0.019	3.01	Yes	**Yes**
		1.07		3400	51	0.015	2.67	Yes	**Yes**
		0.88		2800	34	0.012	2.40	Yes	**Yes**
		0.75		2400	25	0.010	2.22	Yes	**Yes**
		0.42		1300	7.8	0.0058	1.67	Yes	No
		0.28		900	3.5	0.0039	1.43	No	No

* Obtained using Mao *et al.*'s model (1997) for D_m^*.
Bold letter implies agreement with prediction.

In Table 5-3, Mao *et al.*'s model's predictions are compared with experimental results for particle-laden drops impacting Teflon® film at impact speeds of 2 and 2.55 m/s. The model predicts that rebounding will occur in all 27 of the particle-laden tests, but in the experiments rebounding occurs in only 14 of them. No modification of model was the made to account for particles; however, Krieger's viscosity was used for computing D_m^* using Mao *et al.*'s model (1997). The failure of the model indicates that the effect of particles on rebounding is due to factors other than viscosity.

Rebounding does not occur for high volume fractions for any particle size. As discussed earlier, at high ϕ, there are sufficient particles present in the thread that their individual motions are restricted and the necking of the thread is slowed; therefore, for ϕ of 0.2 and 0.3, the particle volume fraction was sufficiently high to prevent pinch-off. Rebounding was suppressed for drops containing 6- and 250-µm particles at ϕ as low as 0.1. With the 250-µm particles, the speed on retraction is slowed, which is probably associated with the size of the particles. For these drops at an impact speed of 2 m/s, the ratio of thickness of the drop at D_m^* to the particle size (h_m/d_p) of is approximately 1. The reason rebounding does not occur for the drops containing 6-µm particles at ϕ = 0.1 is not clear, but probably related to the phenomenon observed in Figure 4-11 (a) where some of the 6-µm particles appear to be left behind during retraction when particle-laden drops at ϕ = 0.3 impact on Teflon® film.

Table 5-3. Summary of rebounding of particle-laden liquid on Teflon® film.

Liquid	d (mm)	d_p (μm)	v (m/s)	ϕ	θ	Re	We	Ca	D_m^*	Does rebounding occur?	
										Experimental Result	Mao *et al.*'s prediction
S1	2.7	0.47	2	0	95	5400	160	0..030	3.60	Yes	**Yes**
				0.15		3000	170	0.058	3.40	Yes	**Yes**
Mixture 1	2.9	20	2	0	112	2700	170	0.064	3.20	Yes	**Yes**
				0.05		2400		0.072	3.18	Yes	**Yes**
				0.1		2000		0.083	3.16	Yes	**Yes**
				0.15		1800		0.097	3.10	Yes	**Yes**
				0.2		1500		0.12	3.04	No	Yes
			2.55	0		3400	280	0.081	3.65	Yes	**Yes**
				0.10		2600		0.11	3.52	Yes	**Yes**
				0.20		1900		0.15	3.37	Yes	**Yes**
				0.25		1600		0.18	3.29	Yes	**Yes**
				0.30		1300		0.22	3.20	No	Yes
		40	2	0		2700	170	0.064	3.20	Yes	**Yes**
				0.1		2000		0.083	3.16	Yes	**Yes**
				0.2		1500		0.12	3.04	No	Yes
				0.3		990		0.17	2.88	No	Yes
			2.55	0		3400	280	0.081	3.65	Yes	**Yes**
				0.05		3000		0.092	3.59	Yes	**Yes**
				0.10		2600		0.11	3.52	Yes	**Yes**
				0.15		2200		0.12	3.44	Yes	**Yes**
				0.20		1900		0.15	3.37	Yes	**Yes**
				0.25		1600		0.18	3.29	No	Yes
				0.30		1300		0.22	3.20	No	Yes
M1S100	3.9	6	2	0	90	3600	380	0.11	3.84	Yes	**Yes**
				0.1		2800		0.14	3.71	No	Yes
				0.2		2000		0.20	3.54	No	Yes
				0.3		1300		0.29	3.22	No	Yes
	4.0	40	2	0		3600	380	0.11	3.84	Yes	**Yes**
				0.1		2800	390	0.14	3.72	Yes	**Yes**
				0.2		2000	390	0.20	3.55	Yes	**Yes**
				0.3		1400	390	0.29	3.37	No	Yes
	3.4	250	2	0		3600	380	0.11	3.84	Yes	**Yes**
				0.1		2400	340	0.14	3.58	No	Yes
				0.2		1700	340	0.20	3.41	No	Yes
				0.3		1200	340	0.29	3.24	No	Yes

* Mao *et al.*'s (1997) model is used to get D_m^*.

CHAPTER 6

CONCLUSIONS

The effects of particles on the impact process are discussed in this dissertation. Bouncing and ejection of droplet for low impact speeds are also discussed. The energy balance model for maximum spreading ratio of pure liquid drop is adapted to predict the maximum spreading ratio for particle laden liquid. Also Mao *et al*.'s (1997) model for rebounding is evaluated.

The effect of particle volume fraction on the spreading process depends on impact speed and substrate. At low impact speed, particles have little effect on the spreading except for surfaces where the equilibrium contact angle is low. For this case, the maximum spreading ratio of particle-laden drop is lower than that of pure liquid drop. The liquid spreads to the equilibrium spreading ratio with almost no overshoot for the glass slide and silicon oxide wafer, and with a small overshoot for the Teflon® film (for the 690-μm drop, no overshoot occurs on Teflon® film). For high impact speed, the influence of particles on spreading can largely be described by the effective viscosity: as particle volume fraction is increased, viscosity increases, and Re is decreased; as a result, the particle-laden liquid does not spread as far as pure

liquid.

The effect of particle size on the spreading process also depends on impact speed and substrate. Since spreading is dominated by liquid-surface interfacial energy at low impact speed, the drop does not have enough kinetic energy to overcome the energy barrier associated with the large particles, consequently D_m^* is lower for the drop containing 250-μm particles. The effect of particle size is small for the impact speed of 2 m/s and for $\phi = 0.1$ and 0.2. For all surfaces and $\phi = 0.3$, D_m^* is largest for $d_p = 40$ μm, second largest for $d_p = 250$ μm, and smallest for $d_p = 6$ μm; however, the difference in D_m^* for the glass slide and silicon oxide wafer is small.

For particle-laden liquids, retraction depends on particle volume fraction, ϕ, and ratio of particle diameter to drop diameter, d_p/d. When pure liquid drops retract from D_m^*, the retraction appears to be symmetric around the point of impaction. In contrast, sometimes retraction of the particle-laden drop is asymmetric. The wetted area is not circular and particle distribution appears to be non-uniform. Drops containing 250-μm particles do not retract beyond the equilibrium position even for $\phi = 0.1$ while other drops retract beyond the equilibrium position.

Rebounding on the Teflon® surface depends on impact speed, particle volume fraction and particle size. The impact speed must reach a critical value for rebounding to occur. For 3.2-mm water drops, rebounding is observed at an impact

speed as low as 0.42 m/s. The addition of particle affects rebounding. At low concentrations, the drop stretches further up before a drop is pinched off; however, if particle fraction is increased sufficiently, no rebounding occurs. Particles increase the viscosity of the liquid, and at high ϕ, the viscosity is sufficiently high to prevent pinch-off. At low ϕ, stretching for the particle-laden fluid is greater that of pure liquid and pinch-off can occur at a weak point devoid of particles.

For larger pure liquid drops, Mao *et al.*'s rebounding model (1997) correctly predicts when rebounding occurs; however, it fails for the 690-μm pure liquid drop and for most of the particle-laden drops, especially for high ϕ. The failure of the model indicates that the effect of particles on rebounding are due to factors other than apparent viscosity.

Bouncing results suggest that the probability of bouncing decreases as viscosity increases, impact speed increases, and surface tension decreases. The non-wetting behavior and bouncing probably involves an air layer between the surface and the drop, and further work is needed.

When a low-velocity liquid drop impacts on a surface, ejection of a secondary drop from the top of the impacting drop is sometimes observed. Drop ejection is due to a spreading capillary wave, which is initiated at the impact point and progresses from the bottom of the drop to the top of the drop. The ejected drop eventually falls

due to gravity, impacts on the mother drop which is spread over the surface, and then bounces several times on the mother drop and coalesces with it. During coalescence, the ejected drop sometimes ejects a daughter drop. When Renardy *et al.*'s (2003) criteria for the range of velocities for existence of a capillary wave is applied to for a 3.2-mm water drop, the range is found to be between 0.2 to 1.5 m/s. However, drop ejection was observed at impact speed of 0.08 m/s.

Smaller drops spread faster and reach the equilibrium spreading ratio, D_e^*, sooner than the bigger drops for low and high impact speeds.

When apparent viscosity of the particle-laden liquid obtained from Krieger's equation (1972) was used in the pure liquid models for predicting D_m^*, good agreement between model predictions and experimental results was obtained. For impact speeds of 0.01 m/s and 0.3 m/s, Pasandideh-Fard *et al.*'s (1996) and Mao *et al.*'s (1997) model greatly over estimate D_m^*, especially for the low contact angle; however, Park *et al.*'s model (2003) is in close agreement with the experimental results. For an impact speed of 2 m/s, Mao *et al.*'s (1997) model overestimated some values while Pasandideh-Fard *et al.* (1996) and Park *et al.*'s (2003) models are good agreement with the measured maximum spreading ratio.

CHAPTER 7

RECOMMENDATIONS

The present study is a first attempt to understand the effect of particles on impact process, and many areas are still open for further study.

Almost all of the investigations on the impacting and spreading of liquid drops on solid surfaces have been limited to smooth surfaces. Surface morphology such as roughness and surface energy is important in inkjet printing on textiles. Study of the impacting, spreading, and wicking on textile-like surfaces is needed. The study could use various surfaces with filament yarns mounted on smooth surfaces. The surfaces should have different levels of surface energy, such as nylon, polypropylene, and cellulose acetate. Also, it is suggested that images of real inkjet drops impacting and spreading on real fabrics be taken. The research should lead to a better understanding of the effects of surface roughness on the impacting and spreading process.

As shown in Chapter 4, rebounding behavior can be greatly affected by particles. It may be related with elongational viscosity being lower for higher particle volume fraction. McKinley and Sridhar (2002, 2004) developed a liquid bridge

apparatus which consists of two endplates with liquid between them. The endplates are pulled apart in a constant speed, and the deformation of the liquid stretching can be studied. This technique has been mostly used to study the stretching of complex polymer fluids. Using this technique, the motions of the particles within a stretching liquid column could be studied, as well as particle interactions with the free surface. Even though measuring quantitative values of elongational viscosity is difficult, one can use qualitative values of the particle-laden liquid relative to those of pure liquid. By using qualitative elongational viscosity of particle-laden liquid, effects of ϕ and d_p on drop formation and rebounding might be explained.

APPENDIX A

BASIS FOR USING APPARENT VISCOSITY CALCULATED USING KRIEGER'S EQUATION FOR THE PARTICLE-LADEN LIQUIDS

Reynolds number (Re = $\rho vd/\eta$) is an important dimensionless group in drop impaction studies. Thus, viscosity, η, is needed in calculating this important dimensionless group. For pure liquids, η can be obtained from the literature or by measurement. Determining η for particle-laden liquids is more difficult since it is not available in the literature and measurements of apparent viscosity of particle-laden liquids is difficult. In this dissertation research, viscosity was obtained in two ways. One was measuring the apparent viscosity of the particle-laden liquids using a Brookfield viscometer. The other (referred to as Krieger's viscosity) was by using Krieger's equation (1972). Tests using several particle-laden liquids were conducted to determine which viscosity would be used in presenting the results of this dissertation research. For each particle-laden liquid, two pure liquid mixtures of water and glycerin were made. One had a viscosity that match the measured viscosity, and the other had a viscosity that matched Krieger's viscosity. Impact tests were conducted using the particle-laden liquids and the matching pure liquid mixtures, and D^* versus time (t) plots were made. The purpose of the tests was to determine which method of determining apparent viscosity would give better fits between the plots for the particle-laden liquid and those for the pure liquid. When the plots of the pure liquid drops were compared with those for the particle-laden drops, much better agreement was obtained for the pure liquid drops with viscosities matching Krieger's

viscosity. Comparison of the plots revealed that during spreading, the D^* versus t plots of the pure liquid drops with viscosities matching Krieger's viscosity agreed much closer with those for the particle-laden drops. Based on these results, Krieger's viscosity was used for calculating Re in this dissertation. It should be noted that during retraction from D_m^*, the D^* versus t plots of the particle-laden drops are usually different from those for the pure liquid drops with viscosities obtained by either method. This result indicates that behavior of particle-laden drops during retraction can not be accounted for simply by proper selection of apparent viscosity.

In the tests discussed above, 40-μm particles were used with Mixtures 2 and 3 to produce particle-laden liquids with volume fractions of 0, 0.1, and 0.2. Plots of D^* versus t for the particle-laden drops are compared with those based on measured viscosity in Figure A-1. Note that close agreement was not obtained using measured viscosity.

The 40-μm particles were also used with Mixtures 4, 5, and 6 to produce particle-laden liquids with volume fractions of 0, 0.1, 0.2, and 0.3. Plots of D^* versus t for the particle-laden drops are compared with those based on Krieger's viscosity in Figures A-2 and A-3.

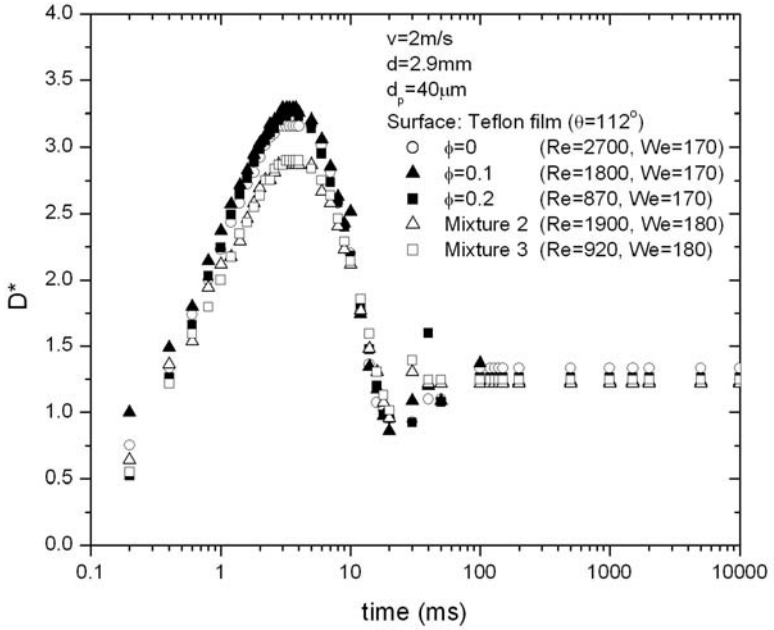

Figure A-1. Comparison of impact process of pure liquid (Mixtures 2 and 3) drops with those of particle-laden (40-μm particles) drops with Re based on measured viscosity. Drops impact at a speed of 2 m/s on Teflon film.

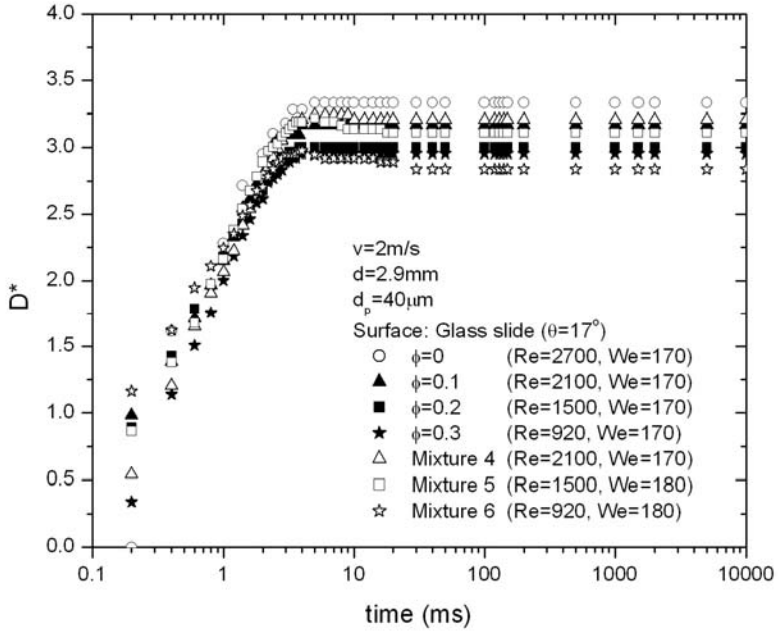

(a) Glass slide

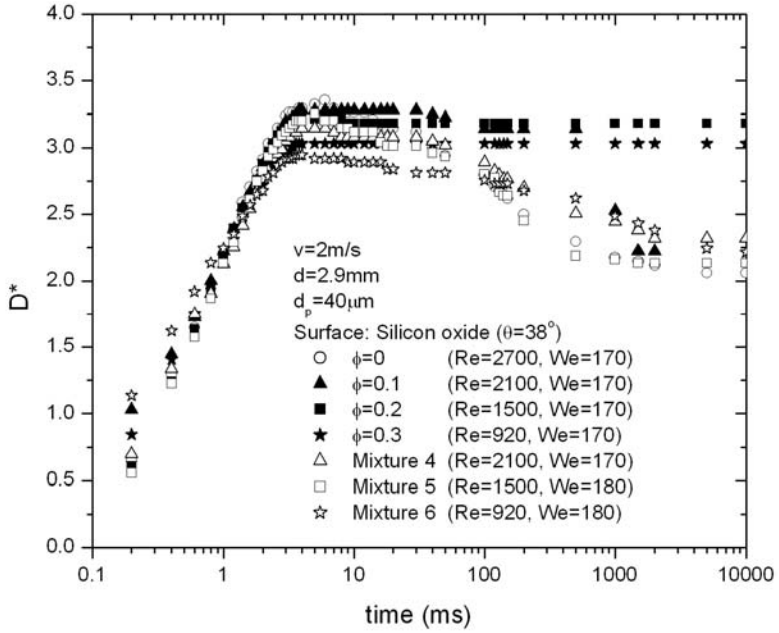

(b) Silicon oxide wafer

Figure A-2. Comparison of impact process of pure liquid (Mixtures 4, 5, and 6) drops with those of particle-laden (40-μm particles) drops with Re based on Krieger's viscosity. Drops impact at a speed of 2 m/s on: (a) glass slide, (b) silicon oxide wafer, and (c) Teflon® film.

Figure A-2. (continued).

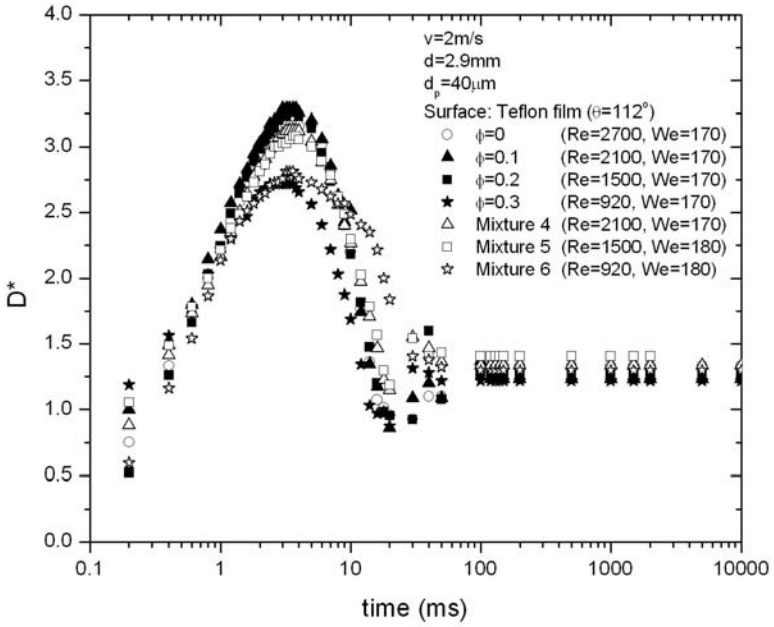

(c) Teflon® film

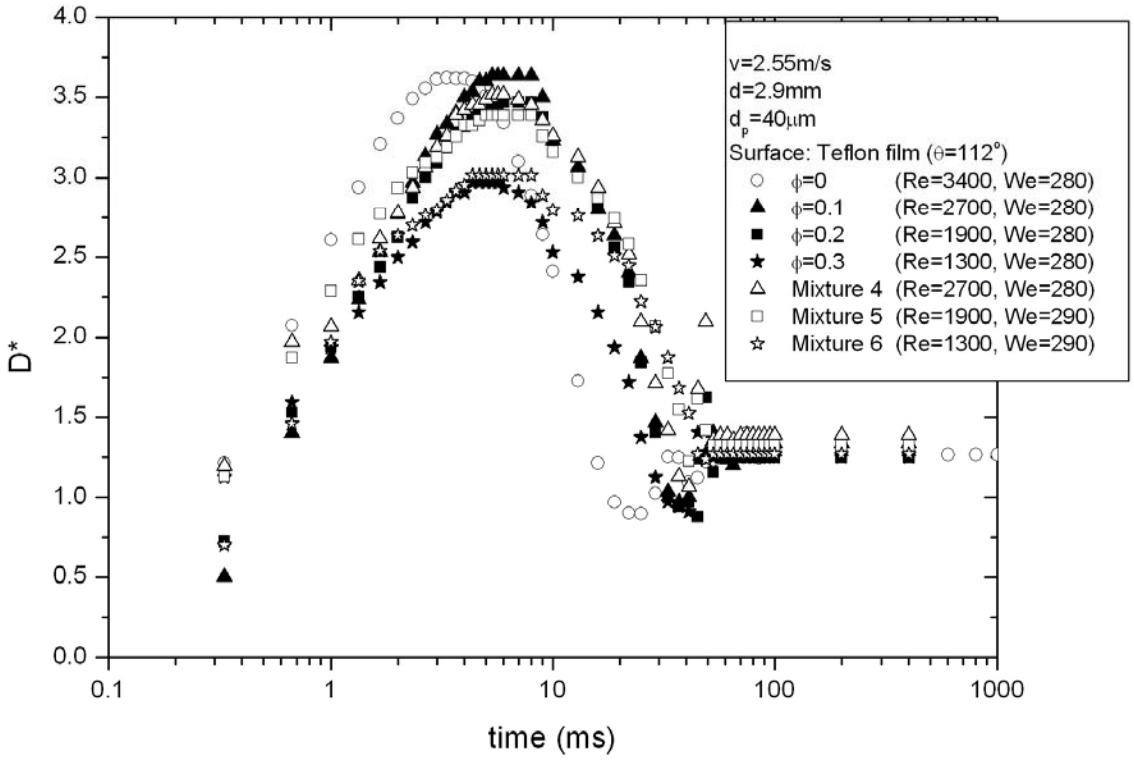

Figure A-3. Comparison of impact process of pure liquid (Mixtures 4, 5, and 6) drops with those of particle-laden (40-μm particles) drops with Re based on Krieger's viscosity. Drops impact at a speed of 2.55 m/s on Teflon® film.

APPENDIX B

SPREADING RATIO VERSUS TIME

In Figure B-1 and 2, spreading ratio, D^*, is plotted against time for a 690-μm drop containing either 20 or 40-μm particles with impact speeds of 0.3 and 2 m/s impacting on three surfaces: glass slide, silicon oxide, and fluorocarbon plasma treated silicon wafer. In Figure B-3 and 5, spreading ratio, D^*, is plotted as a function of time for 2.9-mm drop containing 20-μm particles with impact speeds of 0.01, 1, and 2 m/s impacting on five surfaces: glass slide, silicon oxide wafer, silicon wafer, HMDS coated silicon wafer, and Teflon® film. In Figure B-6 and 7, the plot of spreading ratio, D^*, versus time is for 2.9-mm drop containing 40-μm particles with impact speeds of 0.01 and 2 m/s impacting on five surfaces: glass slide, silicon oxide wafer, silicon wafer, HMDS coated silicon wafer, and Teflon® film. The impact process of particle-laden fluid is illustrated for a drop containing 6-, 40-, and 250-μm particles in M1S100 solution in Figure B-8 to 13. Three surfaces (glass slide, silicon oxide, and Teflon® film) are used, and the impact speed is varied from 0.01 to 2 m/s. In Figure B-14 and 15, D^* is plotted against time for a drop containing 0.47-μm particles impacting on glass slide, silicon oxide wafer, and Teflon® film with impact speed of 0.01 and 2 m/s.

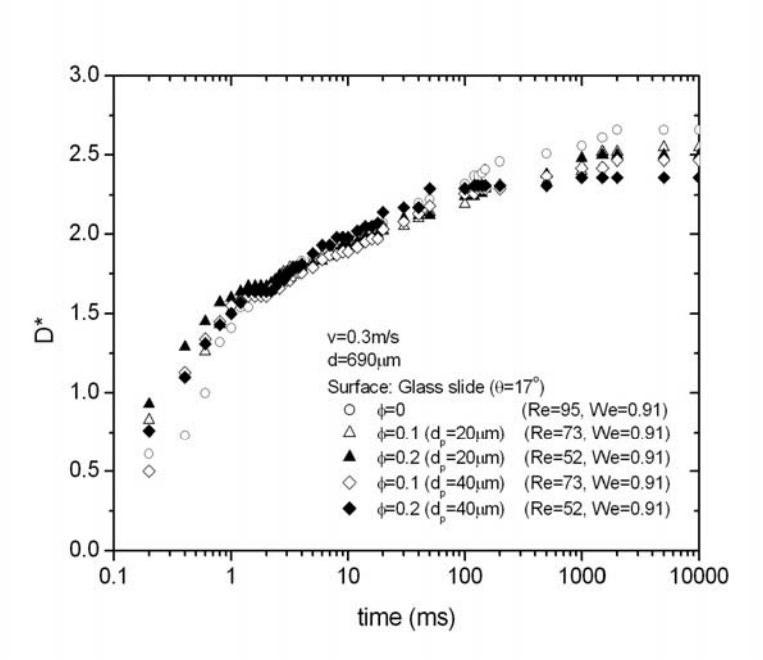

(a) Glass slide

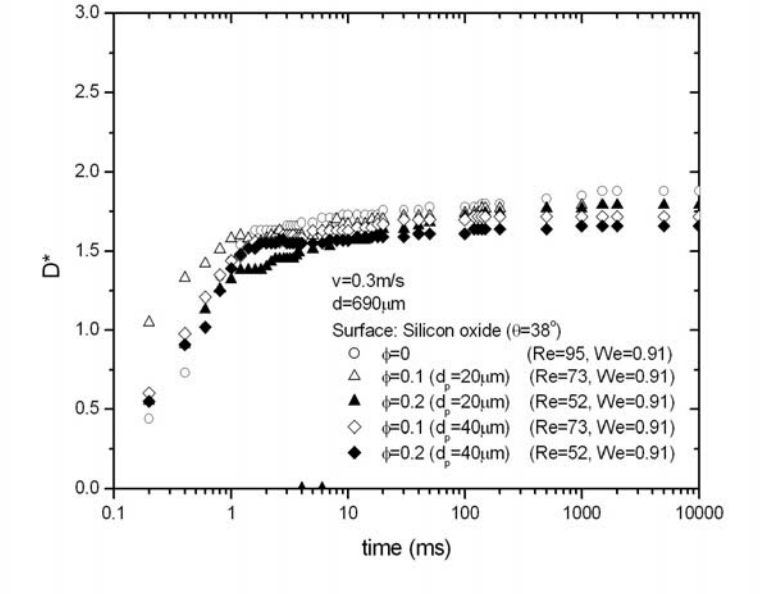

(b) Silicon oxide wafer

Figure B-1. Impact process of particle-laden fluid. The particles were dispersed in Mixture 1, the drop size is 690μm, and the impact speed is about 0.3m/s: (a) glass slide, (b) silicon oxide wafer, and (c) fluorocarbon plasma treated silicon wafer.

Figure B-1. (continued).

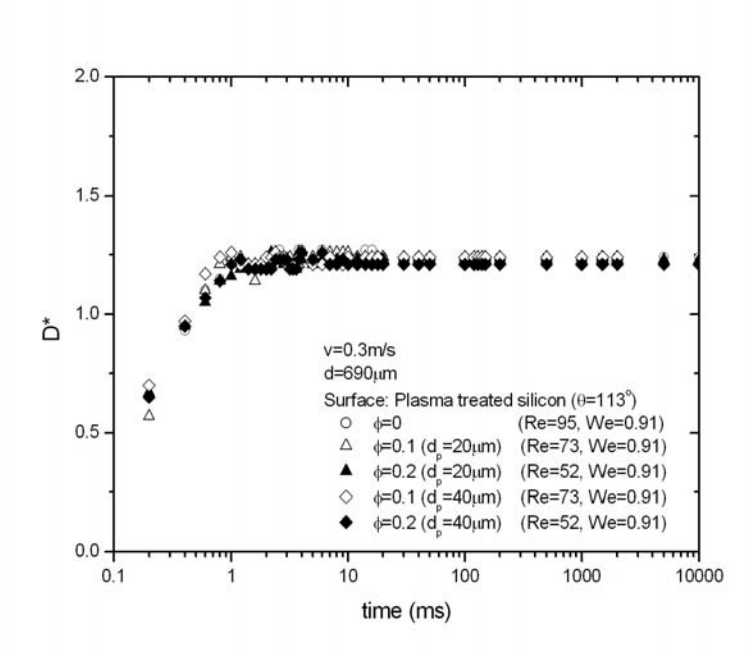

(c) Fluorocarbon plasma treated silicon wafer

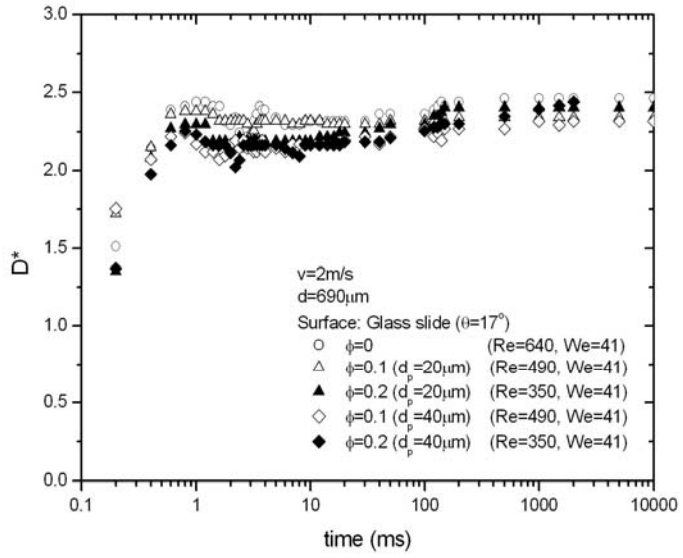

(a) Glass slide

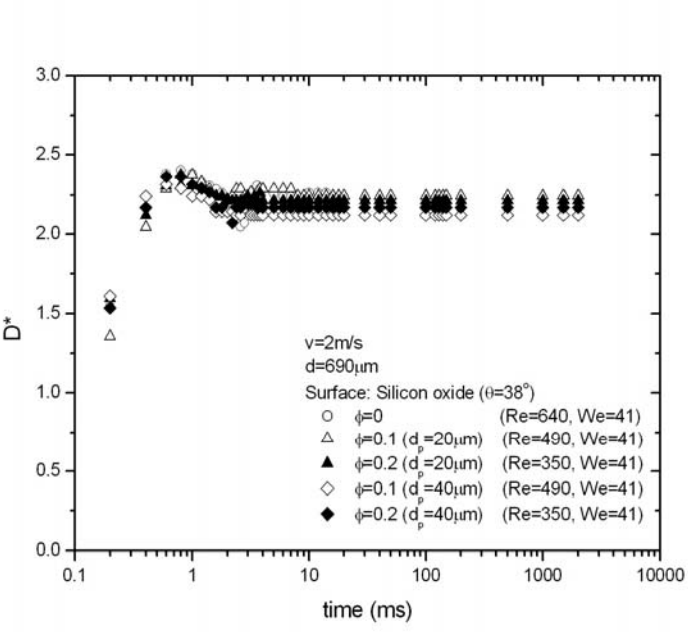

(b) Silicon oxide wafer

Figure B-2. Impact process of particle-laden fluid. The particles were dispersed in Mixture 1, the drop size is 690μm, and the impact speed is about 2m/s: (a) glass slide, (b) silicon oxide wafer, and (c) fluorocarbon plasma treated silicon wafer.

Figure B-2. (continued).

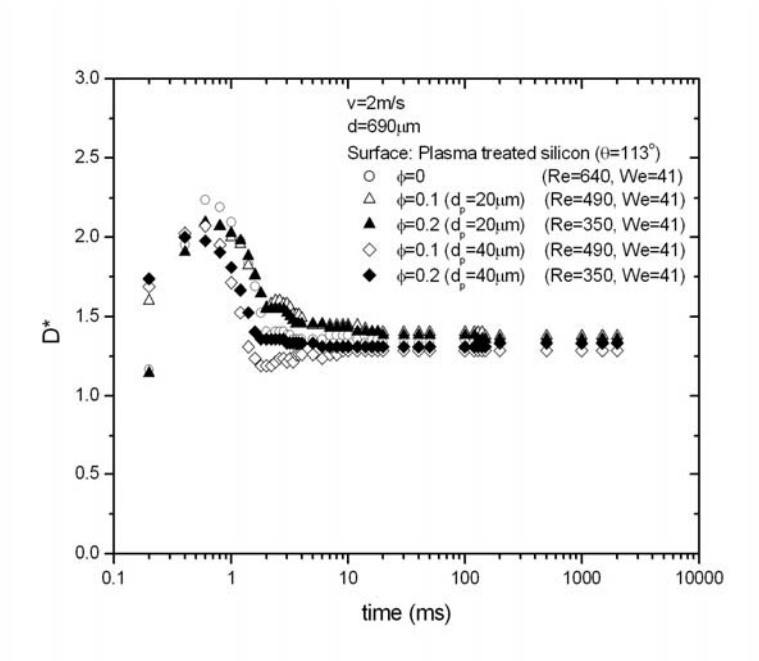

(c) Fluorocarbon plasma treated silicon wafer

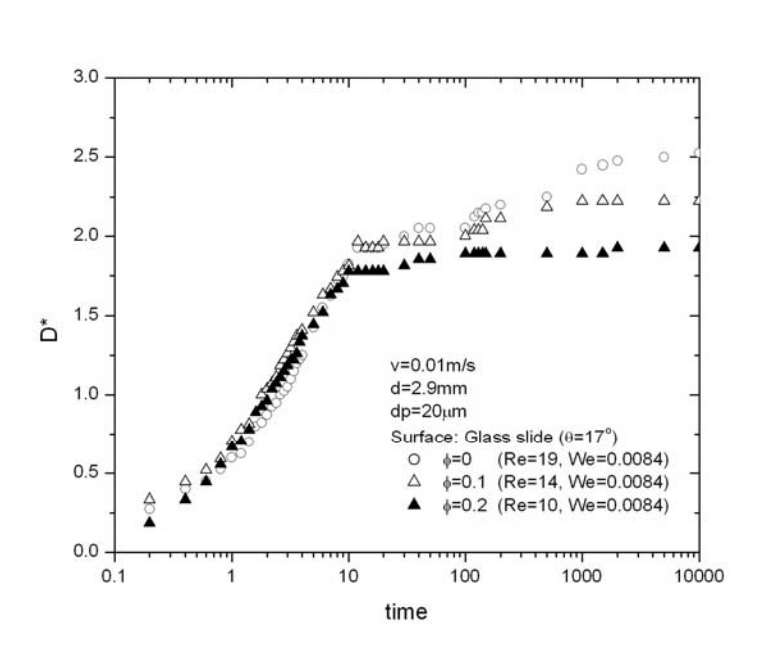

(a) Glass slide

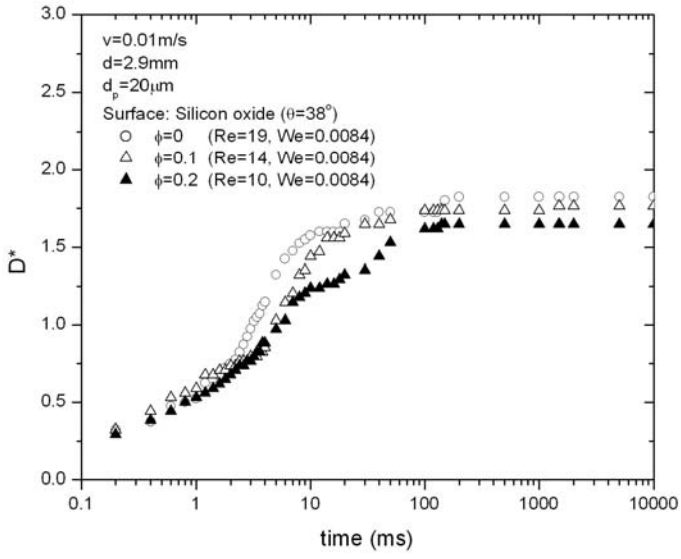

(b) Silicon oxide wafer

Figure B-3. Impact process of particle-laden fluid. The 20-μm particles were dispersed in Mixture 1, the drop size is 2.9mm, and the impact speed is about 0.01m/s: (a) glass slide, (b) silicon oxide wafer, (c) silicon wafer, (d) HMDS coated silicon wafer and (e) Teflon® film.

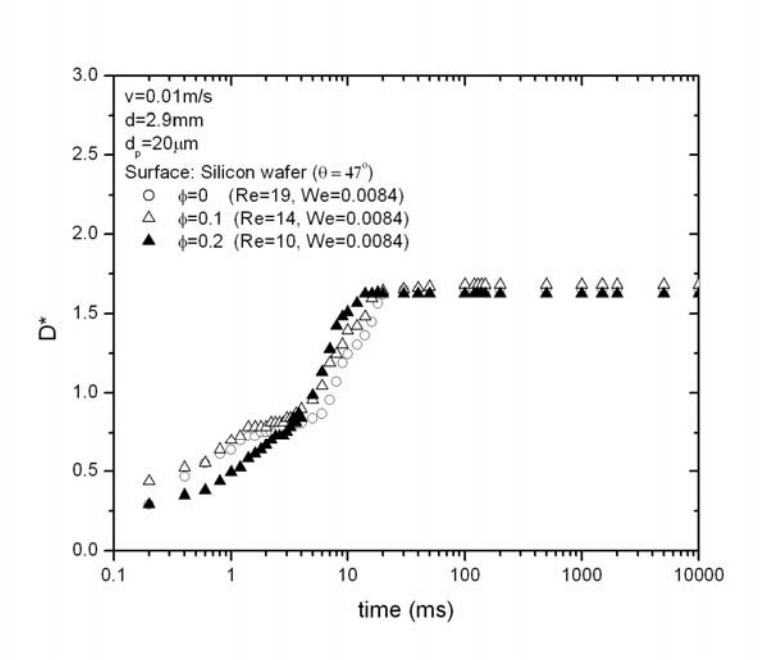

(c) Silicon wafer

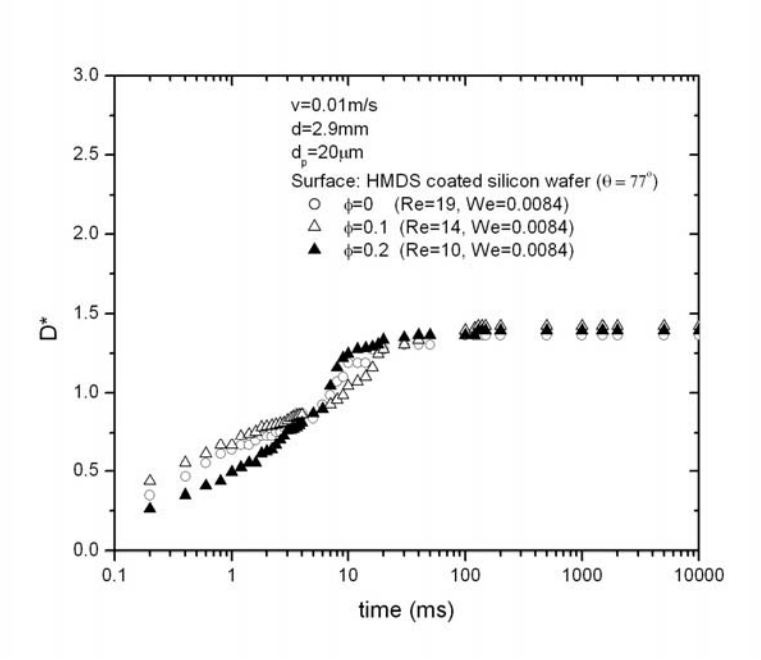

(d) HMDS coated silicon wafer

Figure B-3. (continued).

Figure B-3. (continued).

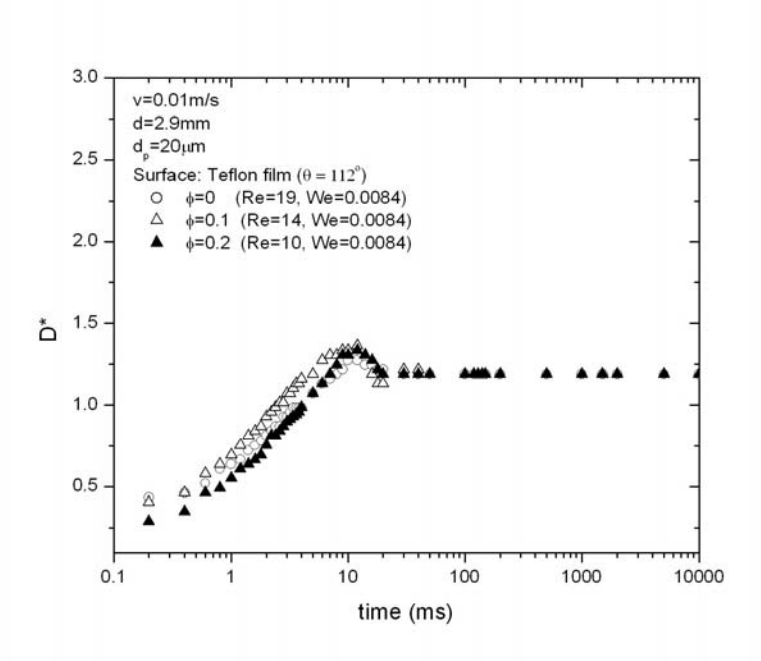

(e) Teflon® film

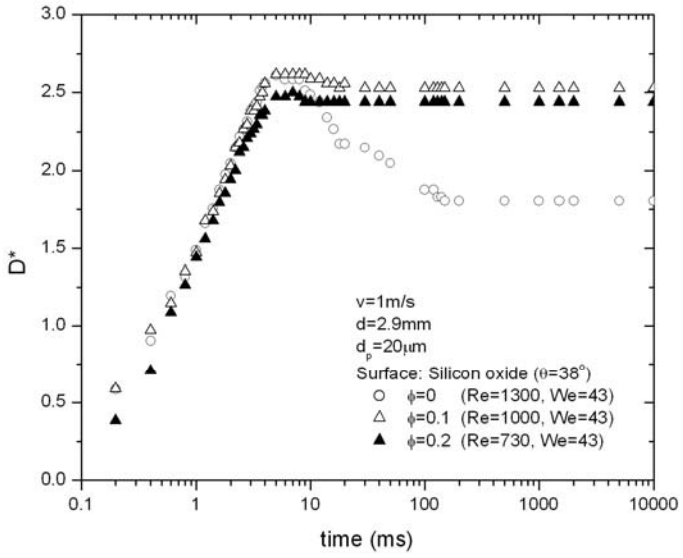

(a) Silicon oxide wafer

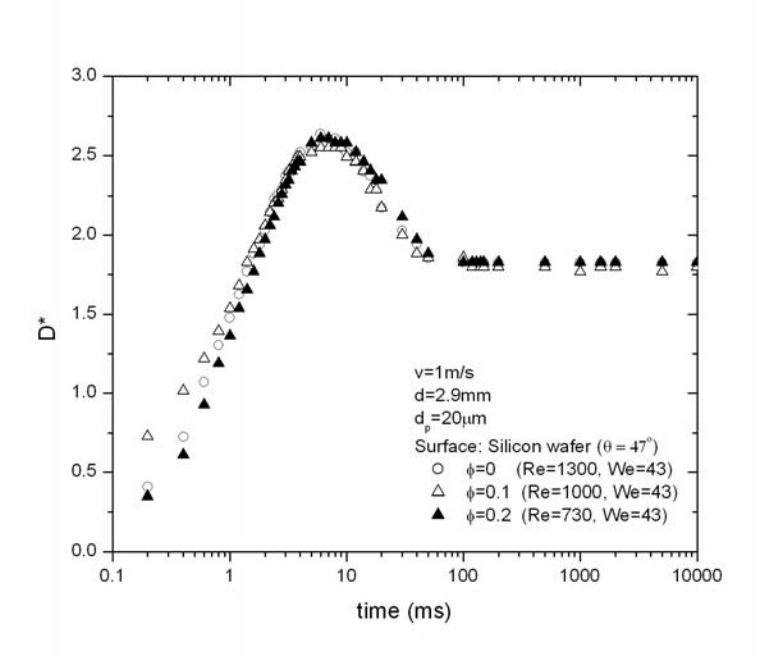

(b) Silicon wafer

Figure B-4. Impact process of particle-laden fluid. The 20-μm particles were dispersed in Mixture 1, the drop size is 2.9mm, and the impact speed is about 1m/s: (a) silicon oxide wafer, (b) silicon wafer, (c) HMDS coated silicon wafer and (d) Teflon® film.

Figure B-4. (continued).

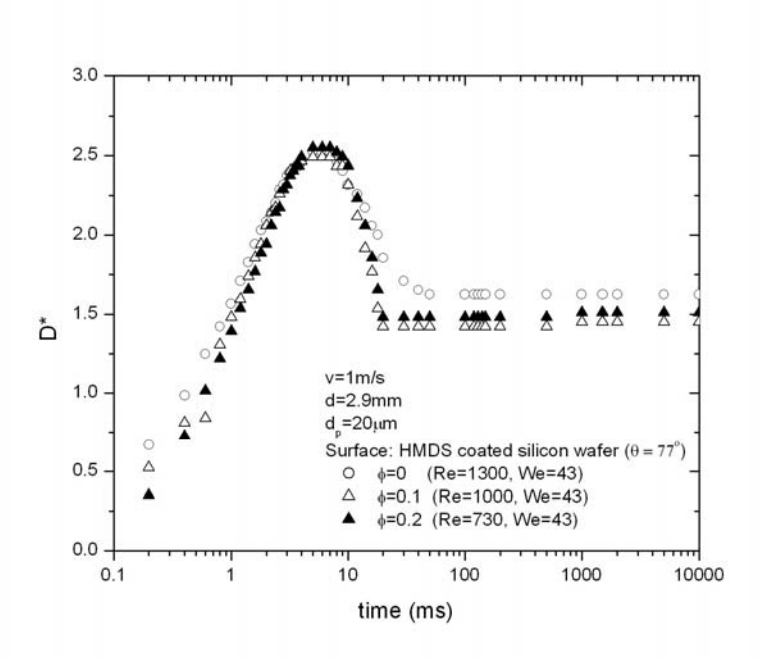

(c) HMDS coated silicon wafer

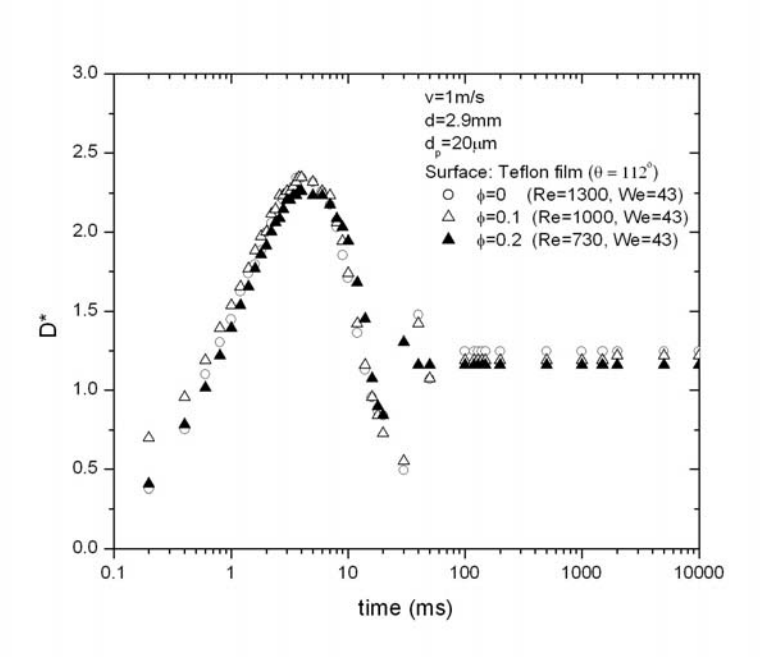

(d) Teflon® film

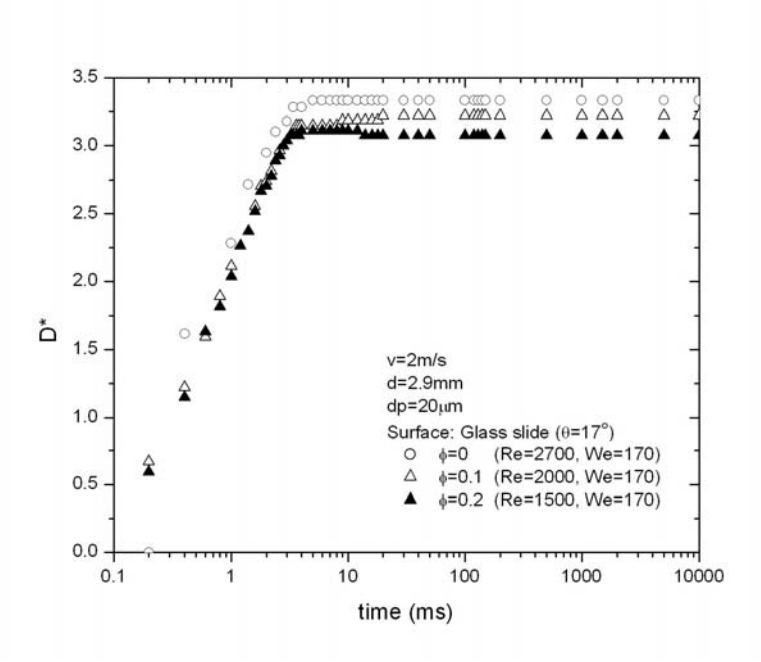

(a) Glass slide

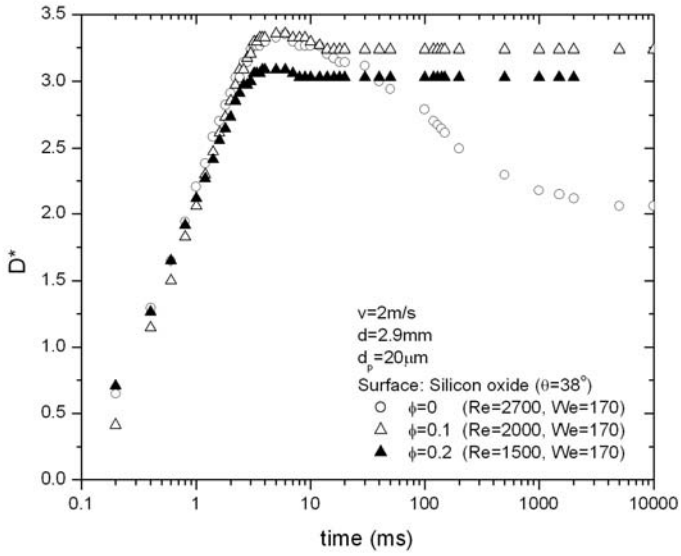

(b) Silicon oxide wafer

Figure B-5. Impact process of particle-laden fluid. The 20-μm particles were dispersed in Mixture 1, the drop size is 2.9mm, and the impact speed is about 2m/s: (a) glass slide, (b) silicon oxide wafer, (c) silicon wafer, (d) HMDS coated silicon wafer and (e) Teflon® film.

Figure B-5. (continued).

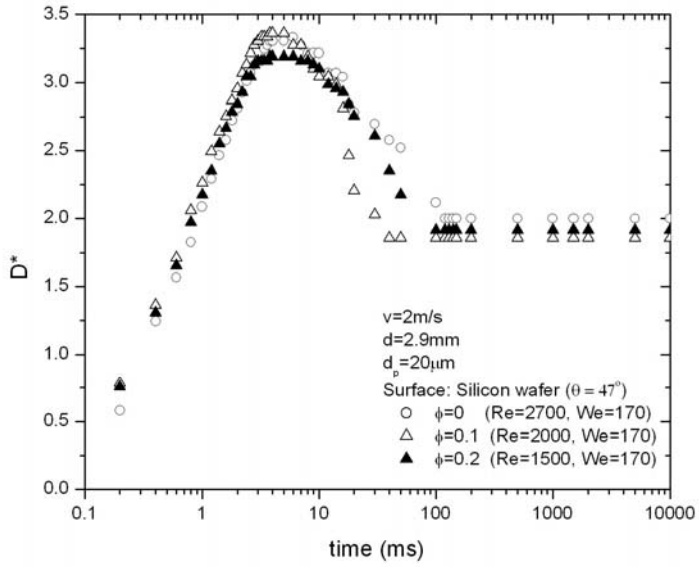

(c) Silicon wafer

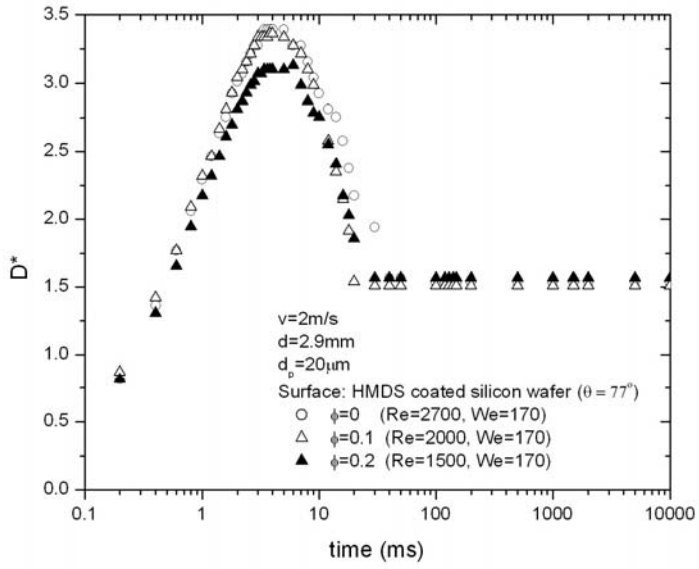

(d) HMDS coated silicon wafer

Figure B-5. (continued).

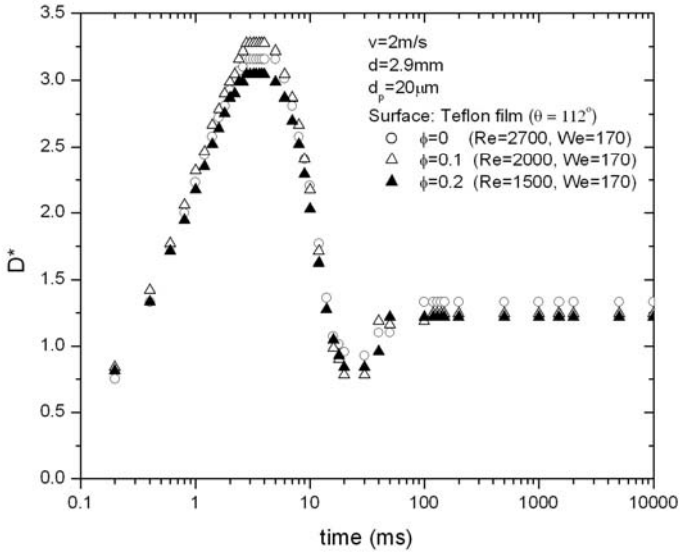

(e) Teflon® film

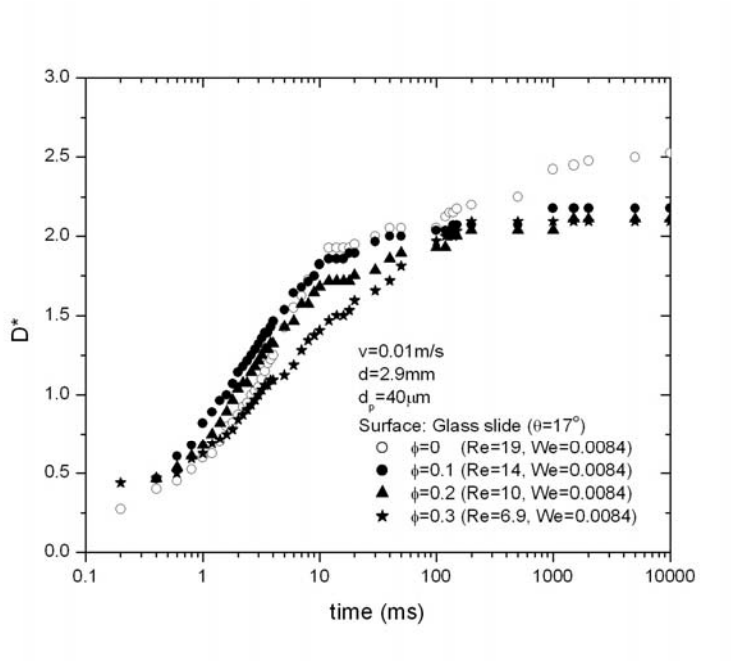

(a) Glass slide

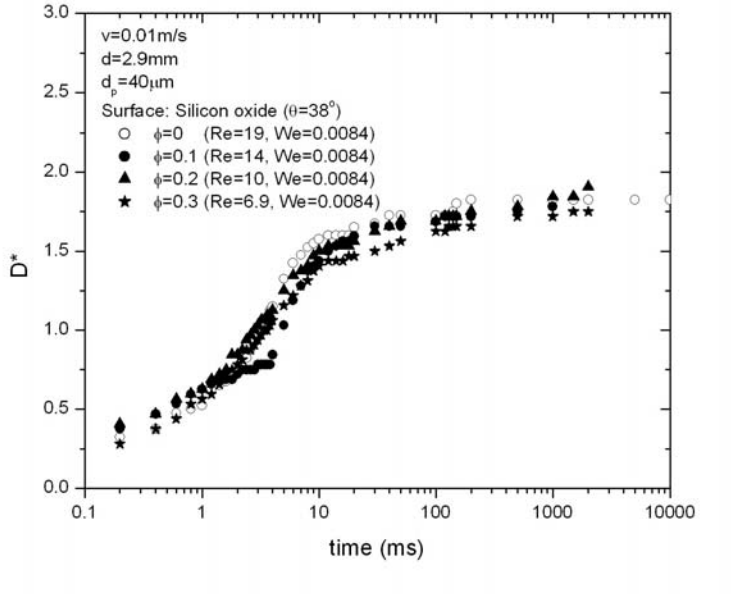

(b) Silicon oxide wafer

Figure B-6. Impact process of particle-laden fluid. The 40-μm particles were dispersed in Mixture 1, the drop size is 2.9mm, and the impact speed is about 0.01m/s: (a) glass slide, (b) silicon oxide wafer, (c) silicon wafer, (d) HMDS coated silicon wafer and (e) Teflon® film.

Figure B-6. (continued).

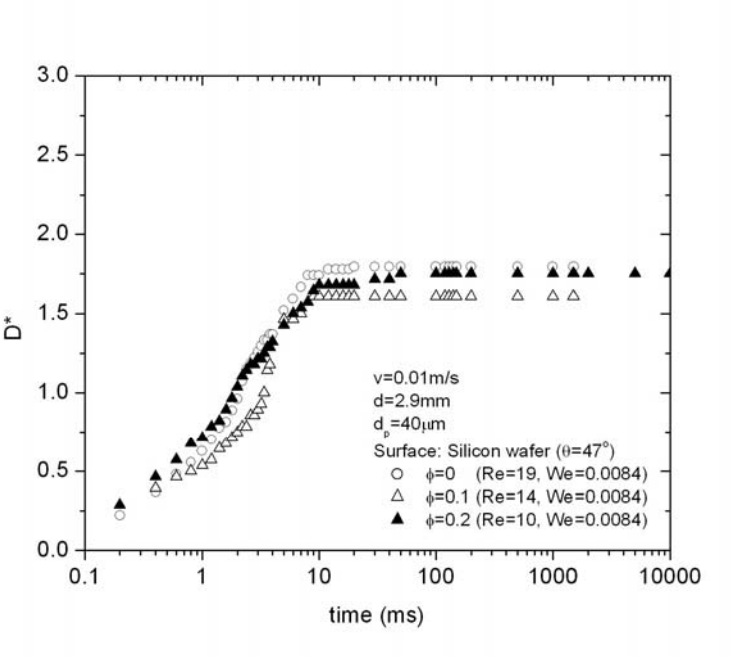

(c) Silicon wafer

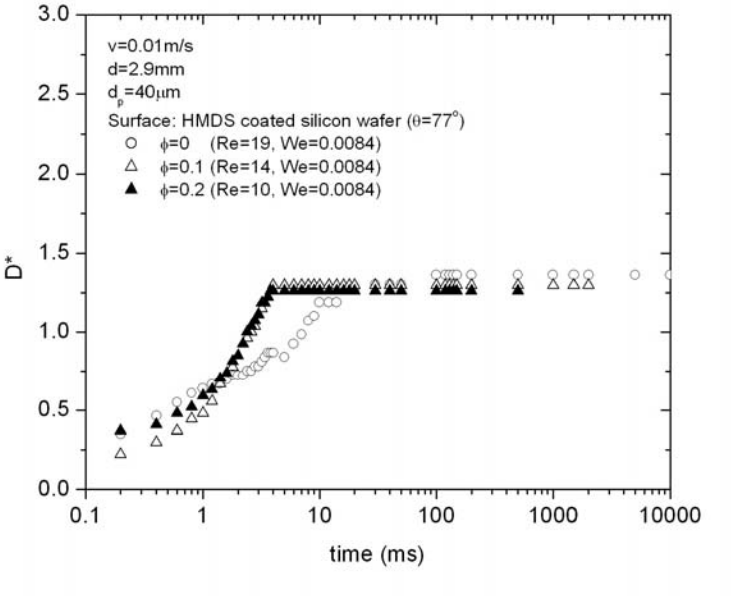

(d) HMDS coated silicon wafer

Figure B-6. (continued).

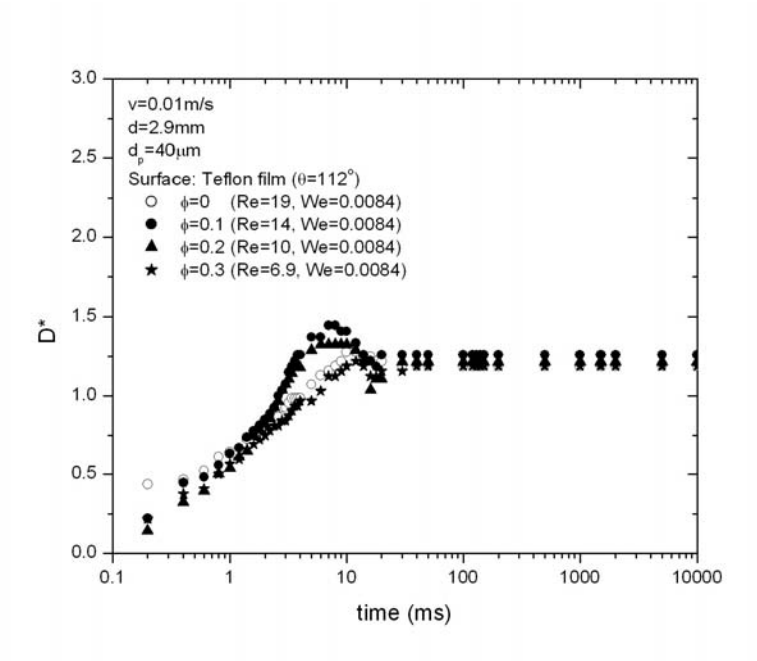

(e) Teflon® film

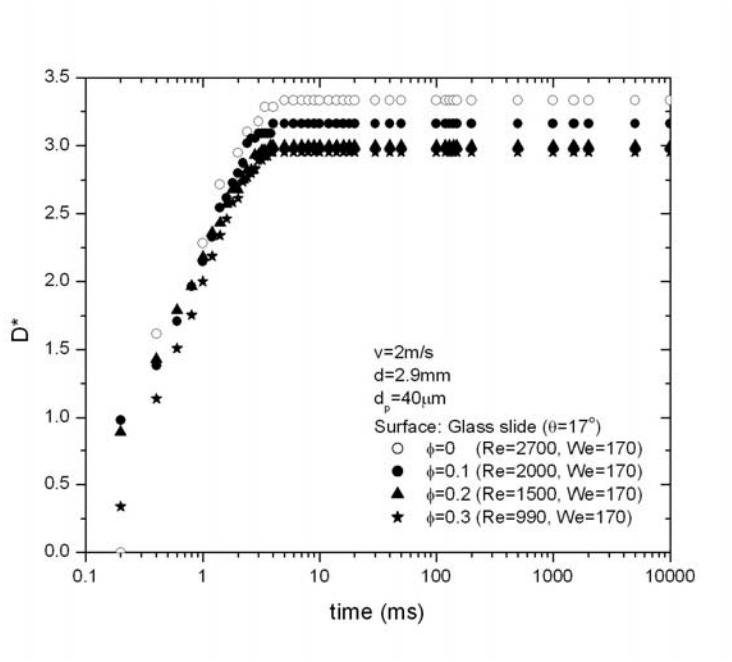

(a) Glass slide

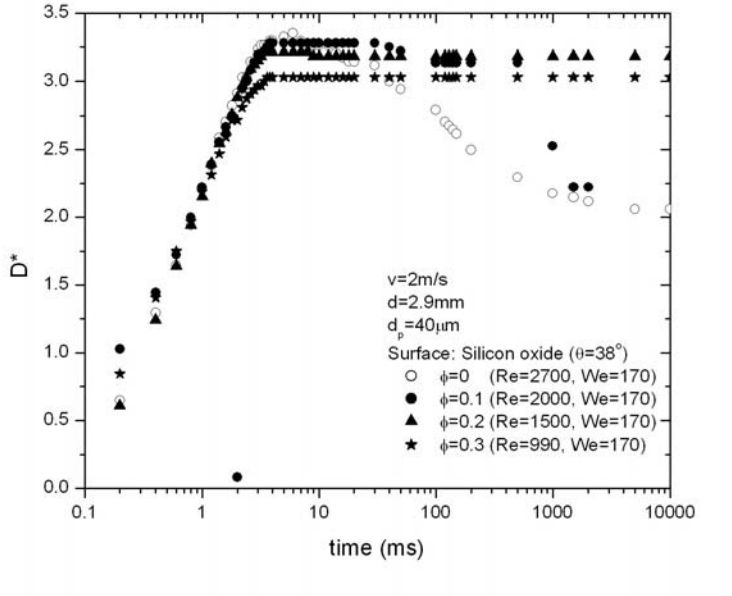

(b) Silicon oxide wafer

Figure B-7. Impact process of particle-laden fluid. The 40-μm particles were dispersed in Mixture 1, the drop size is 2.9mm, and the impact speed is about 2m/s: (a) glass slide, (b) silicon oxide wafer, (c) silicon wafer, (d) HMDS coated silicon wafer and (e) Teflon® film.

Figure B-7. (continued).

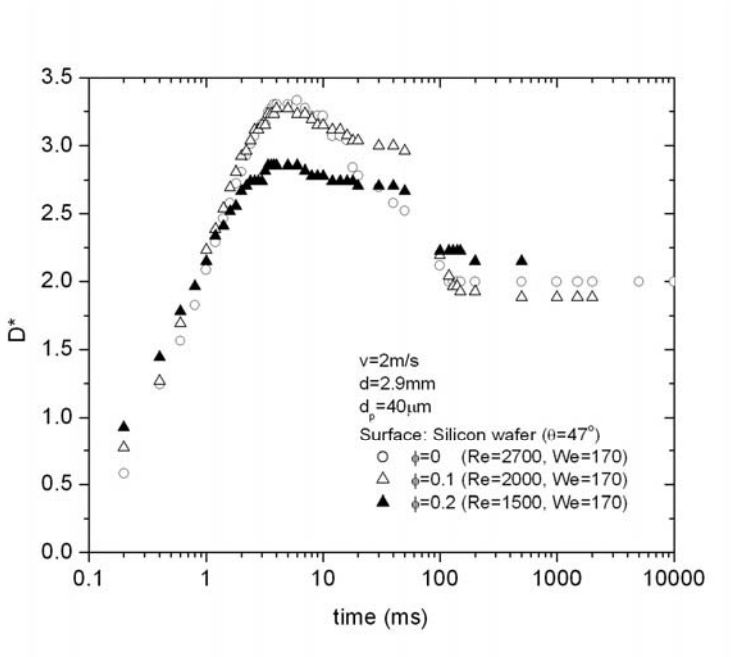

(c) Silicon wafer

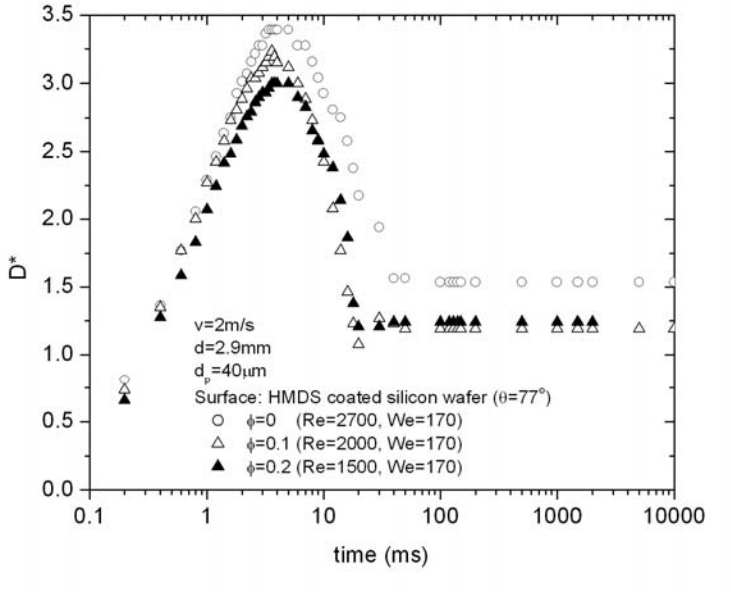

(d) HMDS coated silicon wafer

Figure B-7. (continued).

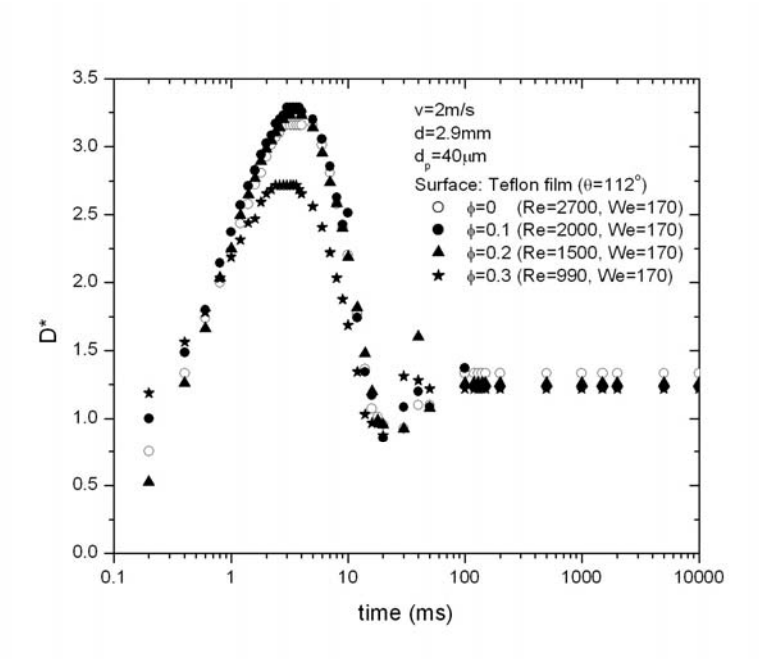

(e) Teflon® film

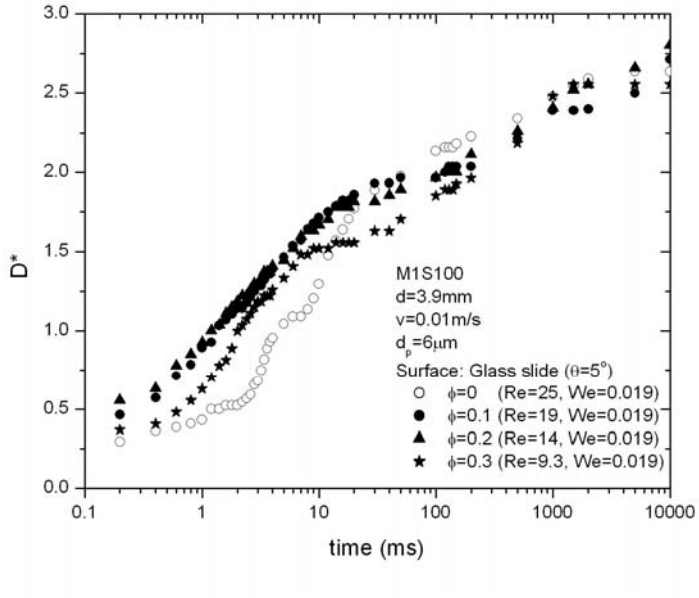

(a) Glass slide

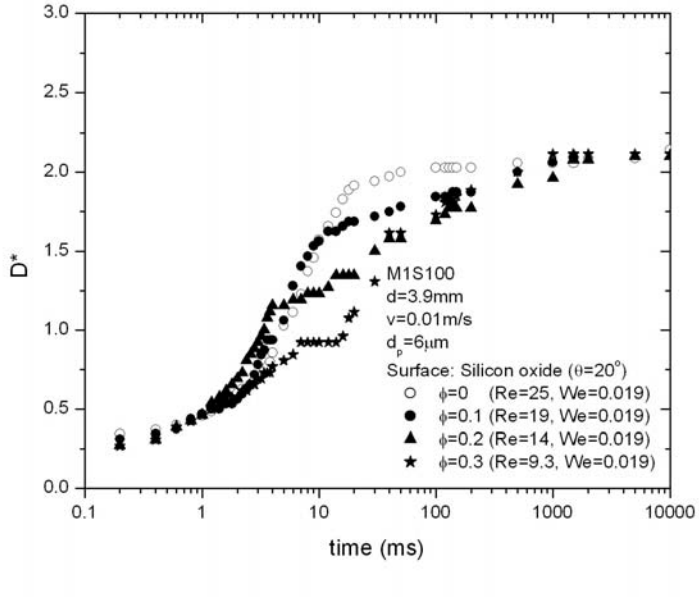

(b) Silicon oxide wafer

Figure B-8. Impact process of particle-laden fluid. The 6-μm particles were dispersed in Mixture 1 with 100ppm surfactant, the drop size is 3.9mm, and the impact speed is about 0.01m/s: (a) glass slide, (b) silicon oxide wafer, (c) Teflon® film.

Figure B-8. (continued).

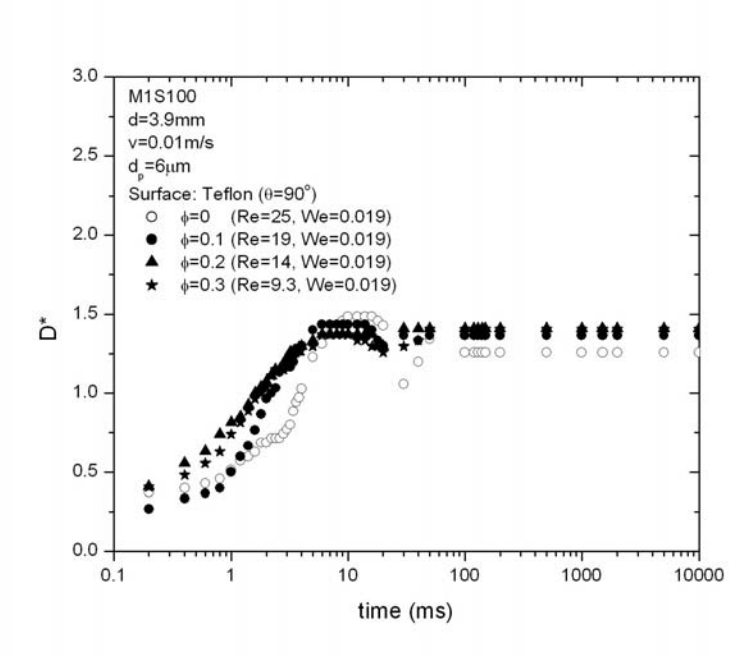

(c) Teflon® film

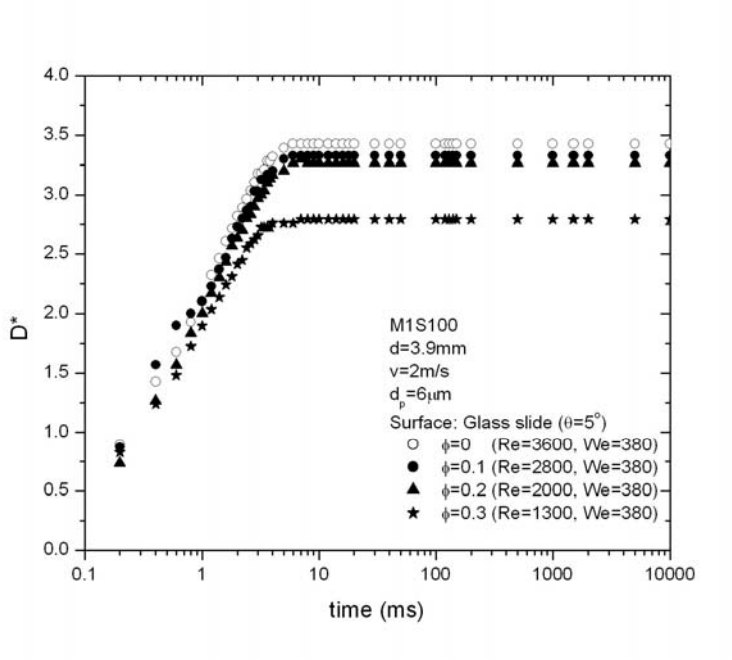

(a) Glass slide

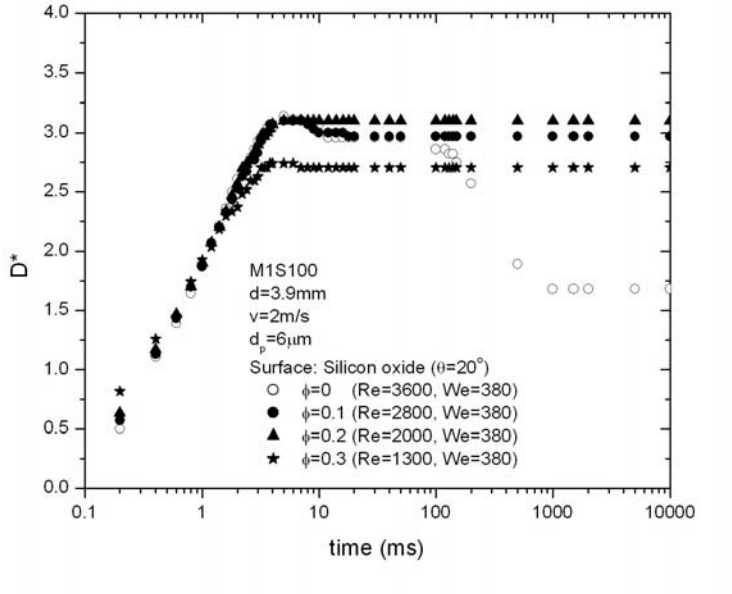

(b) Silicon oxide wafer

Figure B-9. Impact process of particle-laden fluid. The 6-μm particles were dispersed in Mixture 1 with 100ppm surfactant, the drop size is 3.9mm, and the impact speed is about 2m/s: (a) glass slide, (b) silicon oxide wafer, (c) Teflon® film.

Figure B-9. (continued).

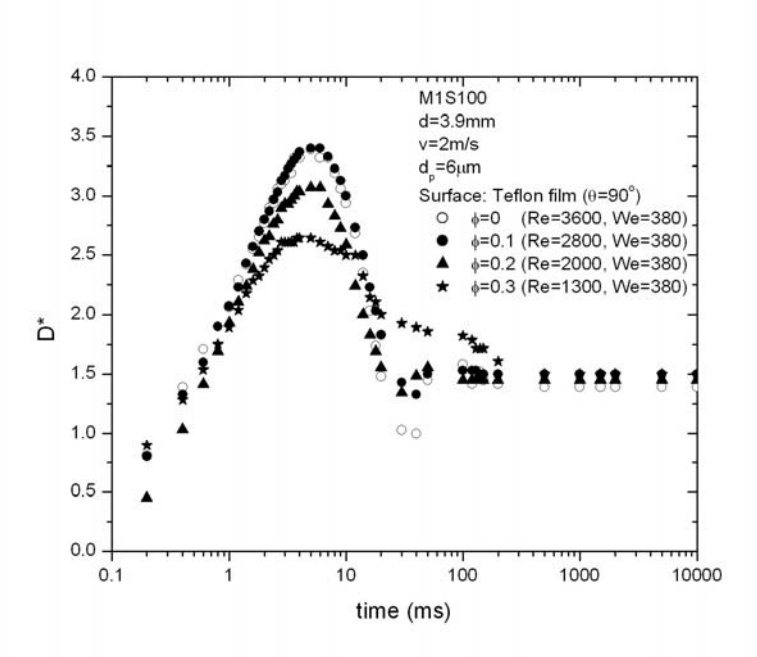

(c) Teflon® film

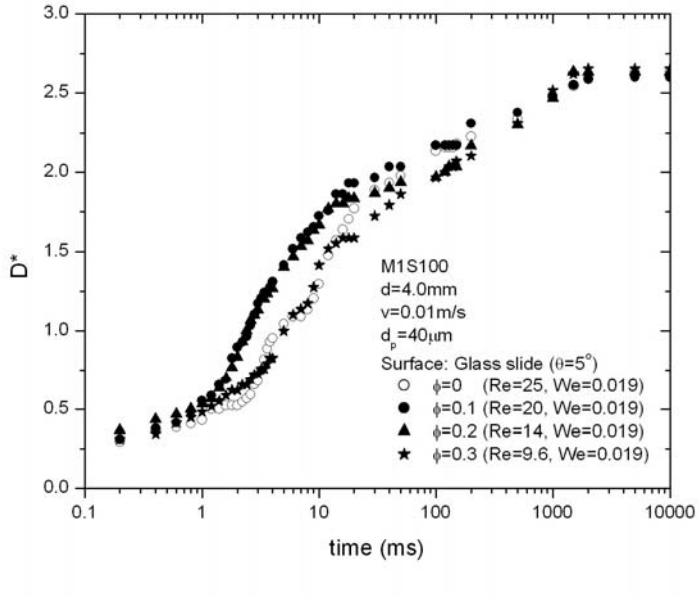

(a) Glass slide

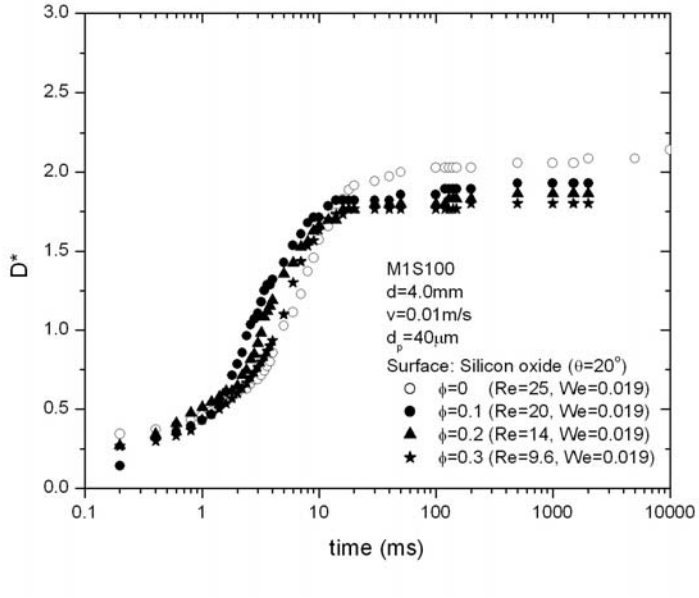

(b) Silicon oxide wafer

Figure B-10. Impact process of particle-laden fluid. The 40-μm particles were dispersed in Mixture 1 with 100ppm surfactant, the drop size is 3.9mm, and the impact speed is about 0.01m/s: (a) glass slide, (b) silicon oxide wafer, (c) Teflon® film.

Figure B-10. (continued).

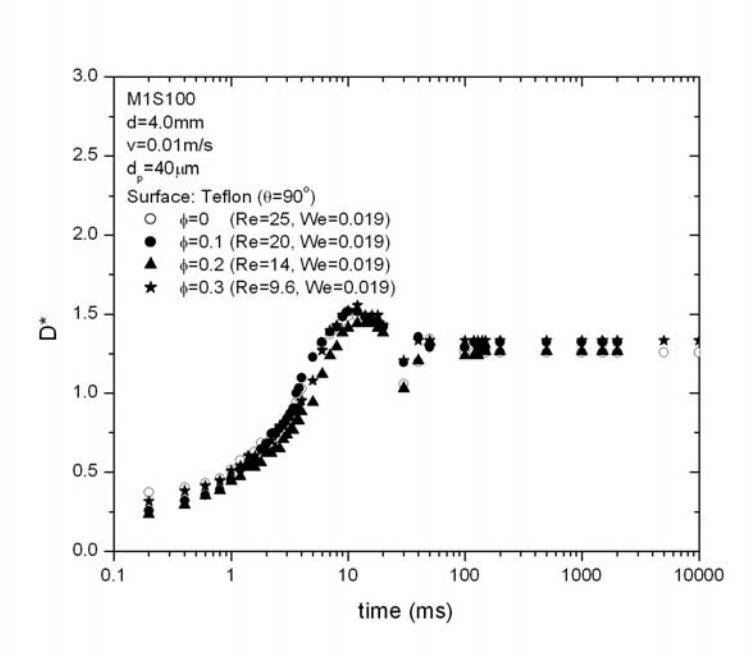

(c) Teflon® film

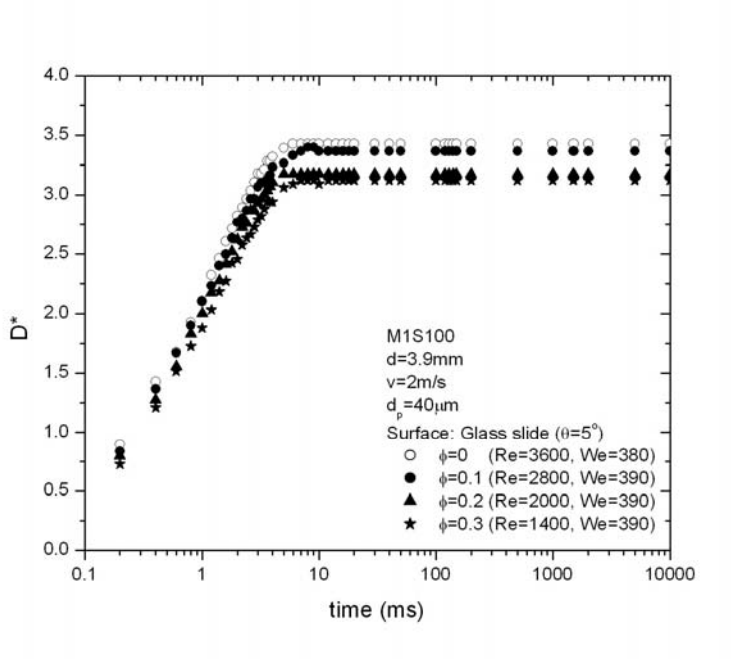

(a) Glass slide

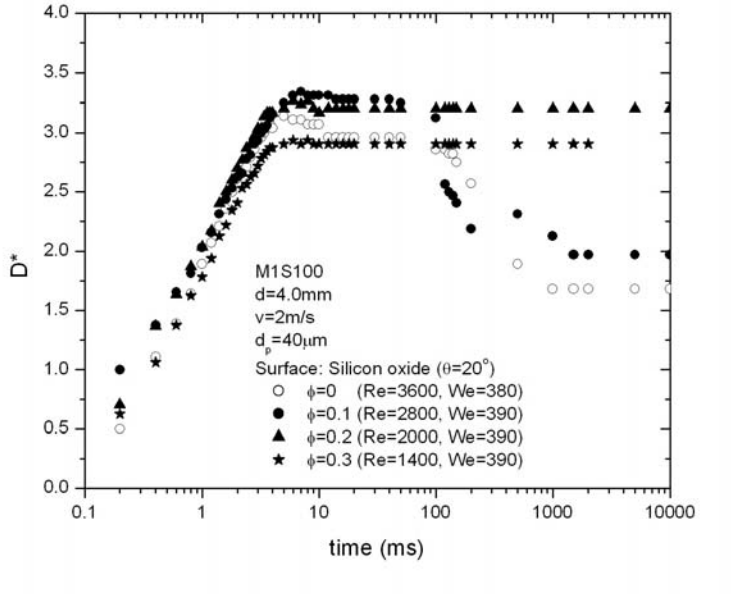

(b) Silicon oxide wafer

Figure B-11. Impact process of particle-laden fluid. The 40-μm particles were dispersed in Mixture 1 with 100ppm surfactant, the drop size is 3.9mm, and the impact speed is about 2m/s: (a) glass slide, (b) silicon oxide wafer, (c) Teflon® film.

Figure B-11. (continued).

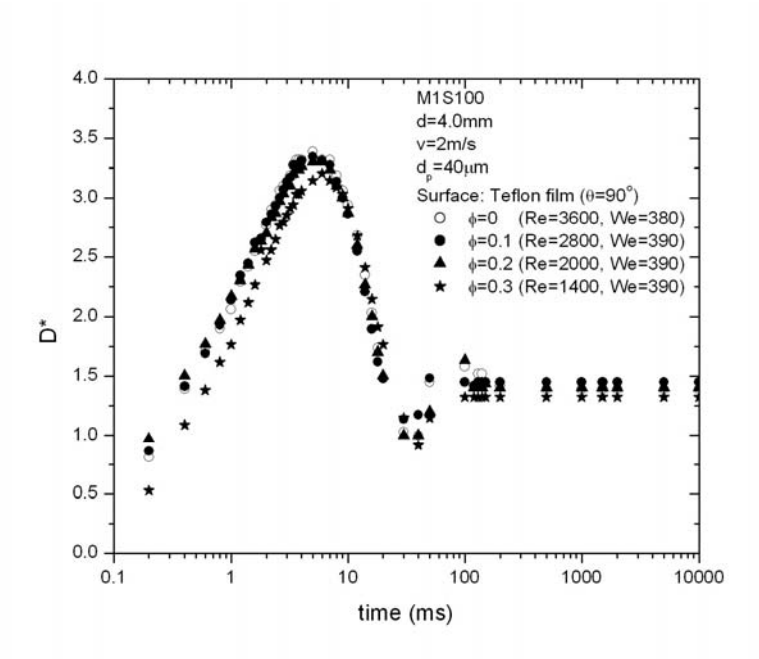

(c) Teflon® film

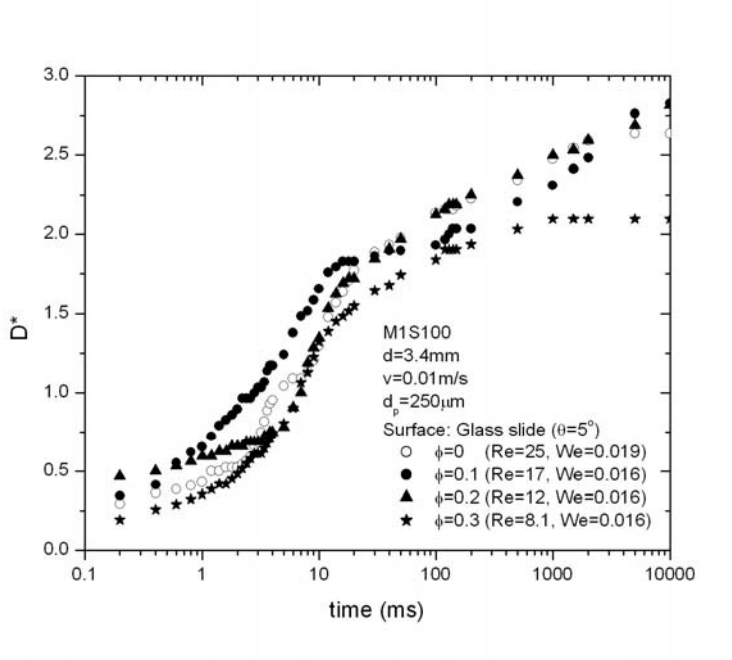

(a) Glass slide

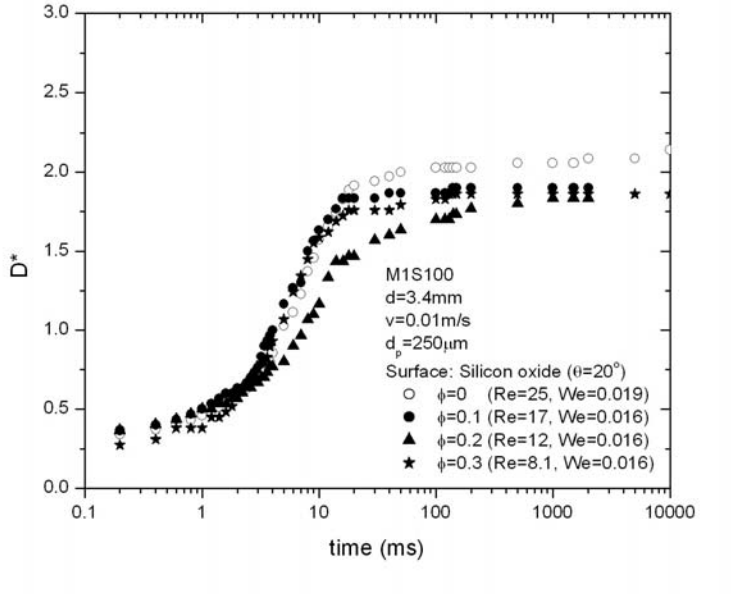

(b) Silicon oxide wafer

Figure B-12. Impact process of particle-laden fluid. The 250-μm particles were dispersed in Mixture 1 with 100ppm surfactant, the drop size is 3.9mm, and the impact speed is about 0.01m/s: (a) glass slide, (b) silicon oxide wafer, (c) Teflon® film.

Figure B-12. (continued).

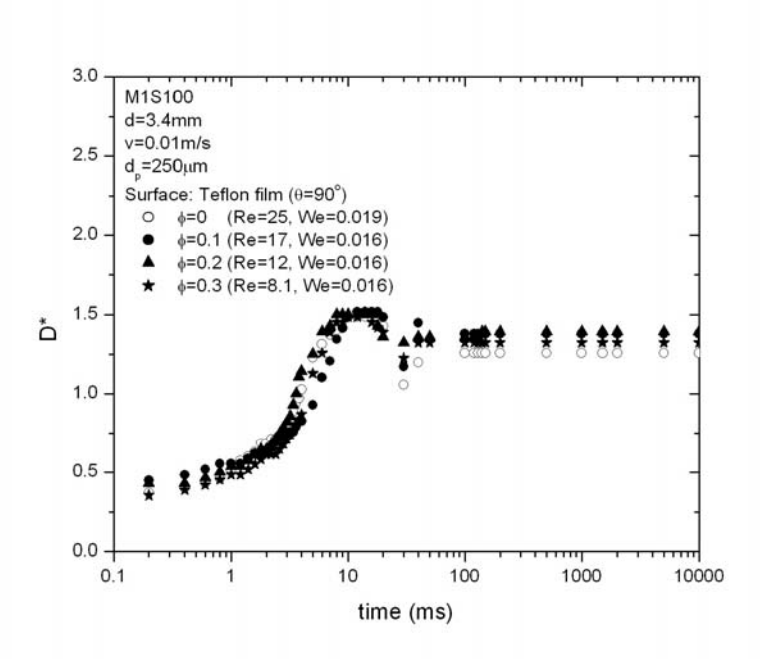

(c) Teflon® film

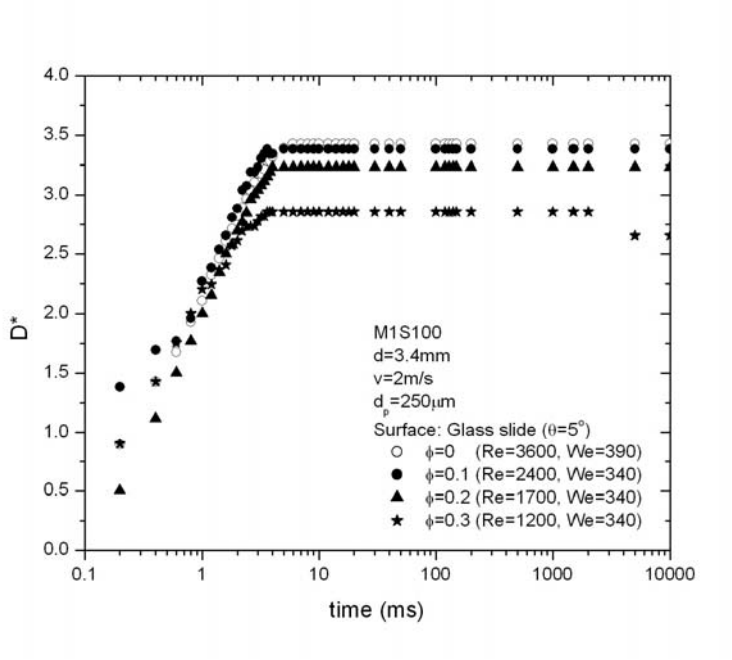

(a) Glass slide

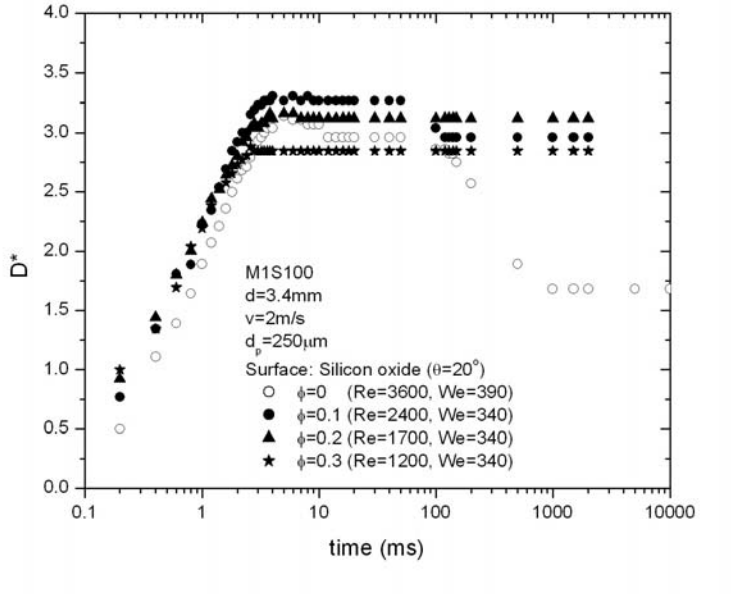

(b) Silicon oxide wafer

Figure B-13. Impact process of particle-laden fluid. The 250-μm particles were dispersed in Mixture 1 with 100ppm surfactant, the drop size is 3.9mm, and the impact speed is about 2m/s: (a) glass slide, (b) silicon oxide wafer, (c) Teflon® film.

Figure B-13. (continued).

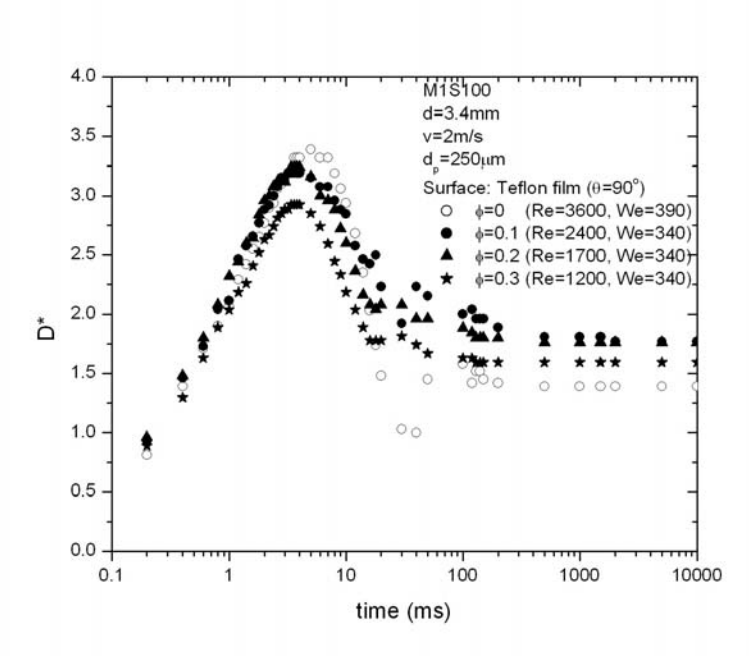

(c) Teflon® film

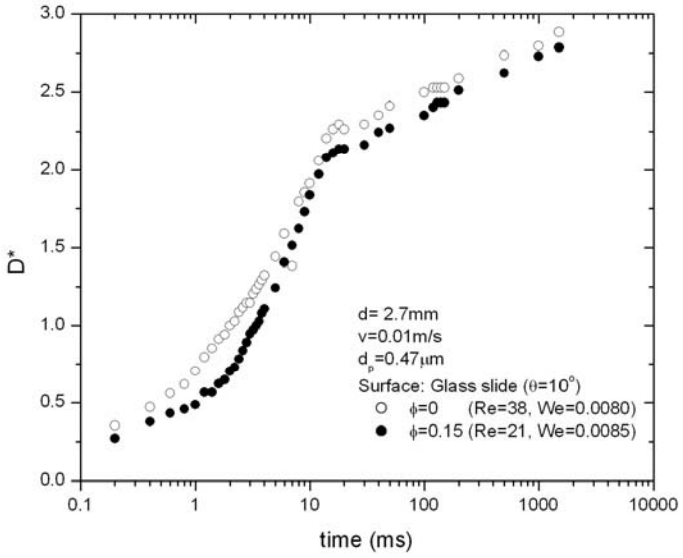

(a) Glass slide

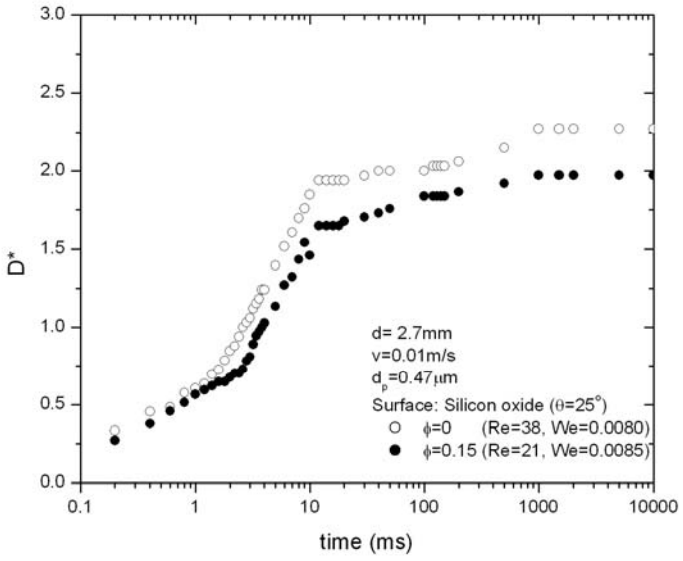

(b) Silicon oxide wafer

Figure B-14. Impact process of particle-laden fluid. The 0.47-μm particle-laden fluid were used, and the impact speed was about 0.01m/s: (a) glass slide, (b) silicon oxide wafer, (c) Teflon® film.

Figure B-14. (continued).

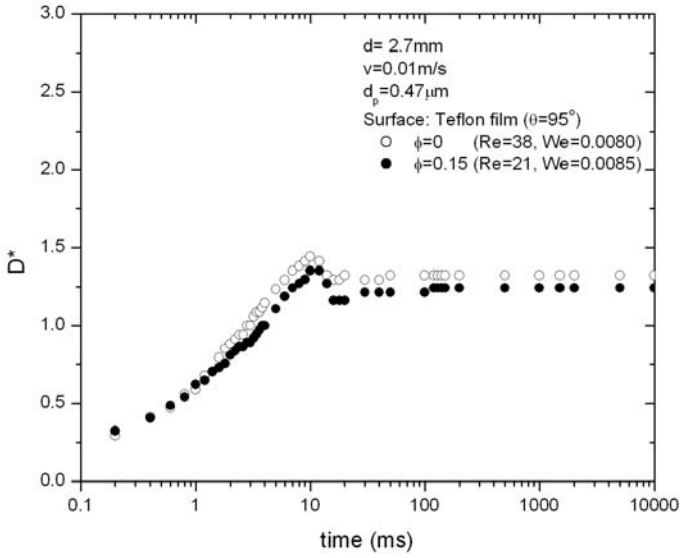

(c) Teflon® film

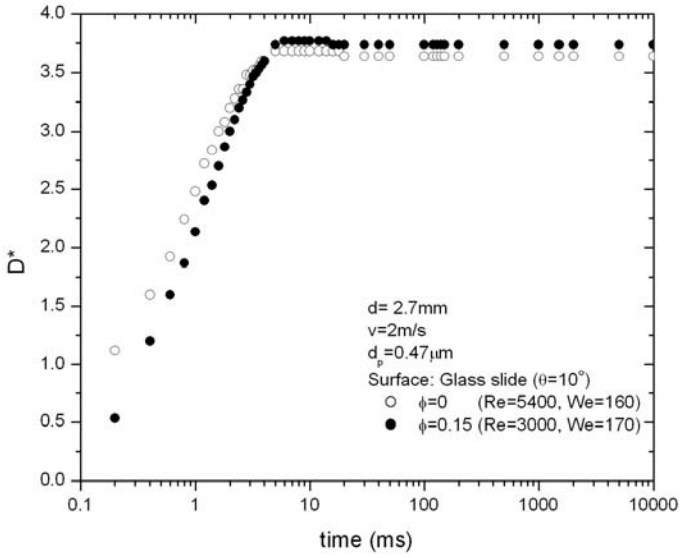

(a) Glass slide

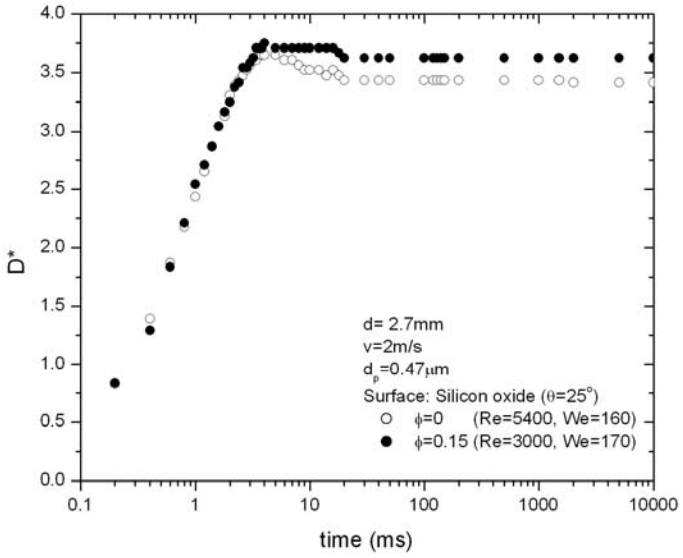

(b) Silicon oxide wafer

Figure B-15. Impact process of particle-laden fluid. The 0.47-μm particle-laden fluid were used, and the impact speed was 2m/s: (a) glass slide, (b) silicon oxide wafer, (c) Teflon® film.

Figure B-15. (continued).

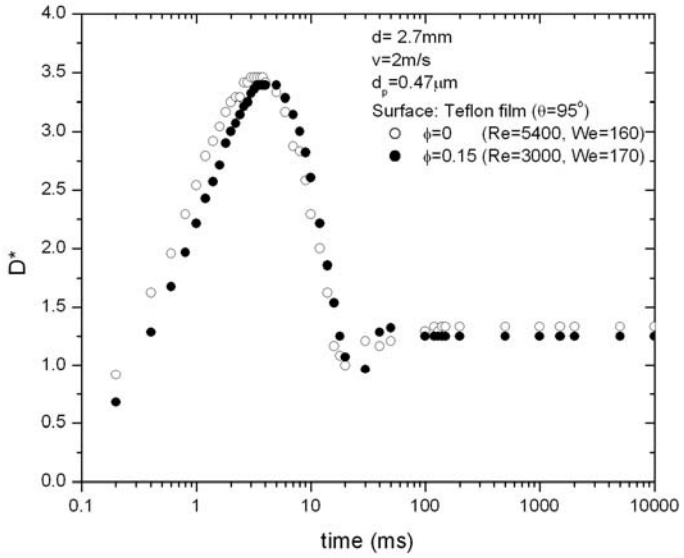

(c) Teflon® film

APPENDIX C

EQUILIBRIUM SPREADING RATIO

When a small drop is placed on a solid surface, it takes the form of a spherical cap with an equilibrium contact angle θ. Ford and Furmidge (1967) derived the spreading ratio of the spherical cap, D_e^*, which can be estimated using the relationship, $D_e^* = \left[\frac{4\sin^3\theta}{2-3\cos\theta+\cos^3\theta}\right]^{\frac{1}{3}}$. The calculated D_e^* is plotted against equilibrium contact angle in Figure C-1. The calculated D_e^* for the surfaces used in this study are shown in Table C-1 through C-3.

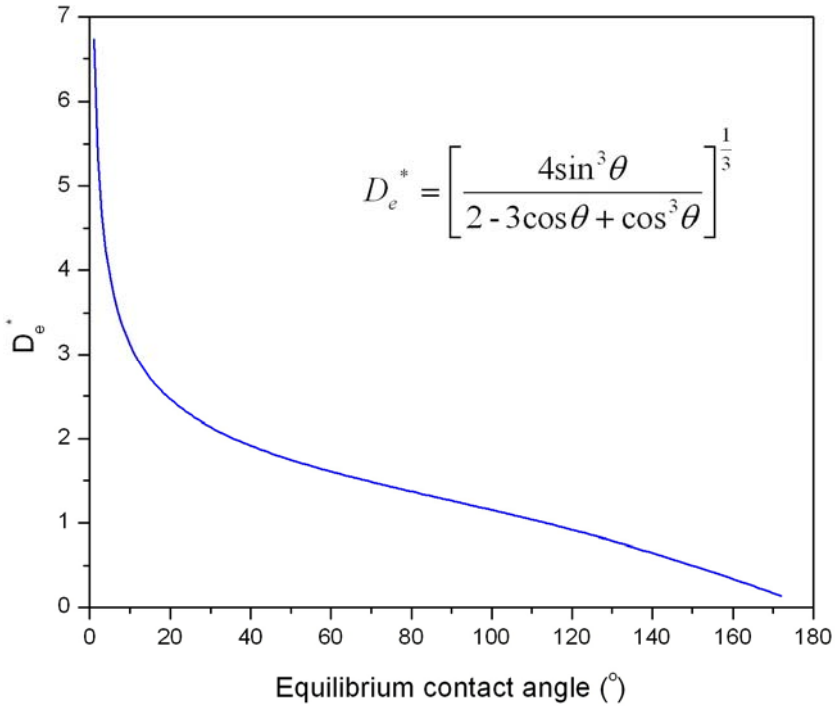

Figure C-1. The calculated D_e^* versus equilibrium contact angle (Ford and Furmidge 1967).

Table C-1. Equilibrium contact angle of distilled water on surfaces and calculated equilibrium spreading ratio

Surface	Contact angle (^{o})	Calculated D_e^*
Glass slide	17	2.6
Silicon oxide wafer	38	1.95
Silicon wafer	47	1.8
Teflon® film	112	1.0

Table C-2. Equilibrium contact angle of distilled water containing 100ppm surfactant and calculated equilibrium spreading ratio.

Surface	Contact angle (^{o})	Calculated D_e^*
Glass slide	5	3.9
Silicon oxide wafer	20	2.5
Teflon® film	90	1.3

Table C-3. Equilibrium contact angle of 0.47μm-polystyrene solution and calculated equilibrium spreading ratio.

Surface	Contact angle (^{o})	Calculated D_e^*
Glass slide	10	3.1
Silicon oxide wafer	25	2.3
Teflon® film	95	1.2

APPENDIX D

EFFECT OF PARTICLE SIZE ON IMPACT PROCESS

The effect of particle size on impact process is shown in Figure D-1 through 6. Three surfaces (glass slide, silicon oxide wafer, and Teflon® film) are used. The drop contains either 6-, 40-, or 250-μm particles, and the volume fractions are varied from 0.1 to 0.3.

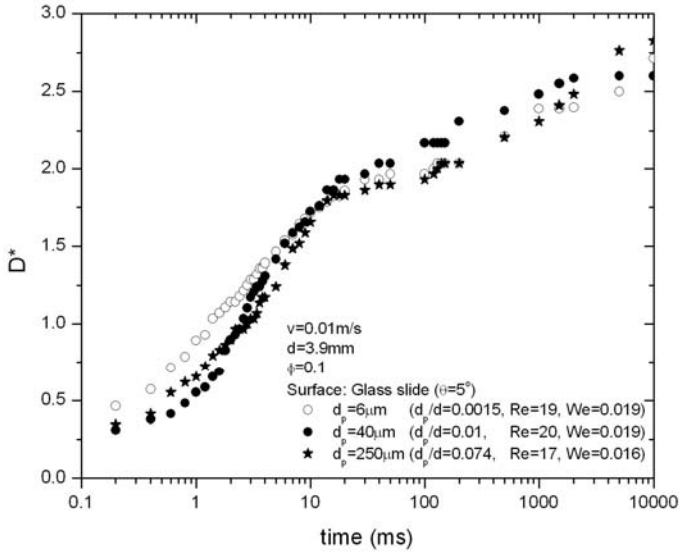

(a) Glass slide

Figure D-1. Effect of particle size on impact. The drop size is 3.9mm with $\phi = 0.1$ and the impact speed is about 0.01 m/s: (a) glass slide, (b) silicon oxide wafer, (c) Teflon® film.

Figure D-1. (continued).

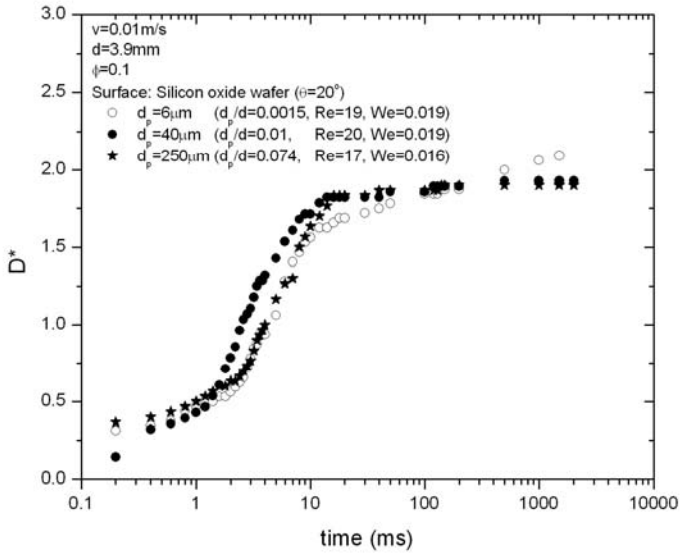

(b) Silicon oxide wafer

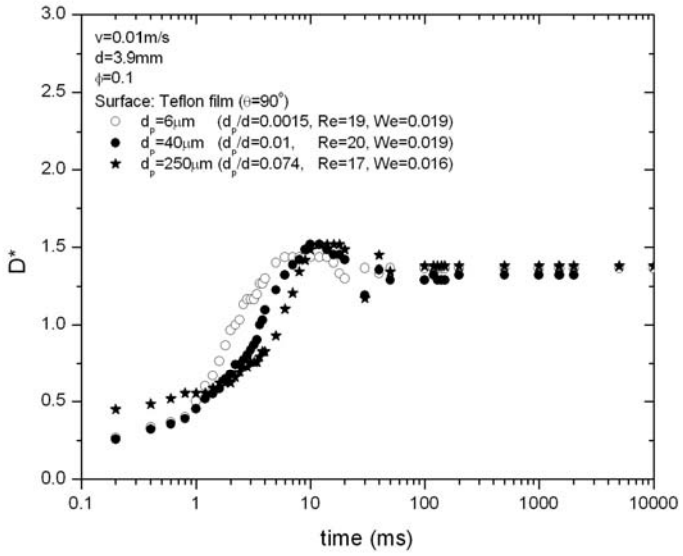

(c) Teflon® film

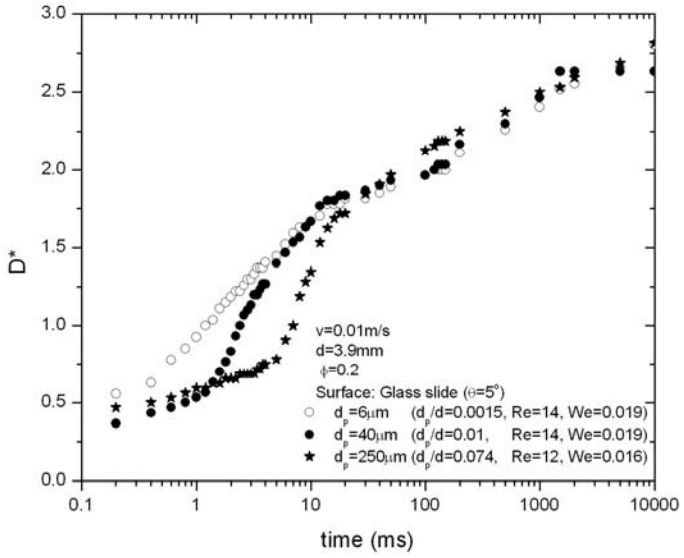

(a) Glass slide

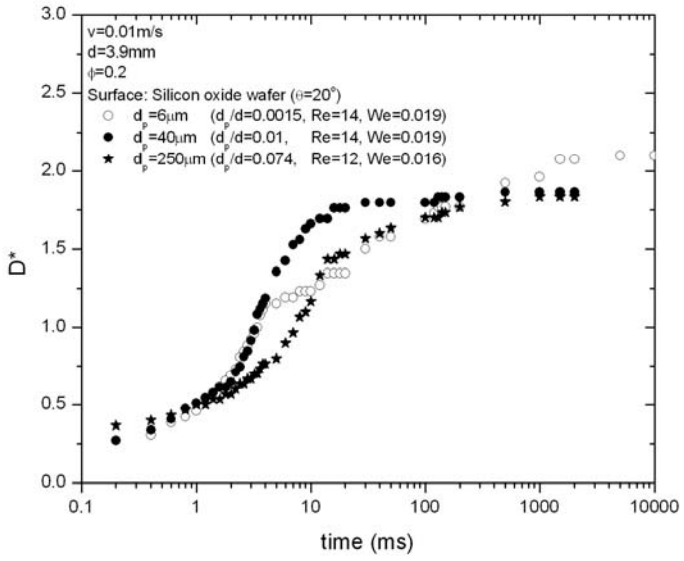

(b) Silicon oxide wafer

Figure D-2. Effect of particle size on impact. The drop size is 3.9mm with $\phi = 0.2$ and the impact speed is about 0.01 m/s: (a) glass slide, (b) silicon oxide wafer, (c) Teflon® film.

Figure D-2. (continued).

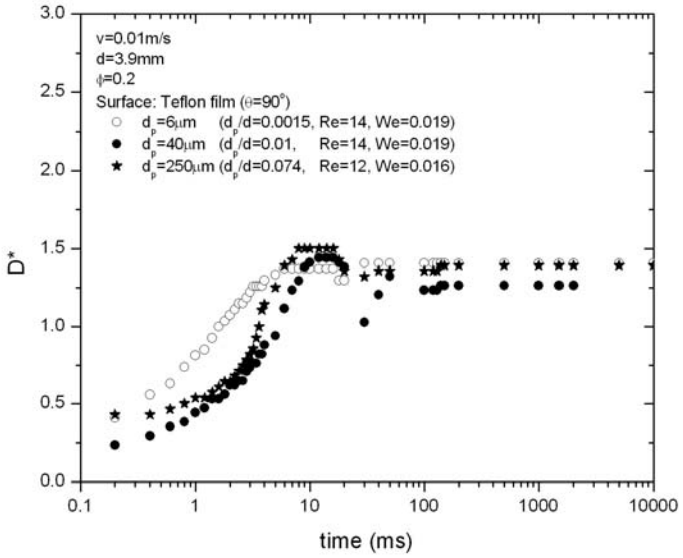

(c) Teflon® film

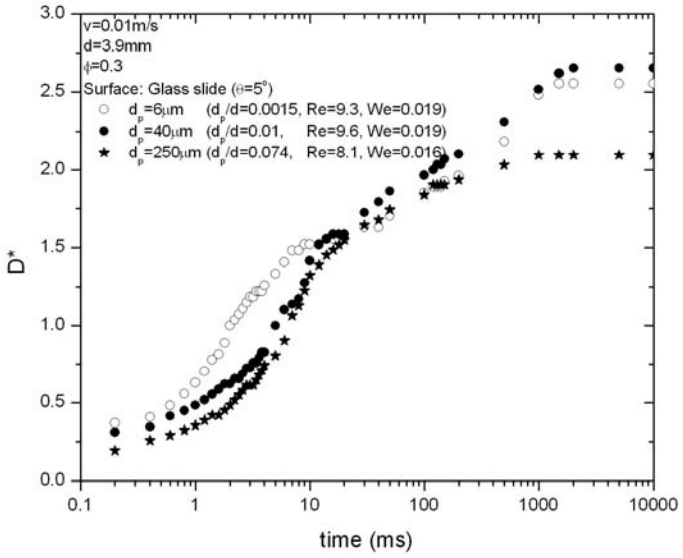

(a) Glass slide

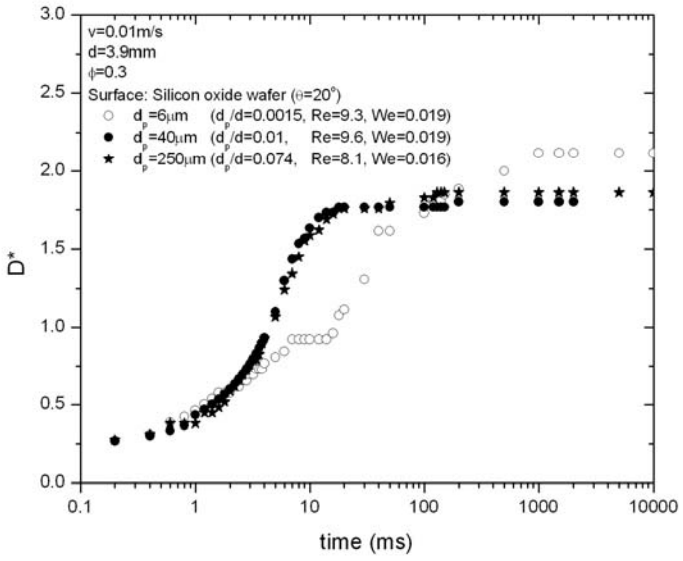

(b) Silicon oxide wafer

Figure D-3. Effect of particle size on impact. The drop size is 3.9mm with $\phi = 0.3$ and the impact speed is about 0.01 m/s: (a) glass slide, (b) silicon oxide wafer, (c) Teflon® film.

Figure D-3. (continued).

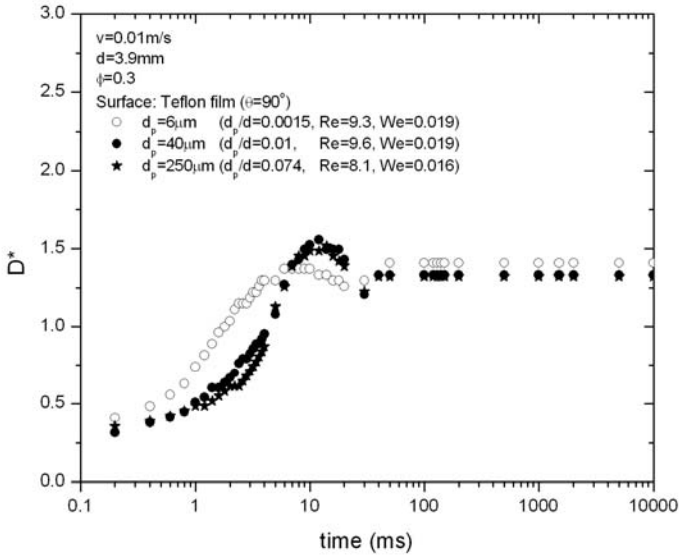

(c) Teflon® film

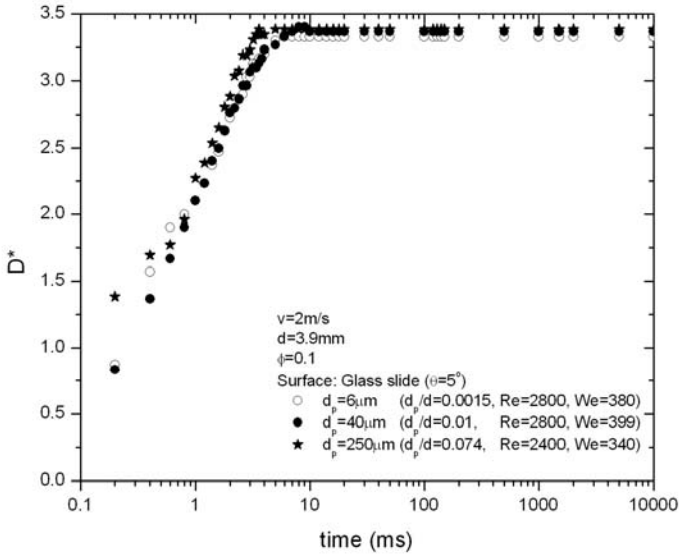

(a) Glass slide

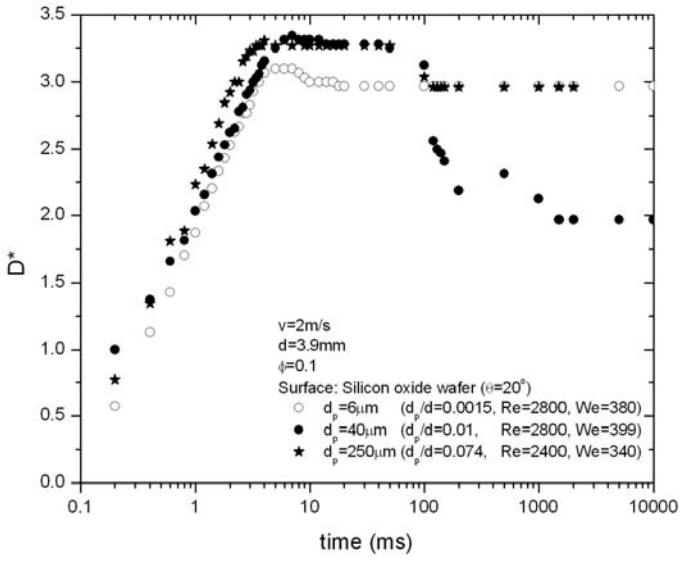

(b) Silicon oxide wafer

Figure D-4. Effect of particle size on impact. The drop size is 3.9mm with $\phi = 0.1$ and the impact speed is 2 m/s: (a) glass slide, (b) silicon oxide wafer, (c) Teflon® film.

Figure D-4. (continued).

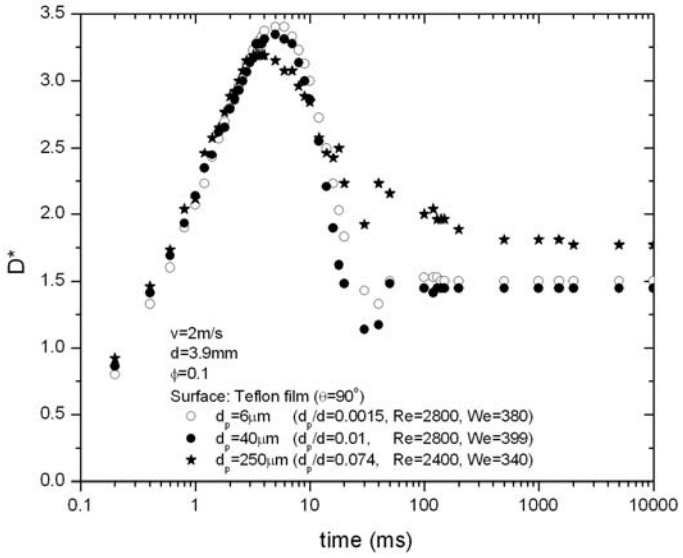

(c) Teflon® film

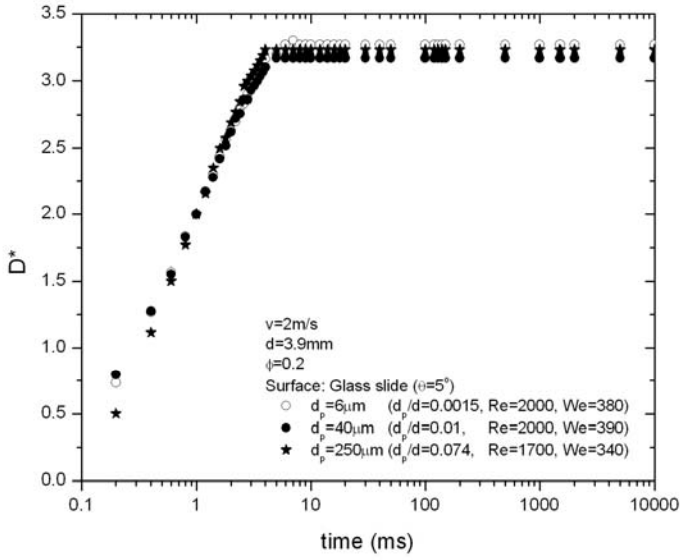

(a) Glass slide

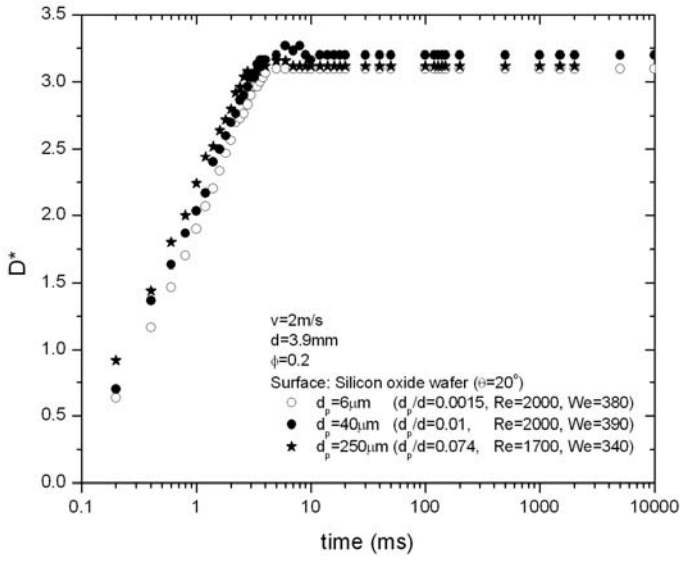

(b) Silicon oxide wafer

Figure D-5. Effect of particle size on impact. The drop size is 3.9mm with $\phi = 0.2$ and the impact speed is 2 m/s: (a) glass slide, (b) silicon oxide wafer, (c) Teflon® film.

Figure D-5. (continued).

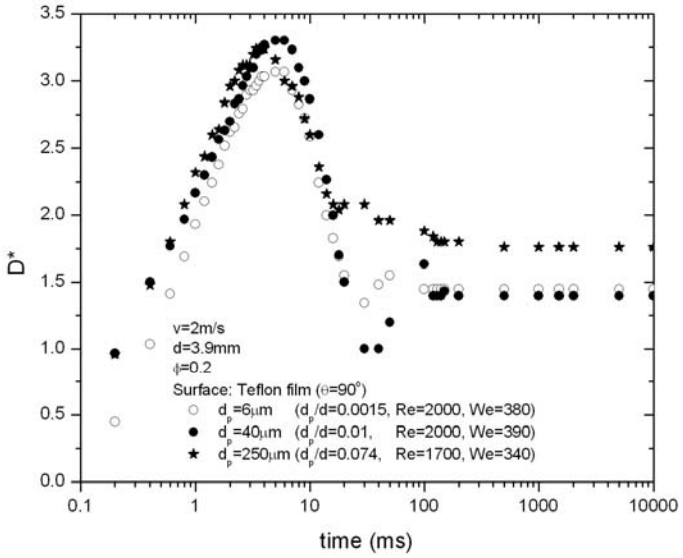

(c) Teflon® film

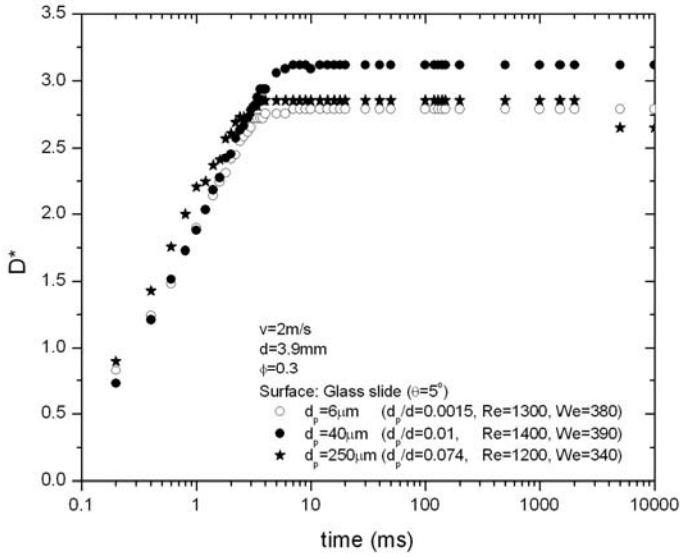

(a) Glass slide

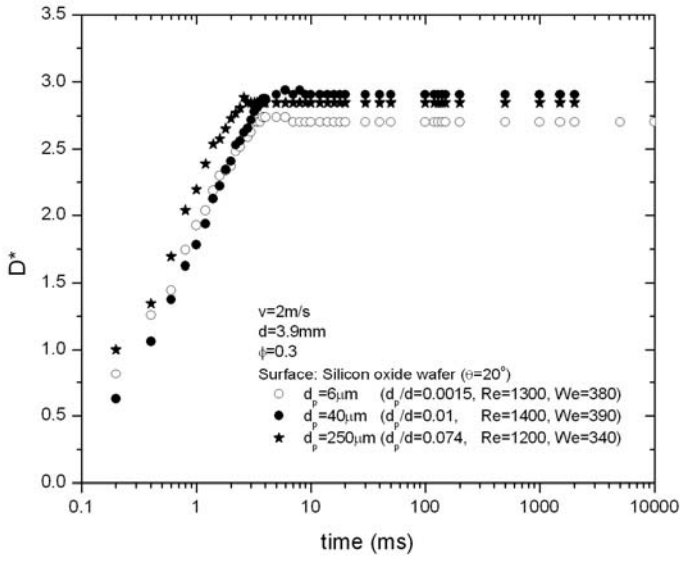

(b) Silicon oxide wafer

Figure D-6. Effect of particle size on impact. The drop size is 3.9mm with $\phi = 0.3$ and the impact speed is 2 m/s: (a) glass slide, (b) silicon oxide wafer, (c) Teflon® film.

Figure D-6. (continued).

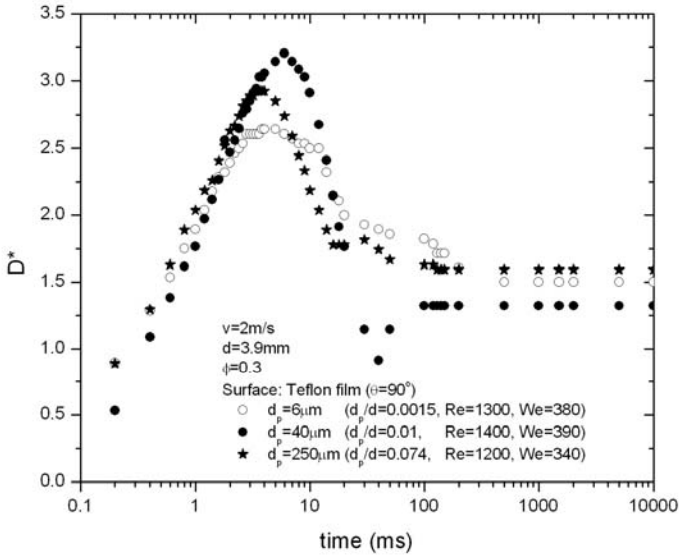

(c) Teflon® film

APPENDIX E

PROBABILITY OF BOUNCING VERSUS DIMENSIONLESS NUMBERS

The effect of particles on bouncing was investigated using 20-μm particles added to Mixture 1 at ϕ of 0.1 and 0.2. In Figure E-1 through 3, the probability of bouncing for both pure and particle-laden liquids is plotted versus Re, We and Ca.

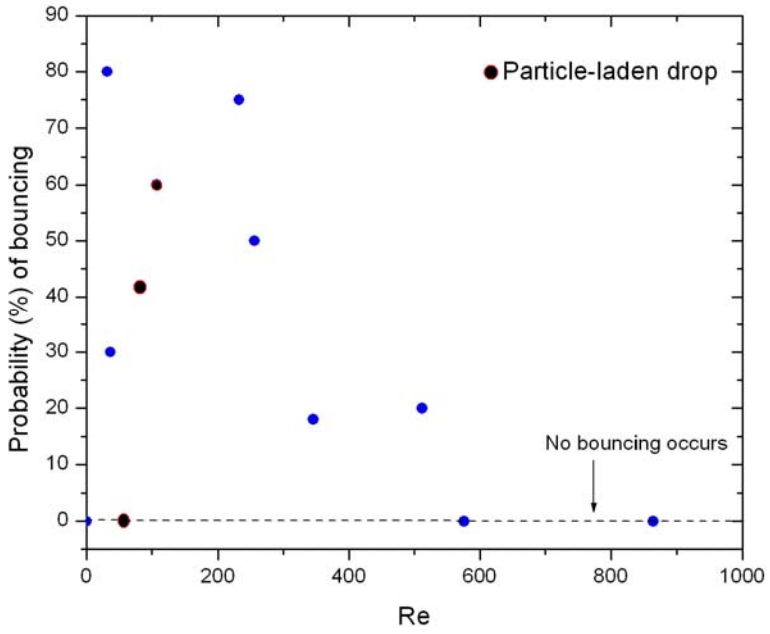

Figure E-1. Probability (%) of bouncing as a function of Re.

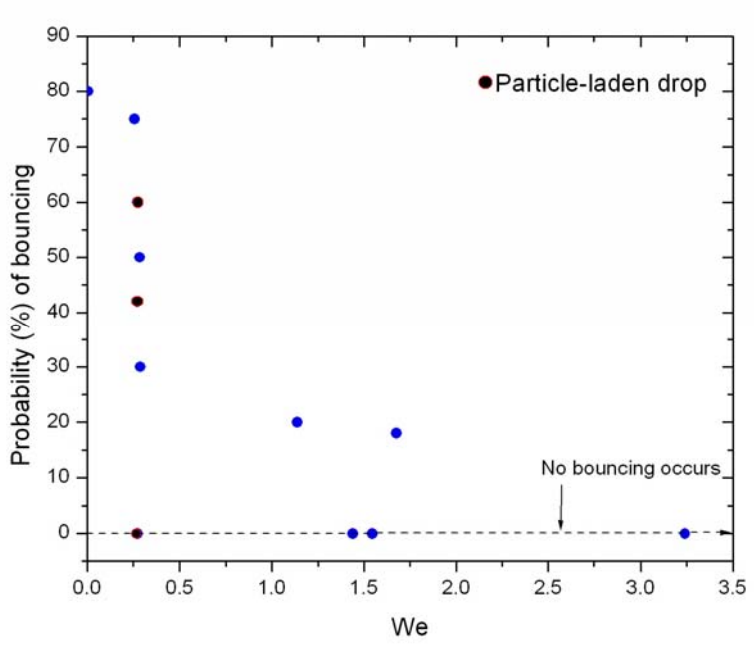

Figure E-2. Probability (%) of bouncing as a function of We.

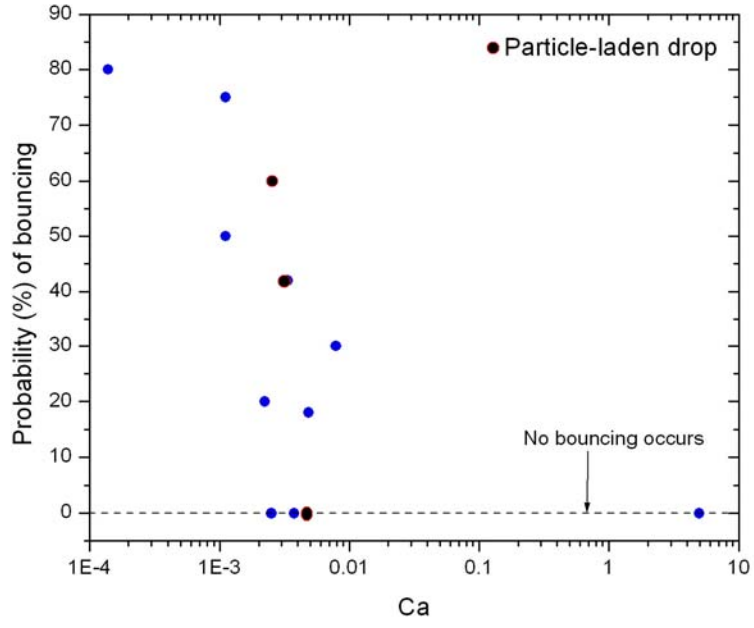

Figure E-3. Probability (%) of bouncing as a function of Ca.

APPENDIX F

EXAMPLES OF NONWETTING OF DROP AT LOW IMPACT SPEED

Even if a low-velocity drop does not bounce from the surface, non-wetting behavior of the drop is sometimes observed for hydrophilic drops on both hydrophilic and hydrophobic surfaces, but most frequently on the silicon oxide wafer. The drop contacts the surface, but appears not to wet it for sometime after the contact is made. When this happens, the D^* versus time curve is not almost straight from the origin to the maximum spreading ratio as usually occurs. Examples are shown in Figure E-1 to 3, which illustrates D^* versus time until 10 ms for a 2.7-mm drop containing 0.47-μm particles impacting at a speed of 0.01 m/s on three surfaces: glass slide, silicon oxide wafer, and Teflon® film. The images in the first three regions of this figure show a drop that is in contact with the surface, but is not wetting the surface. In Region I, the drop impacts on surface, and the contact area increases. The contact area stays almost constant while the drop shape deforms slowly in Region II. The deformation of the drop is large in Region III; however, the drop still does not wet the surface in this region. At the beginning of Region IV, the drop finally wets the surface.

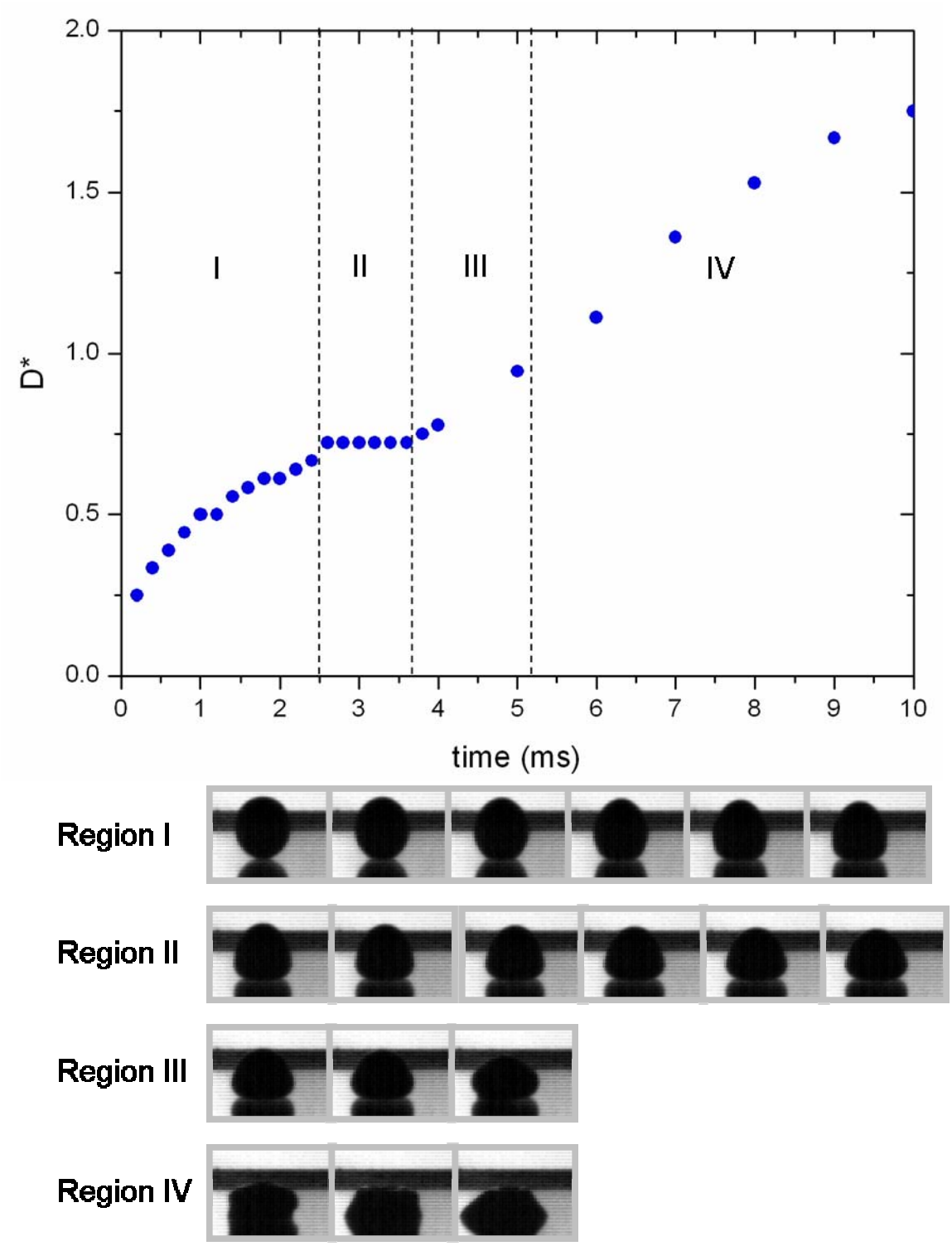

Figure F-1. Changing of drop shape after impact on glass slide surface (d = 2.7 mm, d_p= 0.47 μm, ϕ=0.15, v=0.01 m/s).

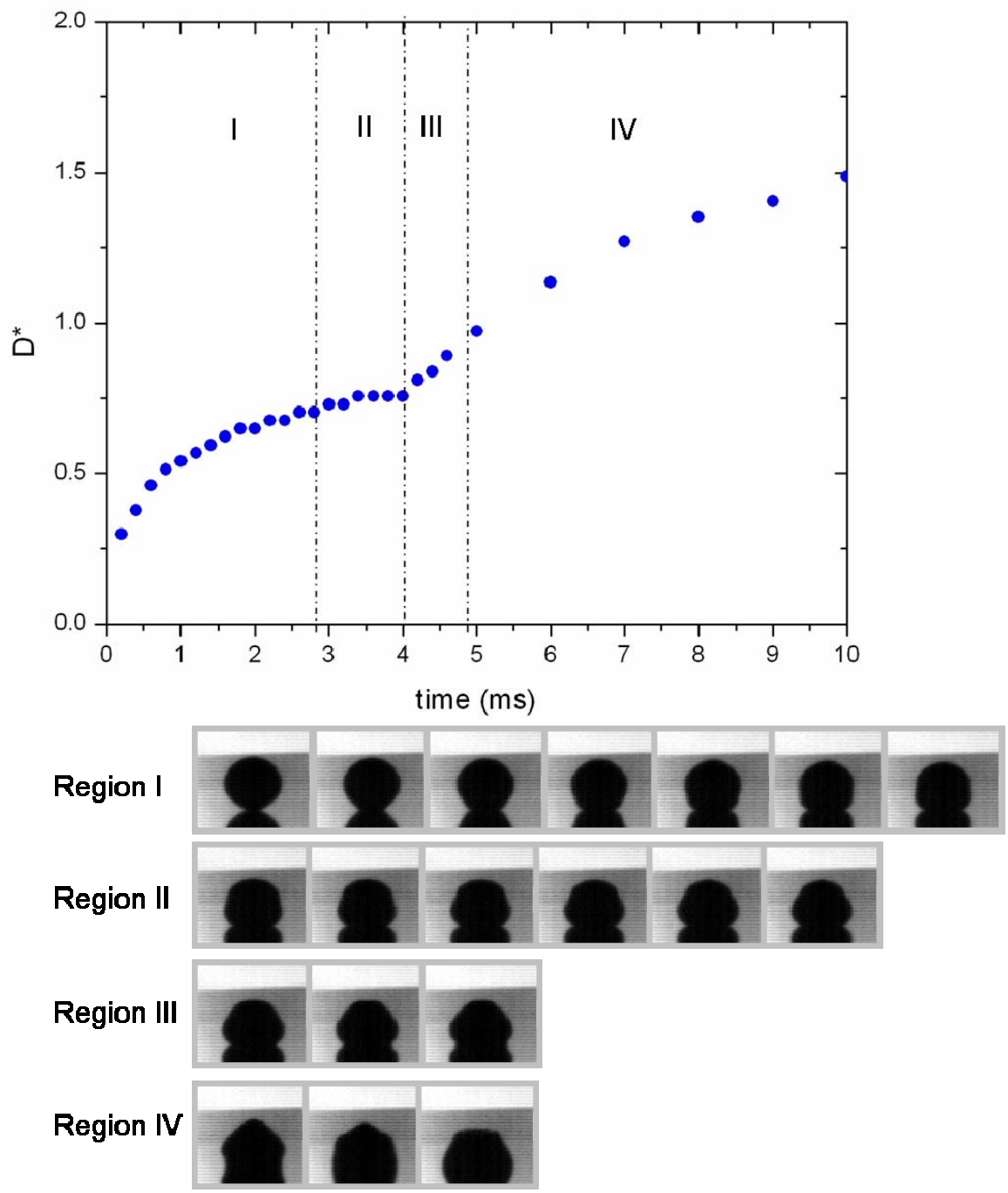

Figure F-2. Changing of drop shape after impact on silicon oxide wafer surface (d = 2.7 mm, d_p= 0.47 μm, ϕ=0.15, v=0.01 m/s).

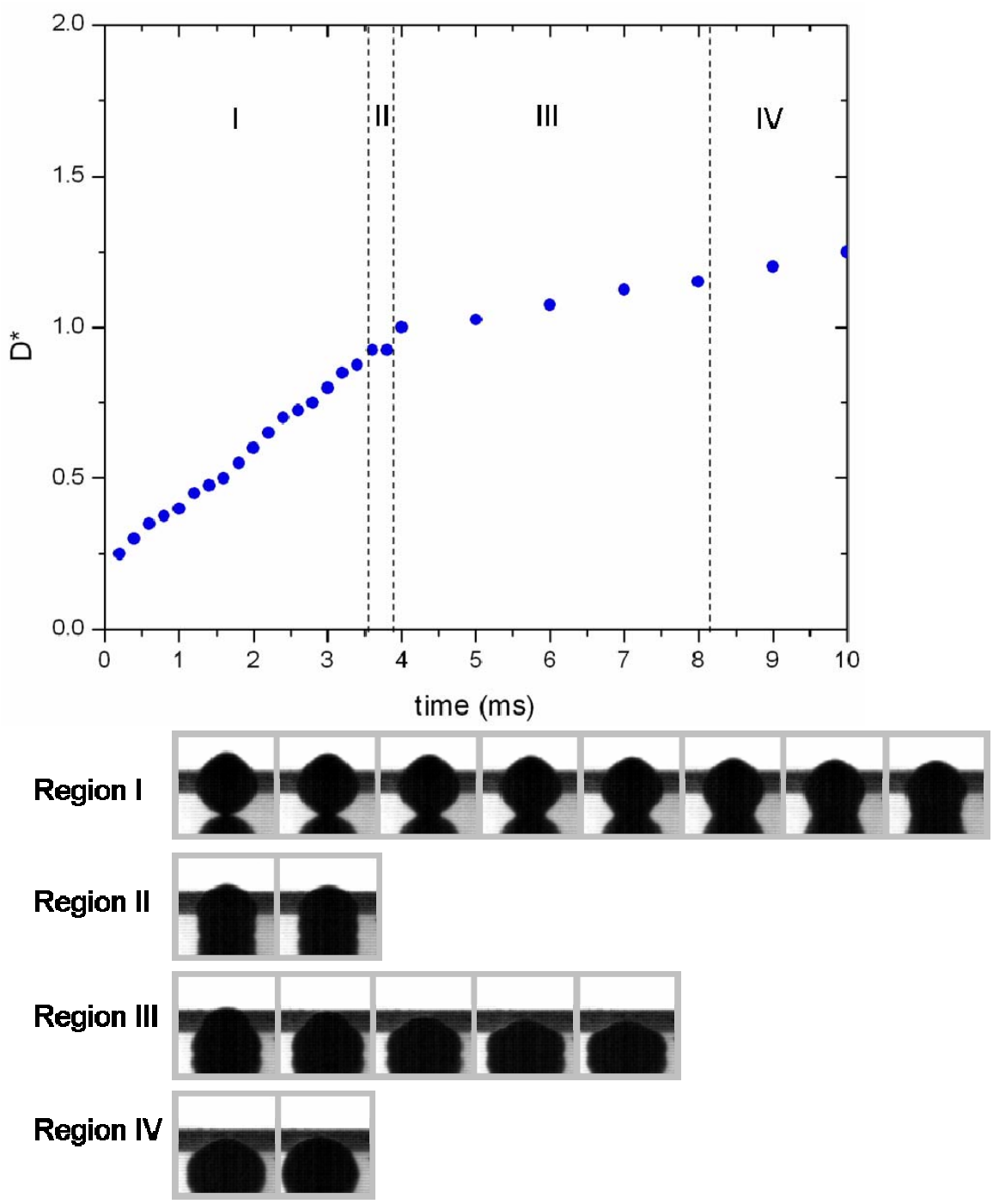

Figure F-3. Changing of drop shape after impact on Teflon® film surface (d = 2.7 mm, d_p= 0.47 μm, ϕ=0.15, v=0.01 m/s).

APPENDIX G

EFFECT OF DROP SIZE ON IMPACT PROCESS

Figure G-1 to 6 show D^* versus time for different drop sizes (340, 690, and 2900 μm) for pure liquid drops impacting a hydrophobic surface at 0.01 and 2 m/s. The small drop spreads faster and reaches the equilibrium spreading ratio, D_e^*, sooner than the bigger drop.

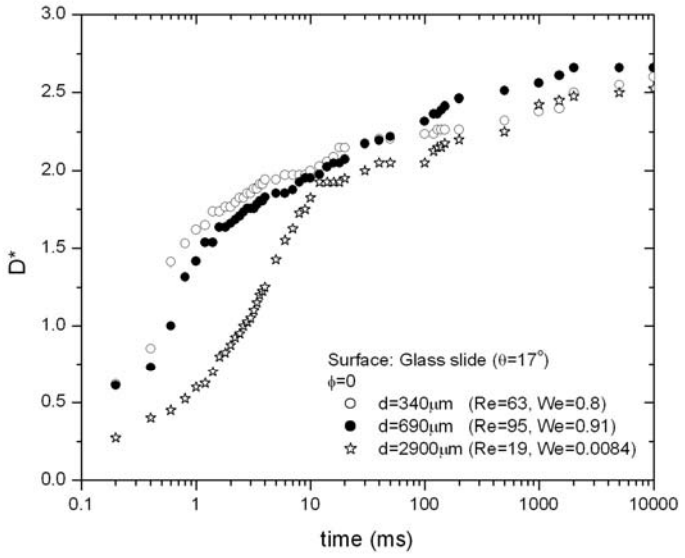

(a) D^* versus time

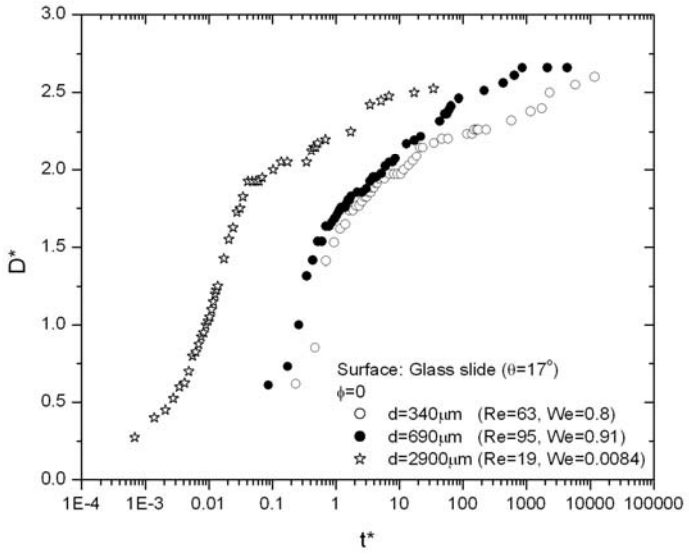

(b) D^* versus dimensionless time

Figure G-1. Effect of drop size on impact process on glass slide surfaces for pure liquid. Impact speed is 0.4 m/s for 340-μm drop, 0.3 m/s for 690-μm drop, and 0.01 m/s for 2900-μm drop: (a) D^* versus time and (b) D^* versus dimensionless time.

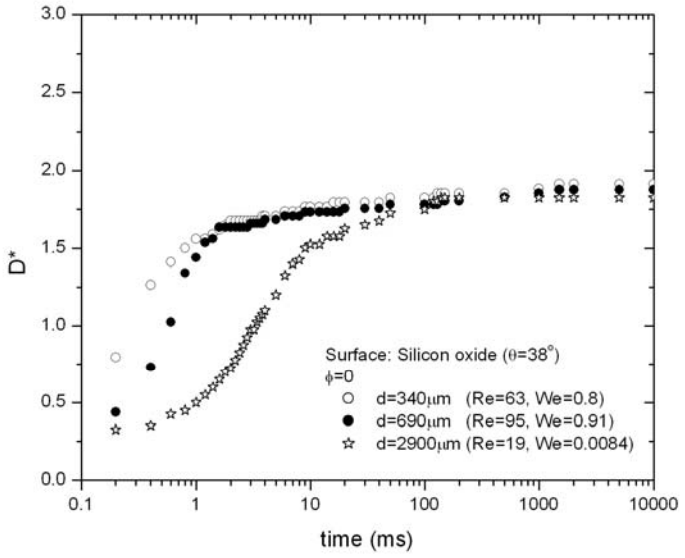

(a) D^* versus time

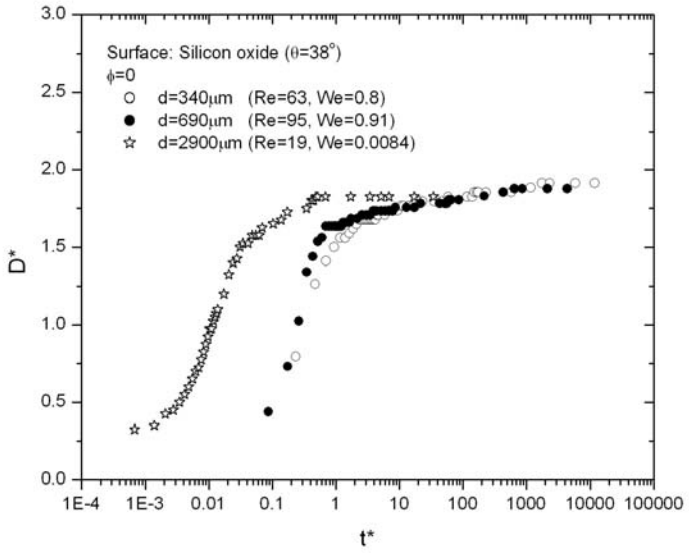

(b) D^* versus dimensionless time

Figure G-2. Effect of drop size on impact process on silicon oxide surfaces for pure liquid. Impact speed is 0.4 m/s for 340-μm drop, 0.3 m/s for 690-μm drop, and 0.01 m/s for 2900-μm drop: (a) D^* versus time and (b) D^* versus dimensionless time.

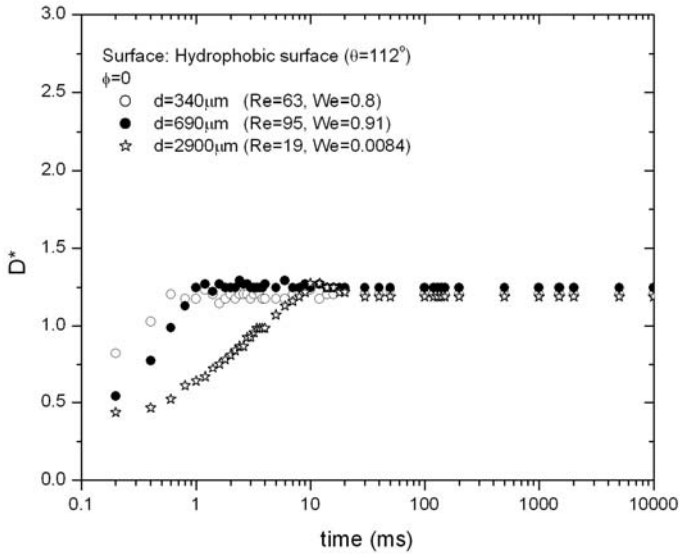

(a) D^* versus time

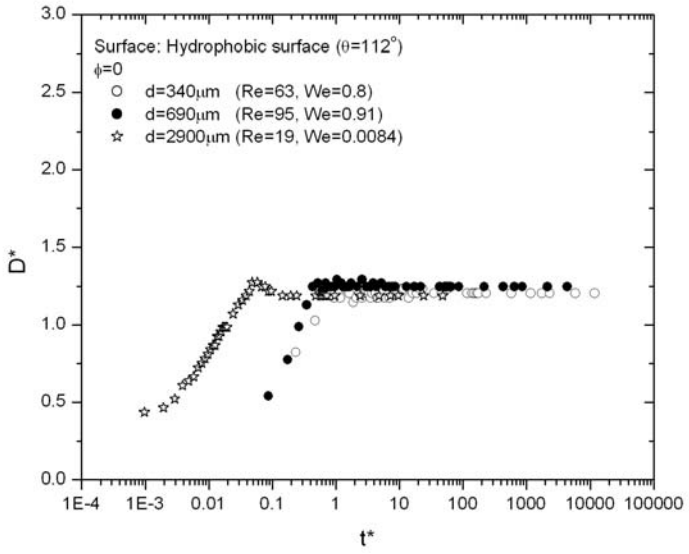

(b) D^* versus dimensionless time

Figure G-3. Effect of drop size on impact process on hydrophobic surfaces for pure liquid. Impact speed is 0.4 m/s for 340-μm drop, 0.3 m/s for 690-μm drop, and 0.01 m/s for 2900-μm drop: (a) D^* versus time and (b) D^* versus dimensionless time.

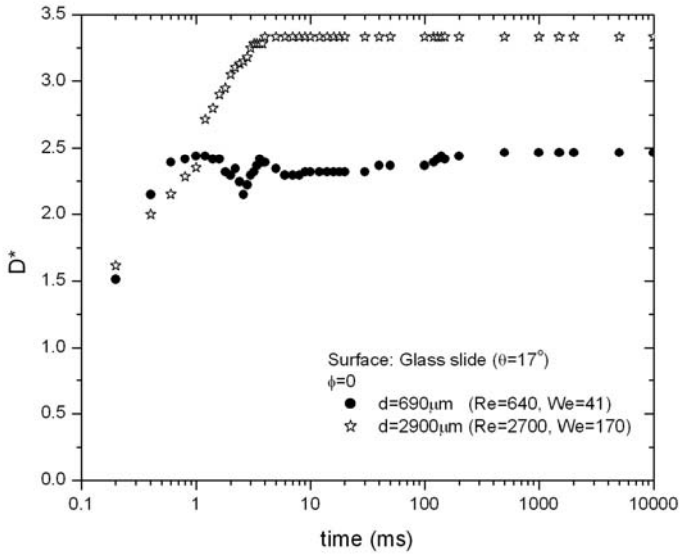

(a) D^* versus time

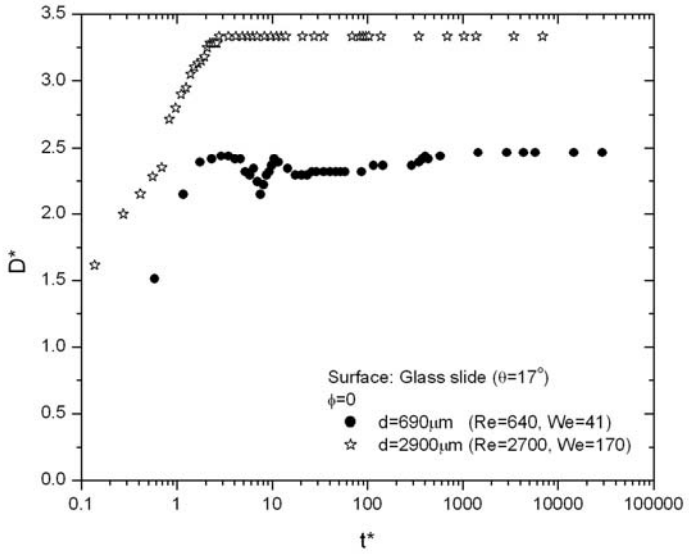

(b) D^* versus dimensionless time

Figure G-4. Effect of drop size on impact process on glass slide surfaces for pure liquid. Impact speed is 2 m/s: (a) D^* versus time and (b) D^* versus dimensionless time.

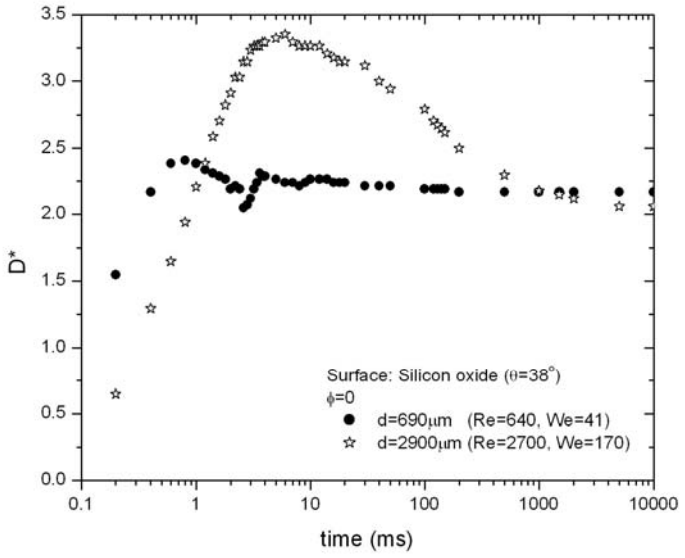

(a) D^* versus time

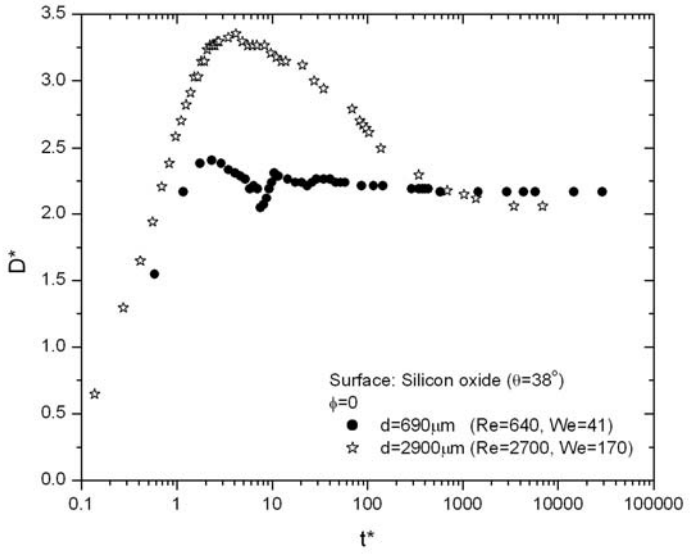

(b) D^* versus dimensionless time

Figure G-5. Effect of drop size on impact process on silicon oxide surfaces for pure liquid. Impact speed is 2 m/s: (a) D^* versus time and (b) D^* versus dimensionless time.

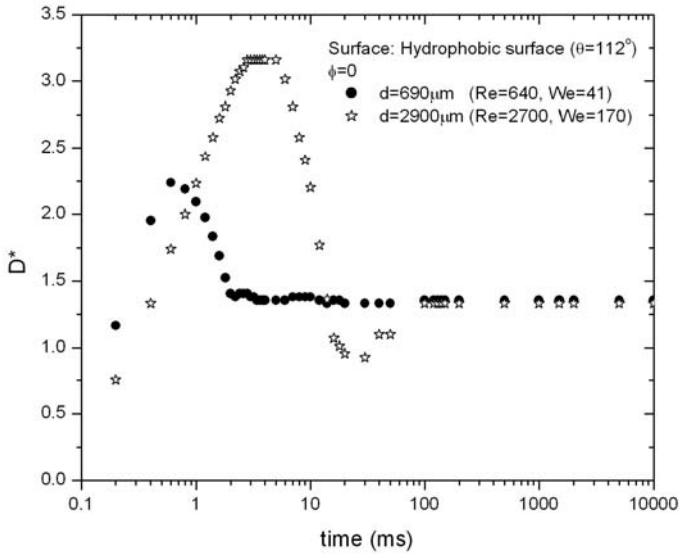

(a) D^* versus time

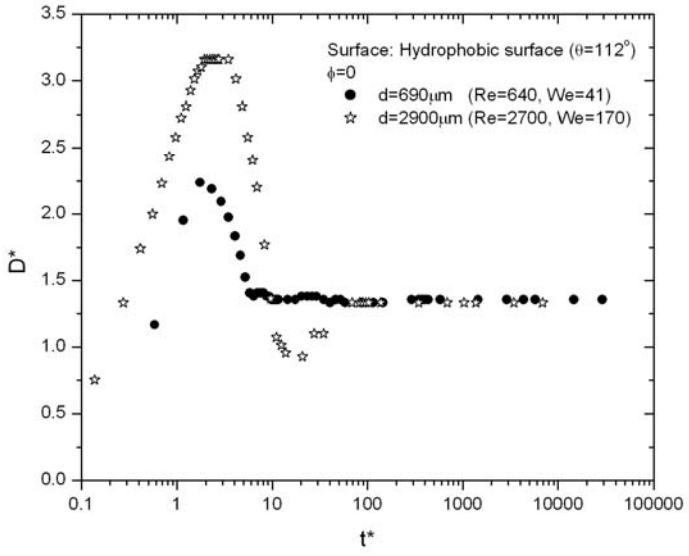

(b) D^* versus dimensionless time

Figure G-6. Effect of drop size on impact process on hydrophobic surfaces for pure liquid. Impact speed is 2 m/s: (a) D^* versus time and (b) D^* versus dimensionless time.

APPENDIX H

COMPARISON OF MEASURED D_m^* WITH MODEL PREDICTIONS

Table H-1 to 11 and Figure H-1 to 4 show the comparison of the measured maximum spreading ratio and model predictions value for the particle-laden drop on glass slide, silicon oxide wafer, and Teflon® film for low and high impact speed experiments. For impact speeds of 0.01 m/s and 0.3 m/s, Pasandideh-Fard *et al.*'s (1996) and Mao *et al.*'s (1997) model greatly over estimate D_m^*, especially for the low contact angle; however, Park *et al.*'s (2003) model is in close agreement with the experimental results. For low impact speeds, Park *et al.*'s model gives better results because it is assumed that the drop shape is a cap of sphere at the maximum spreading state while other models (Pasandideh-Fard *et al.* (1996), Mao *et al.* (1997)) assume that it is cylindrical. For an impact speed of 2 m/s, Mao *et al.*'s (1997) model over estimates some values while Pasandideh-Fard *et al.* (1996) and Park *et al.*'s (2003) models are good agreement with the measured maximum spreading ratio. For large drop sizes (3.4 to 4.0 mm), Pasandideh-Fard *et al.*'s and Park *et al.*'s model predictions are close to the experimental values, but Mao's model over estimates D_m^* for most of the cases.

Table H-1. Comparison of measured D_m^* with model predictions for 690-μm drops impacting glass slide.

v (m/s)	d_p (μm)	ϕ	Re	We	Measured D_m^*	Modeled D_m^*		
						Pasandideh-Fard *et al.*'s	Mao *et al.*'s	Park' *et al.*s
0.3	20	0	95	0.91	**2.66**	5.06	4.20	2.61
		0.1	73		**2.55**	4.81	4.04	2.61
		0.2	52		**2.50**	4.50	3.84	2.60
	40	0	95	0.91	**2.66**	5.06	4.20	2.61
		0.1	73		**2.47**	4.81	4.04	2.61
		0.2	52		**2.37**	4.50	3.84	2.60
2	20	0	640	41	**2.46**	2.83	2.81	2.53
		0.1	490		**2.34**	2.61	2.69	2.37
		0.2	350		**2.41**	2.44	2.54	2.17
	40	0	640	41	**2.46**	2.83	2.81	2.53
		0.1	490		**2.32**	2.61	2.69	2.37
		0.2	350		**2.44**	2.44	2.54	2.17

Table H-2. Comparison of measured D_m^* with model predictions for 690-μm drops impacting silicon oxide wafer.

v (m/s)	d_p (μm)	ϕ	Re	We	Measured D_m^*	Modeled D_m^*		
						Pasandideh-Fard *et al.*'s	Mao *et al.*'s	Park' *et al.*s
0.3	20	0	95	0.91	**1.88**	3.58	3.01	1.90
		0.1	73		**1.79**	3.49	2.95	1.48
		0.2	52		**1.79**	3.36	2.86	1.40
	40	0	95	0.91	**1.88**	3.58	3.01	1.90
		0.1	73		**1.72**	3.49	2.95	1.48
		0.2	52		**1.66**	3.36	2.86	1.40
2	20	0	640	41	**2.40**	2.73	2.70	2.53
		0.1	490		**2.38**	2.57	2.59	2.37
		0.2	350		**2.31**	2.37	2.46	2.17
	40	0	640	41	**2.40**	2.73	2.70	2.53
		0.1	490		**2.21**	2.57	2.59	2.37
		0.2	350		**2.16**	2.37	2.46	2.17

Table H-3. Comparison of measured D_m^* with model predictions for 690-μm drops impacting Teflon® film.

v (m/s)	d_p (μm)	ϕ	Re	We	Measured D_m^*	Modeled D_m^*		
						Pasandideh-Fard *et al.*'s	Mao *et al.*'s	Park' *et al.*s
0.3	20	0	95	0.91	**1.27**	1.69	1.11	1.26
		0.1	73		**1.26**	1.68	1.10	1.24
		0.2	52		**1.26**	1.67	1.08	1.20
	40	0	95	0.91	**1.27**	1.69	1.11	1.26
		0.1	73		**1.26**	1.68	1.10	1.24
		0.2	52		**1.26**	1.67	1.08	1.20
2	20	0	640	41	**2.24**	2.24	2.19	2.20
		0.1	490		**2.09**	2.14	2.13	2.11
		0.2	350		**2.10**	2.03	2.05	1.99
	40	0	640	41	**2.24**	2.24	2.19	2.20
		0.1	490		**2.07**	2.14	2.13	2.11
		0.2	350		**2.00**	2.03	2.05	1.99

Table H-4. Comparison of measured D_m^* with model predictions for 2.7-mm drops impacting glass slide.

v (m/s)	d_p (μm)	ϕ	Re	We	Measured D_m^*	Modeled D_m^*		
						Pasandideh-Fard *et al.*'s	Mao *et al.*'s	Park' *et al.*s
0.01	0.47	0	38	0.0080	**3.10**	15.38	14.00	3.12
		0.15	21	0.0085	**3.20**	15.05	14.00	3.12
0.01	0.47	0	5400	160	**3.68**	4.43	4.20	4.30
		0.15	3000	170	**3.77**	3.82	3.80	3.73

Table H-5. Comparison of measured D_m^* with model predictions for 2.7-mm drops impacting silicon oxide wafer.

v (m/s)	d_p (μm)	ϕ	Re	We	Measured D_m^*	Modeled D_m^*		
						Pasandideh-Fard *et al.*'s	Mao *et al.*'s	Park' *et al.*s
0.01	0.47	0 0.15	38 21	0.0080 0.0085	**2.27** **1.97**	6.48 6.45	6.00 6.00	2.22 2.21
0.01	0.47	0 0.15	5400 3000	160 170	**3.65** **3.75**	4.37 3.79	4.20 3.80	4.24 3.70

Table H-6. Comparison of measured D_m^* with model predictions for 2.7-mm drops impacting Teflon® film.

v (m/s)	d_p (μm)	ϕ	Re	We	Measured D_m^*	Modeled D_m^*		
						Pasandideh-Fard *et al.*'s	Mao *et al.*'s	Park' *et al.*s
0.01	0.47	0 0.15	38 21	0.0080 0.0085	**1.32** **1.24**	1.92 1.92	1.40 1.40	1.22 1.20
0.01	0.47	0 0.15	5400 3000	160 170	**3.43** **3.39**	3.79 3.41	3.60 3.40	3.66 3.32

Table H-7. Comparison of measured D_m^* with model predictions for 2.9-mm drops impacting glass slide.

v (m/s)	d_p (μm)	ϕ	Re	We	Measured D_m^*	Modeled D_m^*		
						Pasandideh-Fard *et al.*'s	Mao *et al.*'s	Park' *et al.*s
0.01	20	0	19	0.0084	**2.53**	9.30	8.65	2.57
		0.1	14		**2.22**	9.26	8.59	2.57
		0.2	10		**1.93**	9.21	8.52	2.44
	40	0	19	0.0084	**2.53**	9.30	8.65	2.57
		0.1	14		**2.18**	9.26	8.59	2.57
		0.2	10		**2.11**	9.21	8.52	2.42
		0.3	6.9		**2.09**	9.14	8.44	2.3
2	20	0	2700	170	**3.33**	3.17	3.76	3.56
		0.1	2000		**3.22**	3.44	3.58	3.36
		0.2	1500		**3.07**	3.21	3.42	3.12
	40	0	2700	170	**3.34**	3.17	3.76	3.56
		0.1	2000		**3.16**	3.44	3.58	3.36
		0.2	1500		**3.00**	3.21	3.42	3.12
		0.3	990		**2.95**	2.89	3.19	2.86

Table H-8. Comparison of measured D_m^* with model predictions for 2.7-mm drops impacting silicon oxide wafer.

v (m/s)	d_p (μm)	ϕ	Re	We	Measured D_m^*	Modeled D_m^*		
						Pasandideh-Fard *et al.*'s	Mao *et al.*'s	Park' *et al.*s
0.01	20	0	19	0.0084	**1.83**	4.32	3.90	1.84
		0.1	14		**1.76**	4.31	3.90	1.84
		0.2	10		**1.65**	4.31	3.89	1.84
	40	0	19	0.0084	**1.83**	4.32	3.90	1.84
		0.1	14		**1.78**	4.31	3.90	1.84
		0.2	10		**1.91**	4.31	3.89	1.84
		0.3	6.9		**1.75**	4.30	3.89	1.84
2	20	0	2700	170	**3.35**	3.64	3.69	3.52
		0.1	2000		**3.33**	3.39	3.52	3.36
		0.2	1500		**3.09**	3.16	3.36	3.12
	40	0	2700	170	**3.35**	3.64	3.69	3.52
		0.1	2000		**3.28**	3.39	3.52	3.36
		0.2	1500		**3.18**	3.16	3.36	3.12
		0.3	990		**3.03**	2.86	3.15	3.00

Table H-9. Comparison of measured D_m^* with model predictions for 2.7-mm drops impacting Teflon® film.

v (m/s)	d_p (μm)	ϕ	Re	We	Measured D_m^*	Modeled D_m^*		
						Pasandideh-Fard *et al.*'s	Mao *et al.*'s	Park' *et al.*s
0.01	20	0	19	0.0084	**1.28**	1.70	*	1.03
		0.1	14		**1.36**	1.70	*	1.03
		0.2	10		**1.33**	1.70	*	1.03
	40	0	19	0.0084	**1.28**	1.70	*	1.03
		0.1	14		**1.44**	1.70	*	1.03
		0.2	10		**1.32**	1.70	*	1.03
		0.3	6.9		**1.22**	1.70	*	1.03
2	20	0	2700	170	**3.33**	3.26	3.28	3.25
		0.1	2000		**3.36**	3.07	3.16	3.07
		0.2	1500		**3.19**	2.90	3.04	2.90
	40	0	2700	170	**3.33**	3.26	3.28	3.25
		0.1	2000		**3.29**	3.07	3.16	3.07
		0.2	1500		**3.26**	2.90	3.04	2.90
		0.3	990		**2.72**	2.66	2.88	2.66

* imaginary number was obtained.

Table H-10. Comparison of measured D_m^* with model predictions for 3.9-mm drops impacting glass slide.

v (m/s)	d_p (μm)	ϕ	Re	We	Measured D_m^*	Modeled D_m^*		
						Pasandideh-Fard *et al.*'s	Mao *et al.*'s	Park' *et al.*s
0.01	6	0	25	0.019	**2.83**	21.25	8.26	3.26
		0.1	19		**2.71**	20.41	8.18	3.14
		0.2	14		**2.80**	19.46	8.09	3.00
		0.3	9.3		**2.56**	18.19	7.96	2.80
	40	0	25	0.019	**2.83**	21.25	8.26	3.26
		0.1	20		**2.60**	20.57	8.20	3.16
		0.2	14		**2.63**	19.46	8.09	3.00
		0.3	9.6		**2.66**	18.29	7.97	2.82
	250	0	25	0.019	**2.83**	21.25	8.26	3.26
		0.1	17	0.016	**2.83**	21.12	8.15	3.23
		0.2	12	0.016	**2.81**	20.05	8.04	3.07
		0.3	8.1	0.016	**2.10**	18.83	7.91	2.88
2	6	0	3600	380	**3.43**	3.93	4.17	3.89
		0.1	2800		**3.33**	3.69	4.00	3.66
		0.2	2000		**3.30**	3.40	3.79	3.36
		0.3	1300		**2.79**	3.05	3.53	3.02
	40	0	3600	380	**3.43**	3.93	4.17	3.89
		0.1	2800	390	**3.40**	3.69	4.01	3.66
		0.2	2000	390	**3.17**	3.39	3.80	3.36
		0.3	1400	390	**3.12**	3.10	3.58	3.02
	250	0	3600	380	**3.43**	3.93	4.17	3.89
		0.1	2400	340	**3.38**	3.56	3.87	3.52
		0.2	1700	340	**3.23**	3.27	3.66	3.23
		0.3	1200	340	**2.86**	2.99	3.41	2.93

Table H-11. Comparison of measured D_m^* with model predictions for 3.9-mm drops impacting silicon oxide wafer.

v (m/s)	d_p (μm)	ϕ	Re	We	Measured D_m^*	Modeled D_m^*		
						Pasandideh-Fard *et al.*'s	Mao *et al.*'s	Park' *et al.*s
0.01	6	0	25	0.019	**2.14**	7.83	3.86	2.38
		0.1	19		**2.09**	7.78	3.85	2.38
		0.2	14		**2.10**	7.73	3.84	2.38
		0.3	9.3		**2.12**	7.64	3.82	2.35
	40	0	25	0.019	**2.14**	7.83	3.86	2.38
		0.1	20		**1.93**	7.79	3.85	2.38
		0.2	14		**1.86**	7.73	3.84	2.38
		0.3	9.6		**1.80**	7.65	3.83	2.35
	250	0	25	0.019	**2.14**	7.83	3.86	2.38
		0.1	17	0.016	**1.90**	7.82	3.85	2.38
		0.2	12	0.016	**1.83**	7.76	3.84	2.38
		0.3	8.1	0.016	**1.86**	7.69	3.82	2.38
2	6	0	3600	380	**3.11**	3.92	4.13	3.89
		0.1	2800		**3.10**	3.68	3.96	3.65
		0.2	2000		**3.10**	3.39	3.75	3.36
		0.3	1300		**2.74**	3.04	3.50	3.02
	40	0	3600	380	**3.11**	3.92	4.13	3.89
		0.1	2800	390	**3.34**	3.68	3.97	3.65
		0.2	2000	390	**3.27**	3.39	3.76	3.36
		0.3	1400	390	**2.94**	3.10	3.55	3.02
	250	0	3600	380	**3.11**	3.92	4.13	3.89
		0.1	2400	340	**3.31**	3.55	3.83	3.52
		0.2	1700	340	**3.16**	3.26	3.62	3.23
		0.3	1200	340	**2.85**	2.99	3.42	2.93

Table H-12. Comparison of measured D_m^* with model predictions for 3.9-mm drops impacting Teflon® film.

v (m/s)	d_p (μm)	ϕ	Re	We	Measured D_m^*	Modeled D_m^*		
						Pasandideh-Fard *et al.*'s	Mao *et al.*'s	Park' *et al.*s
0.01	6	0	25	0.019	**1.48**	2.00	*	1.27
		0.1	19		**1.43**	2.00	*	1.27
		0.2	14		**1.37**	1.99	*	1.27
		0.3	9.3		**1.37**	1.99	*	1.27
	40	0	25	0.019	**1.48**	2.00	*	1.26
		0.1	20		**1.52**	2.00	*	1.26
		0.2	14		**1.44**	1.99	*	1.27
		0.3	9.6		**1.56**	1.99	*	1.27
	250	0	25	0.019	**1.48**	2.00	*	1.26
		0.1	17	0.016	**1.52**	2.00	*	1.26
		0.2	12	0.016	**1.50**	2.00	*	1.27
		0.3	8.1	0.016	**1.52**	1.99	*	1.27
2	6	0	3600	380	**3.39**	3.72	3.84	3.72
		0.1	2800		**3.40**	3.52	3.71	3.52
		0.2	2000		**3.07**	3.26	3.54	3.26
		0.3	1300		**2.64**	3.00	3.22	2.95
	40	0	3600	380	**3.39**	3.72	3.84	3.72
		0.1	2800	390	**3.34**	3.52	3.72	3.52
		0.2	2000	390	**3.30**	3.26	3.55	3.26
		0.3	1400	390	**3.20**	3.00	3.37	3.02
	250	0	3600	380	**3.39**	3.72	3.84	3.72
		0.1	2400	340	**3.19**	3.38	3.58	3.36
		0.2	1700	340	**3.24**	3.13	3.41	3.26
		0.3	1200	340	**2.93**	2.89	3.24	3.00

* imaginary number was obtained.

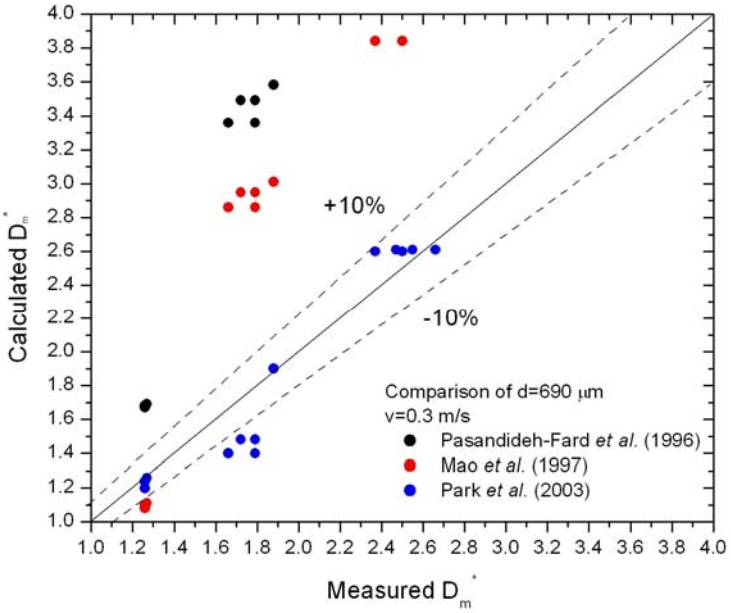

(a) Impact speed of 0.01 m/s.

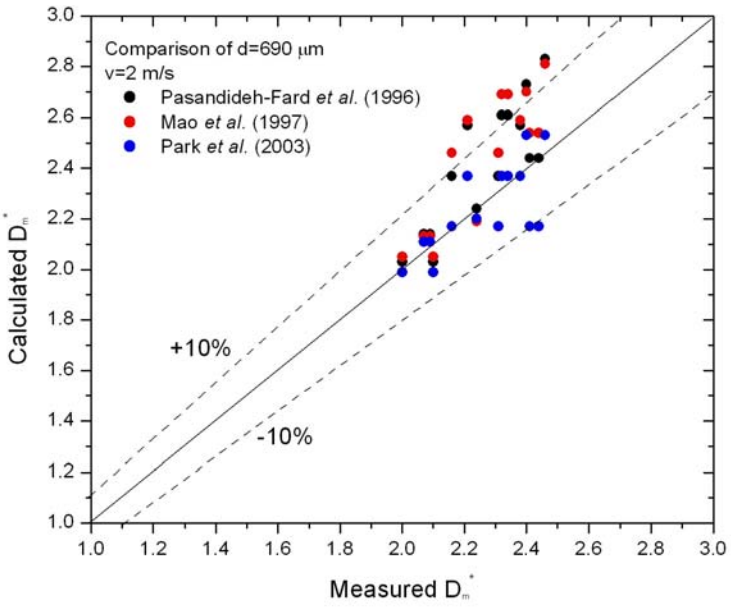

(b) Impact speed of 2 m/s.

Figure H-1. Comparison of Measured D_m^* for d = 690 μm with model predictions: (a) Impact speed of 0.01 m/s and (b) impact speed of 2 m/s.

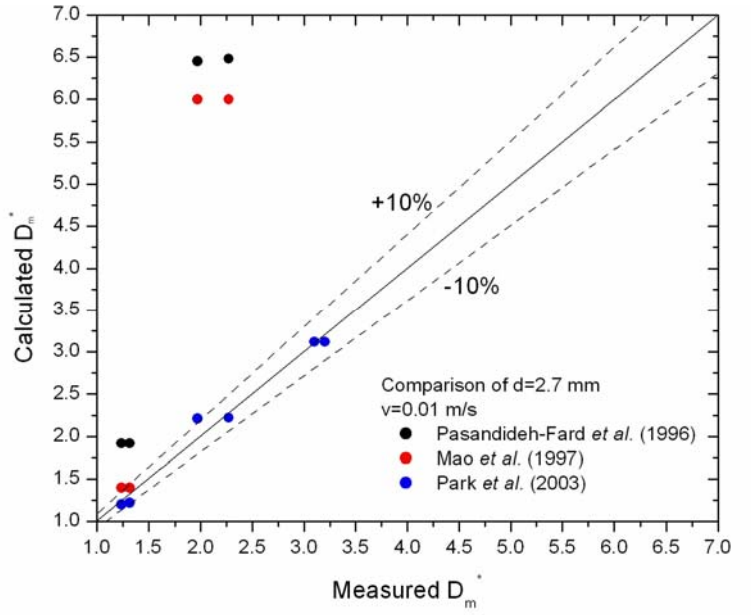

(a) Impact speed of 0.01 m/s.

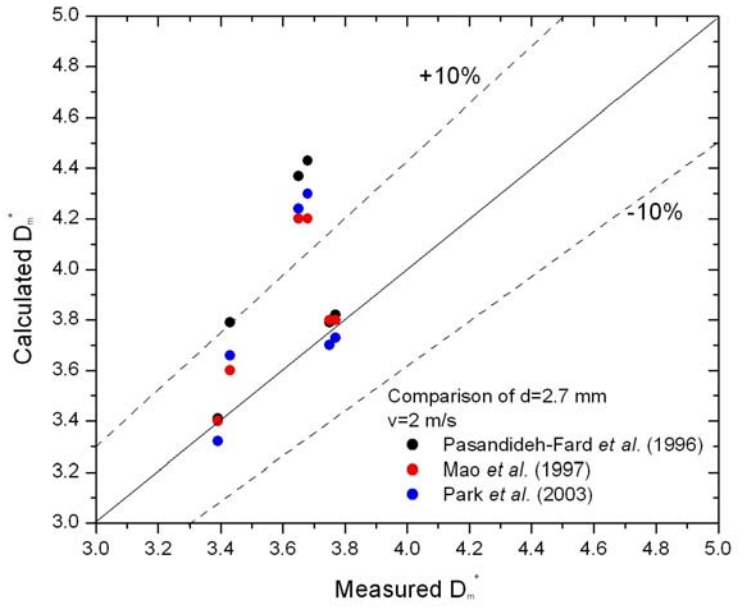

(b) Impact speed of 2 m/s.

Figure H-2. Comparison of Measured D_m^* for d = 2.7 mm with model predictions: (a) Impact speed of 0.01 m/s and (b) impact speed of 2 m/s.

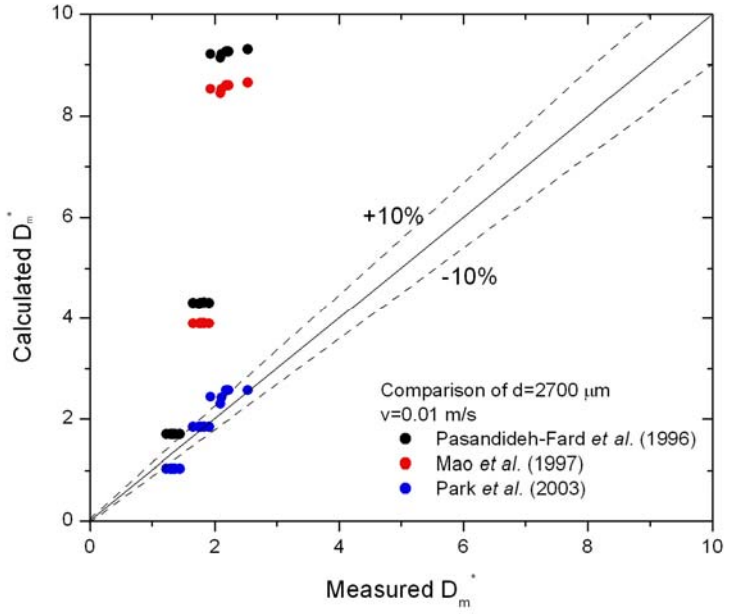

(a) Impact speed of 0.01 m/s.

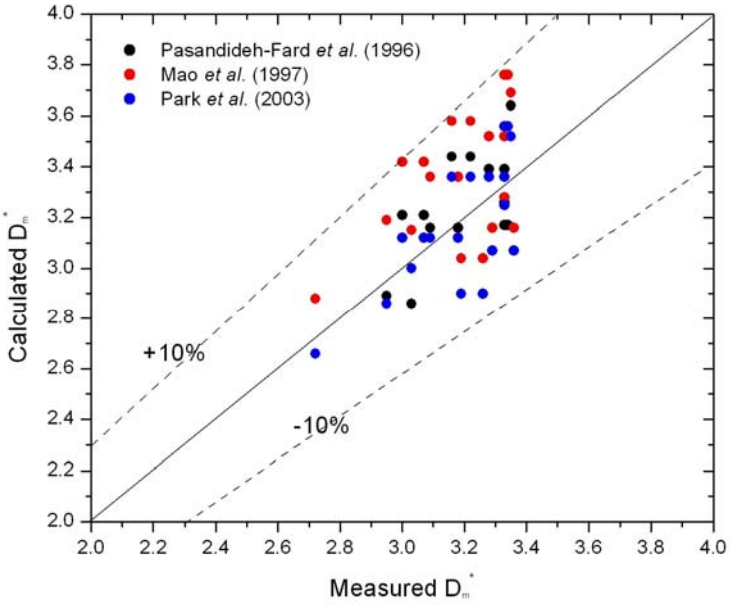

(b) Impact speed of 2 m/s.

Figure H-3. Comparison of Measured D_m^* for d = 2.9 mm with model predictions: (a) Impact speed of 0.01 m/s and (b) impact speed of 2 m/s.

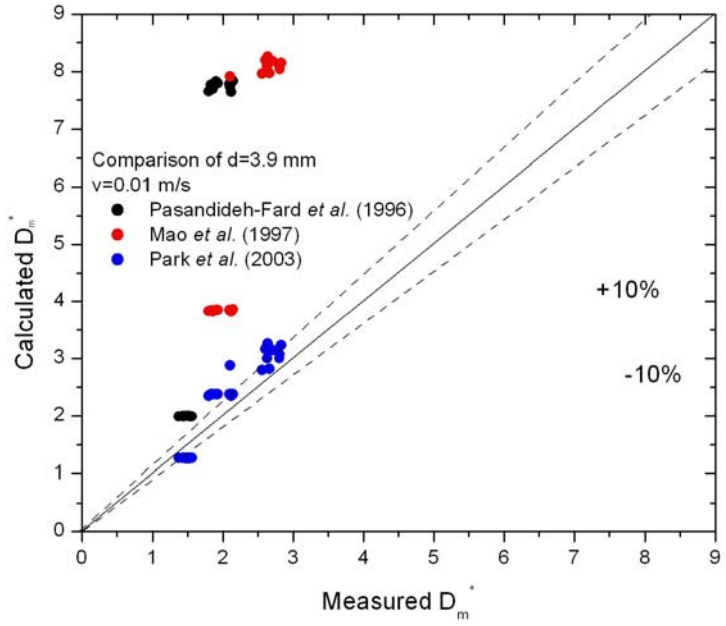

(a) Impact speed of 0.01 m/s.

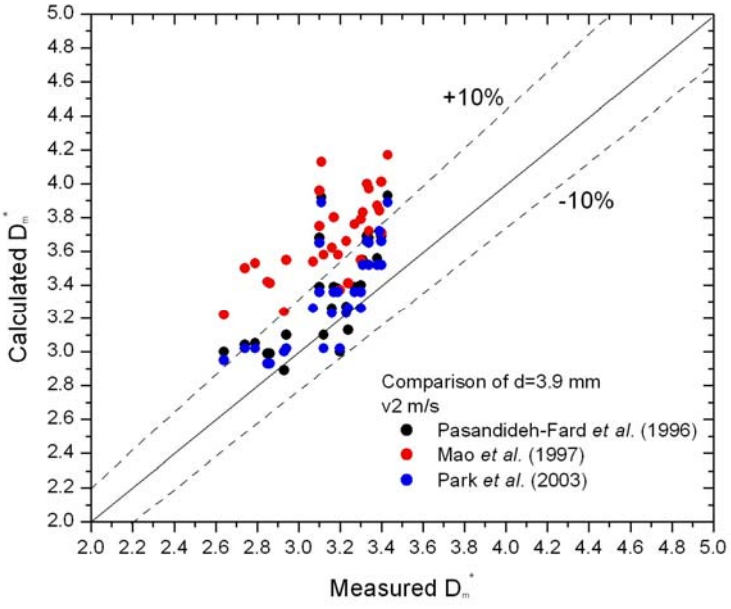

(b) Impact speed of 2 m/s.

Figure H-4. Comparison of Measured D_m^* for d = 3.9 mm with model predictions: (a) Impact speed of 0.01 m/s and (b) impact speed of 2 m/s.

APPENDIX I

AFM IMAGES OF SILICON OXIDE WAFER, SILICON WAFER, AND TEFLON® FILM

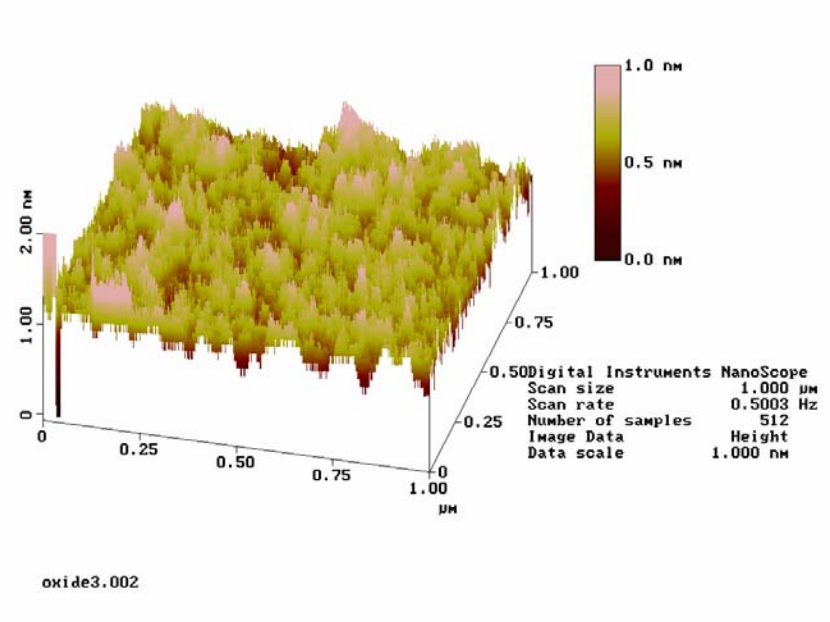

(a) Scanned image

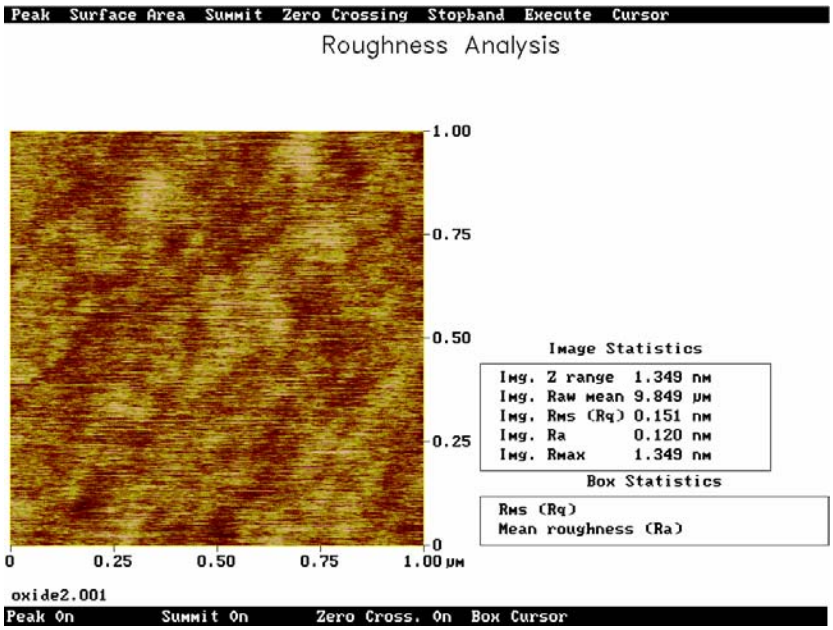

(b) Roughness analysis

Figure I-1. AFM images of silicon oxide wafer: (a) Scanned image, and (b) roughness analysis.

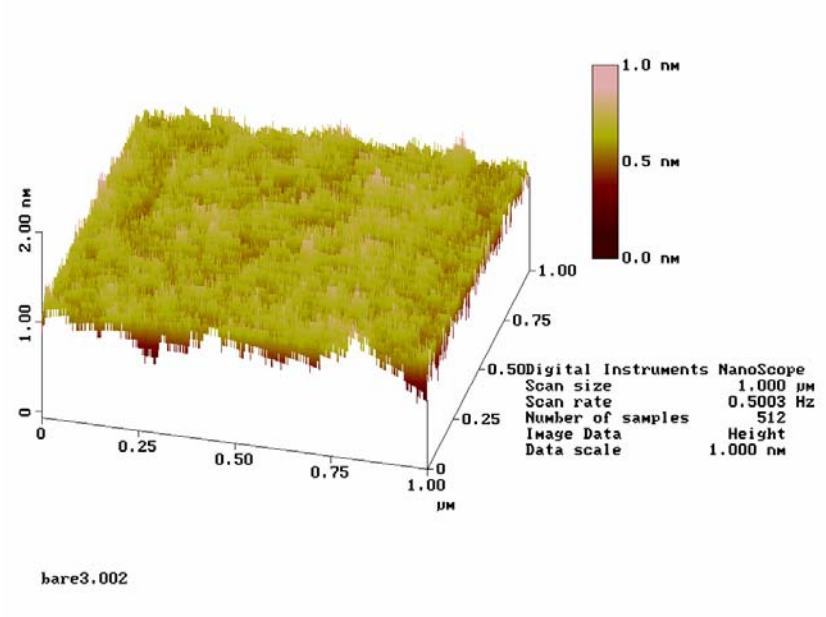

(a) Scanned image

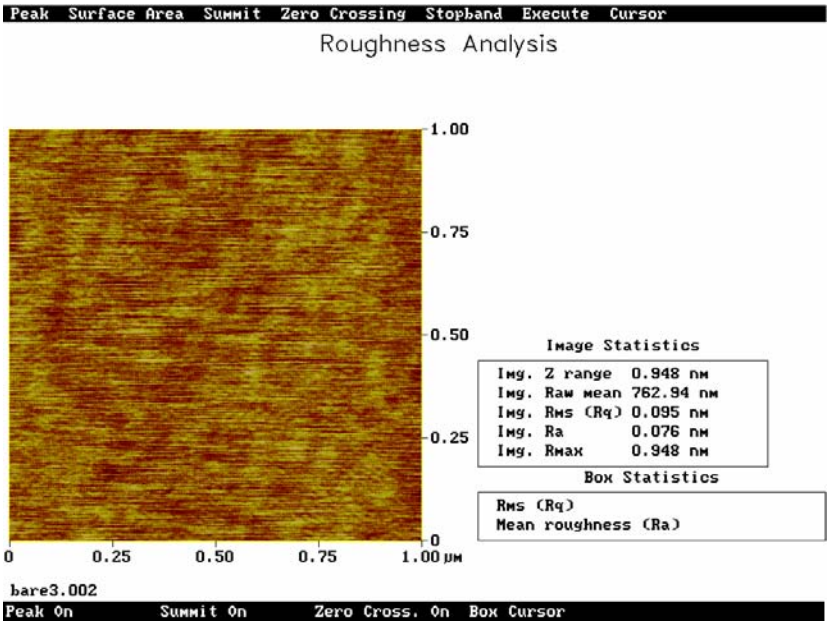

(b) Roughness analysis

Figure I-2. AFM images of silicon wafer: (a) Scanned image, and (b) roughness analysis.

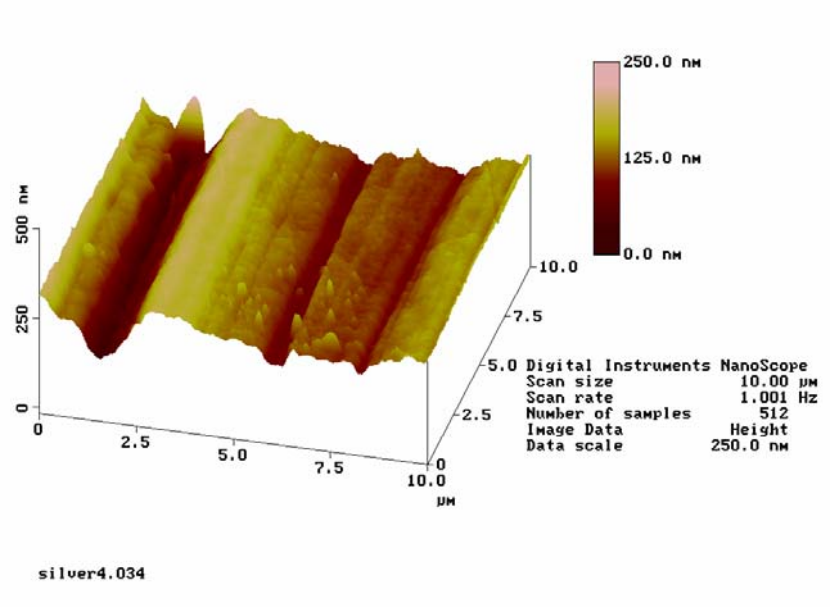

(a) Scanned image

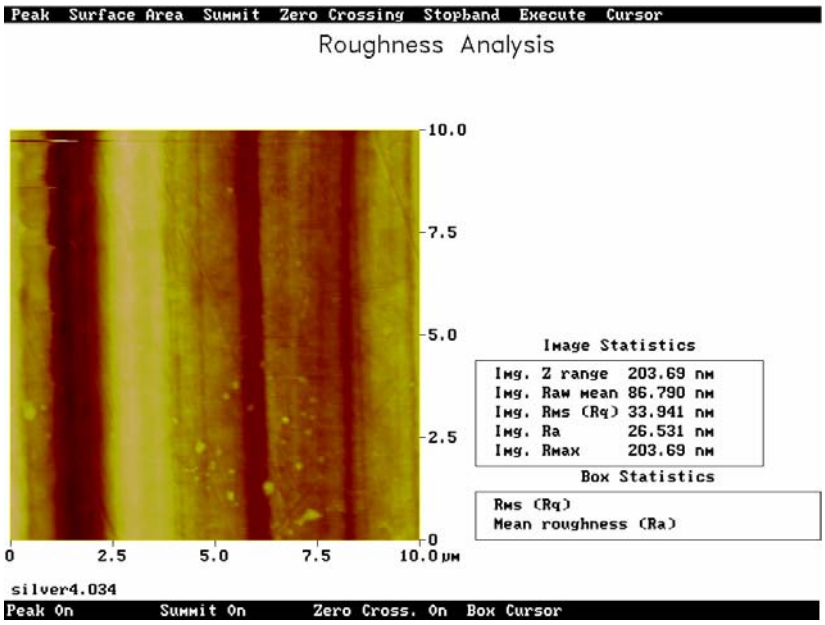

(b) Roughness analysis

Figure I-3. AFM images of Teflon® film: (a) Scanned image, and (b) roughness analysis.

REFERENCES

Asai, A., Shioya, M., Hirasawa, S., and Okazaki, T., Impact of an ink drop on paper, *J. Imaging Sci. Tech.,* **37**(2), pp.205-207, 1993.

Aussillous, P. and Quéré, D., Liquid marbles, Liquid marbles, *Nature*, **411**(21), pp.924-927, 2001.

Bechtel, S.E., Bogy, D.B., and Talke, F.E., Impact of a liquid drop against a flat surface, *IBM J. Res. Develop*, **25**(6), pp.963-971, 1981.

Bergeron, V., Bonn, D., Martin, J.Y., Vovelle, L., Controlling droplet deposition with polymer additives, *Nature*, **405**, pp.772-775, 2000.

Bico, J., Marzolin, C., and Quéré, D., Pearl drops, *Europphysics Letters*, **47**(2), pp.220-226, 1999.

Carr, W.W., Park, H., and Morris, J.F., 'Textile inkjet: drop formation and surface interaction', *National Textile Center Annual Report*, National Textile Center, Wilmington, DE, Project C02-GT07, 2004.

Chandra, S. and Avedisian, C.T., On the collision of a droplet with a solid surface, *Proc. R. Soc. Lond.,* **432**, pp.13-41, 1991.

Crooks, R., Cooper-Whitez, J., and Boger, D.V., The role of dynamic surface tension and elasticity on the dynamics of drop impact, *Chem. Eng. Sci*., **56**, pp.5575-5592, 2001.

Dell'Aversana, P., Tontodonato, V., and Carotenuto, L., Suppression of coalescence and of wetting: The shape of the interstitial film, *Physics of Fluids*, **9** (9), pp. 2475-2485, 1996.

Dell'Aversana, P. and Neitzel G.P., When liquids stay dry, *Physics Today*, **51**, pp. 38-41, 1998.

Dietzel, M., Haferl, S., Ventikos, Y., and Poulikakos, D., Marangoni and variable viscosity phenomena in picoliter size solder droplet deposition, *Journal of Heat Transfer*, **125**, pp. 365-376, 2003.

Doring, M., Ink-jet printing, *Philips Tech. Rev*., **40**, p.192, 1982.

Engel, O.G., Waterdrop Collisions with solid surfaces, *J. Res. Natn. Bur. Stand.*, **54**(5), pp.281-295, 1955.

Ford, R.E. and Furmidge, C.G.L, Impact and spreading of spray drops on foliar surfaces, Wetting, Soc. Chem. Industry Monograph, pp.417-432, 1967.

Fukai, J., Shiiba, Y., Yamamoto, T., Miyataka, O., Poulikakos, D., Megaridis, C.M., Zhao. Z., Wetting effects on the spreading of a liquid droplet colliding with a flat surface: experiment and modeling, *Phys. Fluids*, **7**(2), pp.236-247, 1995.

Fujimoto, H., Ito, S., and Takezaki, I., Experimental Study of Successive Collision of Two Water Droplets with a Solid, *Experiments in Fluids*, **33**, pp. 500-502, 2002.

Funk, H.L., Non-impact printing, *SID 84 digest*, **26**(1), p.349, 1985.

Furbank, R.J.; Morris, J.F. An Experimental study of particle effects on drop formation, *Physics of Fluids*, **16**(5), pp.1777-1790, 2004.

Haferl, S. and Poulikakos, D., Transport and solidification phenomena in molten microdroplet pileup*, Journal of Applied Physics*, **92**(3), pp. 1675-1689, 2002.

Kim, H.Y. and Chun, J.H., The recoiling of liquid droplets upon collision with solid surfaces, *Physics of fluids*, **13**(3), pp.643-659, 2001.

Kim, H., Park, S., and Min, K., Imaging the high-speed impact of microdrop on solid surface, *Review of scientific instruments*, **74**(11), pp.4930-4937, 2003.

Krieger, I.M., Rheology of monodisperse lattices, *Adv. Colloid Interface Sci*., **3** (2), pp.111-136, 1972.

Mao, T., Kuhn, D.C.S., and Tran H., Spread and rebound of liquid droplets upon impact on flat surfaces, *AIChE Journal*, **43**(9), pp.2169-2179, 1997.

McKinley, G. and Sridhar, T., Filament-stretching rheometry of complex fluids, *Annu. Rev. Fluid Mec*., **34**, pp. 375-415, 2002.

McKinley, G., Private communication., 2004.

Mehdi-Nejad, J., Mostaghimi, J., and Chandra, S., Air bubble entrapment under an impacting droplet, *Physics of fluids*, **15**(1), pp.173-183, 2003.

Moita, A.S. and Moreira, A.L., The dynamic behaviour of single droplets impacting onto a flat surface., *ILASS-Europe 2002*, , Zaragoza, September 2002.

Mourrougou-Candoni, N., Prunet-Foch, B., Legay, F., and Vignes-Adler, M., Retraction Phenomena of Surfactant Solution Drops upon Impact on a Solid Substrate of Low Surface Energy, *Langmuir*, **15**, pp.6563-6574, 1999.

Neitzel, G.P. and Dell'Aversana, P., Noncoalescence and nonwetting behavior of liquids, *Annu. Rev. Fluid Mech.,* **34**, pp. 267-289, 2002.

Ok, H., Park, H., Carr, W.W., Morris, J.F., and Zhu, J., Particle-laden drop impingement on solid surfaces, *Journal of Dispersion Science and Technology*, **25** (4), pp.449-456, 2004.

Okumura, K., Chevy, F., Richard, D., Quéré, D., and Clanet, C., Water spring : A model for bouncing drops, *Europhysics Letters*, **62**(2), pp.237-243, 2003.

Oliver, J.F., Role of paper surface properties in non-impact printing, *J. Imaging Technology*, **14**(5), p.144-148, 1988.

Onda, T., Shibuichi, S., Satoh, N., and Tsujii, K., Super-water-repellent fractal surfaces, *Langmuir*, **12**(9), pp.2125-2127, 1996.

Orme, M., Experiments on droplet collisions, bounce, coalescence and disruption, *Progress in Energy and Combustion Science*, **21**(1), pp.65-79, 1997.

Park, H., Carr, W.W., and Zhu, J., Interactions of a single ink-jet droplet with textile printing surfaces, *IS&T's NIP 17: International Conference on Digital Printing Technologies*, pp.438-441, 2001.

Park, H., Carr, W.W., and Zhu, J., Interactions of a single inkjet droplet with well-characterized surfaces, *IS&T's NIP18: International Conference on Digital Printing Technologies*, pp.620-626, 2002.

Park, H., Drop impingement and interaction with a solid surface, Doctorial dissertation, Georgia Institute of Technology, Atlanta, GA, 2003.

Park, H., Carr, W.W., Zhu, J., and Morris, J.F., Single drop impaction on a solid surface, *AIChE Journal*, **49**(10), pp. 2461-2471, 2003.

Pasandideh-Fard, M., Qiao, Y.M., Chandra, S., and Mostaghimi, J., Capillary effects during droplet impact on a solid surface, *Phys. Fluids*, **8**(3), pp.650-659, 1996.

Pasandideh-Fard, M., Qiao, Y.M., Chandra, S., and Mostaghimi, J., On the spreading and solidification of molten particles in a plasma spray process: effect of thermal contact resistance, *Plasma Chemistry and Plasma Processing*, **16**(1), pp.83S-98S, 1996.

Pasandideh-Fard, Aziz, S.D, Chandra, S., and Mostaghimi, J., Surface cooling by an impinging water drop, *Proceeding of the 33rd National Heat Transfer Conference*, pp. 1-8, Albuquerque, New Mexico, August 15, 1999.

Proebster, W.E. and Reiner, H, VLSI and Computer Peripherals, IEEE, Washington, pp.246, 1989.

Quéré, D., Rough ideas on wetting, *Physica A*, **313**, pp.32-46, 2002.

Range, K. and Feuillebois, F., Influence of surface roughness on liquid drop impact, *Journal of colloid and interface science*, **203**, pp.16-30, 1998.

Rayleigh, L., *The Theory of Sound*, 2nd Ed., Vol. II. Dover, New York, 1945.

Renardy, Y., Popinet, S., Duchemin, L., Renardy, M., Zaleski, S., Josserand, C., Drumright-Clarke, M.A., Richard, D., Clanet, C., and Quéré, D., Pyramidal and toroidal water drops after impact on a solid surface, *Journal of Fluid Mechanics*, **484**, pp.69-83, 2003.

Richard D., and Quéré, D., Bouncing Water Drops, *Europphysics Letters*, **50**(6), pp.769-775, 2000.

Richard D., Clanet, C., and Quéré, D., Contact time of a bouncing drop, *Nature*, **417**, p.811, 2002.

Rioboo, R., Marengo, M., and Tropea, C., Time evolution of liquid drop impact onto solid, dry surfaces, *Experiments in fluids*, **33**, pp.112-124, 2002.

Roux, D.C.D. and Cooper-Whiter J.J., Dynamics of water spreading on a glass surface, *Journal of Colloid and Interface Science*, **277**, pp.424-436, 2004.

Scheller, B.L. and Bousfield, D.W., Newtonian drop impact with solid surface, *AIChE Journal*, **41**(6), pp.1357-1367, 1995.

Šikalo, S., Marengo, M., Tropea, C., and Ganic, E., Analysis of impact of droplets on horizontal sufaces, *Experimental thermal and fluid science*, **25**, pp.503-510, 2002.

Tincher, W.C., Hu, Q., Li, X., and Tian, Y., Ink jet systems for printing fabric, *Textile Chemist and Colorist*, **30**(5), pp.24-27, 1998.

Tincher, W.C., Hu, Q., Li, X., Tian, Y., and Zang, J., Coloration systems for ink jet printing of textiles, *IS&T's NIP 14: International Conference on Digital Printing Technologies*, p.243, 1998.

Tincher, W.C., AATCC Symposium Printing 2000: Entering the jet age, AATCC, Research Triangle Park, NC, p.11, 1999.

Thoroddsen, S.T. and Sakakibara, J., Evolution of the fingering pattern of an impacting drop, *Physics of Fluids*, **10**(6), pp.1359-1374, 1998

Thoroddsen S.T and Takehara, K., The coalescence cascade of a drop, *Physics of Fluids*, **12**(6), pp. 1265-1267, 2000

Tristram-Nagle, S., Petrache, H.I., Suter, R.M., and Nagle, J.F., Effect of substrate roughness on D spacing supports theoretical resolution of vapor pressure paradox, *Biophysical Journal*, **74**, pp. 1421-1427, 1998.

Tsurutani, K, Yao, M., Senda, J., and Fujimoto, J., Numerical analysis of the deformation process of a droplet impinging upon a wall, *JSME International Journal Series II*, **33**(3), pp.555-561, 1990

Ugelstad, J., Kaggerud, K.H., Hansen, F.K., and Berge, A., Absorption of low molecular weight compounds in aqueous dispersions of polymer-oligomer particles: A two step swelling process of polymer particles giving an enormous increase in absorption capacity, *Makromol. Chem*., **180**, pp.737-744, 1979.

Worthington, A.M., On the forms assumed by drops of liquids falling vertically on horizontal plate, *Proc. R. Soc. Lond*., **25**, pp.261-272, 1876.

Xu, M., Private communication, 2003.

Zhang, X. and Basaran, O.A., Dynamic surface tension effects in impact of a drop with a solid surface, *Journal of colloid and interface science*, **187**, pp.166-178, 1997.